IEEE microwave MAGAZINE

for the Microwave & Wireless Engineer

Volume 23 • Number 6 • June 2022

Breadth of MTT

IMS2022 Advance Program

MTT-S

IEEE

IMWS-AMP 2022

2022 IEEE MTT-S International Microwave Workshop Series on Advanced Materials and Processes for RF and THz Applications

November 13-15, 2022, Guangzhou, China

Call for Papers

http://www.em-conf.com/imws-amp2022

Organizing Committee

IEEE MTT-S International Microwave Workshop Series on Advanced Materials and Processes for RF and THz Applications (IMWS-AMP 2022) is co-organized by South China University of Technology, and co-sponsored by IEEE Guangzhou Joint AP/MTT Chapter. IMWS-AMP 2022 is a continuation of a series of annual international events held in Suzhou, China (2015), Chengdu, China (2016), Pavia, Italy (2017), Michigan, USA (2018), Bochum, Germany (2019), Virtual (2020) and Chongqing, China (2021). The purpose of this platform is to boost technical and educational activities as well as exchanges and collaborations within the international microwave community.

IMWS-AMP2022 will be held in Guangzhou, China on Nov. 13-15, 2022. IMWS-AMP2022 will feature both invited and contributed papers. Distinguished researchers will be invited to deliver keynote speeches on technology trends and significant advances in relevant topics. Contributed papers are solicited for the same topics as listed below:

Topics

The topics include, but are not limited to, the following technical areas:

- Emerging electronic and optoelectronic devices (e.g. carbon nanotube, 2D materials and beyond)
- Wide bandgap and other emerging semiconductor materials (e.g. ionic materials) based electronic devices and circuits
- Advanced silicon, integrated passive devices and integrated circuits
- Monolithic integrated circuits
- Low-temperature co-fired ceramic and liquid crystal polymer based microwave devices and circuits
- Large-area printing, inkjet printing and 3D printing materials and processes for RF and THz applications
- Integrated passive devices and advanced packaging for RF applications
- Advanced materials (flexible, ferromagnetic and superconducting materials etc.) for RF electronics and antennas
- Engineered metamaterials and plasmonics for absorption, cloaking, and wave manipulation
- Passive/active microwave and terahertz devices and circuits
- Antennas with advanced/complex/artificial materials and processes
- Microwave and millimeter wave antennas and antenna arrays

Electronic Paper Submission

Prospective authors are invited to submit manuscripts in electronic (PDF) format only. All papers must be written in English and limited to three pages including text, references, and figures. A template is available on the IMWS-AMP 2022 website. Papers submitted will be peer reviewed and all papers presented at the conference will be included in IEEE Xplore pending quality review. Note that one-page abstracts can also be acceptable, but it will not be included in IEEE Xplore.

Special Issues in IEEE Transactions on Microwave Theory and Techniques:

Authors of all papers presented at IEEE IMWS-AMP 2022 are invited to submit an expanded version of their papers to a Mini-Special Issue of IEEE Transactions on Microwave Theory and Techniques. Every paper will be reviewed by the respective journal in the same manner as all other regular submissions.

Best Paper Awards

Awards for Best Student Papers will be presented to the winners at the conference. The Awards Committee will judge the papers primarily on originality, significance, technical soundness, presentation, and reviewers' reports. To qualify for the Best Student Paper, the author must be a full-time student who presents, as the first author, the paper at the conference.

Important Dates

Paper Submission Deadline: August 15, 2022
Notification of Acceptance: September 15, 2022
Pre-registration: September 30, 2022

Special Sessions

Special sessions of Young Professionals (YP) and Women in Microwaves (WiM) will be organized in the conference.

Exhibitions

Exhibition of company products is solicited for the areas related to the topics. Interested parties could contact the Conference Secretariat.

Digital Object Identifier 10.1109/MMM.2022.3162510

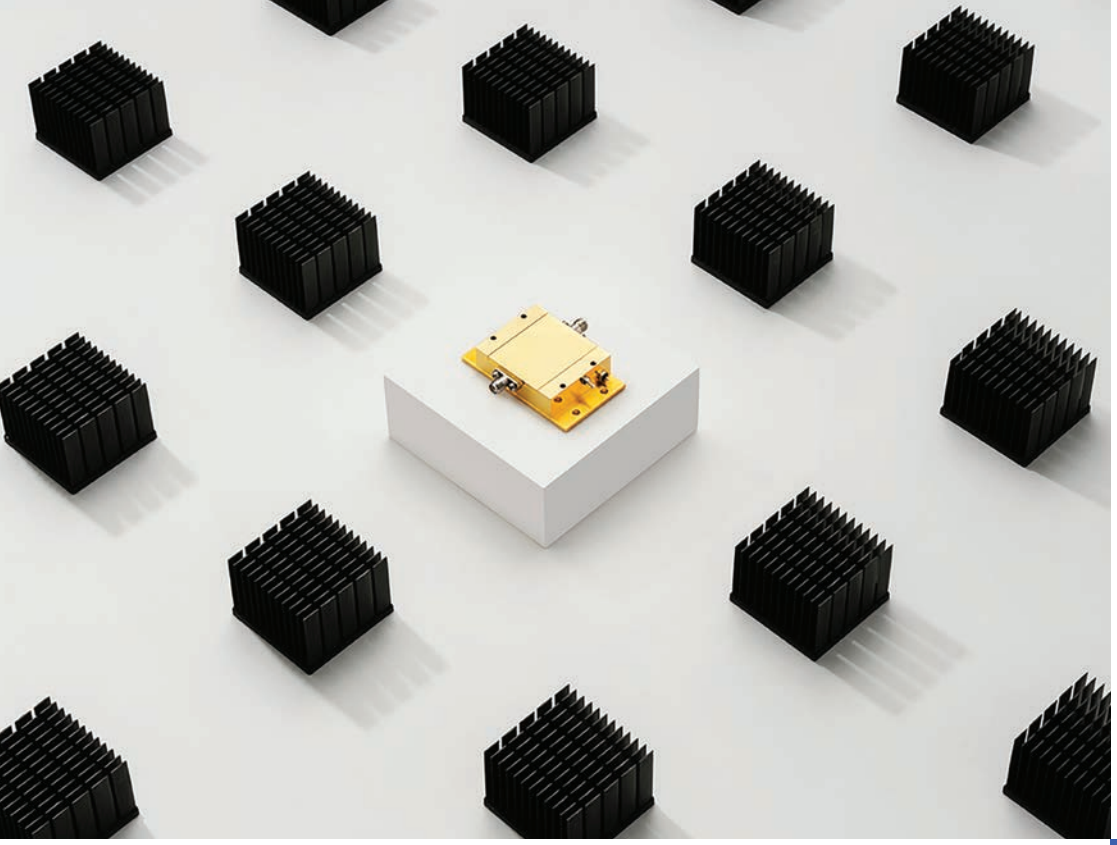

0.05 MHZ TO 86 GHZ

High-Frequency Amplifiers

Ultra-Wideband Performance

Features for Almost Any Requirement Now up to E-Band

- High gain, up to 45 dB
- Noise figure as low as 1.7 dB
- Output power up to 1W
- Rugged designs with built-in protections
- Wide DC input voltage range

NEW TO MARKET

ZVA-71863+ Series

- 71 to 86 GHz
- Low Noise & Medium Power Models

ZVA-35703+

- 35 to 71 GHz

Mini-Circuits®

cadence®

Design Smarter with AWR Software

See for yourself how easy and effective it is to streamline your design process, improve end-product performance, and accelerate time to market for MMICs, RF PCBs, microwave modules, antennas, communications systems, radar systems, and more.

Get started at **cadence.com/go/awr/try**.

Visit us at IMS in Booth #5050

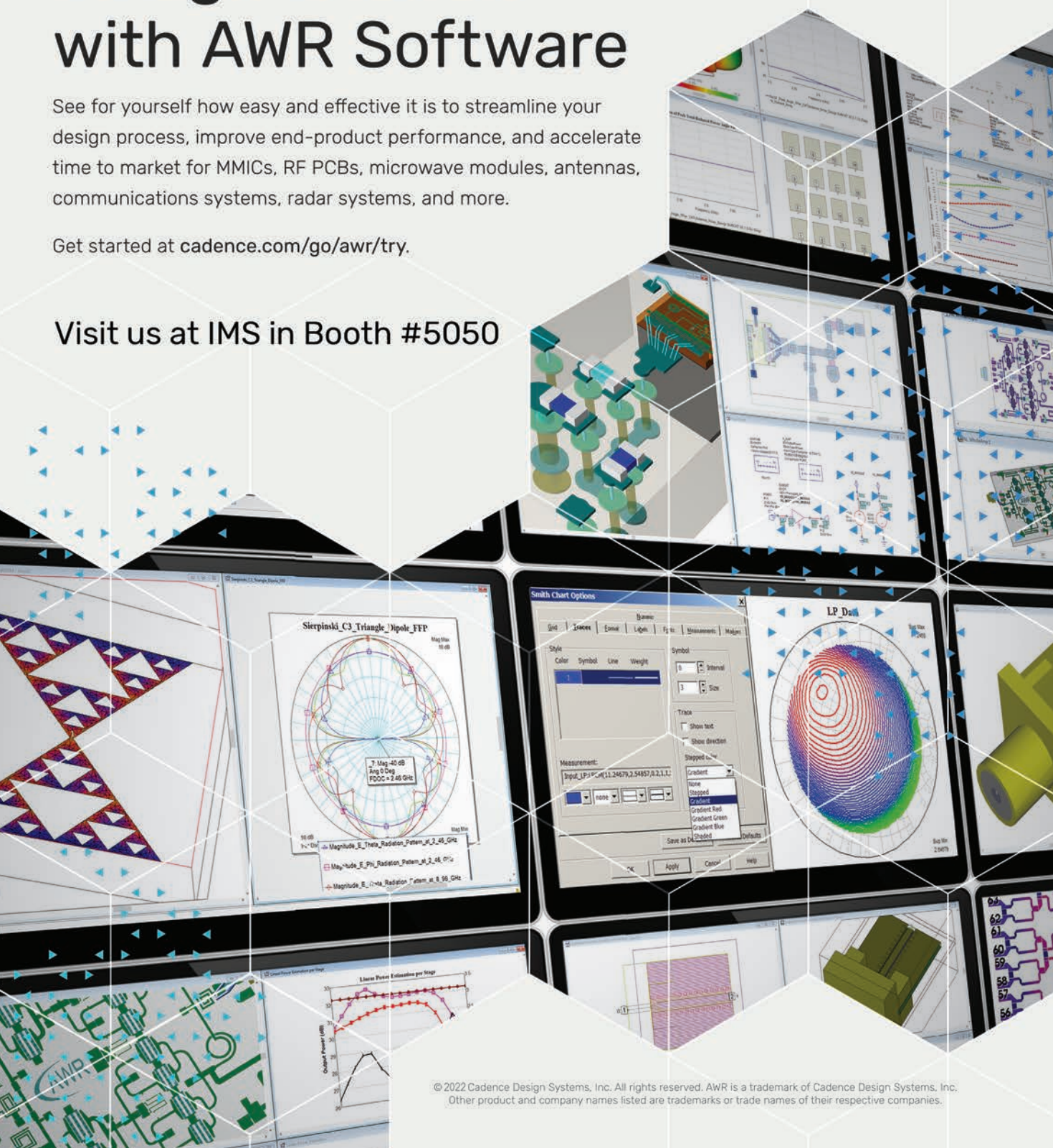

Digital Object Identifier 10.1109/MMM.2022.3144751

IEEE microwave MAGAZINE
for the Microwave & Wireless Engineer

Volume 23 • Number 6 • June 2022 • ISSN 1527-3342

features

on the cover:

©SHUTTERSTOCK.COM/GARRYKILLIAN

IEEE microwave MAGAZINE
for the Microwave & Wireless Engineer

IEEE Microwave Magazine (ISSN 1527-3342) (IEMMFF) is published 12 times a year by the Institute of Electrical and Electronics Engineers, Inc. Headquarters: 3 Park Avenue, 17th Floor, New York, NY 10016-5997 USA. Responsibility for the contents rests upon the authors and not upon the IEEE, the Society, or its members. IEEE Service Center (for orders, subscriptions, address changes): 445 Hoes Lane, Piscataway, NJ 08854. Telephone: +1 732 981 0060, +1 800 678 4333. Individual copies: IEEE members US$20.00 (first copy only), nonmembers US$38.00 per copy. Subscription rates: Subscriptions for Society members are included with membership dues. Nonmember subscription rates available upon request. Periodicals postage paid at New York, N.Y., and at additional mailing offices. Ride along enclosed. Postmaster: Send address changes to *IEEE Microwave Magazine*, IEEE Operations Center, 445 Hoes Lane, Piscataway, NJ 08854 USA. Canadian GST #125634188
PRINTED IN THE USA
Digital Object Identifier 10.1109/MMM.2022.3144752

columns & departments

Technology. Support. Success.

Powerful EM Simulation Software and Real-World Expertise.

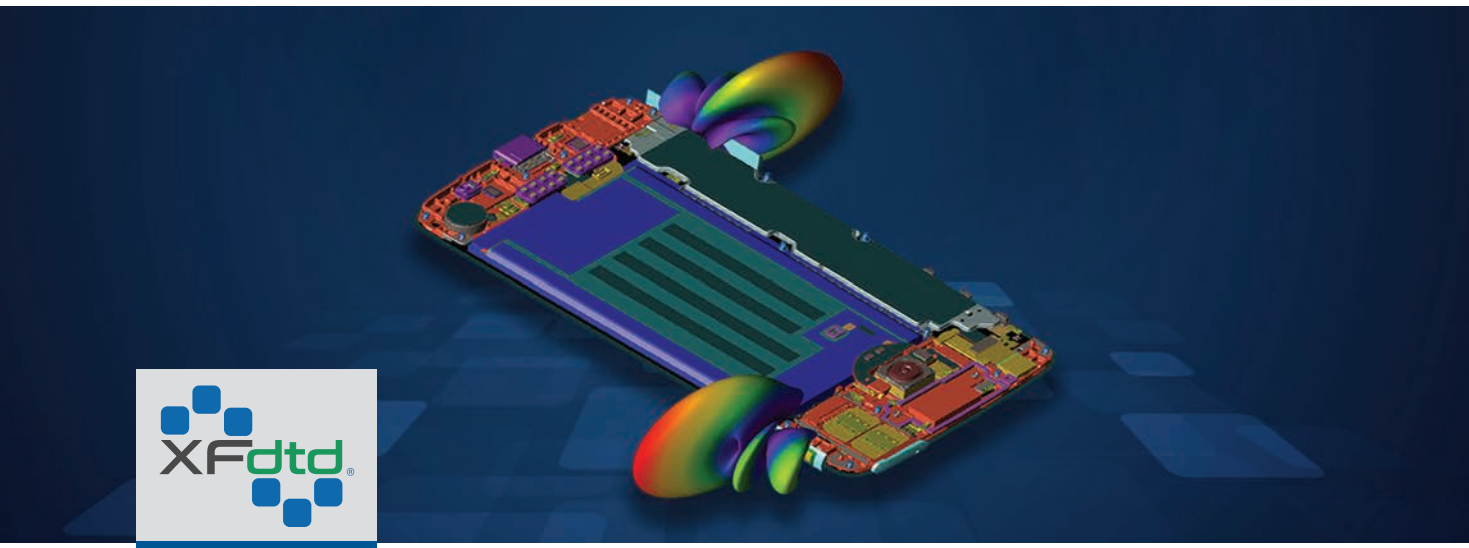

XFdtd
Electromagnetic
Simulation Software

XFdtd® 3D EM Simulation Software has evolved alongside modern antenna design, meeting industry requirements and solving today's most advanced antenna design challenges.

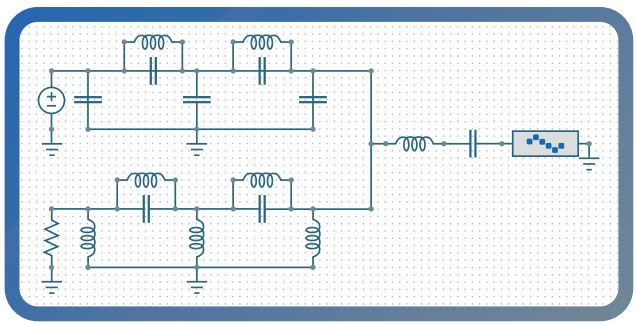

XFdtd's new schematic editor enables advanced antenna matching network and corporate feed network analyses as part of a unified solver workflow, including multi-state and multi-port devices.

Explore all of XFdtd's powerful features at | **www.remcom.com/xfdtd** ›››

Superior Support

Remcom provides an extraordinary level of support to our customers, giving you direct access to EM experts who are dedicated to your success. Our team is there to guide you through all of your EM challenges, from the simple to the technically complex.

Learn more about the Remcom difference at | **www.remcom.com/about-remcom** ›››

REMCOM®

+1.888.7.REMCOM (US/CAN) | +1.814.861.1299 | **www.remcom.com**

From the Editor's Desk

Welcome to the June Issue

■ **Robert H. Caverly**

For many years, the issues of *IEEE Microwave Magazine* are not only sent out to IEEE Microwave Theory and Techniques Society (MTT-S) members in the manner in which they subscribe (hard copy or electronic), but they are also placed inside the delegate bags at the MTT-S's flagship conference, the International Microwave Symposium (IMS). For 2022, we are again including this month's issue, the June 2022 issue, as the second insert for the delegate bags as a way to show the "Breadth of the MTT-S," that is, examples of the wide-ranging topics that fall within our field of interest (see the MTT-S field of interest statement at https://mtt.org/field-interest-statement/).

This issue complements the May 2022 IMS2022 focus issue with an updated advance program as well as four technical features, our regular columns, and the annual special feature on the newly inducted Fellows of IEEE, which focuses on members associated with the MTT-S. The elevation to Fellow of IEEE is an honor reserved for a select group of engineers, with the number of IEEE Members elevated to Fellow not exceeding one-tenth of 1% of the total voting membership. This highest grade of membership is conferred by the IEEE Board of Directors in recognition of an individual's outstanding record of accomplishments in any IEEE field of interest. Before going into the overview of the issue, I would like to thank one of the magazine's associate editors, Chia-Chan Chang, for her efforts in the development of the Fellows recognition article and for interacting with all of the new IEEE Fellows to bring this article to fruition.

As previously mentioned, our four technical features this month span a wide range of topics within the MTT-S. The first article, by Cuadrado-Calle et al., "Solid-State Diode Technology for Millimeter and Submillimeter-Wave Remote Sensing Applications," is a timely look at the advances in high-frequency diode technology and related applications up to 5 THz. The article covers key global players in diode fabrication and then discusses the applications of many of these devices, including mixers, multipliers, detectors, and noise sources, finishing with a look down the technology road.

Robert H. Caverly (rcaverly@villanova.edu) is with Villanova University, Villanova, Pennsylvania, 19085, USA.

Digital Object Identifier 10.1109/MMM.2021.3136635
Date of current version: 5 May 2022

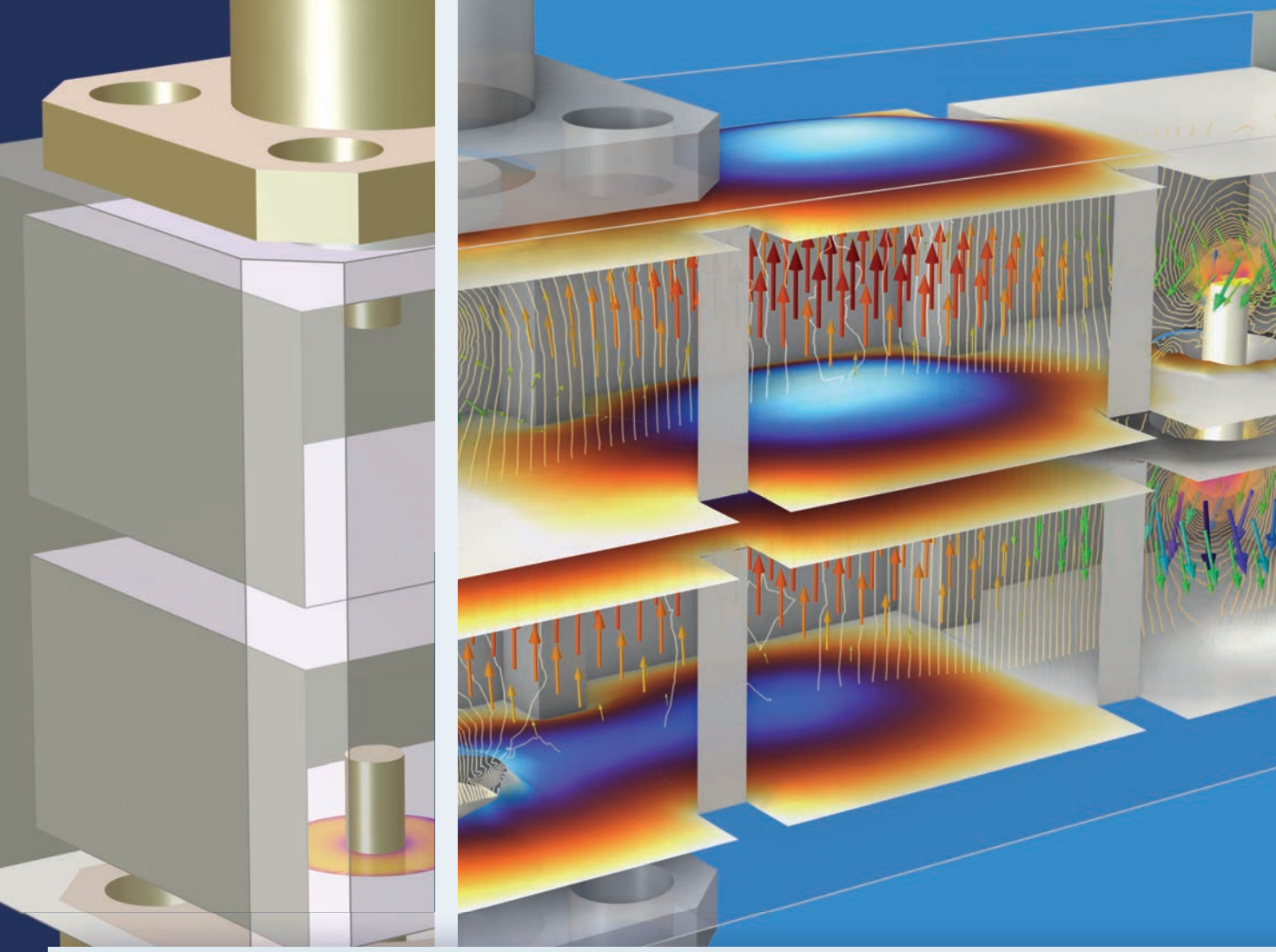

Take the Lead in RF Design

with COMSOL Multiphysics®

Multiphysics simulation is expanding the scope of RF analysis to higher frequencies and data rates. Accurate models of microwave, mmWave, and photonic designs are obtained by accounting for coupled physics effects, material property variation, and geometry deformation. Ultimately, this helps you more quickly see how a design will perform in the real world.

» *comsol.com/feature/rf-innovation*

In the second feature, Gao et al. take a more system-oriented approach in "Integrated Filter–Amplifiers." Here, the authors consider filters and antennas in a microwave system as a single circuit block, rather than separate blocks, to reduce the parts count and simplify the system design. The authors describe a synthesis approach in the co-design of filters and antennas and then move to the presentation of various published designs to show the importance of the co-design approach.

In our third feature, "Microwave Power Detectors in Different CMOS Design Architectures," Ravanne et al. discuss the current state of the art in detector design. The feature reviews the important requirements for a microwave power detector and then proceeds to present several active power detector circuits.

The final technical feature by Dutta et al., "Spatiotemporal Nonreciprocal Filters," looks at current active nonreciprocal filter circuits, which are integrated substitutes for traditional magnetic material-based nonreciprocal filters. The authors present the necessary theoretical background governing nonreciprocity and then discuss design techniques for nonreciprocal filters, concluding with nonreciprocal filter examples from the literature. While these four feature articles do not represent the entire field of interest of the MTT-S, they are excellent examples of our wide-ranging field.

Our traditional monthly columns are in this issue as well, starting with Rashaunda Henderson's "President's Message." Fred Schindler, in our "Micro-Business" column, talks about the need to perform due diligence when taking on new industry partners or acquisitions. The MTT-S currently has 26 technical committees (TCs) that span our core technologies and techniques as well as the systems and applications that fall within our field of interest. In this month's "MTT-S Society News" column, we hear from one of those TCs, TC-2 Design Automation, with its biennial report on the activities and accomplishments of the TC since 2019. With the various workshops, conferences, talks, and publications in TC-2's technical area, it is clear that the TC is active in spite of the constraints of the last two years.

Sherry Hess, a member of the MTT-S Administrative Committee (AdCom) as well as chair of the AdCom's Marketing and Communication Committee, provides a 12-year retrospective look at the activities and accomplishments of the MTT-S Women in Microwaves group. In addition to the solution to last month's "Enigmas, etc." problem, we also have the IMS2022 advance program.

Finally, we have our monthly "Conference Calendar." When putting the calendar together for this month, I noticed a distinct trend toward returning to in-person events, which is a trend that I hope can continue at a rapid pace. Be sure to check the websites of the conferences to see if there are any changes in conference modalities as the conference date approaches. We hope you enjoy this month's issue, and I look forward to seeing you at IMS2022.

MiCIAN

µWave Wizard™

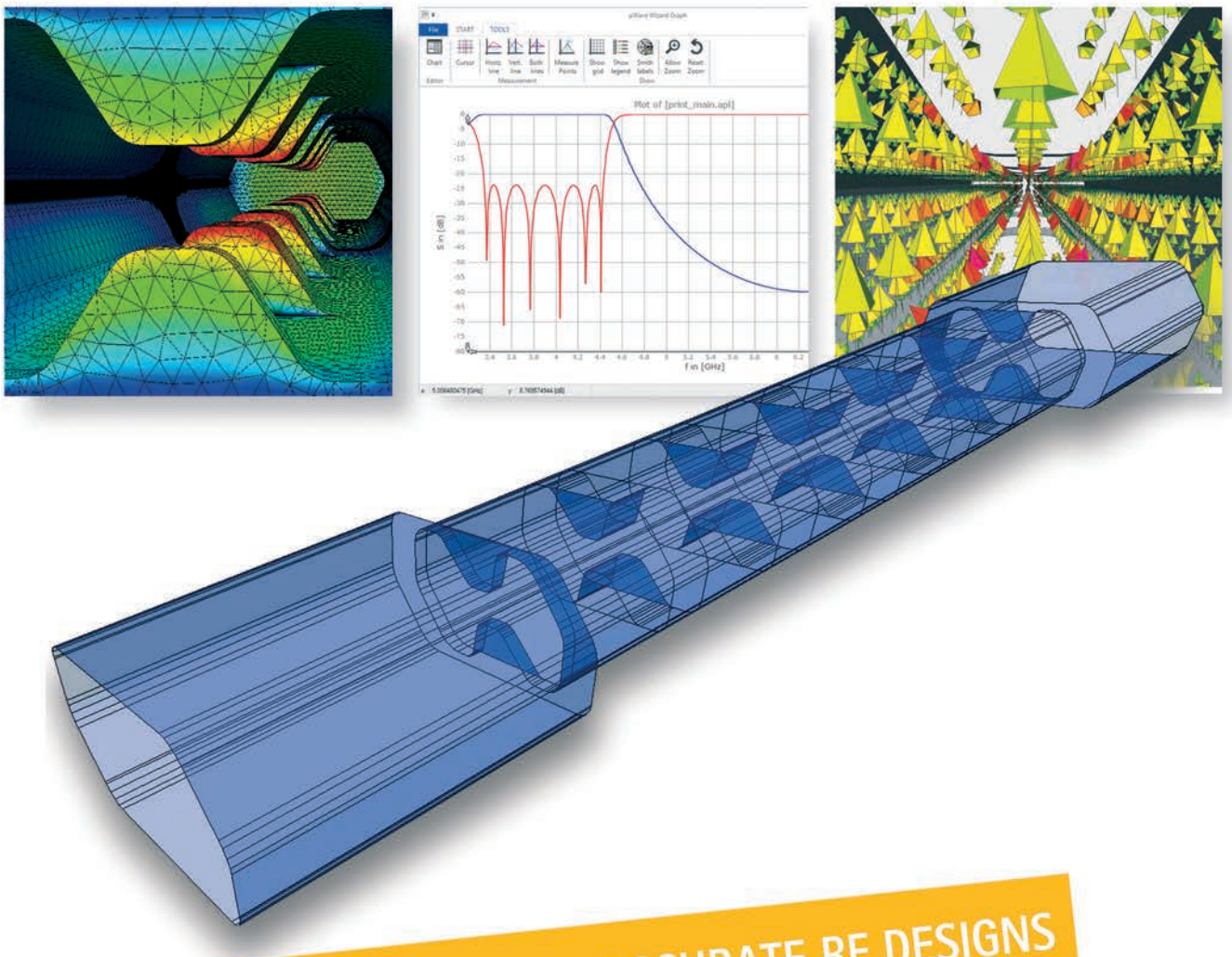

THERE'S MAGIC IN FAST AND ACCURATE RF DESIGNS

µWave Wizard™ EDA software for fast and accurate designs and analysis of passive components and antennas

- Hybrid solver with six different EM methods
- Rapid development with more than 400 building blocks
- User friendly modeling capabilities
- Full parameterization of structure geometries
- Various powerful synthesis tools and optimizers
- Several import and export CAD formats

MiCIAN

See us at IMS 2022, booth #9068

Mician GmbH, Schlachte 21, 28195 Bremen, Germany, Tel.: +49 42116899351, www.mician.com

President's Column

Membership Has Its Privileges

■ **Rashaunda Henderson**

That was a slogan American Express used years ago, when I was younger and an avid TV watcher. The company's commercials always showed people on great vacations, living lavishly. The implication was that if you had membership with American Express through its credit card services, you, too, would have all the privileges displayed in the ads. As I embarked on writing this article, I wanted to mention the benefits of membership in the IEEE Microwave Theory and Techniques Society (MTT-S).

Many of us joined the Society as students in undergraduate school and perhaps were part of IEEE as a whole. We benefited from *IEEE Spectrum* and being tutored or serving as tutors in challenging electrical engineering, math, and physics courses. There are strong IEEE Student Branch Chapters that compete across respective regions and do outreach representing their universities, resulting in bonds with on-campus peers. After graduation, you may have started working in industry or government and moved away from the college campus. As a new employee learning the company, you may have been encouraged to read articles and journals to get up to speed with the state of the art in a concentration area.

Digital Object Identifier 10.1109/MMM.2022.3158032
Date of current version: 5 May 2022

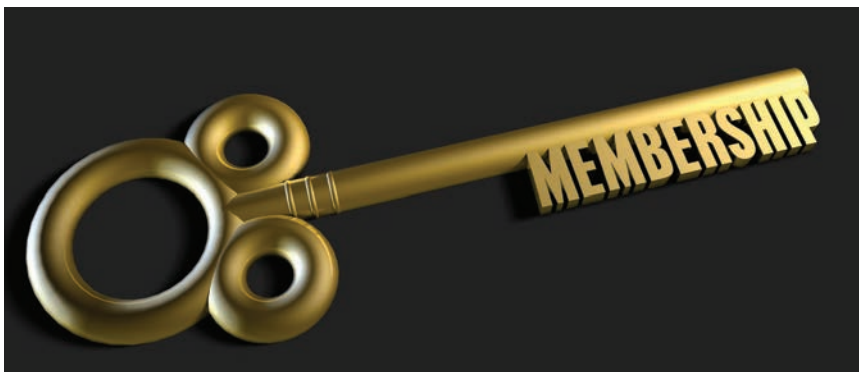

Perhaps if you attended graduate school like me, you began research in a specific area and were encouraged to join a Society within IEEE. In this way, you may have unknowingly become involved in the IEEE Technical Activities Organizational Unit. If one is still in school, student membership is still at a reasonable rate but increases when you select a Society for your affiliation. Student and Society memberships provide direct benefits toward IEEE-sponsored conference registration rates. This is a particular perk that one takes advantage of as a student because the difference in conference registration rates can be significant. Once again, maybe unknowingly, as a Society member, you are eligible for additional benefits. Examples include being added to email lists for Society newsletters that keep one abreast of opportunities in a technical area and journals and magazines that can be mailed. In the past 15 years or so, we have moved away from hard-copy journals to accessing content using IEEE *Xplore*. If you have membership in a Society, there is free access to IEEE's digital library to view all the archives. This is an extremely valuable benefit.

Rashaunda Henderson (rmhen@ieee.org), 2022 MTT-S president, is with the University of Texas at Dallas, Richardson, 75080, Texas, USA.

Anokiwave

mmW Solutions. Enabling a new world

Industry's Trusted Choice for mmW 5G Systems,

Built Green

Introducing our 4th generation

- Silicon Beamformer ICs
- IF Up/Down Converter ICs
- IF Transceiver ICs NEW
- mmW Antenna Kits NEW

anokiwave.com/5g

Highest efficiency and linear power ICs

Enabling greener radios for a net-zero emissions future

Multi-band ICs for fewer SKUs

Just 5 total ICs for a complete mmW to IF, including LO, solution for all 5G bands from 24 to 50 GHz

Smallest form factor radios

More than 70% antenna form factor reduction over 4 generations of ICs

Production assurance

Assured supply to support all mmW 5G market demand

mmW Silicon ICs

Intelligent Array IC Solutions™

mmW Algorithms to Antennas™

www.anokiwave.com/5g | innovation@anokiwave.com

Please See Us At IMS-MTT-s Booth #11022

As young engineers in industry, we are often surprised by the rate increase from student membership to full membership. Justifying why we should invest in IEEE membership becomes important and worthy of debate. In one sense, if you work for a company that subscribes to IEEE *Xplore*, there is no real reason why you should pay for that access through your own membership. Graduate student members also gain access to IEEE *Xplore* through university libraries. However, IEEE wants to be more than a repository for technical content. IEEE wants to be your professional home. This means that throughout your career, IEEE is part of your life. Whether you are a Student Member or a Life Member, IEEE wants to be your source for technical advancements, networking, professional development, and community service opportunities.

Not only can you gain from Society membership but you can also give to others. This can take many forms and develop skills that can be used in the marketplace. You can volunteer for leadership roles ranging from treasurer to committee chair. You can be trained to manage conferences, become an editor, and contribute to the development of global standards for industry. The benefits of leadership training within IEEE are as vast as the number of technical areas IEEE covers. If you are not interested in IEEE membership but only in the MTT-S, you could become a Society affiliate. Affiliates are members of a Society. MTT-S affiliates are not IEEE Members and are eligible to receive benefits and services from the Society, not IEEE. There are pros and cons to becoming an affiliate, but there is a clear reduction in membership costs.

IEEE Young Professionals (YP) is the former Graduates of the Last Decade (GOLD) program that focused on retaining and meeting the needs of recent graduate student members. In 2014, GOLD was replaced with YPs and is now defined by members who are within 15 years of receiving their first professional degree. The YP Affinity Group has traditionally been focused at the IEEE level, but Society YP groups are being formed and helping provide benefits that are specific to the technical activities of professionals who are early in their career.

Let's think about advancing in one's career and integrating it with IEEE membership. That happens in two ways: one is through senior member grade and the other is IEEE Fellow status. Senior Member is achieved by application and requires experience within a profession. The application process occurs between April and June and requires a reference from a Senior Member. Candidates typically have been in professional practice for at least 10 years and shown notable performance during at least five of them in many areas in IEEE-designated fields. A subset of the areas of performance includes the following: substantial responsibility and achievement; the publication of papers, books, and inventions; the technical direction and management of important work, with evidence of accomplishments; and recognized contributions to the welfare of the professions encompassed by IEEE. As a member of the IEEE Phoenix Section, I applied for Senior Member grade and had support from colleagues who were fellow Members and with whom I worked at Motorola. Often, your daily role in technology and product development may be sufficient for seeking Senior Member grade. Your service to a Society and technical achievements can help you achieve this grade. When you achieve senior membership, you receive a recognition plaque.

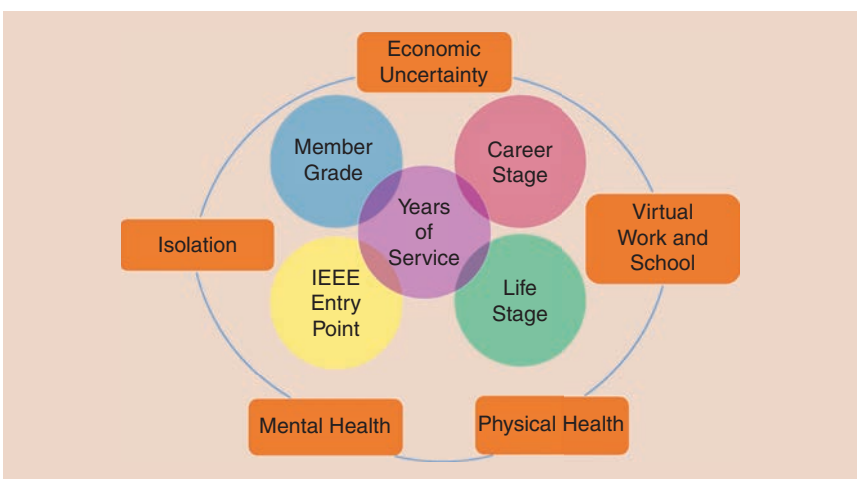

Figure 1. *The IEEE membership life cycle as presented by Ievgen Pichkalyov (chair of the 2021 IEEE Membership Recruitment and Recovery Committee) and Elyn Perez (MGA staff).*

The grade of IEEE Fellow recognizes unusual distinction in a profession and is conferred only by invitation of the Board of Directors on people with extraordinary accomplishments in any of IEEE's designated fields of interest. This month, we celebrate the Fellows of 2021, who were announced at the beginning of the year. Members of this group have been elevated through the MTT-S or had accomplishments that led to elevation through another Society. We congratulate them and look forward to their continued success.

Fast-forward through your career and consider Life Member grade. You must be at least 65, and your age and the number of years you have been an IEEE Member must equal 100 or more. When that happens, you become a Life Member. There are benefits, some of which mimic those for students, including conference registrations. I recently received the *IEEE Life Members Newsletter* and enjoyed reading it. IEEE Members are eligible for group insurance rates. I have used the life insurance for additional coverage and avoid rates associated with my employer.

IEEE Members enjoy discounts (as listed at https://www.ieee.org/membership/join/index.html) from companies such as UPS, Dell, and the GE Appliances Store, to name a few. Not only do we have financial benefits but there are intangible perks that include lifelong friendships and collaborations providing disaster relief. The IEEE Special Interest

YOUR PARTNER IN SIMULATION AND VALIDATION

dSPACE

Radar Testing Over-the-Air? We just call it DARTS.

Over-the-air simulation of radar echoes has never been as easy, quick, and thorough as with the new dSPACE Automotive Radar Test Systems (DARTS). They reliably meet even the strictest requirements of safety-critical applications. DARTS get the job done in chip testing, R&D, end-of-line testing, type approval, you name it.

dspace.com

IMS Connecting Minds. Exchanging Ideas. EXPLORE THE PEAKS OF MICROWAVE ENGINEERING DENVER2022

Visit us at IMS 2022
June 19-24 | Booth #2014

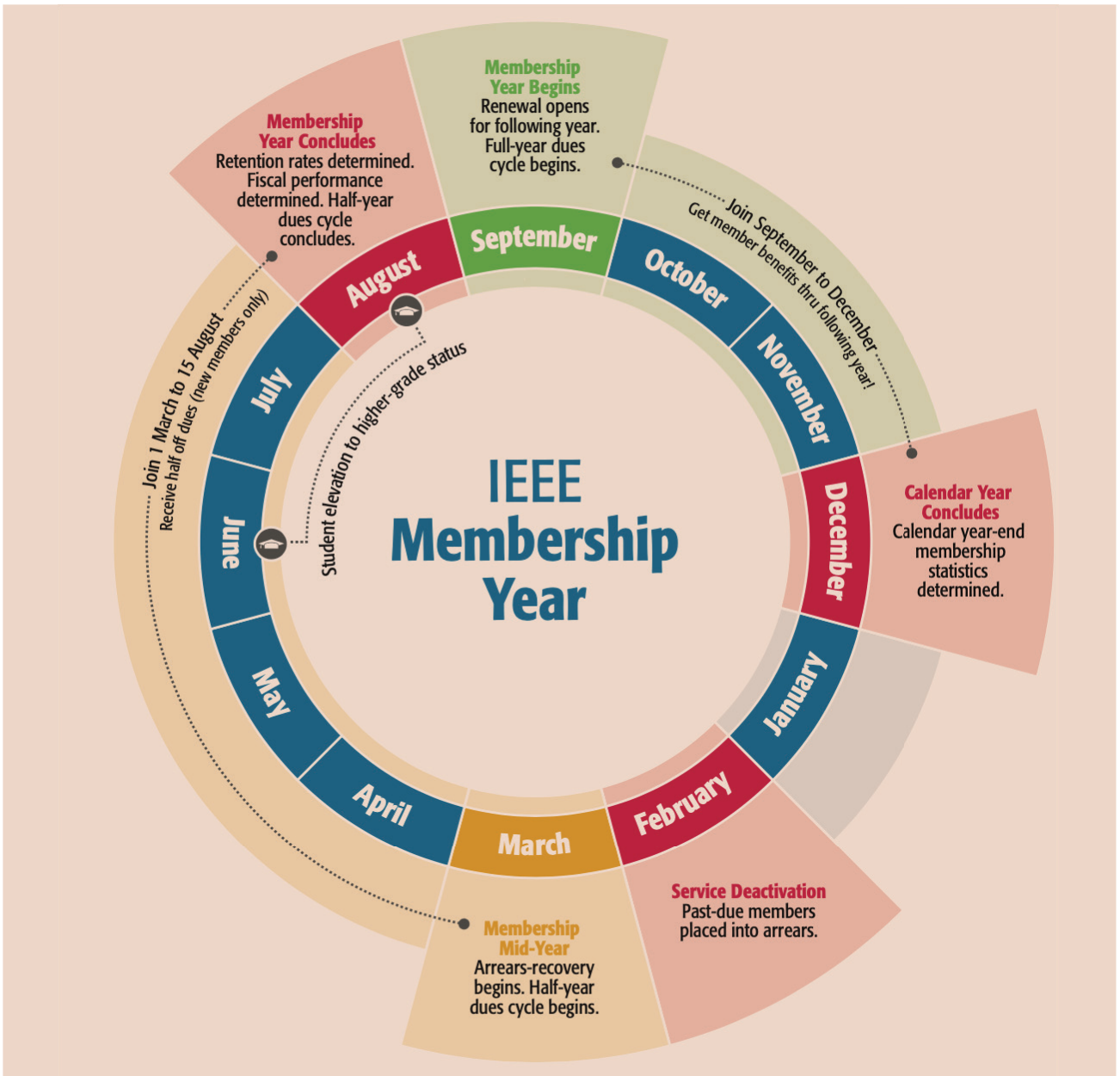

Figure 2. *The IEEE membership development cycle through a calendar year.*

Group on Humanitarian Technology program is free to join and provides an opportunity to get involved by using technical skills. It can be as easy as explaining to nontechnical Red Cross volunteers how to set up Wi-Fi, for example.

The responsibility of providing Member benefits is part of the IEEE Membership and Geographical Activities (MGA) Board's mission. MGA has a membership development portal full of content that technical activities committees can utilize to encourage and retain student and YP members. MGA is studying how to better support IEEE Members and focusing on ways to understand how to best assist them through their lifetime (Figure 1).

I would like to highlight the IEEE Center for Leadership Excellence and the Volunteer Leadership Training (VoLT) Program. These initiatives provide a vast set of resources for mentoring and self-study.

I would like to remind MTT-S students and professors to tell their peers and pupils who are not MTT-S members that the cost to join is US$1, with an IEEE Member rate of US$24. Since this is June, those numbers are reduced by 50% (Figure 2). Reduced IEEE membership dues can be requested for special circumstances and the MTT-S has a membership fee subsidy program as well. This information can be found on the IEEE website. There are also regional subsidies available to members. In conclusion, IEEE would like to be a professional home for you and me. I believe it is a good place for us to establish connections and advance in our areas of interest. Let's grow together.

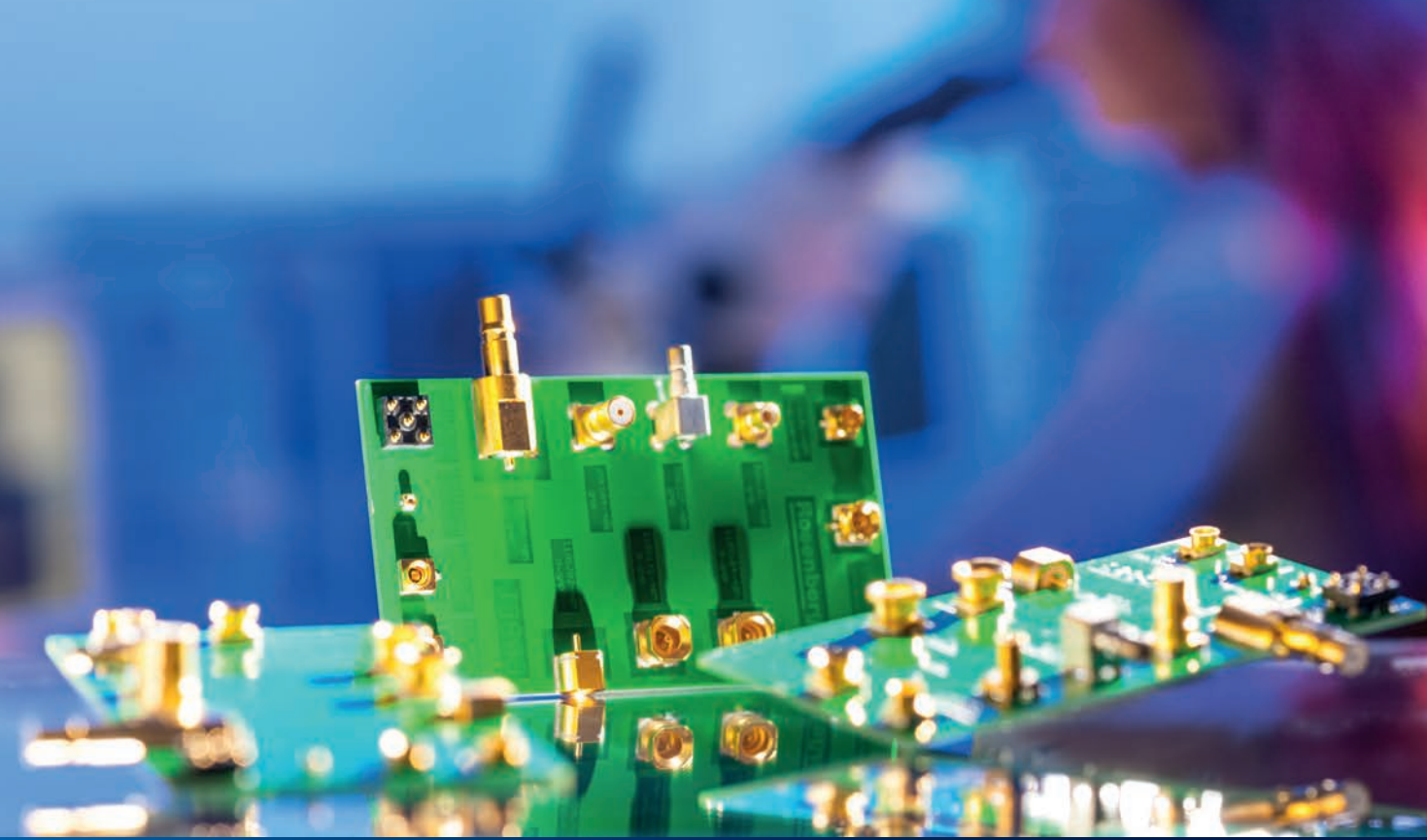

SURFACE MOUNT TECHNOLOGY

PCB Connectors

Rosenberger provides a wide range of RF coaxial connectors for PCB applications – for board-to-board- and also for cable-to-board connections.

Whether well-established standard connector series or newly developed innovative connectors – Rosenberger PCB connectors feature a lot of customer benefits:

- Minimum board-to-board distances
- Radial and axial misalignment using bullets
- Space-saving and cost-effective assembly design
- Excellent transmission quality
- Variety of back end types, e.g. SMT, edge mount, pin-in-paste, solder pin, solderless connectors as well as bullets

www.rosenberger.com

Rosenberger

MicroBusiness

Do Diligence

■ **Fred Schindler**

Mergers and acquisitions happen all the time. They are often a means for a company to obtain new technologies, products, and services. They can bring companies with complementary capabilities together. They can help reduce costs. However, it seems that many of them fail. An article in the *Harvard Business Review* claims that companies spend more than US$2 trillion on acquisitions every year, but 70–90% of them are failures [1]. That many failures represent not only the loss of trillions of dollars in acquisition costs but also the loss of businesses, product lines, and careers.

With so many failures and so much economic loss, why are mergers and acquisitions still so common? It's worth keeping in mind that there are also many successful mergers and acquisitions. They often make a lot of sense. I've seen some successful mergers and acquisitions up close. I've also seen some failures. Most importantly, I've seen some successful nonacquisitions.

Fred Schindler (m.schindler@ieee.org) consults on management issues in the Boston, Massachusetts, USA, area.

Digital Object Identifier 10.1109/MMM.2022.3157965
Date of current version: 5 May 2022

IMAGE LICENSED BY INGRAM PUBLISHING

Sometimes, the greatest success comes from not going through with a prospective acquisition.

That is where due diligence comes in. Due diligence is a process where the potential acquiring company closely evaluates a potential acquisition before making a final decision. I've had the opportunity to participate in some due diligence processes. I've also had the opportunity to watch some and see the results of others. There are plenty of guides available for how to best complete a due diligence exercise, but the most important guidance is to be diligent with your due diligence.

Doing due diligence well takes time, though, typically, time is limited. There is also the matter of resources. People with expertise need to spend time investigating the target and making careful evaluations. However, for most companies, employees with the necessary expertise already have a full-time job. They can't afford to take a few weeks away from all of their ongoing projects and commitments to focus adequately on the due diligence

ORDER OF MAGNITUDE AHEAD

WIPL-D Pro V18

3D EM simulation environment for Medical Microwave Imaging

released!

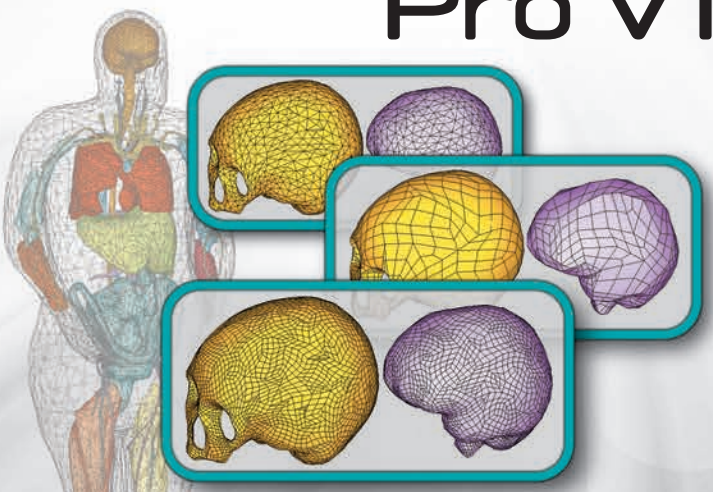

New:

- New STL Editor Options
  - Automatic Validation and Healing options
  - Fully controlled decimation and quad meshing
  - Export selected model part
  - Model settings and manipulations in STL model
- NEVA based models of human phantoms
- New module for graphic representation of output results
- Library of antennas suited for medical microwave imaging

- Material library with over 80 predefined materials
- Frequency dependent material properties using Frequency table, Cole-Cole and Djordjevic-Sarkar approximation
- Near field calculation in selected domains
- Averaging material properties for specified set of domains
- Accelerated in-core and out-of core GPU inversion for large number of excitations
- Custom defined merge tolerance
- Export and re-use of inverted matrix
- Repair projects option at their opening

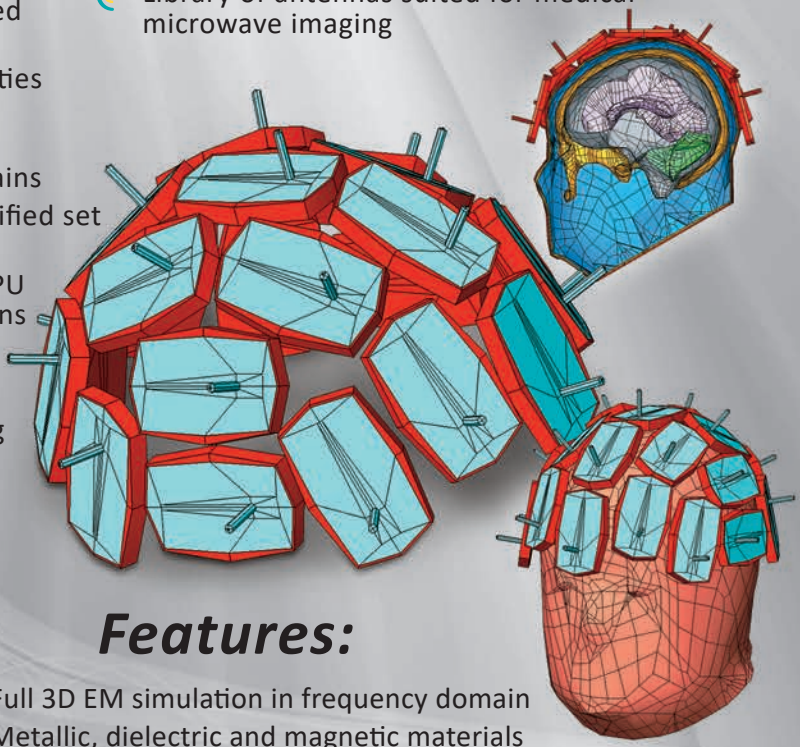

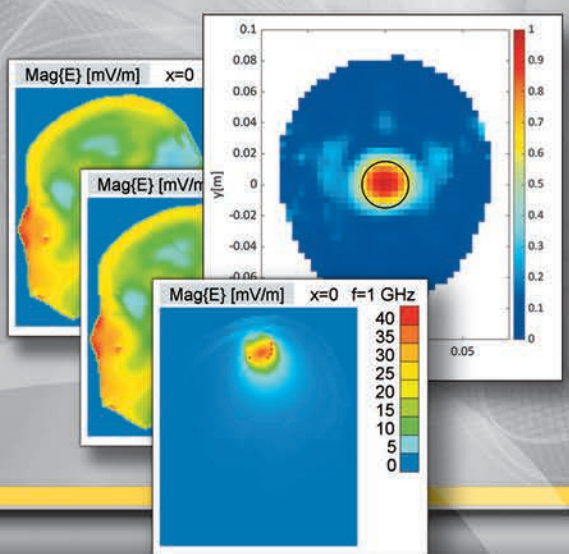

Features:

- Full 3D EM simulation in frequency domain
- Metallic, dielectric and magnetic materials
- Lumped elements and distributed loadings
- Add-ons: GPU Solver, Optimizer, Time Domain Solver, Circuit Solver (Microwave) and 2D Solver
- Applications: antenna design and placement, scatterers, microwave circuits and waveguides, EMC ...

www.wipl-d.com

for a potential acquisition. There are companies that maintain a staff to continually evaluate potential acquisitions and to do due diligence. Even these companies often find it useful to hire outside experts.

With trillions of dollars spent on mergers and acquisitions, it's a big business. There are organizations that focus on helping companies find acquisition targets and, on the other side of things, sell companies or parts of companies to new organizations. These investment bankers collect a fee for closing a deal. Their incentive is to close the deal, not necessarily to ensure a thorough due diligence process and the long-term success of the acquisition.

There are plenty of guides available for how to best complete a due diligence exercise, but the most important guidance is to be diligent with your due diligence.

There are lots of reasons why so many mergers and acquisitions fail. I believe most of these can be avoided with appropriate due diligence. In the technology space, a larger company often acquires a smaller one to gain a new technology or a complementary capability. Then the key questions include the following: Does a unique technology or capability actually exist? Does the technology work? Is the talent that developed and understands the technology still with the company? Is the technology worth the price that's being paid in the acquisition? Are employees likely to stay? Is there a cultural difference? All of these questions can be, at least partially, addressed with good due diligence.

You would think that the question of whether a technology works would be simple to address, yet I know of a number of counterexamples. In one case, a large acquisition was made primarily on the basis of a presentation on the product family the target company was developing. What wasn't appreciated, even months after the acquisition was completed, was that the slides were aspirational. The company that made the acquisition started aggressively selling the promised products and didn't realize—until customers complained about the lack of samples—that the product development had just started.

In another case, a target company had developed a product to operate to a standard. As part of due diligence, the acquiring company observed the product functioning, but only in the target company's lab. The parts functioned well when they interacted with parts made by the same company, but there was no test of the product's performance when operating with a competitor's products. The acquiring company missed a serious flaw that prevented full compliance with the standard.

There are a range of techniques that can be employed in good due diligence. The acquiring company typically receives sets of data about the target. Due diligence may uncover claims that exaggerate realities. For example, digging into the target's financial summaries might show that they've lost most of their research and development engineering talent. It's also possible to learn quite a bit by carefully reviewing public materials on the company's website. It's not difficult to judge how technologically advanced or obsolete a company's products are. If most of the company's products use 10- to 20-year-old technology, it's likely that the company is more interested in milking the business than growing new revenue.

Site visits are an invaluable part of any due diligence exercise. Meeting with leaders, observing processes, seeing facilities, and interacting with employees can be very revealing. I recall one site visit where we visited adjoining buildings, one with up-to-date equipment and excellent process control. The building was well maintained, and the employees conveyed pride. The other building wasn't bad, but it was less well maintained, the employees were less enthusiastic, and the equipment was not as modern. It was clear which products the company was investing in. That can be a valuable insight.

Very small companies are often dominated by one person—typically the technical leader. In these cases, it's important to not only assess the technology but also the leader's vision for the technology. We need to consider the perspectives of the other employees. Are they are engaged and aligned? If there is disharmony in a small company, there's a good chance that the organization won't survive an acquisition.

Often the target company is a start-up—a venture- or angel-funded company that is developing a new concept, product, or technology. The investors have an incentive to sell the company and recognize a profit or, sometimes, just recoup some of their investment. Some start-ups develop valuable technologies and, for the right purchaser, can add lasting value. However, for some start-ups, the real product is the company itself. The goal is to sell the company so that the investor and maybe even the founders realize a profit, even though there isn't much underlying value. Consider my first example, where the acquirer essentially bought a concept on a set of slides. That was a due diligence failure.

There are plenty of shortcomings and qualities that good due diligence can expose. Good due diligence will also guide the integration of the companies once the acquisition is consummated. However, the key for due diligence is to do it well.

Reference

[1] C. M. Christensen, R. Alton, C. Rising, and A. Waldeck. "The big idea: The new M&A playbook," in *Harv. Bus. Rev.*, Mar. 2011. [Online]. Available: https://hbr.org/2011/03/the-big-idea-the-new-ma-playbook

YOUR INNOVATIONS. OUR SOLUTIONS.

Printed Circuit Board Fabrication • Photo-Chemical Metal Etching

For 25 years Transline has focused on making quality RF/Microwave and
High Performance boards, Flex, Rigid-Flex PCB and Photo-Chemical & Metal Etching.

AS9100D
ISO9001:2015
ITAR REGISTERED
UL & IPC COMLIANT
SBD 8(a) CERTIFIED
MINORITY OWNED

TTI TRANSLINE TECHNOLOGY INCORPORATED

INDUSTRIES SERVED:

COMMUNICATIONS • WIRELESS
SATELLITE • GPS • RF • MICROWAVE
MEDICAL • OEM • UAV
DEFENSE & AEROSPACE

1106 S TECHNOLOGY CIRCLE, ANAHEIM CA 92805 TEL: 714.533.8300 FAX: 714.533.8791 WWW.TRANSLINETECH.COM

MTT-S Society News

TC-2 Technical Committee Report

■ Qijun Zhang and Roni Khazaka

Technical Committee 2 (TC-2) is the IEEE Microwave Theory and Techniques Society (MTT-S) TC on Design Automation (https://mtt.org/technical-committees/mtt-2-design-automation/). TC-2 spearheads advances in all aspects of methods, software, and technologies of high-frequency circuit and system design. From RF to terahertz (THz), engineering innovation hinges on the availability of state-of-the-art design automation. Our mission is thus fundamental to the MTT-S, and our activities are often in collaboration with many other MTT committees. Fields of interests to TC-2 include the following:

- modeling and simulation of devices, circuits, and systems
- optimization techniques
- multiphysics modeling
- design automation technologies from megahertz to THz
- emerging design automation technologies such as artificial intelligence (AI), machine learning, and quantum computing.

Qijun Zhang (qijunzhang@cunet.carleton.ca) is with Carleton University, Ottawa, K1S 5B6, Canada. Roni Khazaka (roni.khazaka@mcgill.ca) is with McGill University, Montréal, H3A 0E9, Canada.

Digital Object Identifier 10.1109/MMM.2022.3157968
Date of current version: 5 May 2022

Membership

Chaired by Dr. Qijun Zhang, and with Vice Chair Dr. Roni Khazaka, TC-2 had 24 members and two affiliate members in 2021, including 12 IEEE Fellows. New members are added to the committee through nomination and voting by the committee members. During 2021, three new members and two affiliate members were added. The members of TC-2 have representation in microwave design automation from both academia and industry, and various parts of the globe including North America, Latin America, Europe, Asia, and Oceania.

TC-2 spearheads advances in all aspects of methods, software, and technologies of high-frequency circuit and system design.

The members of TC-2 are expected to be active in the microwave design automation field, and to participate in MTT-S and TC-2 activities related to TC-2's fields of interests. TC-2 members contribute to the nomination of Distinguished Microwave Lecturers as well as to proposals of workshops, short courses, focus sessions, the Three Minute Thesis (3MT) competition, and student design competitions for the IEEE MTT-S International Microwave Symposium (IMS). TC-2 members also play pivotal roles in several MTT-S-sponsored conferences, including the IEEE MTT-S International Conference on Numerical Electromagnetic and Multiphysics Modeling and Optimization (NEMO), the IEEE MTT-S Latin America Microwave Conference (LAMC), and the Conference on Electronic Performance of Electronic Packaging and Systems (EPEPS). TC-2 members also represent the MTT-S in the IEEE Council on Electronic Design Automation. TC-2 members give keynote and other important talks related to microwave design automation in conferences and professional events. In addition, TC-2 also contributes to special issues related to design automation in *IEEE Microwave Magazine*

and *IEEE Transactions on Microwave Theory and Techniques*.

Activities Report (2020–2021)

IMS Workshops

TC-2 sponsored the workshop on "Recent Advances in the Efficient Small- and Large-Signal Stability Analysis of Microwave Circuits" at IMS 2021. The workshop was organized by Dr. A. Suarez and TC-2 member Dr. Marco Pirola. The workshop presents new achievements in the field of small- and large-signal stability analysis with state-of-the-art results presented in the last few years. The five speakers are recognized authorities in the field of stability analysis. This workshop addresses a topic that has not been covered in any workshop for many years. Emerging areas are covered through stability-analysis examples linked to RF and microwave identification and active antenna arrays, among others.

A workshop for IMS 2022 sponsored by TC-2 and proposed by Dr. N.C. Miller and TC-2 member S. Khandelwal has been approved. The workshop is titled "Measurement and Modeling of Trapping, Thermal Effects, and Reliability of GaN HEMT Microwave PA Technology." This workshop aims to inform and excite the attendees on the advances in multiple aspects of this technology. Starting with a gallium nitride (GaN) technology overview, the planned talks will inform the audience about measurement and characterization of this technology, including the complex thermal, charge trapping, and long-term degradation phenomenon in these devices. The next part of the workshop covers modeling and simulation research in GaN. Starting with an overview of modeling challenges in GaN devices, the workshop will cover the latest industry standard compact models and advances in Technology Computer-Aided Design-based modeling of GaN devices.

NEMO

NEMO 2020 was held in Hangzhou, China, in December 2020 (Figure 1). The conference was organized by Prof. Wenyan Yin of Zhejiang University, Prof. Erping Li of Zhejiang University–University of Illinois at Urbana-Champaign Institute, and Prof. Junfa Mao of Shanghai Jiaotong University. NEMO 2020 attracted over 315 in-person participants, with 275 papers presented. The conference presented the Women in NEMO for MAPE Award to five women authors of NEMO papers, and the best student paper award to six winning student papers.

TC-2 members give keynote and other important talks related to microwave design automation in conferences and professional events.

Due to COVID-19, NEMO 2021 was rescheduled to July 2022, to be held in Limoges, France (www.nemo-ieee.org). It is organized by Prof. Dominique Baillargeat of the University of Limoges. The conference aims to bring together experts and practitioners of electromagnetic- and multiphysics-based modeling, simulation and optimization for RF, microwave, and THz applications. This conference is an ideal forum to share new ideas on techniques for electromagnetic and multiphysics modeling, propose efficient design algorithms and tools, and anticipate the modeling/analysis needs of future technologies and applications.

LAMC

LAMC 2021 was held fully virtually in Cali, Colombia, from 26 to 28 May 2021. It included a technical session on computer-aided design techniques for RF and microwave engineering. A Region 9 graduate student initiative was implemented to support the audience. The next edition of LAMC will be in December 2023.

EPEPS

EPEPS 2021 was a milestone occurrence for EPEPS in its 30th year. EPEPS 2021 was held virtually and covered a growing range of electronic packaging topics, which resulted in a very strong program with technical novelty and diversity. The technical paper sessions included 42 papers selected after a robust and thorough review process. The conference technical events included two keynote presentations and one invited presentation on future outlooks and pertinent efforts on electronic packaging given by Bradley McCredie of AMD, Mike (Peng) Li of Intel, and Sunil Sudhakaran of Nvidia. Furthermore, the first day of the conference included eight technical tutorials given by highly respected experts from the industry. In celebration of 30 years of EPEPS, a panel was held bringing together several individuals who have made lasting and distinguished contributions to EPEPS, including Andreas Cangellaris, Albert Ruehli, Madhavan Swaminathan, Jose Schutte-Aine, and W. Dale Becker. Three paper awards were given at EPEPS 2021: the Best Conference Paper Award, the Best Student Paper Award, and the Best Benchmark Paper Award.

Figure 1. *NEMO2020 was held in Hangzhou, China, in December 2020.*

Figure 2. *TC-2 Member Dr. Feng Feng of Tianjin University organized the first IEEE MTT-S Young Professionals Workshop on Electromagnetic Modeling and Optimization (EMO 2021) in October 2021.*

TC-2 Members Playing Key Roles in Other MTT-Sponsored Conferences

TC-2 member Sourabh Khandelwal served as the technical program committee (TPC) cochair of the 2021 Asia Pacific Microwave Conference (APMC), which was held virtually from 28 November to 1 December 2021. APMC 2021 had four technical sessions covering design automation topics including active and passive device modeling and simulations, design optimization of antennas, and microwave systems.

TC-2 members have made a significant impact on the Signal and Power Integrity (SPI) Workshop over many years of its history. SPI 2021 was held as a virtual event from 10 to 12 May 2021. TC-2 members Michel Nakhla and Madhavan Swaminathan served on the standing committee, and Peter Aaen, Francesco Ferranti, and Andreas Weisshaar served on the TPC.

3MT in IMS

Dr. John Bandler is the founding organizer for the 3MT competition at IMS. Since 2017, Dr. Bandler and Erin Kiley have organized the 3MT for each IMS, with the first year in Honolulu (2017), the second year in Philadelphia (2018),

the third year (2019) in Boston, and the fourth and fifth years (2020, 2021) virtually. Selected videos of the competition can be found on the MTT-S IMS YouTube channel https://www.youtube.com/user/mttims. Participation in 2020 and 2021 included the collocated RF Integrated Circuit and the Automatic Radio Frequency Techniques Group conferences (Microwave Week). Aline Eid and Daniel Tajik joined the 3MT team in 2021.

In connection with the 3MT, John Bandler, Erin Kiley, Aline Eid, and Daniel Tajik presented a webinar titled "Exploring Online Presentation Skills for Engaging Your Audience" as an IEEE MTT-S Webinar, 11 March 2021 (www.tinyurl.com/kzj498yv). They further described the 3MT in an article, "The IMS2021 Microwave Week Virtual 3MT Competition," in *IEEE Microwave Magazine* [1].

A 2021 Special Issue on Machine Learning in *IEEE Microwave Magazine*

A special issue on machine learning in microwave engineering was organized jointly by TC-1 and TC-2, with guest editors Costas Sarris and Qijun Zhang. This issue was published in October 2021, including three feature articles that speak to the past, present, and some aspects of the future of machine learning in microwaves. The three feature articles included "Design Space and Frequency Extrapolation: Using Neural Networks" by Osama Waqar Bhatti, Nikita Ambasana, and Madhavan Swaminathan; "ANNs for Fast Parameterized EM Modeling: The State of the Art in Machine Learning for Design Automation of Passive Microwave Structures" by Feng Feng, Weicong Na, Jing Jin, Wei Zhang, and Qijun Zhang; and "Enabling Automatic Model Generation of RF Components: A Practical Application of Neural Networks" by Lei Zhang, Humayun Kabir, Rick Sweeney, and Kevin Kim.

A future special issue on AI and machine learning technologies for microwaves is scheduled for *IEEE Transactions on Microwave Theory and Techniques* in 2022, with guest editor Qijun Zhang.

Speakers Bureau

The Speakers Bureau speakers elected in TC-2 during 2021 are Prof. Jose Rayas-Sanchez of ITESO and Prof. Francesco Ferranti of Vrije Universiteit Brussel. Prof. Rayas-Sanchez's presentation is titled "Space Mapping Optimization: Power in Simplicity Rooted in Engineering Practice." Prof. Ferranti's presentation is titled "Uncertainty Quantification of Complex Systems Described by Large-Scale Equations."

Young Professionals Workshop on Electromagnetic Modeling and Optimization

TC-2 member Dr. Feng Feng of Tianjin University organized the 2021 IEEE MTT-S Young Professionals Workshop on Electromagnetic Modeling and Optimization (EMO 2021). The workshop, technically sponsored by TC-2, was held as a virtual event on 25 October 2021 (Figures 2 and 3). It provided a platform for young professionals to share their recent research

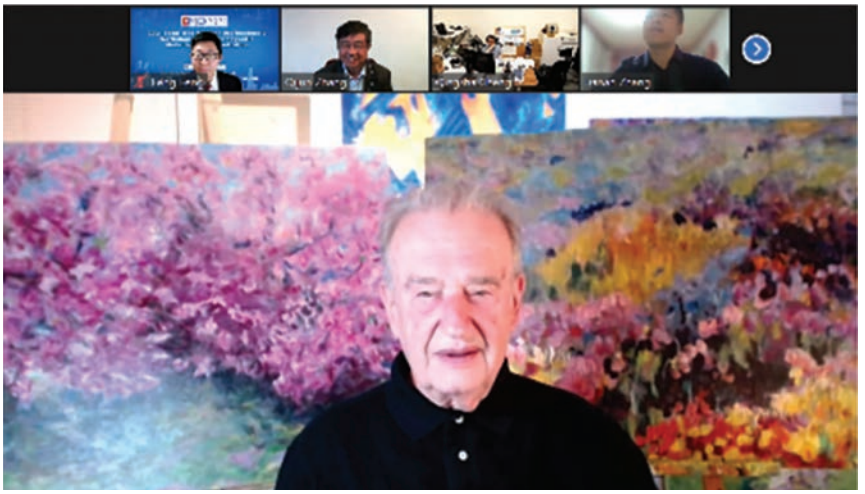

Figure 3. *Dr. John Bandler, a senior professional from TC-2, shared his vision and experiences with the Young Professionals during EMO 2021.*

on electromagnetic modeling and optimization.

The workshop featured young professional talks from Asia, Europe, and North America. Dr. John Bandler, a senior professional from TC-2, shared his vision and experiences with the young professionals. The workshop attracted participation by young faculty members and graduate students from Tianjin University, Beijing University of Technology, Shaanxi University of Science and Technology, Harbin Institute of Technology, Zhejiang University, Beijing University of Posts and Telecommunication, the University of Birmingham, Carleton University, Reykjavik University, and more.

EMO 2021 was the first young professionals workshop technically sponsored by TC-2. It is planned that this workshop will continue as a periodical event offering opportunities for young professionals in similar technical areas to meet and discuss with each other and interact with senior experts.

Talks

TC-2 members gave many technical talks around the world. Samples of talks include:

- Natalia Nikolova, "The Methods of Real-Time Microwave and Millimeter-Wave Imaging," plenary talk at the International Applied Computational Electromagnetics Society Symposium, 3 August 2021
- Natalia Nikolova, "Measured System Point-Spread Functions Enable Real-Time Quantitative Imaging," IEEE MTT-S Webinar Series, 22 June 2021
- Natalia Nikolova, "Microwave and Millimeter-Wave Near-Field Imaging: Applications, Methods and Challenges," University of Toronto, IEEE Antennas and Propagation Society Student Chapter, March 2021
- Christopher Snowden, "Microwaves: Past, Present, Future," an Invited Opening Keynote Presentation in the Antennas and Propagation Conference 2019, Birmingham, U.K., 25 September 2019
- Christopher Snowden, "III-V Nitride Semiconductors for Microwave Applications," an Invited Opening Keynote Presentation in the European Microwave Integrated Circuits Conference at European Microwave Week, London, 4 April 2022
- Qijun Zhang, "Machine Learning and Cognition-Driven Approaches to Microwave Design," an Invited Opening Keynote Presentation in NEMO 2020 Hangzhou, China, on 7 December 2020
- Justin King, "Physics-Based Modeling for Compound Semiconductors," an invited talk at the IEEE International Wireless Symposium in Nanjing, China on 24 May 2021
- David Root, "What Every Microwave Engineer Should Know About Quantum Computation," an invited MTT-S Webinar on 14 December 2021.

Invited Overview Articles

TC-2 members wrote two invited articles representing state-of-the-art design automation topics in the inaugural issue of the new *IEEE Journal of Microwaves* in January 2021. One of the invited articles was by Jose Rayas-Sanchez, Slawomir Koziel, and John Bandler, titled "Advanced RF and Microwave Design Optimization: A Journey and a Vision of Future Trends." The other invited article was by Qijun Zhang, Emad Gad, Behzad Nouri, and Michel Nakhla, titled "Simulation and Automated Modeling of Microwave Circuits: State-of-the-Art and Emerging Trends."

Industrial Application of Design Automation Technologies Traceable to TC-2 Members and Their Students

Many design automation technologies traceable to TC-2 members and their students have been adopted in industrial applications over the years. A recent example of such applications during the reporting period is the PathWave Device Modeling (IC-CAP, Keysight Technologies) 2022 Update that contains a new artificial neural network (ANN) model generator that trains ANNs to data, including partial derivative data, and exports nonlinear model building blocks in Verilog-A format that can be consumed by many industrial simulators.

Reference

[1] J. W. Bandler, E. M. Kiley, D. Tajik, and A. Eid, "The IMS2021 Microwave Week Virtual 3MT Competition," *IEEE Microw. Mag.* vol. 22, no. 5, pp. 63–65, May 2021. doi: 10.1109/MMM.2021.3056985.

The Design and Analysis Frontier of Electronic Packaging

31th Conference on Electrical Performance of Electronic Packaging and Systems

October 9th to 12th, 2022

Call for Papers

EPEPS is the premier international conference on advanced and emerging issues in electrical modeling, measurement, analysis, synthesis, and design of electronic interconnections, packages, and systems. It also focuses on new methodologies and CAD/design techniques for evaluating signal, power, and thermal integrity and ensuring performance in high-speed, RF, and wireless designs. EPEPS is jointly sponsored by IEEE Electronics Packaging Society, IEEE Microwave Theory and Techniques Society, and IEEE Antennas and Propagation Society. Submitted papers should describe new technical contributions related to the area of the electrical performance of high-performance interconnect systems, covering:

- System-level, board-level, package-level and on-chip interconnects
- High-speed channels, links, backplanes, serial and parallel interconnects, SerDes
- RF/microwave/mm-wave packaging structures and components, antenna-in-package and RFIC co-design, mixed signal modules and wireless switches
- Signal and thermal integrity
- Power integrity and power distribution networks
- Low power mobile and personal applications
- Memory and DDR interfaces
- Jitter and noise management
- Electronic packages and microsystems
- Heterogeneous integration, 2.5D/3D interconnects and packages, TSVs and MCMs
- Electromagnetic (EM) and EM interference modeling, simulation algorithms, tools, and flows
- Macro-modeling and model order reduction as it applies to electrical analysis
- Advanced and parallel CAD techniques for signal, power, and thermal integrity analysis
- Measurement and data analysis techniques for system-level and on-chip structures
- High volume testing for electronic packages.

Submission Deadline: **July 10, 2022**

Conference Chairs:
Zhen Peng, zvpeng@illinois.edu
Swagato Chakraborty, Swagato_Chakraborty@mentor.com

For more information/contact: **epeps-admin@illinois.edu**

Submission Format: **2-column, 3-page PDF format only.** Selected papers will be invited for a special issue in *IEEE Transactions on Components, Packaging, and Manufacturing Technology.* Information for authors can be found at www.epeps.org. Submitted manuscripts should be camera-ready and compliant with the general standards of the IEEE, including appropriate referencing. Noncompliant manuscripts will not be considered for review.

Location: San Jose Marriott, 301 South Market Street, San Jose, CA 95113, USA.

Tutorials: EPEPS offers tutorials on state-of-the-art topics including latest advances: on CAD software tool techniques for package/PCB design, SI and PI modeling, high-speed SerDes simulation, high precision measurement techniques and novel interconnect design.

IEEE Education Credits: IEEE offers professional development hours (PDHs) and continuing education units (CEUs) for attending the EPEPS program.

Simulation Benchmarking: EPEPS 2022 organizers invite paper submissions covering simulation tool development advances that utilize benchmarks established and released publicly by the IEEE TC-EDMS Packaging Benchmarks Committee *(http://www.packaging-benchmarks.org/)*.

Exhibits: EPEPS offers an excellent array of vendor exhibits. EPEPS is an exciting forum for vendors to demonstrate their state-of-the-art tools to attendees. Interested vendors can contact the conference administration for more details.

Conference Website: **www.epeps.org**

Digital Object Identifier 10.1109/MMM.2022.3157971

2022 IEEE Fellows Elevation and Recognition

©SHUTTERSTOCK.COM/SAFRIIBRAHIM

Chia-Chan Chang and Robert H. Caverly

Chia-Chan Chang (ccchang@ee.ccu.edu.tw) is with National Chung-Cheng University, Chiayi, 621301, Taiwan, and Robert H. Caverly (r.caverly@ieee.org) is with Villanova University, Villanova, Pennsylvania, 19805, USA.

Digital Object Identifier 10.1109/MMM.2022.3157967

Date of current version: 5 May 2022

Elevation to Fellow of the IEEE is an honor reserved for a select group of engineers each year. The number of Fellows elevated in any year cannot exceed one-tenth of 1% of the total voting membership. This highest grade of membership in the IEEE is conferred by the IEEE Board of Directors in recognition of an individual's outstanding record of accomplishments in any IEEE field of interest. This year, 13 honorees were awarded the status of Fellow of the IEEE, with the IEEE Microwave Theory and Techniques Society (MTT-S) as the evaluating Society. Another five new Fellows are members of the MTT-S but were awarded the level of Fellow by other Societies or Councils. In alphabetical order, those awarded the level of Fellow by the MTT-S are

This highest grade of membership in the IEEE is conferred by the IEEE Board of Directors in recognition of an individual's outstanding record of accomplishments.

- Dominique Baillargeat, for contributions to developments of nanomaterials for RF packaging and sensors
- James F. Buckwalter, for contributions to high-efficiency millimeter-wave power amplifiers and optical transceivers in SOI technologies
- Wenquan Che, for contributions to planar transmission line structures for microwave passive components
- Alessandra Costanzo, for contributions to nonlinear electromagnetic co-design of RF and microwave circuits
- Apostolos Georgiadis, for contributions to designs of RF energy harvesting circuits
- Jeffrey L. Hesler, for contributions to development of terahertz components and instrumentation
- Slawomir Koziel, for contributions to modeling and optimization of microwave devices and circuits
- Moriyasu Miyazaki, for leadership in developments of airborne active phased-array radars and satellite communication microwave subsystems
- Anh-Vu Pham, for contributions to organic packaging technologies
- Christopher T. Rodenbeck, for contributions to radar microsystems for ultrawideband and millimeter-wave applications
- Daniel van der Weide, for contributions to ultrafast terahertz electronics and biomedical applications of microwave technologies
- Christian Waldschmidt, for contributions to millimeter-wave automotive radar sensors
- Anding Zhu, for contributions to behavioral modeling and digital predistortion of RF power amplifiers.

In honor of their contributions, short biographies of our Society's new IEEE Fellows are presented in the following pages. These new Fellows have worked very hard and made many sacrifices for this work. Please join us in congratulating each of them.

Dominique Baillargeat
University of Limoges
Limoges, France

for contributions to developments of nanomaterials for RF packaging and sensors

Dominique Baillargeat is a professor of exceptional class at the University of Limoges. He is the scientific executive director of the French National Center for Scientific Research Campus for Research and Technological Enterprise framework of the National Research Foundation of Singapore. He conducts his research between Limoges (XLIM laboratory) and Singapore (Centre national de la recherche scientifique-International-NTU-Thales Research Alliance laboratory) where, in 2019, he initiated a research area on RF nanotechnology. Dr. Baillargeat is among the pioneers of the use of nanomaterials for the design and packaging of innovative RF and millimeter-wave components. This cross-disciplinary activity is based on fundamental research on nanomaterials, such as graphene, 2D materials, and carbon nanotubes, for the design of RF components by considering the constraints of integration, electromagnetic shielding, connectivity, and thermal management.

Dr. Baillargeat is among the pioneers of the use of nanomaterials for the design and packaging of innovative RF and millimeter-wave components.

Dr. Baillargeat has pioneered new technological processes and characterization methods to fabricate and understand nanomaterials as well as full-wave modeling tools for RF component design and integration. His main achievements are in the following areas:

- *Nanomaterial characterization*: This contribution is crucial to well characterize 2D materials for their future use in disruptive RF nanotechnology.
- *Nanomaterial modeling*: This work proposes the first equivalent full-wave model of nanotubes and nanowires in arrays and bundles of arbitrary shape and size. This pioneering work is crucial for the efficient design of RF components.
- *Nanomaterial-based RF nanopackaging*: This seminal work demonstrates that carbon nanotubes can be used for RF interconnects operating at 40 GHz and can be a promising platform for interconnects at higher operating frequencies. In 2020, this work was extended to the W band.

In 2012, Dr. Baillargeat widened the scope of his RF nanotechnology research to the design and fabrication of nanomaterial-based sensors by considering the constraints of integration, flexibility, and sensitivity, helping to address needs of future smart cities that promote a human-centered approach with particular attention to safety and health. In this direction, the Internet of Things (IoT) is becoming essential for the large-scale deployment of sensors. Dr. Baillargeat's research addresses nanomaterial-based sensors for the following:

- *Biological and chemical applications*: His work on graphene-based sensors demonstrates how nanomaterials can significantly enhance ultrasensitive plasmonic nanosensors. He reviews trends and challenges in the engineering and application of nanomaterial-enhanced surface plasmon resonance sensors for detecting "hard-to-identify" biological and chemical analytes, providing a platform for designing future ultrasensitive plasmonic nanosensors.
- *Volatile organic compound monitoring*: His work proposes a differential sensor printed on a flexible

substrate through low-cost technologies and based on two planar microwave transducers with and without nanomaterials, such as graphene and carbon nanotubes. The device can be integrated into real-time multiple-sensing platforms dedicated to applications requiring low power consumption for the IoT.

Dr. Baillargeat has been the advisor of 33 graduated Ph.D. students. He has coauthored 84 journal publications, 170 conference publications, three patents, and five book chapters.

Relevant Publications

- L. Hong *et al.*, "From bulk to monolayer MoS_2: Evolution of Raman scattering," *Adv. Functional Mater.*, vol. 22, no. 7, pp. 1385–1390, 2012.
- P. Franck, D. Baillargeat, and B. K. Tay, "Mesoscopic model for the electromagnetic properties of arrays of nanotubes and nanowires: A bulk equivalent approach," *IEEE Trans. Nanotechnol.*, vol. 11, no. 5, pp. 964–974, 2012, doi: 10.1109/TNANO.2012.2209457.
- C. Brun *et al.*, "Flip chip based on carbon nanotube-carbon nanotube interconnected bumps for high-frequency applications," *IEEE Trans. Nanotechnol.*, vol. 12, no. 4, pp. 609–615, 2013, doi: 10.1109/TNANO.2013.2264534.
- S. Zeng, D. Baillargeat, H. P. Ho, and K. T. Yong, "Nanomaterials enhanced surface plasmon resonance for biological and chemical sensing applications," *J. Chem. Soc. Rev.*, vol. 43, no. 10, pp. 3426–3452, 2014, doi: 10.1039/c3cs60479a.
- P. Bahoumina *et al.*, "Microwave flexible gas sensor based on polymer multi wall carbon nanotubes sensitive layer," *Sensors Actuators B, Chem.*, vol. 249, pp. 708–714, Oct. 2017, doi: 10.1016/j.snb.2017.04.127.

James F. Buckwalter
University of California, Santa Barbara
Santa Barbara, California, United States

for contributions to high-efficiency millimeter-wave power amplifiers and optical transceivers in SOI technologies

James F. Buckwalter received the B.S. degree (with honors) in electrical engineering from the California Institute of Technology (Caltech) in 1999. After working at Telcordia Technologies, in Morristown, New Jersey, he earned the M.S. degree in electrical engineering from the University of California, Santa Barbara (UCSB) and returned to Caltech to complete his Ph.D. degree. He joined the Department of Electrical and Computer Engineering, University of California, San Diego in 2006, becoming an associate professor in 2012, and he returned to UCSB as a full professor of electrical and computer engineering in 2014. He was the recipient of a 2004 IBM Ph.D. fellowship, 2007 DARPA Young Faculty Award, 2011 National Science Foundation (NSF) CAREER Award, and 2015 IEEE MTT-S Young Engineer Award. He has supervised more than 20 Ph.D. and 15 M.S. degree students. He has published 200-plus conference and journal papers on research related to RF, millimeter-wave, and high-speed optoelectronic circuits and systems.

Dr. Buckwalter is recognized for significant early contributions to circuit design for millimeter-wave and high-speed optoelectronic transceivers.

Dr. Buckwalter is recognized for significant early contributions to circuit design for millimeter-wave and high-speed optoelectronic transceivers based on SOI CMOS. His research group published the first comprehensive studies of millimeter-wave and broadband stacked-field-effect transistor (FET) PAs based on SOI CMOS. Alongside collaborators at UCSB, he showed that FETs could be stacked at high frequency by using novel methods and presented new design approaches for load line and power scaling. The results demonstrated a power-added efficiency of 32% in a two-stack PA design at 45 GHz, which, at the time, was a tremendous advance in silicon-based millimeter-wave PAs. His research group subsequently fabricated the first silicon-based millimeter-wave Doherty PA, with an efficiency exceeding 20%, and pushed stacked-FET PAs toward 100 GHz and proposed a multidrive technique. The work, supported under the DARPA Efficient Linearized All-Silicon Transmitter Integrated Circuits program, invigorated industry and academic research on SOI CMOS processes for emerging millimeter-wave markets.

Dr. Buckwalter has also made significant research contributions to the advancement of SOI CMOS in energy-efficient optoelectronic interfaces. Through collaborations with Oracle, he realized the first fully integrated 25-Gb/s transceiver based on photonic microring resonators and achieved energy efficiency under 10 pJ/bit. He continued to chart a course for future energy-efficient optical transceivers based on 45-nm CMOS SOI. By leveraging the insight that the FET-stacking design techniques were inherently broadband, his research group proposed optical driver amplifiers with a differential voltage swing of 4 V over a bandwidth of 30 GHz.

Dr. Buckwalter has volunteered for the IEEE Custom Integrated Circuits Conference, IEEE BiCMOS and Compound Semiconductor Integrated Circuits and Technology Symposium (BCICTS), IEEE MTT-S International Microwave Symposium (IMS), and International Solid-State Circuit Conference and was the cochair of the Technical Program Committee

(TPC) for IMS 2010 and 2020. He has served as an associate editor of *IEEE Transactions on Circuits and Systems II: Express Briefs* and *IEEE Transactions on Microwave Theory and Techniques* (*TMMT*) and a guest editor for the *IEEE Journal of Solid-State Circuits* special issue on the BCICTS and *TMMT* special issue on microwave and millimeter-wave communication and sensor systems. He is currently the chair of MTT-S Technical Committee 14.

Relevant Publications

- H. Dabag, B. Hanafi, F. Golcuk, A. Agah, J. F. Buckwalter, and P. M. Asbeck, "Analysis and design of stacked-FET millimeter-wave power amplifiers," *IEEE Trans. Microw. Theory Techn.*, vol. 61, no. 4, pp. 1543–1556, 2013, doi: 10.1109/TMTT.2013.2247698.
- A. Agah, J. A. Jayamon, P. M. Asbeck, L. E. Larson, and J. F. Buckwalter, "Multi-drive stacked-FET power amplifiers at 90 GHz in 45 nm SOI CMOS," *IEEE J. Solid-State Circuits*, vol. 49, no. 5, pp. 1148–1157, May 2014, doi: 10.1109/JSSC.2014.2308292.
- A. Agah, H. Dabag, B. Hanafi, P. M. Asbeck, J. F. Buckwalter, and L. E. Larson, "Active millimeter-wave phase-shift Doherty power amplifier in 45-nm SOI CMOS" *IEEE J. Solid-State Circuits*, vol. 48, no. 10, pp. 2338–2350, Oct. 2013, doi: 10.1109/JSSC.2013.2269854.
- J. Buckwalter, X. Zheng, G. Li, K. Raj, and A. V. Krishnamoorthy, "A monolithic 25-Gb/s transceiver with photonic ring modulators and Ge detectors in a 130-nm CMOS SOI process," *IEEE J. Solid-State Circuits*, vol. 47, no. 6, pp. 1309–1322, 2012, doi: 10.1109/JSSC.2012.2189835.
- J. Kim and J. F. Buckwalter, "A 40-Gb/s optical transceiver front-end in 45nm SOI CMOS technology," *IEEE J. Solid-State Circuits*, vol. 47, no. 3, pp. 1–4, 2012, doi: 10.1109/CICC.2010.5617418.

Wenquan Che
School of Electronic and Information Engineering
South China University of Technology
Guangzhou, China

for contributions to planar transmission line structures for microwave passive components

Wenquan Che received the B.Sc. degree from the East China Institute of Science and Technology, Nanjing, in 1990; M.Sc. degree from the Nanjing University of Science and Technology (NUST) in 1995; and Ph.D. degree from the City University of Hong Kong (CITYU), Kowloon, Hong Kong, in 2003. In 1999, she was a research assistant with the CITYU. In 2002, she was a visiting scholar at Polytechnique de Montréal. She had been with NUST as a lecturer, associate professor, and professor since 1995. In November 2018, she joined South China University of Technology as a full professor. From 2007 to 2008, she conducted academic research at the Technical University of Munich (TUM). In 2005 and 2006 and from 2009 to 2016, she was with the CITYU as a research fellow and visiting professor. She was a visiting professor at TUM and Paris Nanterre University in 2015. She has authored or coauthored more than 300 internationally refereed journal papers and 100-plus international conference papers, and she holds more than 30 Chinese patents. Her research interests include microwave and millimeter-wave circuits and systems, antenna technologies, and medical applications of microwave technologies.

Her research interests include microwave and millimeter-wave circuits and systems, antenna technologies, and medical applications of microwave technologies.

Dr. Che is an elected member of the IEEE MTT-S Administrative Committee (AdCom) (2018–2023) and the chair of the AdCom Education Committee. Among many recognitions, she was a recipient of the 2007 Humboldt Research Fellowship, presented by the Alexander von Humboldt Foundation, of Germany; the fifth China Young Female Scientists Award, in 2008; and a National Natural Science Foundation Committee of China Distinguished Young Scientist in 2012. She received several IEEE Best Student Paper Awards at, for instance, the 2017 Global Symposium on Millimeter Waves, 2016 IEEE International Conference on Microwave and Millimeter-Wave Technology, and 2016 IEEE MTT-S International Microwave Workshop Series on Advanced Materials and Processes for RF and Terahertz Applications. She is the editor-in-chief of *Microwave and Optical Technology Letters* (2019–2022) and a reviewer for several IEEE transactions and journals (see "Dr. Che: Main Achievements").

Dr. Che: Main Achievements

- *Theoretical modeling of substrate integrated waveguide (SIW)-related guiding structures*: In particular, she derived a group of analytical equations for quick designs of SIW circuits. She derived the formula for characteristic impedance for the offset double-sided parallel stripline (DSPSL) and further implemented several novel DSPSL components.
- *Innovative structures of planar transmission lines and related circuits*: She proposed a ridged SIW featuring a much wider bandwidth than its counterparts and created a framework for its exploitation. Furthermore, she designed a couple of novel microwave and millimeter-wave SIW components, including an H-plane horn antenna with a dielectric lens, a planar magic T, and a ferrite circulator. These contributions make SIWs more flexible and effective for microwave systems, promoting wide applications of SIW technology.
- *SIW-based subsystems and massive products*: She implemented several high-performance SIW-based antenna arrays from the X to W bands and SIW-based microwave subsystems for industries. These inventions have been commercialized by different companies.
- *Novel resonant structures, design methods, and filtering circuits*: These have a very compact size and good performance and can be easily applied in packaging and on-chip systems, even up to millimeter-wave bands.
- *Innovative electromagnetic field manipulation structures and applications on circuits and antennas*: She made important accomplishments in the exploration of artificial magnetic conductors, metasurfaces, and frequency-selective surfaces to flexibly control the amplitude, phase, frequency, and polarization of electromagnetic fields. Several of her novel electromagnetic structures have been proposed and used for implementing innovative antennas featuring a low profile, broadband, high aperture efficiency, easy reconfiguration, and a low radar cross section. These antennas have application potential for advanced wireless communication systems. Several designs have been commercialized.

Alessandra Costanzo
Department of Electrical, Electronic, and Information Engineering "Guglielmo Marconi"
University of Bologna
Bologna, Italy

for contributions to nonlinear electromagnetic co-design of RF and microwave circuits

Alessandra Costanzo is a full professor at the University of Bologna, where she leads the RF and wireless laboratories on the Bologna and Cesena campuses. Her research activities began, under the supervision of Prof. Vittorio Rizzoli, in the areas of nonlinear microwave circuit simulation and design, with an emphasis on the electromagnetic analysis and design of microwave integrated circuits and the nonlinear/electromagnetic cosimulation and co-design of communications links.

Prof. Costanzo has conceived and developed algorithms to simultaneously handle nonlinear components and circuits, such as oscillators, mixers and amplifiers, with electromagnetic entities, such as antennas, antenna arrays, and multilayered RF structures, exploiting domain partitioning, space mapping, and neural network modeling. She has played a key role in establishing the bridge between system- and circuit-level design techniques for RF/microwave wireless links, which are essential prerequisites for the reliable design of current RF/microwave miniaturized systems. She was able to demonstrate end-to-end circuit-level optimization of entire multiple-input, multiple-output links, including the actual radio channel model, adopting layout-based radiating elements as the true source and load terminations of the nonlinear circuits.

Prof. Costanzo has developed pioneering work in the field of wirelessly powering devices and systems, adopting near- and far-field techniques. She has anticipated fundamental results for the theoretical understanding of interactions between the transmitter and receiver sides of wireless power transfer (WPT) systems to quantify the overall efficiency of the wireless powering mechanism. She was able to develop original system architectures for different application scenarios in various frequency and power ranges.

In the far-field radiative energy transfer case, she demonstrated not only full operation of battery-less wireless sensors but also the possibility of their localizing and tracking in harsh electromagnetic environments, which are key enabling features for the effective exploitation of the IoT paradigm in industrial plants and e-health. In the near-field case, she proposed a novel modular system for the load- and coupling-independent wireless powering of "on-the-move" small cars, adopting a gallium nitride-based class EF inverter in the megahertz range. She developed original architectures that integrate microwave devices with WPT systems to combine energy and information transfer, thus enabling remote sensing capabilities.

Prof. Costanzo is the cofounder of European Union Cooperation in Science and Technology action IC1301 to address wireless power transmission, and she is an elected vice-president of the IEEE Council on RFID for publications, where she also serves as a Distinguished Lecturer. She is a past associate editor of *TMMT* and a former chair of MTT-S Technical Committee 26. She was the TPC chair of the 2018 IEEE MTT-S International Microwave and RF Conference and 2019 IEEE Wireless Power Transfer Conference.

Relevant Publications

- V. Rizzoli, A. Costanzo, D. Masotti, A. Lipparini, and F. Mastri, "Computer-aided optimization of nonlinear microwave circuits with the aid of electromagnetic simulation," *IEEE Trans. Microw. Theory Techn.*, vol. 52, no. 1, pp. 362–377, Jan. 2004, doi: 10.1109/TMTT.2003.820898.
- A. Costanzo *et al.*, "Electromagnetic energy harvesting and wireless power transmission: A unified approach," *Proc. IEEE*, vol. 102, no. 11, pp. 1692–1711, Nov. 2014, doi: 10.1109/JPROC.2014.2355261.
- V. Rizzoli, A. Costanzo, D. Masotti, P. Spadoni, and A. Neri, "Prediction of the end-to-end performance of a microwave/RF link by means of nonlinear/electromagnetic co-simulation," *IEEE Trans. Microw. Theory Techn.*, vol. 54, no. 12, pp. 4149–4160, Dec. 2006, doi: 10.1109/TMTT.2006.885566.
- R. Trevisan and A. Costanzo, "A UHF near-field link for passive sensing in industrial wireless power transfer systems," *IEEE Trans. Microw. Theory Techn.*, vol. 64, no. 5, pp. 1634–1643, May 2016, doi: 10.1109/TMTT.2016.2544317.
- A. Costanzo and D. Masotti, "Energizing 5G: Near- and far-field wireless energy and data Tran transfer as an enabling technology for the 5G IoT," *IEEE Microw. Mag.*, vol. 18, no. 3, pp. 125–136, May 2017, doi: 10.1109/MMM.2017.2664001.

Apostolos Georgiadis

for contributions to designs of RF energy harvesting circuits

Apostolos Georgiadis was born in Thessaloniki, Greece. He received the B.S. degree in physics and the M.S. degree in telecommunications from the Aristotle University of Thessaloniki in 1993 and 1996, respectively. He received the Ph.D. degree in electrical engineering from the University of Massachusetts, Amherst in 2002. In 2002, he joined Global Communications Devices, North Andover, Massachusetts, as a systems engineer and worked on CMOS transceivers for wireless network applications. In June 2003, he began at Bermai, Minnetonka, Minnesota, as an RF/analog systems architect. In 2005, he transitioned to the University of Cantabria, Spain, as a Juan de la Cierva fellow. In March 2007, he went to the Catalonia Telecommunications Technology Center (CTTC), Barcelona, Spain, as a senior research associate in the area of communications subsystems. In 2013–2016 he was the group leader of the CTTC Microwave Systems and Nanotechnology Department. In July 2016, he joined Heriot-Watt University, Edinburgh, U.K., as an associate professor. During 2016, he was a visiting scholar at the Georgia Institute of Technology, Atlanta, as a Marie Curie Global Fellow. Since 2017, he has been with the European Patent Office, The Hague, The Netherlands.

Dr. Georgiadis was the general chair of the 2011 IEEE international Conference on RFID Technology and Applications and general cochair of the 2011 IEEE MTT-S International Microwave Workshop Series on Advanced Materials and Processes. He has been an associate editor of *IEEE Journal of Radio Frequency Identification*; *IEEE Microwave and Wireless Components Letters*; *IET Microwaves, Antennas & Propagation*; and *IEEE RFID Virtual Journal*. He cofounded and was the editor-in-chief of *Cambridge Wireless Power Transfer Journal*. He has been a Distinguished Lecturer of the IEEE Council on RFID, and he was the chair of International Union of Radio Science (URSI) Commission D: Electronics and Photonics. He was the recipient of the 2016 Bell Labs Prize (third place) and has been a Fulbright scholar. An URSI fellow, his research interests include energy harvesting and wireless power transmission, RFID technology, active antennas and phased-array antennas, inkjet and 3D printed electronics, and millimeter-wave systems. He has published more than 200 papers in peer-reviewed journals and international conferences.

Relevant Publications

- A. Georgiadis, A. Collado, and M. M. Tentzeris, *Energy Harvesting: Technologies, Systems, and Challenges (EuMA High Frequency Technologies Series)*. Cambridge, U.K.: Cambridge Univ. Press, 2021.
- A. Georgiadis, E. Tentzeris, and G. Goussetis (third place), "Nokia announces its 2016 Bell Labs prize winners: 3D/Inkjet printed millimeter wave systems", Nokia, Espoo, Finland, 2016. [Online]. Available: https://www.nokia.com/about-us/news/releases/2016/12/15/nokia-announces-its-2016-bell-labs-prize-winners/
- S. Kim *et al.*, "Ambient RF energy-harvesting technologies for self-sustainable standalone wireless sensor platforms," *Proc. IEEE*, vol. 102, no. 11, pp. 1649–1666, Nov. 2014, doi: 10.1109/JPROC.2014.2357031.
- A. Collado and A. Georgiadis, "Optimal waveforms for efficient wireless power transmission," *IEEE Microw. Wireless Compon. Lett.*, vol. 24, no. 5, pp. 354–356, May 2014, doi: 10.1109/LMWC.2014.2309074.
- A. Georgiadis, G. Andia Vera, and A. Collado, "Rectenna design and optimization using reciprocity theory and harmonic balance analysis for electromagnetic (EM) energy harvesting," *IEEE Antennas Wireless Propag. Lett.*, vol. 9, pp. 444–446, May 2010, doi: 10.1109/LAWP.2010.2050131.

Jeffrey L. Hesler
Virginia Diodes
Charlottesville, Virginia, United States

for contributions to development of terahertz components and instrumentation

Jeffrey L. Hesler received the B.S. degree in electrical engineering from Virginia Tech, Blacksburg, in 1989 and the M.S. degree (1991) and Ph.D. degree (1996) from the University of Virginia (UVA), Charlottesville, both in electrical engineering. He joined the UVA faculty as a research assistant professor of electrical engineering in 1997, and in 2001, he went to Virginia Diodes (VDI), becoming a full-time employee in 2004. He became the VDI chief technology officer in 2008, a position he continues to hold. Dr. Hesler was a member and secretary of the IEEE P1785 Standards Working Group, which, from 2008 to 2016, developed and published IEEE standards for terahertz waveguide interfaces. He is an associate editor of *IEEE Transactions on Terahertz Science and Technology* (2018–present) and has been a member (2014–present) and the chair (2021–2022) of MTT-S Technical Committee 21 on Terahertz Technology and Applications.

Beginning with his time as a student at UVA, Dr. Hesler's career has focused on the creation of new technologies to make possible the full exploitation of the terahertz frequency band for scientific, defense, and industrial applications. During his early work, he focused on the development of broadband frequency mixers and multipliers that do not require mechanical tuning and bias adjustments to achieve optimal performance and broad operational bandwidth in the terahertz frequency band. In doing so, he was a pioneer in fully utilizing the capabilities of newly available planar diode fabrication technologies. In addition, he developed modeling techniques that enabled the use of commercial electromagnetic and harmonic balance simulation tools to develop terahertz devices and components. These advances made the technology practical for a much greater range of applications, leading to the rapid development of terahertz technology over the past two decades.

Perhaps the best example of the use and impact of these components is the existence and routine operation of the Atacama Large Millimeter Array (ALMA). ALMA is a big science international project that developed a 66-dish radio astronomy array on a 5,000-m Chilean plateau, with receivers operating across the ~100–1,000-GHz range (in ten bands). ALMA receivers above about 100 GHz rely on broadband frequency multipliers to generate the required local oscillator signals. These multipliers were produced by VDI, and some 2,000 of them were delivered as part of the project. One well-known result from ALMA was the first image of a black hole, at ~230 GHz (https://www.almaobservatory.org/en/press-releases/astronomers-capture-first-image-of-a- black-hole/).

Dr. Hesler also used broadband terahertz components for the development of advanced test and measurement equipment to characterize materials, devices, components, and systems. An important example is the vector network analyzer (VNA), which is commonly used to measure complex S-parameters. Before this work, wideband terahertz VNA extenders were limited to about 300 GHz, with a modest dynamic range (~50 dB), and higher-frequency systems were narrow band and required mechanical tuning. In 2010, VDI delivered the first VNA frequency extenders that enabled full two-port measurements (magnitude and phase) across the entire 500–750-GHz (WM380) waveguide band. This system had a dynamic range approaching 90 dB. Since then, the frequency range has been extended to 1.5 THz, with increased dynamic range and improved measurement stability. Terahertz VNA frequency extenders and associated signal analyzers and generators are now ubiquitous in microwave laboratories throughout the United States, Europe, and Asia, and the broad commercial availability of these test and measurement tools has fundamentally changed the methods by which engineers and scientists develop and evaluate materials, components, and systems throughout the terahertz range.

Slawomir Koziel
Department of Engineering
Reykjavík University
Reykjavík, Iceland

for contributions to modeling and optimization of microwave devices and circuits

Slawomir Koziel received the M.Sc. and Ph.D. degrees in electronic engineering from Gdansk University of Technology, Poland, in 1995 and 2000, respectively. He also received the M.Sc. degrees in theoretical physics and mathematics in 2000 and 2002, respectively, as well as the Ph.D. degree in mathematics in 2003, from the University of Gdansk. He is currently a professor with the Department of Engineering, Reykjavik University.

His research interests include CAD and the modeling of microwave and antenna circuits, simulation-driven design, surrogate-based optimization, space mapping, circuit theory, evolutionary computation, and numerical analysis. In recent years, he has been working extensively on surrogate-based modeling and optimization techniques as well as computationally efficient simulation-driven design methods for microwave and antenna engineering and aerospace engineering. He has published several book chapters and more than 1,000 research papers. He is a founder and director of the Engineering Optimization and Modeling Center, Reykjavik University.

Dr. Koziel was a recipient of a Fulbright Scholarship for the 2003–2004 academic year. He has served on the editorial board of various international journals and on various program committees and been a co-organizer of numerous special sessions and workshops at international conferences. He is an associate editor of several journals (*IET Microwaves, Antennas, and Propagation*; *Electronics Letters*; *International Journal of Mathematical Modeling and Numerical Optimization*; and *International Journal of Numerical Modeling*). He has also been a guest coeditor of several special issues of international journals, including *Optimization and Engineering*; *International Journal of RF and Microwave Computer-Aided Engineering*; *International Journal of Mathematical Modeling and Numerical Optimization*; and *IEEE Transactions on Microwave Theory Techniques*, as well as a coauthor of numerous books, such as *Performance-Driven Surrogate Modeling of High-Frequency Structures* (Springer, 2020), *Simulation-Based Optimization of Antenna Arrays* (World Scientific, 2019), *Multi-Objective Design of Antennas Using Surrogate Models* (World Scientific, 2016), *Simulation-Driven Design by Knowledge-Based Response Correction Techniques* (Springer, 2016), and *Antenna Design by Simulation-Driven Optimization* (Springer, 2014), and a coeditor of several others.

Relevant Publications

- S. Koziel and A. Bekasiewicz, "Expedited geometry scaling of compact microwave passives by means of inverse surrogate modeling," *IEEE Trans. Microw. Theory Techn.*, vol. 63, no. 12, pp. 4019–4026, 2015, doi: 10.1109/TMTT.2015.2490662.
- S. Koziel and J. W. Bandler, "Rapid yield estimation and optimization of microwave structures exploiting feature-based statistical analysis," *IEEE Trans. Microw. Theory Techn.*, vol. 63, no. 1, pp. 107–114, 2015, doi: 10.1109/TMTT.2014.2373365.
- S. Koziel, J. Meng, J. W. Bandler, M. H. Bakr, and Q. S. Cheng, "Accelerated microwave design optimization with tuning space mapping," *IEEE Trans. Microw. Theory Techn.*, vol. 57, no. 2, pp. 383–394, 2009, doi: 10.1109/TMTT.2008.2011313.
- S. Koziel, J. W. Bandler, and K. Madsen, "Space mapping with adaptive response correction for microwave design optimization," *IEEE Trans. Microw. Theory Techn.*, vol. 57, no. 2, pp. 478–486, 2009, doi: 10.1109/TMTT.2008.2011243.
- S. Koziel, J. W. Bandler, and K. Madsen, "A space-mapping framework for engineering optimization—Theory and implementation," *IEEE Trans. Microw. Theory Techn.*, vol. 54, no. 10, pp. 3721–3730, 2006, doi: 10.1109/TMTT.2006.882894.

Moriyasu Miyazaki
Electronic Systems Group
Mitsubishi Electric
Tokyo, Japan

for leadership in developments of airborne active-phased-array radars and satellite communication microwave subsystems

Moriyasu Miyazaki received the B.E. degree in electrical engineering and the M.E. and Ph.D. degrees in electronic engineering from Chiba University, Japan, in 1982, 1984, and 1997, respectively. As a graduate student, he accomplished a novel formulation of edge-guided magnetostatic modes by using the boundary element method (BEM). In 1984, he joined Mitsubishi Electric, where he began to research microwave passive circuits. As one of his noteworthy works in the 1990s, he succeeded in optimizing a planar N-way hybrid power divider with sectorial shape via a design based on the BEM. This accomplishment contributed to the realization of an extremely thin and broadband active phased-array radar (APAR) and was applied to many airborne radars. After 2000, he became a department head of the Information Technology R&D Center, Mitsubishi Electric, and led not only passive circuit developments but also overall RF front-end developments, including semiconductor devices. Gallium nitride RF devices were successfully put into practical onboard use. His achievements are utilized in various APARs and play a role in variety of applications, including mobile communication systems. During this period, he also completed a unique design technique, superior in practicality, for waveguide filters by combining the conjugate gradient method, mode-matching techniques, and the BEM.

Dr. Miyazaki also provided leadership and realized an antenna subsystem for in-flight Internet services utilizing communication satellites, achieving high-accuracy satellite acquisition and sufficient communication speed of 40 Mb/s while maintaining a compact size and low profile for mounting on aircraft. The service adopting this antenna subsystem was commercialized in 2004. Through this work, several inventions were born, such as ultrathin orthomode transducers and an integrated diplexer low-noise amplifier unit. Dr. Miyazaki's pioneering developments 20 years ago resulted in today's in-flight Wi-Fi services. For this project's success, he received the R&D 100 award from *R&D Magazine* (2005). He also led a national project on the development of radio communication systems for aircraft through millimeter waves. He oversaw the development of the antenna subsystem and access control system and succeeded in 100-Mb/s bidirectional communication between aircraft and ground controllers. For this contribution, he received the 58th OHM Technology Award from the Promotion Foundation for Electrical Science and Engineering of Japan (2010).

Dr. Miyazaki moved to the Electronic Systems Group, Mitsubishi Electric, in 2013 as a senior chief engineer to support the business from the perspective of microwave and millimeter-wave applications. He is currently a technical adviser in the group and belongs to the Research Organization for Open Innovation Strategy, Waseda University, Tokyo. He served as the treasurer of the IEEE MTT-S Japan Chapter (2003–2004), vice chair of ceremonies for the 2010 Asia Pacific Microwave Conference (APMC), and chair of the APMC National Committee (2019–2020).

Relevant Publications

- M. Miyazaki, O. Ishida, and T. Hashimoto, "N-way sectorial hybrid power divider design using boundary element method," *Int. J. Microw. Millimeter-Wave Comput.-Aided Eng.*, vol. 3, no. 3, pp. 175–182, Jul. 1993, doi: 10.1002/mmce.4570030305.
- M. Miyazaki, K. Yashiro, and S. Ohkawa, "Edge-guided magnetostatic mode in a ridged-type waveguide," *IEEE Trans. Microw. Theory Techn.*, vol. 33, no. 5, pp. 421–424, May 1985, doi: 10.1109/TMTT.1985.1133023.
- M. Hangai, M. Hieda, N. Yunoue, Y. Sasaki, and M. Miyazaki, "S- and C-band ultra-compact phase shifters based on all-pass networks," *IEEE Trans. Microw. Theory Techn.*, vol. 58, no. 1, pp. 41–47, Jan. 2010, doi: 10.1109/TMTT.2009.2036322.
- A. Monk *et al.*, "Ultra-low profile airborne reflector antenna subsystem for broadband satellite communications," in *Proc. 21st AIAA Int. Commun. Satellite Syst. Conf.*, Apr. 2003, pp. 15–19, doi: 10.2514/6.2003-2316.
- M. Miyazaki, H. Yukawa, T. Nishino, S. Urasaki, T. Katagi, and H. Kurebayashi, "Design of iris-coupled broadband waveguide filter using modified reflection-zero frequencies," *Electron. Commun. Japan (II, Electron.)*, vol. 83, no. 7, pp. 59–67, 2000, doi: 10.1002/1520-6432(200007)83:7<59::AID-ECJB9>3.0.CO;2-7.

Anh-Vu Pham
Department of Electrical and Computer Engineering
University of California, Davis
Davis, California, United States

for contribution to organic packaging technologies

Anh-Vu Pham received the B.E.E. (with high honors), M.S., and Ph.D. degrees in electrical engineering from the Georgia Institute of Technology, Atlanta, in 1995, 1997, and 1999, respectively. He joined the University of California, Davis in 2002 as an assistant professor and was promoted to full professor in 2008. From 1999 to 2002, he was an assistant professor at Clemson University, South Carolina. He is a codirector of the Davis Millimeter Wave Research Center at the University of California, Davis. His research interests include RF-to-terahertz hybrid and integrated circuits, electronic packaging, antennas, radars and sensors, and energy harvesting systems. He has published 200 peer-reviewed articles, several book chapters, and two books and has graduated 22 Ph.D. students.

Dr. Pham received the NSF CAREER Award in 2001 and the MTT-S Outstanding Young Engineer Award in 2008. He served as the TPC cochair of IMS 2016, in San Francisco, and the TPC of the 2017 IEEE Asia Pacific Microwave Conference, in Malaysia, and an MTT-S Distinguished Microwave Lecturer from 2010 to 2012. He has served as a guest editor of *TMMT* special issues on broadband millimeter-wave PAs in 2020 and the Asia-Pacific Microwave Conference in 2017.

Dr. Pham has led the development of organic packaging technologies for microwave and millimeter-wave applications. His contributions to organic packaging technologies include surface-mount packages, multilayered board-integrated passives and antennas, and multichip modules. He and his students explored liquid crystal polymers (LCPs) for lightweight, compact, and reliable packages and modules. LCPs have permeation similar to glass, ultralow moisture absorption, and a coefficient of hygroscopic expansion. These characteristics make LCPs attractive candidates for lightweight and high-reliability packaging. His group developed processes to laminate them on LCPs and semiconductor materials for packaging electronic circuits. Using these processes, his group demonstrated the first LCP Ka-band surface-mount package in which integrated circuits are housed in an all-LCP sealed cavity, and it carried out environmental tests to demonstrate LCPs' packaging capabilities.

Dr. Pham's contributions to organic packaging began in the late 1990s when he developed on-wafer measurement techniques to characterize and model low-cost plastic packages up to 26.5 GHz and demonstrated organic multichip modules up to 110 GHz. Dr. Pham also led the development of integrated passives, including baluns, filters, couplers, and power dividers, and antennas in multilayered organic boards. Utilizing multilayered structures, thin substrates, and design techniques such as a defected ground, his group developed state-of-the-art baluns that achieve record bandwidth ratios up to 46:1.

In 2008, Dr. Pham cofounded PlanarMag and served as the chief technology officer. He led a team to develop the first organic board-integrated transformer products for 10 Gb/s Ethernet applications by using automated manufacturing. Traditionally, Ethernet transformers and common mode chokes are manufactured using hand-wound wires around a ferrite core. Handmade transformers have reliability and electrical variability issues. Dr. Pham's team developed a process to embed ferrite cores in a printed circuit board (PCB) that can be used in fabrication processes to produce transformers. Ferrite-embedded components in PCBs can be designed with controlled linewidth and spacing to achieve wide bandwidth and electrical consistency. This technology has opened new capabilities for PCBs and PCB-integrated magnetic components. PlanarMag was acquired by TE Connectivity in 2010. Also, in 1997, Dr. Pham cofounded RF Solutions, Atlanta, Georgia, a fabless semiconductor company providing PAs and RF integrated circuits for Wi-Fi applications. In 2003, RF Solutions was acquired by Anadigics.

Christopher T. Rodenbeck
U.S. Naval Research Laboratory
Washington, D.C., United States

for contributions to radar microsystems for ultrawideband and millimeter-wave applications

Christopher T. Rodenbeck received the B.S. (summa cum laude), M.S., and Ph.D. degrees in electrical engineering from Texas A&M University, College Station, in 1999, 2001, and 2004, respectively. From 2004 to 2014, he was with Sandia National Laboratories, Albuquerque, New Mexico. At Sandia, he led a multidisciplinary advanced/exploratory technology development program for ultrawideband radar and sensor applications. The principal achievements of this program were the consolidation of more than 800 discrete RF components into a handful of integrated circuits and the development of a monolithic pulsed PA exhibiting the fastest ultrawideband pulse modulation and extinction rates reported at power levels greater than 10 W. The success of this program, including US$84 million in cost savings to the U.S. Air Force alone, was reported by the *Wall Street Journal* and twice the subject of congressional testimony by Sandia's president. Dr. Rodenbeck accepted the prestigious National Nuclear Security Administration Defense Programs Award of Excellence in 2012 on behalf of a large, multisite team.

Dr. Rodenbeck is currently an office head with the U.S. Naval Research Laboratory (NRL), Washington, D.C., where he leads the Advanced Concepts Group within the Radar Division. His programs at NRL have resulted in the development of multiple first-in-class millimeter-wave airborne radar systems for the U.S. Navy and Department of Defense, including the creation of compact millimeter-wave radars for the autonomous guidance of unmanned aerial vehicles. His demonstrations of sound reproduction on moving vehicles are motivating the development of a long-range radar system based on the first 100-W solid-state PA at the W band. Most recently, Dr. Rodenbeck has been leading multiple research programs in microwave power beaming, and he serves as the principal investigator for the Air Force Research Laboratory's Arachne power beaming spacecraft, the flagship experiment under the Space Solar Power Incremental Demonstrations and Research Project.

Dr. Rodenbeck has authored or coauthored numerous publications and patents on a wide range of topics in RF microsystems and applications, including several highly cited patents on transceiver miniaturization. He has mentored numerous engineers in the radar electronics application area. He was an associate editor of the *Encyclopedia of Electrical and Electronics Engineering* (Wiley) from 2011 to 2020 and currently is the editor-in-chief of the forthcoming *Encyclopedia of RF & Microwave Engineering*, *Second Edition* (Wiley).

Relevant Publications

- M. Kirkpatrick. "Sounding the nuclear alarm." The Wall Street Journal. https://www.wsj.com/articles/SB122731227702749413
- P. Hommert, "Oral and written testimony to U.S. House of Representatives," Oct. 29, 2013. [Online]. Available: https://www.hsdl.org/?view&did=755532, https://www.osti.gov/servlets/purl/1673652. "Oral testimony to US Senate," Apr. 18, 2012. [Online]. Available: https://www.hsdl.org/?view&did=729407
- U.S. Patents Appl. 20200284901A1, 11029403, 20180174472, 20180172821, 20180172821.
- Worldwide Patent Appl. WO2018112404.
- U.S. Patent Appl. 63/066932.
- U.S. Patent Appl. US20210156953A1.
- J. Soric *et al.*, "A 100W W-band GaN SSPA," Presented at the IEEE Int. Microwave Symp., to be published.
- C. T. Rodenbeck *et al.*, "Microwave and millimeter wave power beaming," *IEEE J. Microw.*, vol. 1, no. 1, pp. 229–259, Jan. 2021, doi: 10.1109/JMW.2020.3033992.
- C. T. Rodenbeck *et al.*, "Terrestrial microwave power beaming," *IEEE J. Microw.*, vol. 2, no. 1, pp. 28–43, Jan. 2022, doi: 10.1109/JMW.2021.3130765.
- C. Delbert, *The Air Force is Building a Spacecraft that will Beam Solar Power to Earth*. New York, NY, USA: Popular Mechanics, Dec. 30, 2020.
- U.S. Patents 7439935, 7408512, 7345647.

Daniel van der Weide
Department of Electrical and Computer Engineering
University of Wisconsin–Madison
Madison, Wisconsin, United States

for contributions to ultrafast terahertz electronics and biomedical applications of microwave technologies

Daniel van der Weide is a pioneer in terahertz integrated circuits, having designed, fabricated, and quantified the shortest electronically generated and measured pulses, a record that has stood for 28 years. As a Ph.D. student in David Bloom's group at Stanford University, he measured the first subpicosecond electronic circuits; as a postdoctoral researcher in Klaus von Klitzing's group, he measured the current record 480 fs, 3.5-V pulses, using gallium arsenide nonlinear transmission lines and samplers (receiving 126 citations since 1994). He has guided his students to apply a related phase discriminator to high-precision materials measurements (earning first prize in the 2020 IEEE Radio and Wireless Week student paper competition).

At the University of Wisconsin–Madison since 1999, Dr. van der Weide has made extraordinary contributions to the understanding of terahertz electronics, including coherent measurements, ultrabroadband antennas, and remote sensing. With John Booske, he invented and published a scaled slow wave structure for terahertz traveling-wave tubes that has been a reference in this rapidly growing field (receiving 348 citations since 2004). With Fritz Keilmann, he invented a polarization-based interferometer, applying pulse interferometry to femtosecond lasers to produce broad infrared combs, whose development has had worldwide impact. With Robert Blick, he applied these techniques to the spectroscopy of low-dimensional electronics. He invented techniques to localize terahertz to submicrometer dimensions by using micromachined scanning probes as near-field antennas for microwave microscopy.

These small-signal measurements gave way to the exploration of localized microwave power to treat cancer. Challenged by Fred Lee to develop a superior treatment modality to RF ablation, Dr. van der Weide invented a triaxial antenna that could be impedance matched to diseased tissue to efficiently deliver ablative power in a 17-gauge format, enabling percutaneous application under image guidance. With advisees Christopher Brace and Paul Laeseke, he pursued the clinical refinement of this application of 2.45-GHz microwave power, ultimately establishing NeuWave Medical, which has treated thousands of patients and was acquired by Johnson & Johnson in 2016. Subsequently, he cofounded Elucent Medical, which has treated hundreds of patients through a wireless surgical navigation system of his invention that is being hailed as a breakthrough in breast cancer surgery.

Dr. van der Weide's interests in coherent signal analysis in optical fiber for >100 Gb/s communications led him to cofound Optametra in 2007 with Rob Marsland (another Bloom group member). Optametra was acquired by Tektronix 2011. While he has wide-ranging interests and creativity to support them, the examples in the preceding indicate the breadth and depth of his contributions to the use of high-frequency technology to terahertz measurements and human health.

Relevant Publications

- D. W. van der Weide, J. Bostak, B. Auld, and D. Bloom, "All-electronic generation of 880 fs, 3.5 V shockwaves and their application to a 3 THz free-space signal generation system," *Appl. Phys. Lett.*, vol. 62, no. 1, pp. 22–24, 1993, doi: 10.1063/1.108806.
- D. W. van der Weide, "Delta-doped Schottky diode nonlinear transmission lines for 480-fs, 3.5-V transients," *Appl. Phys. Lett.*, vol. 65, no. 7, pp. 881–883, 1994, doi: 10.1063/1.113013.
- A. M. Day, M. M. Dwyer, and D. W. van der Weide, "Phase perturbation as a measurement metric: A novel noncontact in-line production measurement through an all-electronic millimeter-wave system tracking millidegree perturbations in phase," *IEEE Microw. Mag.*, vol. 22, no. 1, pp. 79–85, 2021, doi: 10.1109/MMM.2020.3023270.
- A. Schliesser, M. Brehm, F. Keilmann, and D. W. van der Weide, "Frequency-comb infrared spectrometer for rapid, remote chemical sensing," *Opt. Exp.*, vol. 13, no. 22, pp. 9029–9038, 2005, doi: 10.1364/OPEX.13.009029.
- C. L. Brace, P. F. Laeseke, D. W. van der Weide, and F. T. Lee, "Microwave ablation with a triaxial antenna: Results in ex vivo bovine liver," *IEEE Trans. Microw. Theory Techn.*, vol. 53, no. 1, pp. 215–220, 2005, doi: 10.1109/TMTT.2004.839308.

Christian Waldschmidt
Institute of Microwave Engineering
Ulm University
Ulm, Germany

for contributions to millimeter-wave automotive radar sensors

Christian Waldschmidt received the Dipl.-Ing. (M.S.) and the Dr.-Ing. (Ph.D.) degrees in electrical engineering from the Karlsruhe Institute of Technology, Germany, in 2001 and 2004, respectively. From 2001 to 2004, he was a research assistant at the Institute of Radio Frequency Engineering and Electronics, Karlsruhe Institute of Technology. Since 2004, he has been with Robert Bosch, in the corporate research and chassis systems business units. He has led research and development teams in microwave engineering, RF sensing, and automotive radar. In 2013, Dr. Waldschmidt returned to academia. He was appointed the director of the Institute of Microwave Engineering, University of Ulm, Germany, as a full professor. His research topics include radar and RF sensing, millimeter-wave and submillimeter-wave engineering, antennas and antenna arrays, and RF and array signal processing. He has authored or coauthored 280-plus scientific publications and more than 25 patents.

Dr. Waldschmidt's research team has received 14 best paper awards since 2014. He was a two-time TPC chair and general chair of the IEEE MTT-S International Conference on Microwaves for Intelligent Mobility. Since 2018, he has served as an associate editor for *IEEE Microwave and Wireless Components Letters*. He is member of the Executive Committee of the MTT-S/IEEE Antennas and Propagation Society (AP-S) Joint Chapter in Germany. He was the founding chair of MTT-S Technical Committee 29 on Microwave Aerospace Systems, and he served as chair of MTT-S Technical Committee 27 on Wireless Enabled Automotive and Vehicular Applications. He is a reviewer for multiple IEEE transactions and many IEEE conferences in the field of microwaves. Since 2020, he has been member of the Heidelberg Academy of Sciences and Humanities.

Relevant Publications

- C. Waldschmidt, J. Hasch, and W. Menzel, "Automotive radar — From first efforts to future systems," *IEEE J. Microw.*, vol. 1, no. 1, pp. 135–148, 2021, doi: 10.1109/JMW.2020.3033616.
- J. Hasch, E. Topak, R. Schnabel, T. Zwick, R. Weigel, and C. Waldschmidt, "Millimeter-wave technology for automotive radar sensors in the 77 GHz frequency band," *IEEE Trans. Microw. Theory Techn.*, vol. 60, no. 3, pp. 845–860, 2012, doi: 10.1109/TMTT.2011.2178427.
- M. Hitzler *et al.*, "Ultracompact 160-GHz FMCW radar MMIC with fully integrated offset synthesizer," *IEEE Trans. Microw. Theory Techn.*, vol. 65, no. 5, pp. 1682–1691, 2017, doi: 10.1109/TMTT.2017.2653111.
- B. Schweizer, C. Knill, D. Schindler, and C. Waldschmidt, "Stepped-carrier OFDM-radar processing scheme to retrieve high-resolution range-velocity profile at low sampling rate," *IEEE Trans. Microw. Theory Techn.*, vol. 66, no. 3, pp. 1610–1618, 2018, doi: 10.1109/TMTT.2017.2751463.
- P. Grüner, M. Geiger, and C. Waldschmidt, "Ultracompact monostatic MIMO radar with nonredundant aperture," *IEEE Trans. Microw. Theory Techn.*, vol. 68, no. 11, pp. 4805–4813, 2020, doi: 10.1109/TMTT.2020.3006055.
- C. Waldschmidt, S. Schulteis, and W. Wiesbeck, "Complete RF system model for analysis of compact MIMO arrays," *IEEE Trans. Veh. Technol.*, vol. 53, no. 3, pp. 579–586, May 2004, doi: 10.1109/TVT.2004.825788.

Anding Zhu
School of Electrical and Electronic Engineering,
University College Dublin
Dublin, Ireland

for contributions to behavioral modeling and digital predistortion of RF power amplifiers

Anding Zhu received the Ph.D. degree in electronic engineering from University College Dublin (UCD) in 2004. He is currently a professor with the School of Electrical and Electronic Engineering, UCD. His research interests include high-frequency nonlinear system modeling and device characterization techniques, high-efficiency PA design, wireless transmitter architectures, digital signal processing, and nonlinear system identification algorithms.

The main body of Dr. Zhu's work lies in the behavioral modeling and digital linearization of RF PAs for wireless communications. The RF PA is one of the most critical units in wireless transmitters, as it consumes a large amount of energy and introduces distortion that limits data capacity. Dr. Zhu's most prominent contribution is in developing accurate and compact behavioral models for RF PAs. He belongs to a small group of pioneers who demonstrated, from early 2000, how to use modified Volterra series modeling of RF PAs. He developed various approaches to prune Volterra series to reduce model complexity while maintaining accuracy, which provided a foundation for the use of Volterra series in PA modeling and real-world implementation.

The dynamic deviation reduction Volterra model that Dr. Zhu proposed in 2006 is one of the top three models currently used in real systems. His pioneering work in developing accurate behavioral models has not only enabled accurate characterization of PA behavior to help designers optimizing circuit performance but, more importantly, it enables a digital predistortion technique that applies an inverse function in digital basebands to compensate for the nonlinear distortion encountered in analog PAs to maintain efficiency without losing linearity. Over the past 20 years, Dr. Zhu has continuously contributed to digital predistortion development, from early prototypes to ground-breaking discoveries. He not only provides theorical advancements but also smart solutions in real implementations that have had enormous impact in the field.

Dr. Zhu served as the secretary of the MTT-S AdCom in 2018 and is currently an elected member. He is the chair of Electronic Information Committee and the vice chair of the Marketing and Communications Committee. He served as the chair of the MTT-S Microwave High-Power Techniques Committee in 2020–2021. He was the general chair of 2018 IEEE MTT-S International Microwave Workshop Series on 5G Hardware and System Technologies and the guest editor of a *TMMT* special issue on 5G hardware and system technologies. Dr. Zhu is a track editor of *TMMT* and an associate editor of *IEEE Microwave Magazine*. He has been a member of the IEEE Future Directions Committee since 2020. He was the recipient of the 2021 IEEE MTT-S Microwave Prize.

Relevant Publications

- A. Zhu and T. J. Brazil, "Behavioral modeling of RF power amplifiers based on pruned Volterra series," *IEEE Microw. Wireless Compon. Lett.*, vol. 14, no. 12, pp. 563–565, 2004, doi: 10.1109/LMWC.2004.837380.
- A. Zhu, J. C. Pedro, and T. J. Brazil, "Dynamic deviation reduction-based Volterra behavioral modeling of RF power amplifiers," *IEEE Trans. Microw. Theory Techn.*, vol. 54, no. 12, pp. 4323–4332, 2006, doi: 10.1109/TMTT.2006.883243.
- A. Zhu, P. J. Draxler, C. Hsia, T. J. Brazil, D. F. Kimball, and P. M. Asbeck, "Digital predistortion for envelope-tracking power amplifiers using decomposed piecewise Volterra series," *IEEE Trans. Microw. Theory Techn.*, vol. 56, no. 8, pp. 2237–2247, 2008, doi: 10.1109/TMTT.2008.2003529.
- C. Yu, L. Guan, E. Zhu, and A. Zhu, "Band-limited Volterra series-based digital predistortion for wideband RF power amplifiers," *IEEE Trans. Microw. Theory Techn.*, vol. 60, no. 12, pp. 4198–4208, 2012, doi: 10.1109/TMTT.2012.2222658.
- A. Zhu, "Decomposed vector rotation-based behavioral modeling for digital predistortion of RF power amplifiers," *IEEE Trans. Microw. Theory Techn.*, vol. 63, no. 2, pp. 737–744, 2015, doi: 10.1109/TMTT.2014.2387853.

(continued on page 112)

Solid-State Diode Technology for Millimeter and Submillimeter-Wave Remote Sensing Applications

David Cuadrado-Calle, Petri Piironen, and Natanael Ayllon

Atmospheric data collected through spaceborne millimeter (mm) and submillimeter-wave (sub-mm-wave) radiometry combined with complex numerical weather prediction models allow meteorological offices around the world to deliver accurate weather forecasting services of great socioeconomic value. Additionally, the same radiometric technology is pivotal to other applications that include but are not limited to the study of the upper atmosphere of Earth, the understanding of the effects of climate change, and the study of the atmosphere and geological surface of other planets in the solar system. Table 1 shows some examples of remote sensing instruments where there is a demand for mm-wave, sub-mm-wave, and supra-THz radiometers and whose scientific success is underpinned, in great part, by the performance of the fundamental building blocks that form the instruments.

David Cuadrado-Calle (David.CuadradoCalle@esa.int), Petri Piironen (Petri.Piironen@esa.int), and Natanael Ayllon (Natanael.Ayllon@esa.int) are with the European Space Agency, European Space Research and Technology Centre, Keplerlaan 1, 2200 AG Noordwijk, The Netherlands.

Digital Object Identifier 10.1109/MMM.2022.3155031

Date of current version: 5 May 2022

Frequency mixers, frequency multipliers, total power detectors, and noise sources are key fundamental building blocks in heterodyne and direct detection receivers operating at mm- and sub-mm-wavelengths, and these blocks are usually realized by taking advantage of the nonlinear electrical properties exhibited by certain types of solid-state diodes. Schottky-barrier diode mixers are a central element in all modern heterodyne mm- and sub-mm-wave receivers for Earth observation (EO) and planetary science, and today, they are still the preferred first-detecting component at frequencies higher than 230 GHz [1]; see Figure 1. This is due to their superior maturity and electrical room-temperature performance when compared with their main first-detecting competitor technology: the low-noise amplifier (LNA).

Schottky-barrier diode mixers are a central element in all modern heterodyne mm- and sub-mm-wave receivers for Earth observation and planetary science.

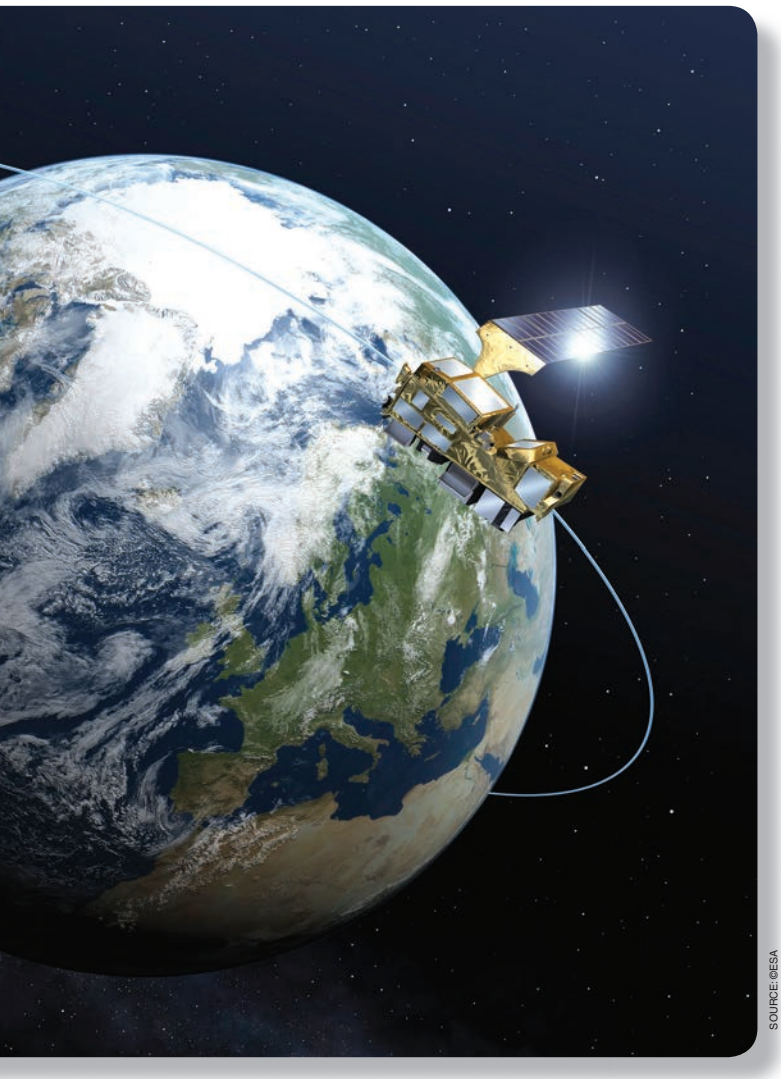

SOURCE: ©ESA

The dominance of Schottky mixers in the sub-mm-wave range is best exemplified through some of the most recent state-of-the-art mm- and sub-mm-wave front-end receiver developments for European Space Agency (ESA) space flight missions: the 243-, 325-, 448-, and 664-GHz front-end receivers on the Ice Cloud Imager (ICI) instrument for the MetOp-Second Generation (MetOp-SG) satellite series and the 600- and 1,200-GHz front-end receivers on the Submillimetre Wave Instrument (SWI) for the JUpiter ICy moons Explorer (JUICE) [2]. All these front-end receivers include a Schottky-barrier mixer as a first-detecting element in the receiving chain, and this component determines many fundamental performance parameters of the system, including the noise temperature and, consequently, the noise equivalent differential temperature ($NE\Delta T$).

At present and despite a recent emergence in heterostructure barrier varactor (HBV) technology for the development of frequency triplers and quintuplers, Schottky-barrier diodes are also the most frequently used technology for developing frequency multipliers due to their superior maturity. The utilization of Schottky varactors at mm-wavelengths is ubiquitous, and to meet the local oscillator (LO) power requirements, it is common to place several diodes in series to increase the power-handling capability of the multiplier.

Another application of Schottky diodes and also of tunnel diodes is small-signal square-law or envelope power detection. The 89-GHz channel on the microwave sounder (MWS) instrument for MetOp-SG is being built with this technology, and the outlook for these detectors at higher frequencies in the coming years is very promising. This is due, in part, to the expected improvements in high-electron mobility transistor monolithic microwave integrated circuit (MMIC) LNA technology at frequencies higher than 100 GHz [4], which is a stepping-stone for the utilization of direct detection systems in future mm- and sub-mm-wave

Editor's Note: The final version of this manuscript was received 17 November 2021. This material was current as of this date.

EO missions. Figure 2 shows the simplified diagram of a direct detection receiver.

The internal calibration of mm-wave radiometers with a noise source is currently considered another concept with high potential for application in the EO community. The radiometric calibration of mm-wave remote sounding and imaging receivers has traditionally been performed by alternating

TABLE 1. Examples of missions with a demand for mm-wave, sub-mm-wave, and supra-THz diode technology.

Instrument	Type	Phase	Diode Development Needs
LEO Meteorological Satellites			
MetOp MHS	mm-wave sounder	Utilization	Radiometers at: 89, 157, 183, and 190 GHz.
MetOp-SG MWS	mm-wave sounder	Production	Radiometers at: 31, 50–57, 89, 166, 183, and 229 GHz.
MetOp-SG MWI	mm-wave imager	Production	Radiometers at: 31, 50–53, 89, 118, 166, and 183 GHz
MetOp-SG ICI	mm-wave imager	Production	Radiometers at: 183, 243, 325, 448, and 664 GHz
CIMR	mm-wave imager	Mission analysis	Radiometers at: 36 GHz
AWS	mm-wave sounder	Mission analysis	Radiometers at: 54, 89, 166, 183, and 325 GHz
GEO Meteorological Satellites			
GEO-sounder	mm-wave sounder	Concept	Radiometers at: 183 GHz
FY-4M GIMS	mm-wave sounder	Concept	Radiometers at: 50–56 GHz
GeoSTAR	MWS	Utilization	Radiometers at: 54 and 183 GHz
Atmospheric Science Missions			
EarthCARE	Cloud profiling radar	Production	Radar at: 94 GHz
Keystone (formerly LOCUS)	Upper-atmospheric sounder	Concept	Radiometers at: 800 GHz, 1.1, 3.5, and 4.7 THz
Planetary Science Missions			
JUICE SWI	Terahertz sounder	Production	Radiometers at: 600 and 1,200 GHz
ORTIS	Terahertz Sounder	Concept	Radiometer at: 2.2 THz.

MHS = Microwave Humidity Sounder; CIMR: Copernicus Imaging Microwave Radiometer; AWS: Arctic Weather Satellite; ORTIS = Oxford RAL Terahertz-Infrared Sensor; LOCUS: Low Cost Upper- atmosphere Sounder.

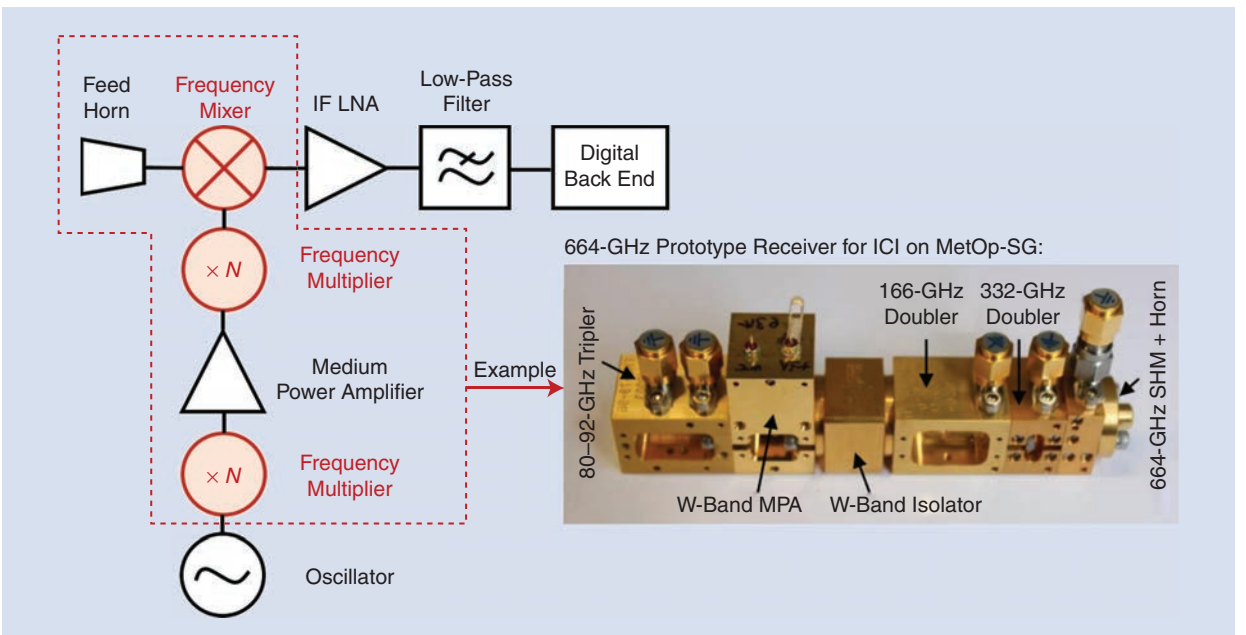

Figure 1. *Simplified functional diagram of a heterodyne receiver operating at frequencies >230 GHz and MetOp-SG receiver developed by Radiometer Physics GmbH (RPG). Diode components are highlighted in red. (Receiver photo source: [3].) IF: intermediate frequency; LNA: low-noise amplifier; MetOp-SG: MetOp-Second Generation; MPA: medium power amplifier.*

measurements of an internal calibration target and the "cold" sky. This requires a "bulky" calibration subsystem that increases the mass of the payload and can also impact the mission efficiency due to the speed limitation of the rotating quasi-optics. In this sense, the future utilization of fast-switching Schottky-diode mm-wave noise source technology can lead to a significant mass reduction and improved mission efficiency.

When considering all the aforementioned applications and because Schottky diodes, tunnel diodes, and HBVs deliver excellent performance when operated at room temperature, these devices are a very versatile and competitive technology, and it is in the best interest of the EO and planetary science communities to have them readily available from commercial sources. However, due to the niche market of these diodes, their development has not always been commercially attractive and, more often than not, the critical mass for R&D and production has had to be supported with public funding.

Scope and Applications

In this article, we present the current development status and a quantitative comparison of different consolidated (e.g., Schottky) and emerging (e.g., HBV and resonant interband tunneling) solid-state diode technologies that are suitable for the implementation of each of the following building blocks for heterodyne and direct signal detection radiometry: frequency mixers, multipliers, total power detectors, and noise sources. The application that will be driving the development road map for these diode technologies is remote sensing—including low-Earth orbit (LEO) meteorological remote sounders and imagers, geostationary (GEO) atmospheric sounders, upper-atmosphere sensors, and so on—where instruments require a very high degree of sensitivity while being operated at room temperature to reduce mass and complexity.

Therefore, it is with this application in mind that we present this technology overview, which covers a broad range of operating frequencies, extending from the mm-wave range (30–300 GHz), to the sub-mm-wave range (300–3,000 GHz) and up to the supra-THz region (<5 THz). With the aforementioned considerations in mind, it must be noted that in addition to remote sensing, the technologies presented in this article are relevant to several other applications, such as astrophysics and cosmology (with the instrument typically operated at <20 K), space-to-space very-long-baseline interferometry, sub-THz intersatellite links, telecoms, nondestructive testing of insulation materials, biomedical imaging, and security scanners.

Several European foundries have developed competitive space-qualified diode processes and demonstrated them in recent ESA missions.

Key Players in Europe and the United States

European Foundries

Planar Schottky diodes were first introduced by Cronin and Law from the University of Bath (United Kingdom) in the early 1980s [6], [7] and developed in the late 1980s and 1990s, thanks to the pioneering work undertaken, first at the University of Virginia (United States) [8], NASA Jet Propulsion Laboratory (JPL) (United States) [9], and the group of H. Hartnagel at the Technical University of Darmstadt (Germany) [10], and subsequently, at other research institutions like the Rutherford Appleton Laboratory (RAL) (United Kingdom) [11]. Rydberg and Kollberg from Chalmers [12] introduced the HBV in 1989, and the work at the Institut d'Electronique et de Microélectronique du Nord (France) was also paramount to bring this technology to maturity [13].

In the early 2000s, Europe did not have competitive diode technology for spaceflight operation in the sub-mm-wave regime. However this situation has changed drastically over the past two decades, thanks in part to several technology development

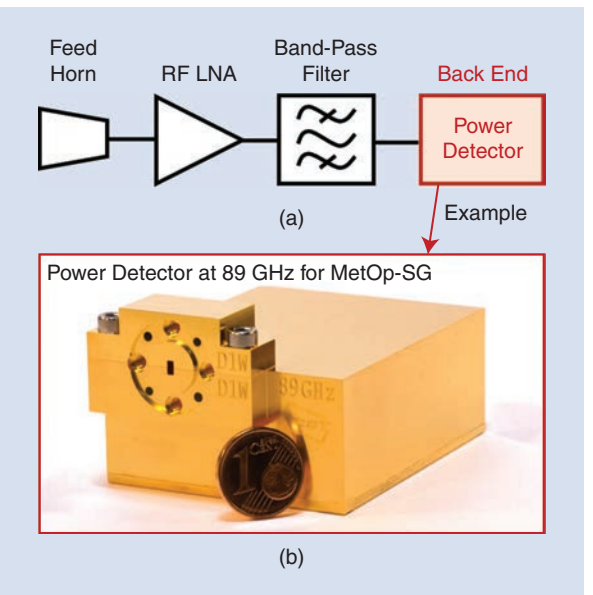

Figure 2. *(a) Simplified functional diagram of (b) a direct detection total power radiometer and power detector for MetOp-SG developed by ACST. (Detector photo source: [5].)*

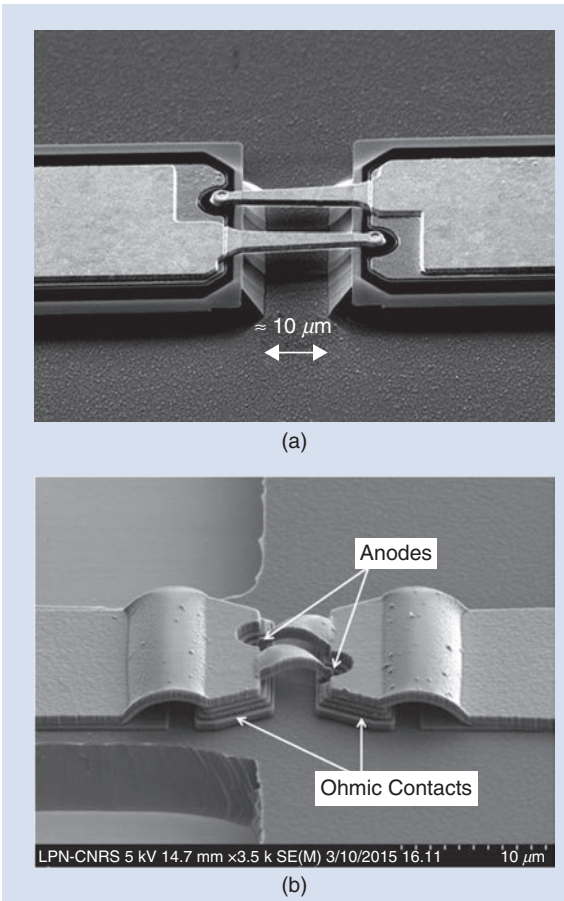

Figure 3. *SEM images of antiparallel air-bridge diode pairs from: (a) RAL ([15]) and (b) OdP-LERMA ([16]).*

programs that have taken place under the framework of MetOp-SG as well as other ESA and national funding sources. Several European foundries, such as ACST GmbH (Germany), Chalmers University of Technology (Sweden), the Observatoire de Paris (OdP) (France), and Teratech Components Ltd./RAL (United Kingdom), have developed competitive space-qualified diode processes and demonstrated them in recent ESA missions.

ACST GmbH and Teratech Components Ltd./RAL have supplied Schottky diodes for the frequency mixers and LO chains developed by both RAL and Radiometer Physics GmbH for the mm- and sub-mm-wave receivers operating up to 664 GHz on the MWS, Microwave Imager (MWI), and ICI instruments for MetOp-SG [1]. Chalmers and the OdP/Laboratoire d'Etudes du Rayonnement et de la Matière en Astrophysique et Atmosphères (LERMA) have supplied Schottky diodes for the frequency mixers and multipliers in the JUICE SWI [2], [14]. United Monolithic Semiconductors (France) have also demonstrated space-qualified planar Schottky diodes, which are included in the ESA Preferred Parts List. Figure 3 shows a scanning electron microscope (SEM) image of two diodes: one from RAL and the other one from OdP-LERMA.

The European foundries employ different techniques to fabricate their Schottky diodes. Teratech Components Ltd./RAL and Chalmers use surface channel etch planar diodes [9], [17]. ACST GmbH uses a quasi-vertical planar structure [9]. The OdP/LERMA uses a reflow process and a photoresist membrane [16]. UMS uses a buried epitaxial Schottky (BES) process [18]. Figure 4 shows a typical layer diagram

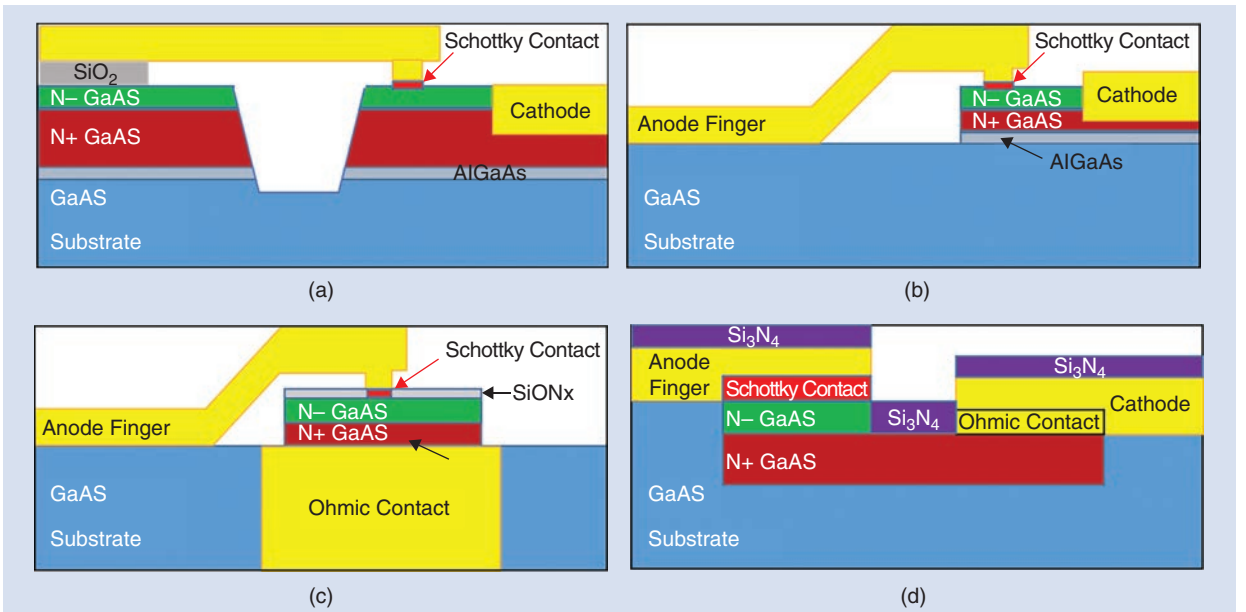

Figure 4. *A typical layer diagram for different diode fabrication techniques. (a) Surface channel etched planar diodes. (b) Air-bridged planar diodes. (c) Quasi-vertical planar diodes. (d) BES. AlGaAs: aluminium gallium arsenide; GaAs: gallium arsenide.*

for some of these techniques. More information on these fabrication methods can be found in [9].

While Schottky diodes have typically been and still remain the reference diode technology for the development of sub-mm-wave remote sensing instrumentation, some European foundries have developed other diode technologies that can also deliver excellent performance. This is the case, for instance, for Chalmers' HBVs [19] and OMMIC's resonant interband tunnel diodes (RITDs) [20].

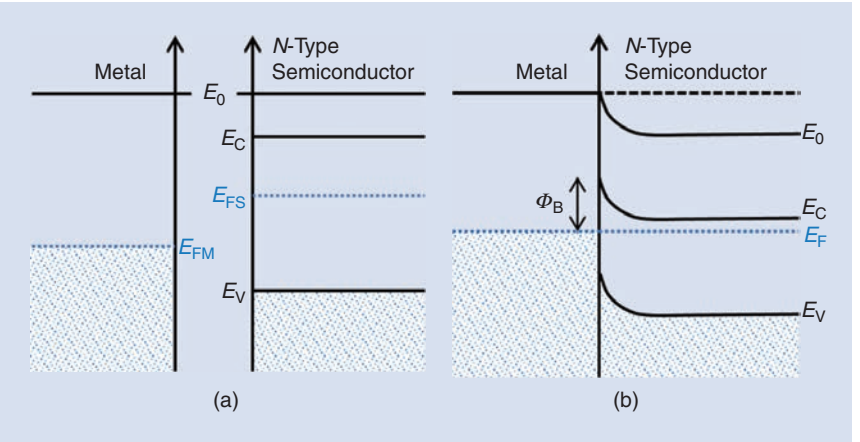

Figure 5. *A simplified energy band of a metal-semiconductor junction. (a) Before contact. (b) After contact. (Based on figure from [29]; used with permission.)*

U.S. Foundries

U.S. foundries NASA JPL and Virginia Diodes (VDI) have long been leading international suppliers of Schottky-barrier diodes for spaceborne applications, pioneering sub-mm-wave and THz integrated diode circuit development since the 1990s, thanks in part to the astrophysics community and the technology development road map for Herschel [6], [21]. As a matter of fact, some of the highest-operating-frequency multipliers and mixers from the open literature use diodes from these two foundries [9], [22]–[24]. The University of Virginia, of which VDI was initially a spin-off, also has in-house space-qualified Schottky-diode fabrication capabilities.

The fabrication processes of these three American foundries have a longstanding space-qualification heritage through multiple space missions. To exemplify this: NASA JPL supplied the diodes for the LO source of the Heterodyne Instrument for Far-Infrared onboard the Herschel Space Observatory; the University of Virginia supplied diodes for the Earth Observing System Microwave Limb Sounder [25]; and VDI supplied a sub-mm-wave receiver for *IceCube* with in-house Schottky diode technology, a satellite that delivered the first map of the global distribution of 883-GHz cloud ice between 2017 and 2018.

Like their European counterparts, these U.S. foundries use different fabrication processes. VDI fabricates the planar Schottky diodes using surface channel etching [9]. JPL uses a reflow process and a photoresist membrane [9]. Finally, the University of Virginia uses a quasi-vertical structure [9].

Although we have not found any evidence for the utilization of this technology on a space mission, HRL Laboratories has produced an antimony (Sb) heterostructure backward tunnel diode, which allows for the development of very sensitive zero-bias detectors and has potential for application in space [26]. More recently, the U.S. Naval Research Laboratory has demonstrated a new gallium nitride (GaN)-based RITD concept whose development should be closely monitored in the future [27].

Frequency Mixers

Schottky-barrier diodes are the central element in all modern room-temperature frequency down-converter systems for atmospheric science and astronomy. A Schottky junction consists of a metal and a semiconductor: typically gallium arsenide (GaAs). When these two elements are brought in contact with each other, a potential barrier builds up in the interface, creating a nonlinear voltage-current relationship that allows the down-conversion of the incident signal by application of an LO signal. Figure 5 shows the band diagram of a Schottky diode, where E_V is the energy of the valence band, E_C is the energy of the conduction band, E_0 is the free space energy level, E_F is the Fermi level, and Φ_B is the Schottky barrier height. Figure 6 shows the internals of a 1.2-THz frequency mixer from JPL [28].

When pumped at their fundamental frequency, Schottky mixers typically deliver their best performance when pumped with an LO signal of 1 mW, and this power requirement usually doubles or triples when using a subharmonic configuration: that is, when

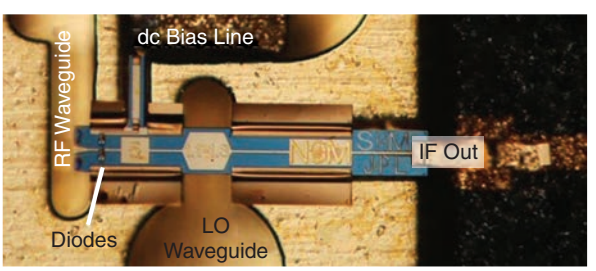

Figure 6. *A 1.2-THz mixer device mounted in its housing. (Source: [28].)*

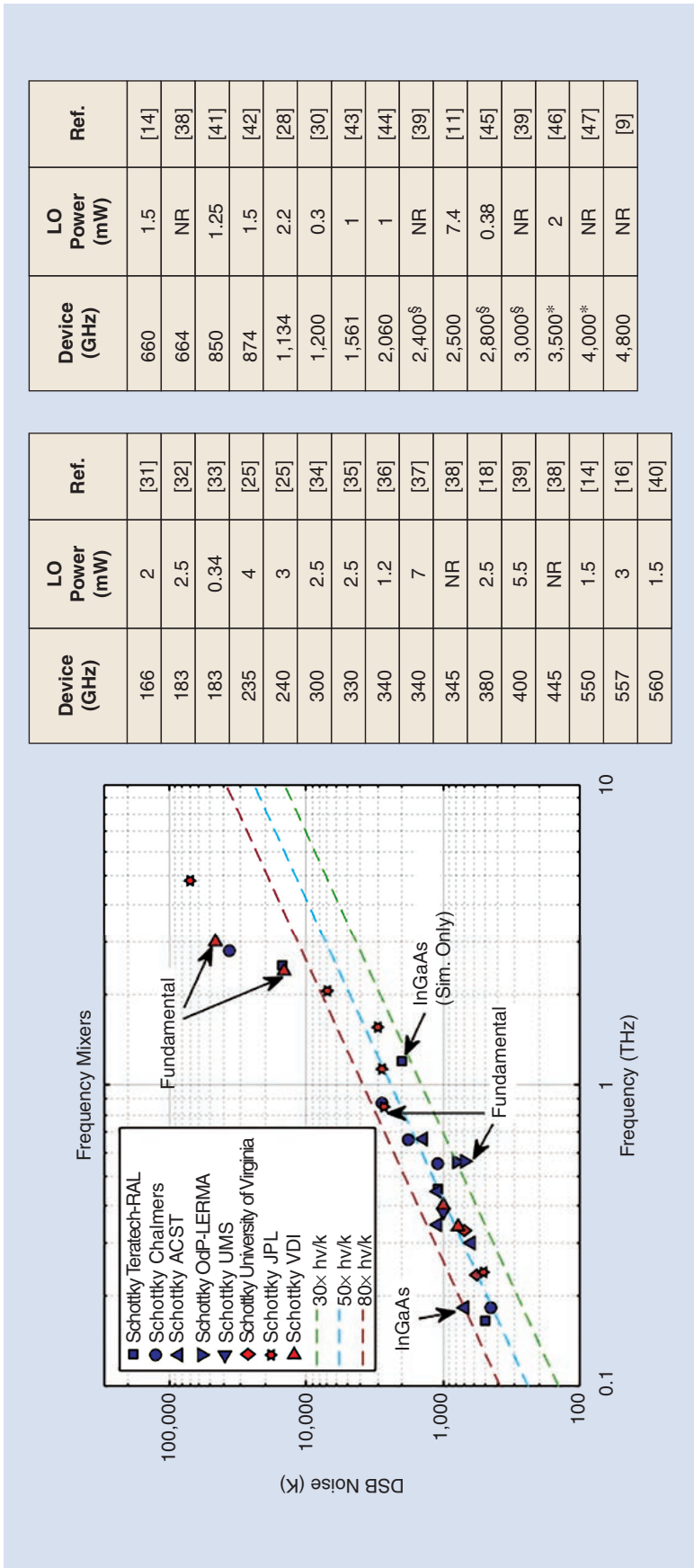

Device (GHz)	LO Power (mW)	Ref.
166	2	[31]
183	2.5	[32]
183	0.34	[33]
235	4	[25]
240	3	[25]
300	2.5	[34]
330	2.5	[35]
340	1.2	[36]
340	7	[37]
345	NR	[38]
380	2.5	[18]
400	5.5	[39]
445	NR	[38]
550	1.5	[14]
557	3	[16]
560	1.5	[40]

Device (GHz)	LO Power (mW)	Ref.
660	1.5	[14]
664	NR	[38]
850	1.25	[41]
874	1.5	[42]
1,134	2.2	[28]
1,200	0.3	[30]
1,561	1	[43]
2,060	1	[44]
2,400§	NR	[39]
2,500	7.4	[11]
2,800§	0.38	[45]
3,000§	NR	[39]
3,500*	2	[46]
4,000*	NR	[47]
4,800	NR	[9]

Figure 7. *Noise temperature versus frequency of several state-of-the-art frequency mixers from the open literature at room temperature. Mixers are harmonic unless otherwise indicated. Noise: *, not reported (NR); §, estimated from losses; sim.: simulated; Ref.: reference.*

the mixer is pumped at half of its fundamental frequency. In this sense, the utilization of low-barrier Schottky diodes with semiconductor materials such as indium GaAs (InGaAs) can bring the LO power requirements down by an order of magnitude [30], thereby opening the door to the development of future multipixel focal plane arrays. However, the tradeoff between the pump power and the noise performance of the mixer needs to be considered.

Current State of the Art Versus Frequency

Figure 7 depicts the double-sideband (DSB) noise temperature of several state-of-the-art Schottky-barrier frequency mixers from the open literature versus frequency and also against the quantum limit, i.e., the noise level limit resulting from the Heisenberg uncertainty principle. The data shown in Figure 7 do not take into account the operating bandwidth of the devices as the goal of this figure is not to compare individual Schottky mixer performances to each other but rather to get an idea of the current noise capabilities of diode technology.

From Figure 7, it can be seen that the best mixers reported to date in the open literature with operating frequencies lower than 1.1 THz feature a DSB noise temperature between 30 and 50 times the quantum limit. Developments at frequencies between 1.1 and 5 THz are pioneered by JPL, VDI, and Chalmers [9], [46], [47], although the noise temperatures reported in this segment are significantly higher than 50 times the quantum limit.

Frequency Multipliers

Frequency multipliers are the cornerstone of LO sources operating in the mm-wave range and beyond [6]. Signal multiplication has traditionally relied on the nonlinear

operating principles of Schottky-barrier metal-semiconductor contacts implemented on GaAs substrates, given the high degree of maturity of this technology. However, GaN is also a promising material due to its wider bandgap (3.4 eV versus 1.4 eV for GaAs), which leads to a higher breakdown voltage, and consequently, higher power-handling capability than GaAs with the same anode size. Figure 8 shows the internals of a Schottky-based 260–307-GHz frequency doubler from OdP-LERMA [16].

HBVs have recently emerged as a competitor to Schottky varactors in some multiplier applications. HBVs consist of a "sandwich" structure with two identical semiconductor materials (e.g., InGaAs) separated by a third different type of semiconductor material (e.g., aluminium arsenide), with the inner layer featuring a larger bandgap than the outer layers [19]. Bringing these three semiconductor layers together results in a symmetric and nonlinear capacitance-voltage characteristic that cancels the even-mode harmonics and allows an incident signal to be multiplied by a factor of ×3 or ×5.

Current State of the Art Versus Frequency

Figure 9 shows the room-temperature performance of several state-of-the-art Schottky and HBV multiplier sources from the open literature. From Figure 9, it can be seen that the output power generation capability of the multiplier sources decreases with frequency and the generation of LO power at frequencies higher than 700 GHz is by no means easy. This is the reason why the maximum powers reported to date in the literature with uncooled LO source technologies (i.e., excluding quantum cascade lasers) at frequencies >700 GHz are generally <2 mW [6], [9]. It is also worth noting that, despite their inferior maturity, the few GaN Schottky multipliers reported in the literature deliver similar output power to the Schottky and HBV multipliers. However, while the efficiency of GaAs Schottky and HBV devices is as high as 30% [9], [38], [56], the efficiency of GaN Schottky multipliers is lower than 11.5% [49], [52], [55].

Detectors

The detector technologies with the best applicability in room-temperature receiver systems for remote sensing are Schottky diodes and Sb heterostructure backward tunnel diodes [26]. Traditional GaAs Schottky junctions have a differential resistance at 0 V in the range of teraohms. Measurement of the dc voltage across this resistance is possible only by the application of a bias signal that reduces the differential resistance but also adds noise to the dc output signal. An alternative approach to overcome this obstacle, which has been adopted by ACST and VDI, consists of lowering the barrier by using materials such as InGaAs/indium

Frequency multipliers are the cornerstone of LO sources operating in the mm-wave range and beyond.

phosphide (InP), which enable the operation under zero-bias conditions.

Sb heterostructure backward tunnel diodes are a proprietary technology of HRL [59] and are based on epitaxial layers of the indium arsenide (InAs)/aluminium antimonide/gallium antimonide (GaSb) family. OMMIC also has developed its own RITD technology on an InP substrate that can be integrated with an MMIC LNA. The bandgap between InAs and GaSb, where the conduction band minimum of InAs lies energetically below the valence band maximum of GaSb, creates a natural asymmetry in the current flow with bias direction. The resulting curvature in the *I*–*V* characteristic is ideal for zero-bias direct detection. Also, it is noteworthy that these devices are very robust against temperature variations [26].

Micro hot electron bolometers (HEBs), transition edge sensors (TESs), kinetic inductor detectors (KIDs), and Golay cells are other detector technologies with potential for achieving exceptional sensitivities. However, HEBs, TESs, and KIDs are operated at cryogenic ambient temperature, and therefore, are not part of the scope of this document. Golay cells are uncooled and feature comparable performance in the sub-mm-wave range to Schottky diodes, but Golay cells feature a slower response time, in the range of 25–30 ms [17] (compared to the response time of Schottky diodes in the order of picoseconds).

The performance of a power detector is quantified by its responsivity and its noise-equivalent power (NEP). The responsivity indicates the output voltage response of the detector to an applied RF power at the input. The NEP is the minimum input power, which produces a signal-to-noise ratio of one at the output

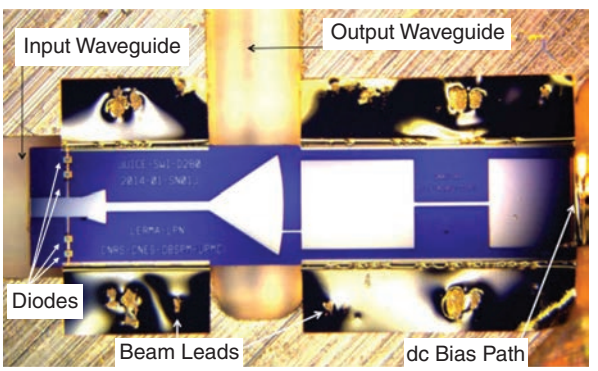

Figure 8. *Internals of a Schottky-based 260–307-GHz frequency doubler for JUICE-SWI. (Source: [16].)*

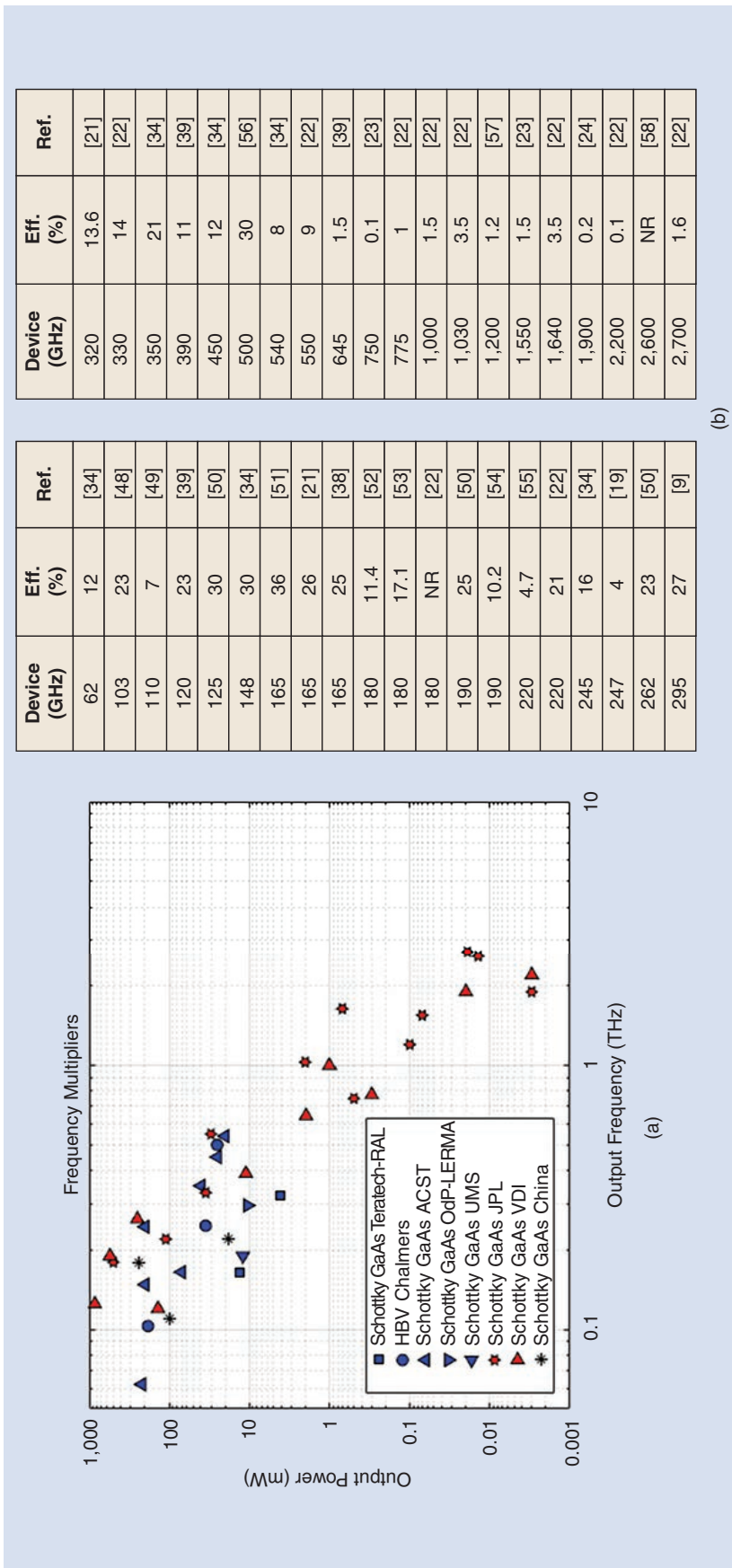

Device (GHz)	Eff. (%)	Ref.
62	12	[34]
103	23	[48]
110	7	[49]
120	23	[39]
125	30	[50]
148	30	[34]
165	36	[51]
165	26	[21]
165	25	[38]
180	11.4	[52]
180	17.1	[53]
180	NR	[22]
190	25	[50]
190	10.2	[54]
220	4.7	[55]
220	21	[22]
245	16	[34]
247	4	[19]
262	23	[50]
295	27	[9]

Device (GHz)	Eff. (%)	Ref.
320	13.6	[21]
330	14	[22]
350	21	[34]
390	11	[39]
450	12	[34]
500	30	[56]
540	8	[34]
550	9	[22]
645	1.5	[39]
750	0.1	[23]
775	1	[22]
1,000	1.5	[22]
1,030	3.5	[22]
1,200	1.2	[57]
1,550	1.5	[23]
1,640	3.5	[22]
1,900	0.2	[24]
2,200	0.1	[22]
2,600	NR	[58]
2,700	1.6	[22]

(b)

Figure 9. *(a) and (b) Output power (a) and efficiency (Eff.) (b) versus frequency of several state-of-the-art frequency multipliers from the open literature at room temperature.*

of the detector. The linearity of the detector (deviation from square law) is also an essential parameter, and a compromise among responsivity, signal-to-noise ratio, and linearity is often needed when selecting the operating point.

Current State of the Art Versus Frequency

Figure 10 shows the responsivity versus frequency and NEP of several state-of-the-art detectors from the open literature. From Figure 10, it can be seen that current state-of-the-art Schottky and tunnel diode-based detectors achieve responsivities without video amplification between 1,000 and 3,000 mV/mW from 60 to 500 GHz, between 700 and 1,000 mV/mW from 500 GHz to 1 THz, and around 100 mV/mW in the 1–1.7-THz frequency range. The NEPs of these devices range from 3 to 6 pW/√Hz at the lower end of the mm-wave spectrum [34], [39] to 12–15 pW/√Hz from 300 to 1,000 GHz [39] and 113 pW/√Hz from 1.1 to 1.7 THz [39].

Noise Sources

As explained at the beginning of this article, noise sources can be used to perform an internal radiometric calibration of spaceflight receivers. State-of-the-art mm-wave noise sources from the open literature have traditionally been implemented in the form of a reverse-biased diode in the avalanche regime. The white noise signal arises from the collision-induced ionization of free carriers in the semiconductor medium [62]. The diodes are often a Schottky device implemented on GaAs [62], similar to those used in frequency mixers and multipliers, or a PN union and a Schottky device in a series implemented on a bipolar CMOS (BiCMOS) structure [63].

Cernex and ELVA-1 use Impact ionization Avalanche Transit-Time (IMPATT) silicon diodes [64], [65].

The performance of a noise source is quantified by its excess noise ratio (ENR), which is the ratio between the output noise power of the diode in its ON and OFF operating states. The ENR can often be adjusted by tuning the bias reverse current.

Current State of the Art Versus Frequency

Figure 11 shows several state-of-the-art noise sources from the open literature. From Figure 11, it can be seen that there is a range of commercial-off-the-shelf noise sources operating in the 30–220-GHz range from commercial vendors, such as VDI, Noisecom, Eravant, Quinstar, Cernex, and ELVA-1. Teratech-RAL proposed a novel approach to noise source development, which is based on the heterodyne mixing of intermediate frequency (IF) signals [69] and which delivers ENRs higher than 23 dB up to 190 GHz. Although this article is focused on solid-state diode technology, a recent work by VTT-Millilab [70] has also been included in Figure 11, showing two noise sources implemented in the form of a silicon germanium BiCMOS amplifier with an input termination that deliver exceptional performance, such as an ENR of 25 dB at 215 GHz. These amplifier sources have a supply voltage requirement of only 2.3 V, compared with the 28 V often required by other technologies, such as Schottky [39] and IMPATT [39]. The only works reported in the sub-mm-wave region with an ENR higher than 10 dB do not use solid-state diodes either but a combination of erbium-doped fiber amplifiers and photodetectors [72], [74].

Noise sources can be used to perform an internal radiometric calibration of spaceflight receivers.

Key Areas for Future Research

The diode technology survey presented in the previous sections allows some key areas of research to be identified to push the boundaries of mm- and sub-mm-wave remote sensing instrumentation. To enable future science objectives, such as the observation of key mesosphere and lower thermosphere species like atomic oxygen, the hydroxyl radical, and nitric oxide, the maturity of Schottky mixer technology needs to be expanded to the THz region. To develop supra-THz mixer and multiplier technology, it is paramount to use high-quality epitaxial layers and air bridges and reduce the junction capacitance of the diodes by reducing the size of the anode to a small fraction of a μm^2 [45]. Other parasitics, such as the

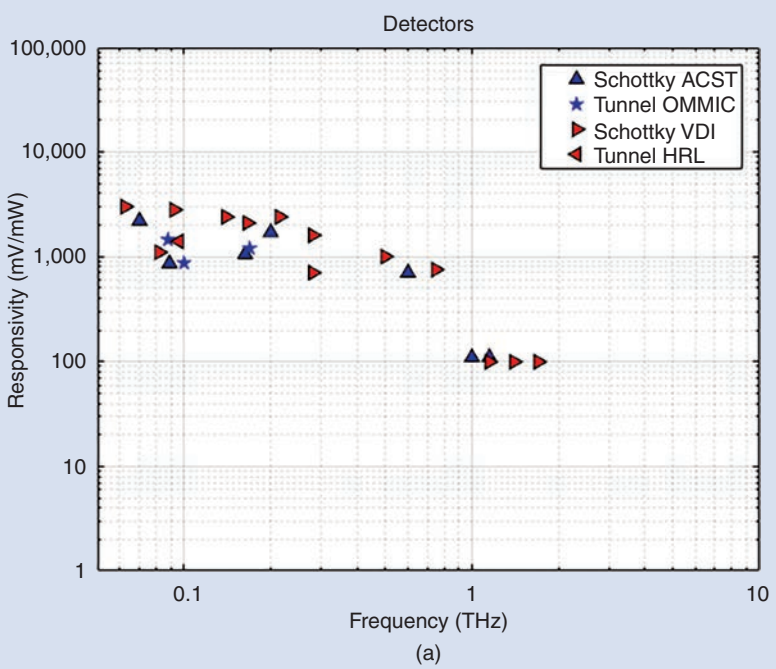

Device (GHz)	NEP (pW/√Hz)	Ref.
62.5	8.9	[39]
70	6	[34]
82	2.65	[59]
89	4.9	[26]
89	5.7	[26]
90	NR	[60]
92.5	9.5	[39]
100	11	[20]
140	11	[39]
166	5	[26]
166	3.7	[26]
166	2.5	[26]
200	6	[34]
215	11	[39]
280	16.5	[39]
280	12.5	[61]
500	11.4	[39]
600	20	[34]
750	15.2	[39]
1,000	15	[34]
1,150	113.7	[39]
1,400	113.7	[39]
1,700	113.7	[39]

(b)

Figure 10. *(a) and (b) Responsivity (a) and NEP (b) versus frequency of several state-of-the-art detectors from the open literature at room temperature, normalized to a video gain of ×1. The video gain of the detectors operating at 70, 82, 90, 100, 200, 600, and 1 THz GHz has been estimated to be ×10.*

series resistance, also need to be minimized, and this can be achieved by shortening the path between the anode and the ohmic contact. Velocity saturation effects can be mitigated by increasing the doping level, although being mindful of the impact on the ideality factory. The thickness of the passivation layers also needs to be reduced to a few tens of nm [6].

An important obstacle for expanding the operation of heterodyne receivers to the THz regime is the lack of LO power. With the advent of power amplifiers operating at frequencies higher than W-band and delivering watts of output power, the development of sub-mm-wave wave Schottky multipliers is commercially viable, and these can be extended to the THz range if precise models that account for nonideal phenomena, such as edge and fringing capacitance effects, are developed [75], [76]. The development of sub-mm-wave HBVs is also commercially viable, but HBV technology has to be brought to maturity in terms of reproducibility and reliability. GaN Schottky devices can handle watt-order input powers but feature less efficiency than their GaAs Schottky or HBV counterparts. Thus, a further investment in GaN Schottky technology is also needed.

Current LO pump requirements of fundamental and subharmonic mixers, combined with the difficulty of spaceborne LO signal generation, are hardly compatible with future focal plane imaging arrays. It is therefore important to investigate low-barrier technologies, such as InGaAs, which can reduce the LO power requirements by an order of magnitude [30].

The upper operating frequency threshold and the maturity of total power detectors and noise sources need to be increased to enable the development of novel spaceborne system architectures, such as direct detection and internal calibration. The atmospheric attenuation at frequencies higher than 300 GHz experiences a gradual increase, and therefore, the development of more sensitive detectors with lower NEP is even more important than at lower frequencies. However, there are very few examples of detectors operating above this frequency threshold, and a further investment is needed to push the limits of this technology.

Lastly, it is worth noting that all the building blocks presented in this article can benefit from using integrated diode structures. Diodes can be fabricated as discrete devices that can be soldered onto a matching network or directly integrated in a filter or a (membrane) MMIC structure. The approach of direct integration is an excellent alternative to the rather complex space-qualified diode soldering process, improves repeatability, and also reduces parasitics and misalignment issues.

Conclusions

Recent advancements in solid-state diode technology, such as a reduction in the device feature size and the use of high-quality semiconductor materials, have allowed the scientific community to develop frequency mixers, multipliers, and power detectors, which have fulfilled the requirements of recently developed single-pixel remote sensors operating in the mm-wave range

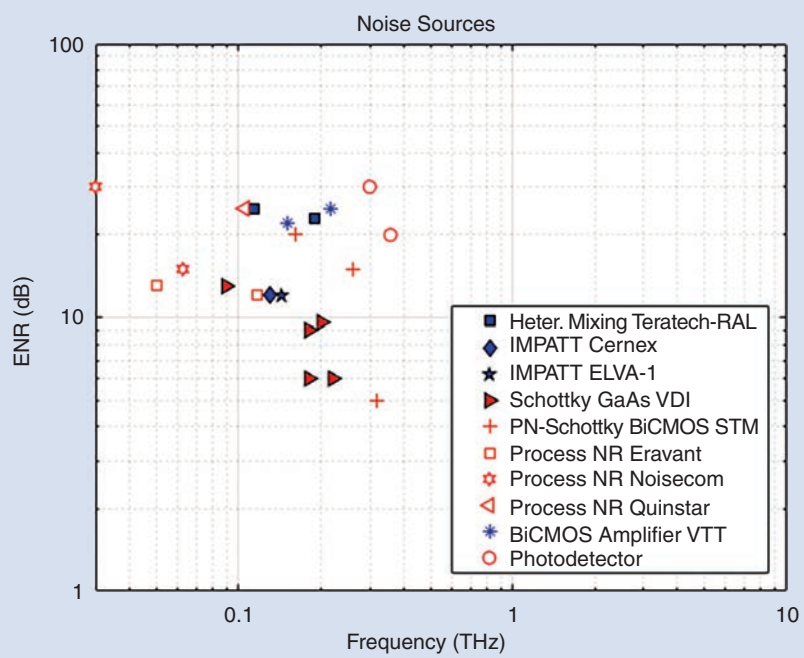

Device (GHz)	Ref.
30	[66]
50	[67]
62.5	[66]
90	[39]
105	[68]
114	[17]
120	[69]
130	[64]
140	[65]
150	[70]
170	[63]
180	[62]
180	[39]
190	[69]
200	[62]
215	[70]
220	[39]
260	[71]
300	[72]
325	[73]
357	[74]

Figure 11. *ENR versus frequency of several state-of-the-art noise sources from the open literature.*

and up to 1.2 THz, such as the MWS onboard *MetOp-SG* and the SWI onboard *JUICE*. However, it is important to continue thinking forward and investing in solid-state diode technologies. This will allow the current performance limits of fundamental receiver building blocks to be pushed forward and future demands for additional LO power in support of future multipixel focal plane arrays to be accommodated. Equally important is to extend the frequency of operation of the diodes in support of future THz sensor development and research novel technologies, such as internal onboard calibration subsystems, to improve the payload design and mission efficiency.

References

[1] D. Cuadrado-Calle *et al*., "EQM front-end receivers at 183 and 229 GHz for the Microwave Sounder on MetOp-SG," in *Proc. 33rd General Assembly Scientific Symp. URSI*, 2020, pp. 1–4, doi: 10.23919/URSIGASS49373.2020.9232214.

[2] A. Maestrini *et al*., "1200GHz and 600GHz Schottky receivers for JUICE-SWI," in *Proc. 27th Int. Symp. Space Terahertz Technol*., 2016, pp. 44–46.

[3] B. Thomas *et al*., "Millimeter & sub-millimeter wave radiometer instruments for the next generation of polar orbiting meteorological satellites – MetOp-SG," in *Proc. 39th Int. Conf. Infrared, Millimeter, Terahertz Waves*, 2014, pp. 1–3, doi: 10.1109/IRMMW-THz.2014.6956005.

[4] D. Cuadrado-Calle, D. George, B. Ellison, G. A. Fuller, and K. Cleary, "Celestial signals: Are low-noise amplifiers the future for millimeter-wave radio astronomy receivers?" *IEEE Microw. Mag*., vol. 18, no. 6, pp. 90–99, 2017, doi: 10.1109/MMM.2017.2712038.

[5] M. Hoefle *et al*., "Low noise 89 GHz detector module for MetOp-SG," in *Proc. Eur. Microw. Conf. (EuMC)*, 2015, pp. 395–398, doi: 10.1109/EuMC.2015.7345783.

[6] A. Maestrini *et al*., "Schottky diode-based terahertz frequency multipliers and mixers," *C. R. Physique*, vol. 11, nos. 7–8, pp. 480–495, 2010, doi: 10.1016/j.crhy.2010.05.002.

[7] N. J. Cronin and V. J. Law, "Planar millimeter-wave diode mixer," *IEEE Trans. Microw. Theory Techn*., vol. 33, n. no. 9, pp. 827–830, 1984, doi: 10.1109/TMTT.1985.1133140.

[8] W. L. Bishop *et al*., "A novel whiskerless Schottky diode for millimeter and submillimeter wave application," in *Proc. IEEE MTT-S Int. Microw. Symp. Dig*., 1987, pp. 607–610, doi: 10.1109/MWSYM.1987.1132483.

[9] I. Mehdi, J. V. Siles, C. Lee, and E. Schlecht, "THz diode technology: Status, prospects, and applications," *Proc. IEEE*, vol. 105, no. 6, pp. 990–1007, Jun. 2017, doi: 10.1109/JPROC.2017.2650235.

[10] A. Simon, A. Grub, V. Krozer, K. Beilenhoff, and H. Hartnagel, "Planar THz Schottky diode based on a quasi vertical diode structure," in *Proc. 4th Int. Symp. Space Terahertz Technol. (ISSTT)*, 1993, pp. 392–403.

[11] B. N. Ellison *et al*., "First results for a 2.5 THz Schottky diode waveguide mixer," in *Proc. 7th Int. Symp. Space Terahertz Technology*, 1996, pp. 12–14.

[12] E. L. Kollberg and A. Rydberg, "Quantum-barrier-varactor diode for high efficiency millimeter-wave multipliers," *IEEE Electron. Lett*., vol. 25, no. 25, pp. 1696–1697, 1989, doi: 10.1049/el:19891134.

[13] X. Melique *et al*., "5-mW and 5% efficiency 216-GHz InP-based heterostructure barrier varactor tripler," *IEEE Microw. Guided Wave Lett. ** (1991–2000), vol. 8, no. 11, pp. 384–386, 1998, doi: 10.1109/75.736253.

[14] P. Sobis *et al*., "Low noise GaAs Schottky TMIC and InP Hemt MMIC based receivers for the ISMAR and SWI instruments," in *Proc. Micro-and Millimetre Wave Technology Techn. Workshop ESA-ESTEC*, Nov. 27, 2014, pp. 25–27.

[15] J. Treuttel *et al*., "Compact sub millimeter wavelength heterodyne radiometer for arrays," in *Proc. 30th URSI General Assembly Scientific Symp.*, 2011, pp. 1–4, doi: 10.1109/URSIGASS.2011.6050797.

[16] J. Treuttel *et al*., "A 520–620-GHz Schottky receiver front-end for planetary science and remote sensing with 1070 K–1500 K DSB noise temperature at room temperature," *IEEE Trans. THz Sci. Technol*., vol. 6, no. 1, pp. 148–155, Jan. 2016, doi: 10.1109/TTHZ.2015.2496421.

[17] C. Viegas, "Broadband Schottky diode components for millimetre-wave instrumentation," Ph.D. thesis, Univ. of Manchester, Manchester, U.K., 2017.

[18] B. Thomas, J. Treuttel, B. Alderman, D. Matheson, and T. Narhi, "Application of substrate transfer to a 190 GHz frequency doubler and 380 GHz sub-harmomic mixer using MMIC foundry Schottky diodes," in *Proc. SPIE Millimeter Submillimeter Detectors Instrumentation Astronomy*, 2008, vol. 7020, pp. 659–667, doi: 10.1117/12.789083.

[19] J. Stake, A. Malko, T. Bryllert, and J. Vukusic, "Status and prospects of high-power heterostructure barrier varactor frequency multipliers," *Proc. IEEE*, vol. 105, no. 6, pp. 1008–1019, Jun. 2017, doi: 10.1109/JPROC.2016.2646761.

[20] OMMIC. Accessed: Nov. 2021. [Online]. Available: https://www.ommic.com/

[21] B. Alderman *et al*., "Schottky diode technology at Rutherford Appleton Laboratory," in *Proc. IEEE Int. Conf. Microw. Technol. Comput. Electromagn.*, 2011, pp. 4–6, doi: 10.1109/ICMTCE.2011.5915577.

[22] J. V. Siles, K. B. Cooper, C. Lee, R. H. Lin, G. Chattopadhyay, and I. Mehdi, "A new generation of room-temperature frequency-multiplied sources with up to 10× Higher output power in the 160-GHz–1.6-THz range," *IEEE Trans. THz Sci. Technol*., vol. 8, no. 6, pp. 596–604, Nov. 2018, doi: 10.1109/TTHZ.2018.2876620.

[23] G. Chattopadhyay *et al*., "An all-solid-state broad-band frequency multiplier chain at 1500 GHz," *IEEE Trans. Microw. Theory Techn*., vol. 52, no. 5, pp. 1538–1547, 2004, doi: 10.1109/TMTT.2004.827042.

[24] A. Maestrini *et al*., "A 1.7 to 1.9 THz local oscillator source," *IEEE Microw. Wireless Compon. Lett*., vol. 14, no. 6, pp. 253–255, Jun. 2004, doi: 10.1109/LMWC.2004.828027.

[25] I. Mehdi *et al*., "Improved 240 GHz subharmonically pumped planar Schottky diode mixers for space-borne applications," *IEEE Trans. Microw. Theory Techn*., vol. 46, no. 12, pp. 2036–2042, Dec. 1998, doi: 10.1109/22.739280.

[26] T. Decoopman *et al*., "Millimetre-wave detectors for direct detection radiometers," in *Proc. Global Symp. Millimeter Waves (GSMM) ESA Workshop Millimetre-Wave Technol. Appl.*, 2016, pp. 1–4, doi: 10.1109/GSMM.2016.7500316.

[27] T. A. Growden *et al*., "Superior growth, yield, repeatability, and switching performance in GaN-based resonant tunneling diodes," *Appl. Phys. Lett*., vol. 116, no. 11, p. 113,501, 2020, doi: 10.1063/1.5139219.

[28] E. Schlecht *et al*., "Schottky diode based 1.2 THz receivers operating at room-temperature and below for planetary atmospheric sounding," *IEEE Trans. THz Sci. Technol*., vol. 4, no. 6, pp. 661–669, Nov. 2014, doi: 10.1109/TTHZ.2014.2361621.

[29] D. Pardo, "Analysis and design of multipliers and mixers via Monte Carlo modelling at THz bands," Tesis Doctoral, Universidad Politecnica de Madrid, 2014.

[30] D. Pardo *et al*., "InGaAs Schottky technology for THz mixers," in *Proc. 28th Int. Symp. Space Terahertz Technol*., 2017, pp. 1–4.

[31] H. Wang *et al*., "Schottky diode components for MetOp SG satellites," in *Proc. 1st Annu. Active Passive RF Devices Seminar*, 2013, pp. 63–63.

[32] M. Anderberg, P. Sobis, V. Drakinskiy, J. Schleeh, A. Emrich, and J. Stake, "A 183-GHz Schottky diode receiver with 4 dB noise figure," in *Proc. IEEE MTT-S Int. Microw. Symp. (IMS)*, 2019, pp. 172–175, doi: 10.1109/MWSYM.2019.8701051.

[33] I. Oprea, A. Walber, O. Cojocari, H. Gibson, R. Zimmermann, and H. L. Hartnagel, "183 GHz mixer on InGaAs Schottky diodes," in *Proc. 21st Int. Symp. Space Terahertz Technol.*, 2010.

[34] ACST GmbH. Accessed: Nov. 2021. [Online]. Available: https://acst.de

[35] B. Thomas, A. Maestrini, and G. Beaudin, "A low-noise fixed-tuned 300–360 GHz sub-harmonic mixer using planar Schottky diodes," *IEEE Microw. Wireless Compon. Lett*., vol. 15, no. 12, pp. 865–867, Dec. 2005, doi: 10.1109/LMWC.2005.859992.

[36] P. J. Sobis, N. Wadefalk, A. Emrich, and J. Stake, "A broadband, low noise, integrated 340 GHz Schottky diode receiver," *IEEE Microw. Wireless Compon. Lett*., vol. 22, no. 7, pp. 366–368, Jul. 2012, doi: 10.1109/LMWC.2012.2202280.

[37] S. Rea, B. Thomas, and D. Matheson, "A 320–360 GHz Sub-Harmonically pumped Image-Rejection Mixer for earth observation applications," in *Proc. 33rd Int. Conf. Infrared, Millimeter Terahertz Waves*, 2008, p. 1, doi: 10.1109/ICIMW.2008.4665707.

[38] B. Thomas *et al*., "Submillimetre-wave receiver developments for ICI onboard MetOP-SG and ice cloud remote sensing instruments," in *Proc. IEEE Int. Geosci. Remote Sens. Symp.*, 2012, pp. 1278–1281, doi: 10.1109/IGARSS.2012.6351306.

[39] Virginia Diodes Inc. Accessed: Nov. 2021. [Online]. Available: https://www.vadiodes.com

[40] J. Treuttel, D. Gonzalez-Ovejero, C. Lee, and I. Mehdi, "Enhancing heterodyne system performances using fundamental millimeter wave mixers with 36 GHz instantaneous IF bandwidth and 35% relative detection bandwidth," in *Proc. Int. Conf. Infrared, Millimeter, Terahertz Waves*, 2018, pp. 1–2, doi: 10.1109/IRMMW-THz.2018.8510158.

[41] B. Thomas *et al*., "A broadband 835–900 GHz fundamental balanced mixer based on monolithic GaAs membrane Schottky diodes," *IEEE Trans. Microw. Theory Techn*., vol. 58, no. 7, pp. 1917–1924, Jul. 2010, doi: 10.1109/TMTT.2010.2050181.

[42] A. Hammar *et al*., "Low noise 874 GHz receivers for the International Submillimetre Airborne Radiometer (ISMAR)," *Rev. Sci. Instrum*., vol. 89, no. 5, p. 055104, 2018, doi: 10.1063/1.5017583,

[43] N. R. Erickson and T. M. Goyette, "Terahertz Schottky-diode balanced mixers," presented at the SPIE OPTO, Integrated Optoelectronic Devices, 2009, vol. 7215, p. 721,508, doi: 10.1117/12.807505.

[44] D. Hayton *et al*., "A compact Schottky heterodyne receiver for 2.06 THz Neutral Oxygen [OI]," in *Proc. 43rd Int. Conf. Infrared, Millimeter, Terahertz Waves*, 2018, pp. 1–2, doi: 10.1109/IRMMW-THz.2018.8510120.

[45] B. T. Bulcha *et al*., "Design and characterization of 1.8–3.2 THz Schottky-based harmonic mixers," *IEEE Trans. THz Sci. Technol*., vol. 6, no. 5, pp. 737–746, Sep. 2016, doi: 10.1109/TTHZ.2016.2576686.

[46] D. Jayasankar, V. Drakinskiy, M. Myremark, P. Sobis, and J. Stake, "Design and development of 3.5 THz Schottky-based fundamental mixer," in *Proc. 50th Eur. Microw. Conf.*, 2021, pp. 595–598, doi: 10.23919/EuMC48046.2021.9338204.

[47] B. T. Bulcha, J. L. Hesler, V. Drakinskiy, J. Stake, and N. S. Barker, "Development of 3–5 THz harmonic mixer," in *Proc. 2017 42nd Int. Conf. Infr., Millim., THz Waves*, pp. 1–2, doi: 10.1109/IRMMW-THz.2017.8067104.

[48] A. Malko, T. Bryllert, J. Vukusic, and J. Stake, "Silicon integrated InGaAs/InAlAs/AlAs HBV frequency Tripler," *IEEE Electron Device Lett*., vol. 34, no. 7, pp. 843–845, Jul. 2013, doi: 10.1109/LED.2013.2262131.

[49] Y. Wang *et al*., "Design of a 110GHz GaN Schottky diode frequency Tripler," in *Proc. 12th* U.K.-*Europe-China Workshop Millim. Waves THz Technol. (UCMMT)*, 2019, pp. 1–2, doi: 10.1109/UCMMT47867.2019.9008344.

[50] E. Bryerton, S. Retzloff, and J. Hesler, "High-power submillimeter wave solid-state sources," in *Proc. 12th Global Symp. Millim. Waves*, 2019, pp. 29–31, doi: 10.1109/GSMM.2019.8797648.

[51] S. Khanal *et al*., "Characterisation of THz Schottky diodes for MetOp-SG instruments," in *Proc. 26th Int. Symp. Space THz Technol*., Cambridge, MA, USA, 2015.

[52] S. Liang *et al*., "A 177–183 GHz high-power GaN-based frequency doubler with over 200 mW output power," *IEEE Electron Device Lett*., vol. 41, no. 5, pp. 669–672, May 2020, doi: 10.1109/LED.2020.2981939.

[53] J. V. Siles, E. Schlecht, R. Lin, C. Lee, and I. Mehdi, "High-efficiency planar Schottky diode based frequency multipliers optimized for high-power operation," in *Proc. 35th Int. Conf. Infr., Millim. THz Waves*, Aug. 2015, pp. 2835–2843, doi: 10.1109/IRMMW-THz.2015.7327677.

[54] J. V. Siles *et al*., "A single-waveguide in-phase power-combined frequency doubler at 190 GHz," *IEEE Microw. Wireless Compon. Lett*., vol. 21, no. 6, pp. 332–334, Jun. 2011, doi: 10.1109/LMWC.2011.2134080.

[55] Y. Yang *et al*., "Development of high power 220 GHz frequency Triplers based on Schottky diodes," *IEEE Access*, vol. 8, pp. 74,401–74,412, Apr. 2020, doi: 10.1109/ACCESS.2020.2988454.

[56] M. Ingvarson, A. O. Olsen, and J. Stake, "Design and analysis of 500GHz heterostructure barrier varactor quintuplers," in *Proc. 14th Int. Symp. Space THz Technol*., 2003.

[57] J. Bruston, A. Maestrini, D. Pukala, S. Martin, B. Nakamura, and I. Mehdi, "A 1.2 THz planar Tripler using GaAs membrane based chips," in *Proc. 12th Int. Symp. Space THz Technol*., San Diego, CA, USA, Feb. 2001, pp. 310–331.

[58] A. Maestrini *et al*., "Frequency tunable electronic sources working at room temperature in the 1 to 3 THz band," in *Proc. SPIE*, Oct. 2012, vol. 8496, p. 84960F, doi: 10.1117/12.929654.

[59] J. Gutiérrez, K. Zeljami, J. P. Pascual, T. Fernández, and A. Tazón, "Comparison of microstrip W-band detectors based on zero bias Schottky-diodes," *Electronics*, vol. 8, no. 12, p. 1450, 2019, doi: 10.3390/electronics8121450.

[60] H. P. Moyer *et al*., "W-band Sb-diode detector MMICs for passive millimeter wave imaging," *IEEE Microw. Wireless Compon. Lett*., vol. 18, no. 10, pp. 686–688, 2008, doi: 10.1109/LMWC.2008.2003471.

[61] L. Liu, J. L. Hesler, H. Xu, A. W. Lichtenberger, and R. M. Weikle, "A broadband quasi-optical terahertz detector utilizing a zero bias Schottky diode," *IEEE Microw. Wireless Compon. Lett*., vol. 20, no. 9, pp. 504–506, Sep. 2010, doi: 10.1109/LMWC.2010.2055553.

[62] N. Ehsan, J. Piepmeier, M. Solly, S. Macmurphy, J. Lucey, and E. Wollack, "A robust waveguide millimeter-wave noise source," in *Proc. 2015 Eur. Microw. Conf.*, pp. 853–856, doi: 10.1109/EuMC.2015.7345898.

[63] J. C. A. Goncalves *et al*., "A 130 to 170 GHz integrated noise source based on avalanche silicon Schottky diode in BiCMOS 55 nm for in-situ noise characterization," in *Proc. 2017 Int. Conf. Microelectron. Test Struct*., pp. 1–3, doi: 10.1109/ICMTS.2017.7954271.

[64] Cernex, Inc. Accessed: Nov. 2021. [Online]. Available: https://cernex.com/

[65] ELVA-1. Accessed: Nov. 2021. [Online]. Available: https://elva-1.com/

[66] Noisecom. Accessed: Nov. 2021. [Online]. Available: https://www.noisecom.com/

[67] Eravant. Accessed: Nov. 2021. [Online]. Available: https://www.eravant.com/

[68] Quinstar. Accessed: Nov. 2021. [Online]. Available: https://www.quinstar.com/

[69] C. Viegas *et al*., "Millimeter-wave noise sources using heterodyne mixing of signals," in *Proc. IEEE MTT-S Int. Microw. RF Conf*., 2019, pp. 1–2, doi: 10.1109/IMaRC45935.2019.9118675.

[70] H. Forstén, J. H. Saijets, M. Kantanen, M. Varonen, M. Kaynak, and P. Piironen, "Millimeter-wave amplifier-based noise sources in SiGe BiCMOS technology," *IEEE Trans. Microw. Theory Techn*., vol. 69, no. 11, pp. 4689–4696, 2021, doi: 10.1109/TMTT.2021.3104028.

[71] J. C. A. Goncalves, Ph.D. thesis, Université de Lille, Lille, France, 2019.

[72] H. Song and M. Yaita, "On-wafer noise measurement at 300 GHz using UTC-PD as noise source," *IEEE Microw. Wireless Compon. Lett*., vol. 24, no. 8, pp. 578–580, 2014, doi: 10.1109/LMWC.2014.2324762.

[73] H. Ghanem *et al*., "Modeling and analysis of a broadband Schottky diode noise source up to 325 GHz based on 55-nm SiGe BiCMOS technology," *IEEE Trans. Microw. Theory Techn*., vol. 68, no. 6, pp. 2268–2277, 2020, doi: 10.1109/TMTT.2020.2980513.

[74] H.-J. Song, N. Shimizu, N. Kukutsu, T. Nagatsuma, and Y. Kado, "Microwave photonic noise source from microwave to sub-terahertz wave bands and its applications to noise characterization," *IEEE Trans. Microw. Theory Techn*., vol. 56, no. 12, pp. 2989–2997, 2008, doi: 10.1109/TMTT.2008.2007325.

[75] D. Moro-Melgar *et al*., "Monte Carlo study of 2-D capacitance fringing effects in GaAs planar Schottky diodes," *IEEE Trans. Electron Devices*, vol. 63, no. 10, pp. 3900–3907, 2016, doi: 10.1109/TED.2016.2601341.

[76] B. Orfao, B. G. Vasallo, D. Moro-Melgar, S. Pérez, J. Mateos, and T. González, "Analysis of surface charge effects and edge fringing capacitance in planar GaAs and GaN Schottky barrier diodes," *IEEE Trans. Electron Devices*, vol. 67, no. 9, pp. 3530–3535, 2020, doi: 10.1109/TED.2020.3007374.

Integrated Filter–Amplifiers

Yang Gao, Xiaobang Shang, Lei Li, Cheng Guo, and Yi Wang

Amplifiers and filters are essential components in microwave systems. An amplifier is used to increase the signal strength, and it is usually cascaded by filters for frequency selection or harmonic rejection [1]–[3]. Their functionalities require a precise design of the individual parts as well as the way in which they are connected. The common approach is to make individual components with a system impedance that is usually 50 Ω. A generic example of the filters and amplifier in a generalized receiver is shown in Figure 1(a).

Rather than the conventional topology, where the amplifiers, matching networks, and filters are separate, the amplifier and the filters can be integrated, allowing the input matching network (IMN) and the output matching network (OMN) of the transistor to be removed [see Figure 1(b)]. In this approach, the filters are designed to replace the matching networks whose elements can be on-chip lumped circuits or planar structures. Thus, loss reduction can be achieved through two aspects: first, the ohmic and dielectric loss of the microstrip matching circuitry can be minimized; secondly, the insertion loss and risk of multiple reflections associated with the port-to-port interconnection can be avoided. Apart from reduced loss, such integrated filter–amplifiers also have appealing advantages, such as significantly reduced size and improved performance in terms of matching and efficiency over the conventional approach based on individually cascaded components. These advantages are particularly attractive for millimeter-wave and terahertz applications,

Yang Gao (gaoyang678@outlook.com) and Lei Li (lilei@zzu.edu.cn) are with the School of Physics and Microelectronics, Zhengzhou University, Zhengzhou, 450001, China. Xiaobang Shang (xiaobang.shang@npl.co.uk) is with the National Physical Laboratory, Teddington, TW11 0LW, U.K. Cheng Guo (guocheng@xjtu.edu.cn) is with Xi'an Jiaotong University, Xi'an, 710049, China. Yi Wang (y.wang.1@bham.ac.uk) is with the University of Birmingham, Birmingham, B15 2TT, U.K.

Digital Object Identifier 10.1109/MMM.2022.3155034
Date of current version: 5 May 2022

where the insertion loss of the matching network is usually a significant concern. Here, we will review the recent advances of the integrated filter–amplifiers and present featured techniques and examples.

Extending Passive Filter Design Methods to Active Circuits

Passive filter synthesis techniques have been well established [3]. These techniques normally deal with filters with real loads (usually 50 Ω), which is a valid assumption for typical microwave filters. However, in general, the loads presented by transistors are not real, and they present a complex frequency-dependent impedance, as shown in Figure 2(a). Filter–amplifier integration concerns the transformation of the transistor port impedances so that the amplifier response can be fully specified using Chebyshev, Butterworth, elliptical, or other filtering functions [see Figure 2(b)]. The challenge is to incorporate the complex impedances presented by the transistors into the design of passive filters where the real-valued source and load impedances are usually considered. The matching filters of the transistor also play an important role in the amplifier's characteristics, such as efficiency, harmonic terminations, stability, and noise figure.

Let us start the discussion with broadband filter–amplifiers, followed by narrow-band filter–amplifiers. For broadband amplifiers, matching filters are commonly realized using multistage *LC* element-based ladder networks, enabling the use of the well-developed classic wideband filter synthesis. The matching filter design techniques can be classified into numerical or analytical methods [4]. A numerical solution, namely the real frequency technique, was proposed by Carlin and Komiak [5] and further developed by Yarman and Carlin [6]. Fano, for the first time, came up with transcendental equations for broadband filter matching

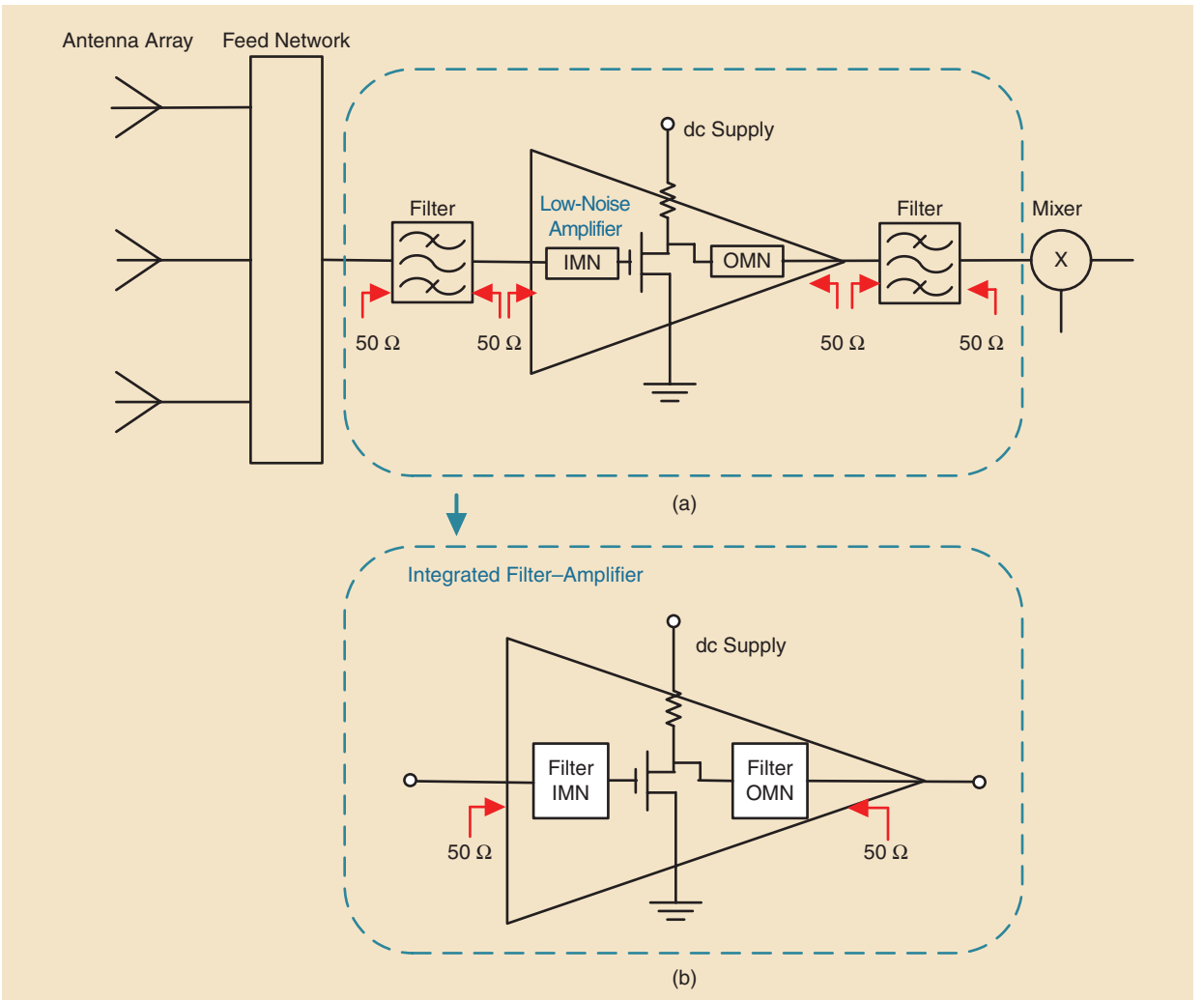

Figure 1. *(a) A typical receiver system and (b) an integrated filter–amplifier. The amplifier and filters can be integrated, eliminating the need for separate impedance matching circuits. IMN: input matching network; OMN: output matching network.*

network with arbitrary impedance to achieve the desired return loss [7]. Dawson proposed closed-form formulas and tabulated methods for broadband amplifier matching [8]. Other analytical techniques were also developed and utilized, such as the clipping contour method [9], simplified real frequency technique [10], even–odd-mode analysis technique [11], and reactance-compensation technique [12]. The distributed amplifier (DA) is also a common solution to broadband amplifications [13]. Unlike these aforementioned techniques, actively coupled resonators, active impedance/admittance inverters, and negative resistance were also applied to satisfy the filter transfer functions in DAs [13]–[15]. Compared with passive filter ladder-based amplifiers, the advantages of the DAs are flat gain, flat group delay, low noise figure, and low voltage standing-wave ratio (VSWR) over a wider bandwidth. The disadvantage of the active distributed filter is the need for multiple transistors, which increase the circuit complexity and cost and result in relatively low efficiency.

Narrowband amplifiers deal with a relatively simpler situation because the complex frequency-dependent impedance can be treated as a constant value within the band of interest. By incorporating the arbitrary complex impedance of the transistor into the filter, the filtering matching can be readily maintained. There exist indirect and direct integration techniques for the filter–amplifiers. For the indirect approach, the imaginary component of the complex impedance is absorbed first and then transferred to the 50-Ω common terminal impedance. This is followed by the classic filter synthesis. The equivalent circuit analysis method can be employed in the conversion of arbitrary complex port impedance. In practice, coupled lines [16] and quarter-wavelength impedance inverters [17] are often used in the conversion of the impedance's imaginary part, and the filter couplings are adjusted to match the real parts. The drawbacks of the indirect approaches lie in the additional circuit complexity and loss introduced by the transformation structure.

Unlike the indirect approach, the direct filter–amplifier integration method treats passive elements and active elements as an entity and utilizes resonator-based filters to offer the matching for amplifiers. Figure 3 shows diagrams of a typical n-coupled resonator filter and an integrated filter–amplifier. In the resonator-based filter–amplifier topology, the complex impedance conversion can be achieved by choosing appropriate coupling values [18]. For example, if the transistor has a complex input admittance $Y_{\text{in}} = a + jb$ (a and b are real constants), to achieve the desired Chebyshev (or other) filtering response, the coupling coefficients can be modified as [19]–[21]

The challenge is to incorporate the complex impedances presented by the transistors into the design of passive filters where the real-valued source and load impedances are usually considered.

$$m_{k,k} = -\frac{b}{a \cdot g_k g_{k+1}}, \tag{1}$$

$$m_{k,\text{in}} = m_{\text{in},k} = \sqrt{\frac{a^2 + b^2}{a \cdot g_k g_{k+1}}}, \tag{2}$$

where g_k and g_{k+1} are the standard g values defined in the Chebyshev low-pass prototype [3]. $m_{k,k}$ is the self-coupling of the kth resonator that is adjacent to the transistor port; $m_{k,\text{in}}$ and $m_{\text{in},k}$ are the couplings between the kth resonator and the transistor.

This resonator-based filter integration technique is ideally suitable for applications at millimeter-wave and terahertz frequencies in that the resonators could have very low loss if made from waveguide structures [22]–[24]. Resonator-based filter matching approaches

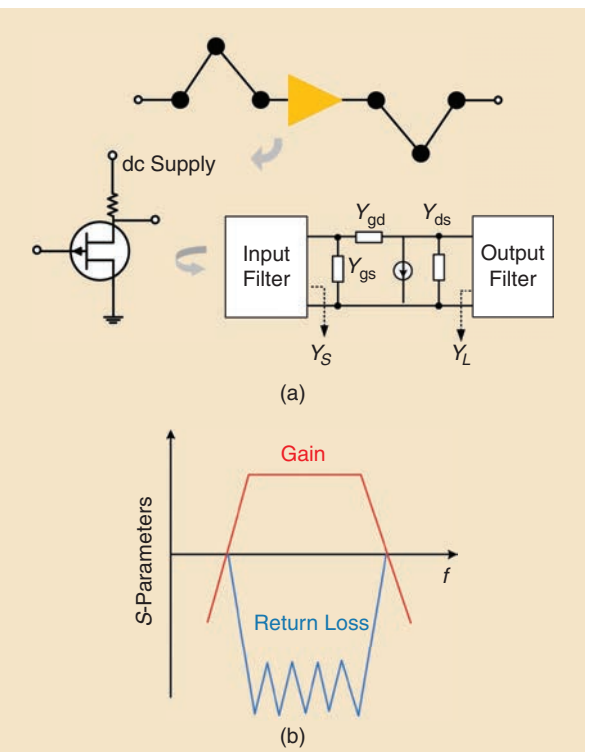

Figure 2. *(a) Filters matching the complex input and output impedances of a transistor. Y_S and Y_L are the optimum source and load admittances depending on the types of amplifiers; Y_{gd}, Y_{gs}, and Y_{ds} are the admittances of the transistor small-signal model. (b) Illustrative filter–amplifier S-parameter response with a filtering function and gain.*

Planar circuit filters are commonly used for matching transistors because of their low production cost and ease of fabrication.

can also be employed to provide the desired matching for other types of microwave circuits with complex port impedance. For example, we have demonstrated this on filter–amplifiers with different topologies [19]–[21], orthomode transducers [25], Schottky diode-based frequency triplers [26], [27] and subharmonic mixers [28]. See also "Active Coupling Matrix Synthesis for Filter–Amplifiers."

Physical Construction of Integrated Filter–Amplifiers

Now let us move on to the practical amplifier design. Electrical and physical characteristics of the integrated filter–amplifiers are closely related to the transistors, packaging process, choice of filter types, and integration techniques. It should be noted that the design of the filter–amplifier is a two-stage approach, where the type of filter (e.g., microstrip, coaxial, waveguide, or dielectric) can be considered at the second stage. The technique described here can be used in different types of filters. The choice of the filter types depends upon the device or system requirements, such as insertion loss, achievable bandwidth, power-handling capability, noise, power, temperature stability, size, and cost. The physical construction of the filter and how it is integrated with the on-chip transistor is an important practical consideration. A few different schemes of filter–amplifier integration using various physical structures will be reviewed later.

The losses of the integrated filters (including dielectric loss, ohmic loss, and radiation loss) are determined not only by the physical and electrical parameters of the materials but also by their physical construction. Table 1 summarizes the typical unloaded Q-factors of several popular microwave resonators. Advanced manufacturing technologies allow various physical constructions to be precisely fabricated. Apart from traditional computer numerical control machining, emerging manufacturing technologies, such as 3D printing, SU-8, laser cutting, and silicon deep reactive ion etching have been utilized in making various passive microwave circuits [30]. Combining these advanced machining technologies with the new packaging and integration scheme is expected to greatly reduce the loss and improve the efficiency of the amplifier and advance the technologies into new applications at increasingly higher frequencies.

Microstrip Filter–Amplifiers

Planar circuit filters are commonly used for matching transistors because of their low production cost and ease of fabrication [31]–[35]. Compared with nonplanar

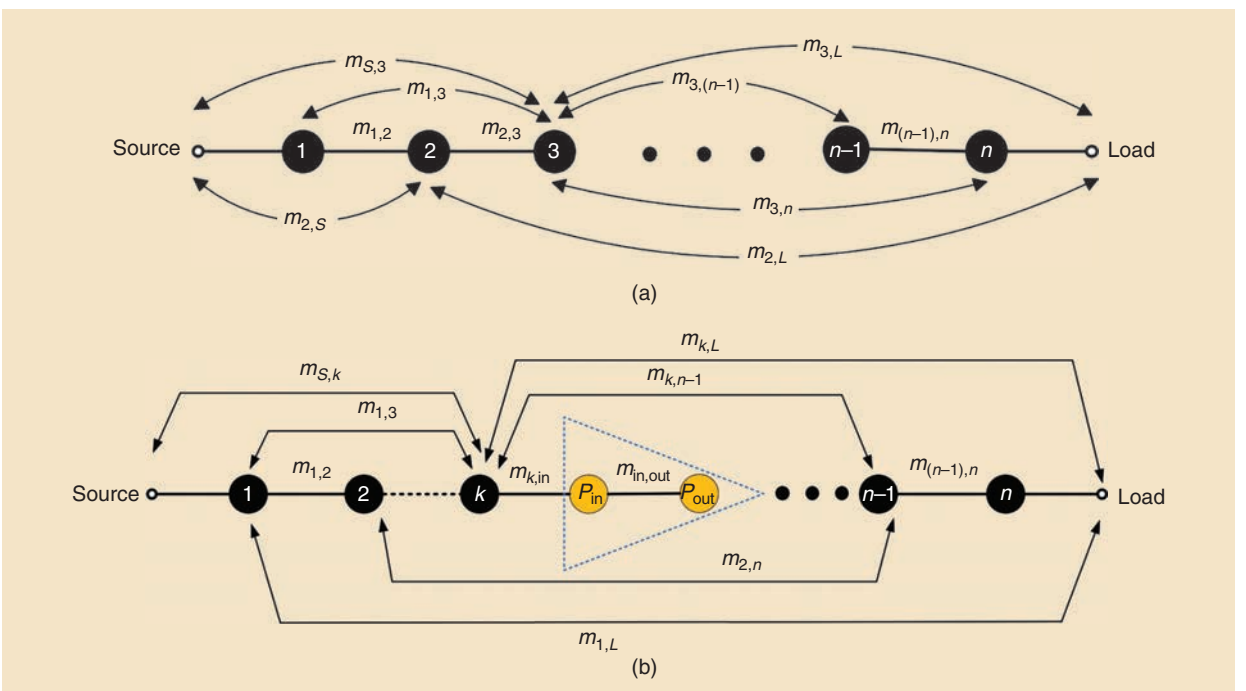

Figure 3. *The general topology of (a) a passive filter and (b) an integrated filter–amplifier with coupling coefficients $m_{i,j}$ and a set of resonators labeled 1 to n showing couplings between the resonators. The active element (transistor) is represented by the nonresonating nodes P_{in} and P_{out}.*

Active Coupling Matrix Synthesis for Filter–Amplifiers

The concept of the coupling matrix was first introduced by Atia and Williams in the 1970s and implemented using waveguide cavity filters [S1]. Initially, an $N \times N$ matrix design approach was developed based on lumped circuit elements and an ideal transformer coupling. This was later extended to the $N+2$ coupling matrix, where port impedances were included [S2]. Recently, $N+3$ and $N+4$ active coupling matrices based on direct-synthesis and optimization methods were developed [19]–[21] to deal with the design of filter–amplifiers. The typical $N+2$ passive coupling matrix and the recently developed active coupling matrix elements are illustrated in Figure S1.

Three topology examples and their corresponding S-parameter responses are given in Figure S2. Their coupling matrices can be directly synthesized for filter matching with a Chebyshev response when resonators are coupled to the input or output of the transistor, as shown in Figure S2(a) and (b). When the transistor is placed between resonators, as shown in Figure S2(c), the coupling matrix can be obtained using the optimization method [21]. This is due to the existence of feedback from the transistor, making it more difficult to calculate the coupling coefficients using the direct synthesis technique. Apart from the S-parameters, noise figures have also been derived using the coupling matrix technique

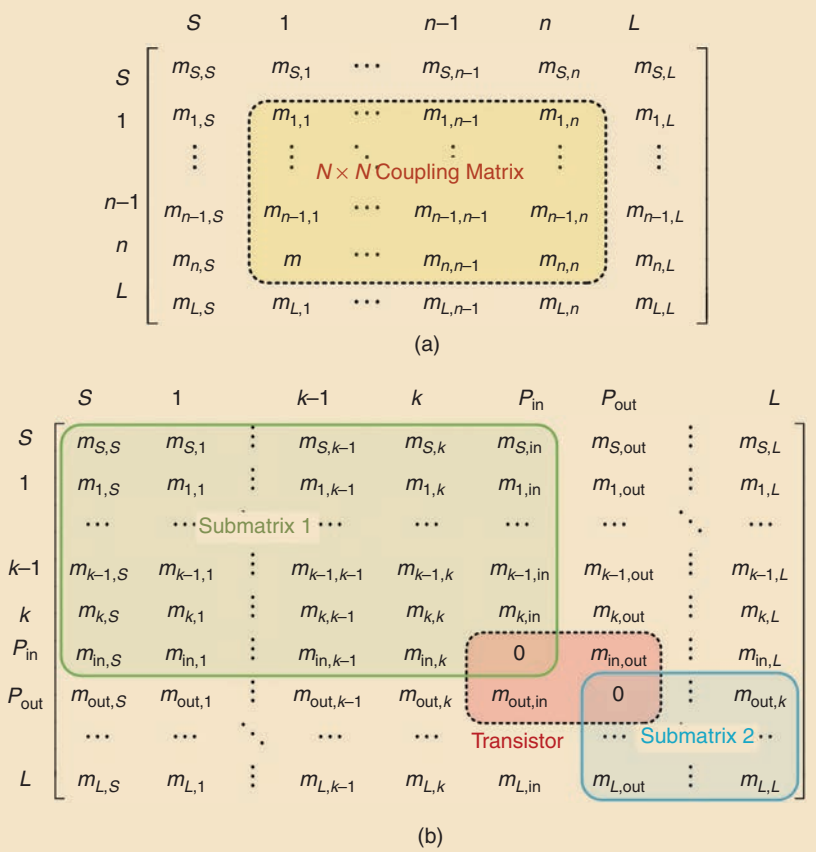

Figure S1. *General coupling matrix of (a) a passive filter and (b) an integrated filter–amplifier. Note that the active coupling matrix includes the active transistor elements $m_{in,out}$ and $m_{out,in}$, which represent the couplings (or feedback) between the transistor's input and output. $m_{i,j}$ represents the interresonator coupling; $m_{S,j} = m_{j,S}$ and $m_{L,j} = m_{j,L}$ ($j = 1$ to n) are the couplings from the source and load; $m_{j,in} = m_{in,j}$ and $m_{out,j} = m_{j,out}$ are the couplings from the resonators to the transistor's gate and drain.*

Continued

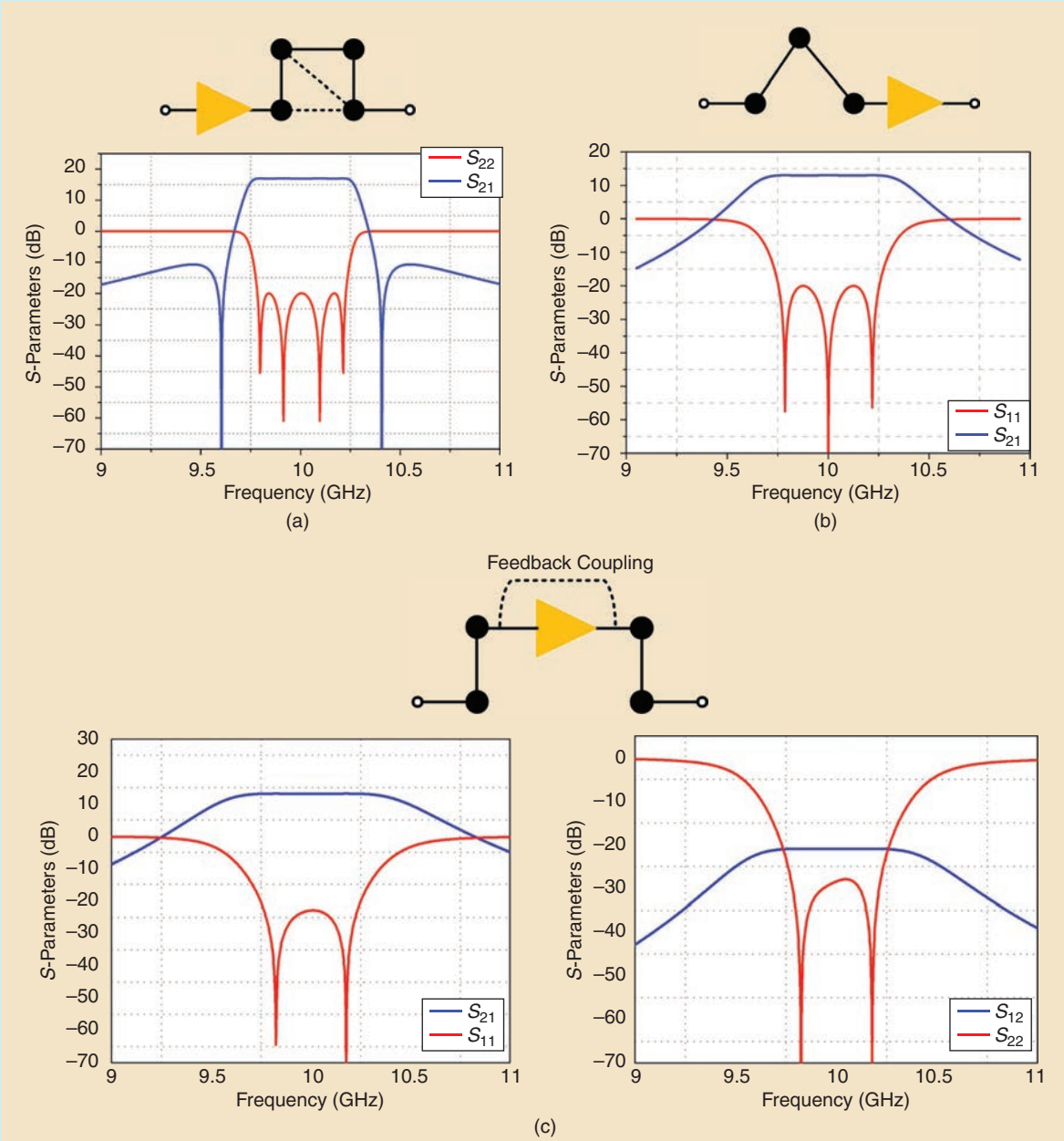

Figure S2. *Examples of filter–amplifier topologies and their corresponding S-parameter responses where resonators are coupled (a) to the input of the transistor, (b) to the output of the transistor, and (c) to both sides of the transistor.*

[21]. It is worth noting that the active coupling matrix approach can also be applicable to other amplifier parameters, such as stability factor, gain, and efficiency. The active coupling matrix represents a new and potentially generic design approach for filter–amplifiers and other types of active and nonlinear circuits.

References

[S1] A. E. Atia and A. E. Williams, "Narrow-bandpass waveguide filters," *IEEE Trans. Microw. Theory Techn.*, vol. 20, no. 4, pp. 258–265, 1972, doi: 10.1109/TMTT.1972.1127732.

[S2] R. J. Cameron, C. M. Kudsia, and R. R. Mansour, "Synthesis of networks: Direct coupling matrix synthesis methods," *Microwave Filters for Communication Systems: Fundamentals, Design, and Applications*. Hoboken, NJ, USA: Wiley, 2018, pp. 247–294.

metallic structures, planar matching filters bring in relatively high losses. As frequencies go higher to the submillimeter or terahertz regime, the losses increase rapidly and impair the amplifier's performance. Therefore, planar filter–amplifiers are often found in relatively low-frequency applications.

Figure 4 shows a schematic of a narrowband microstrip power amplifier with a filter integrated at the transistor output [31]. The equivalent circuit analysis technique is used. Through a microstrip tuning line, the imaginary part of the transistor impedance can be absorbed. The normalized real input impedance was obtained using the coupling coefficients, expressed by

$$Z_{\text{in}} = \frac{M_{1,2}^2}{M_{S,1}^2 M_{2,L}^2}. \tag{3}$$

TABLE 1. Typical *Q*-factors of various types of resonators [29].

	Microstrip/ Stripline	SIW	DR	Rectangular Waveguide
Unloaded *Q*-factor	50–200	150–1,000	200–3,000	1,000–12,000

SIW: substrate integrated waveguide; DR: dielectric resonator.

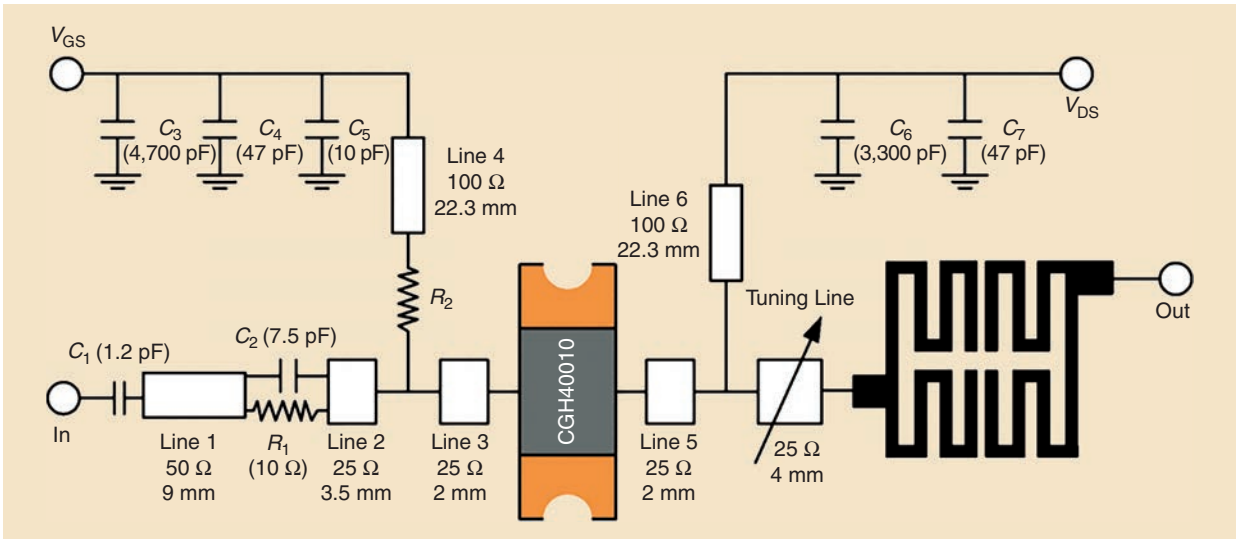

Figure 4. *A schematic of the power amplifier integrated with a filter at its output [31].*

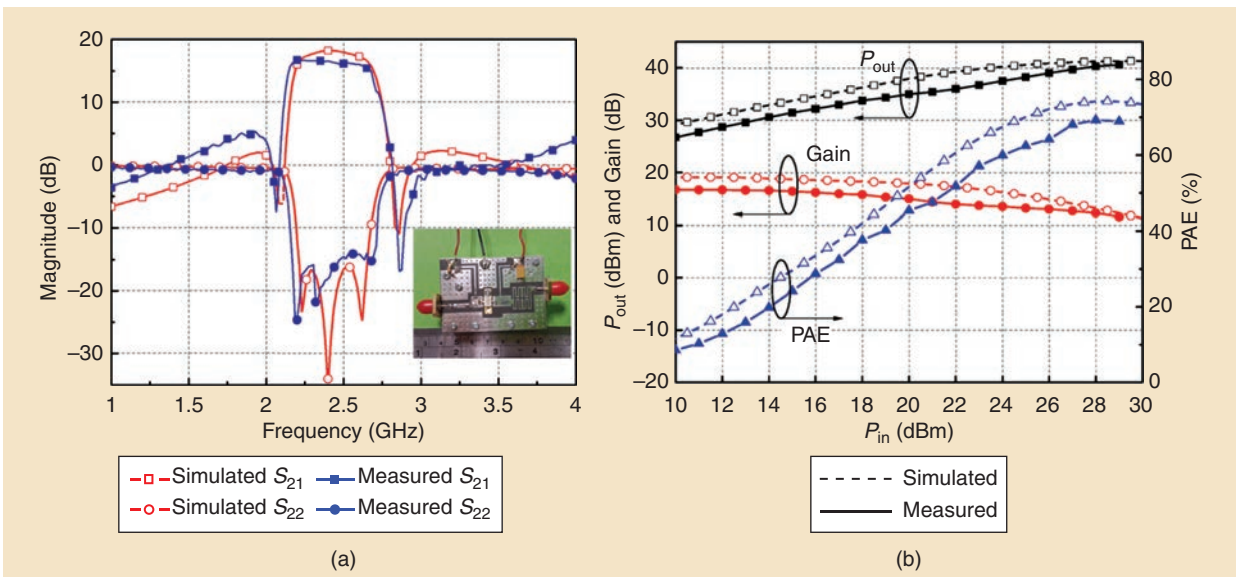

Figure 5. *The performance of the filter–amplifier shown in Figure 4. (a) Simulated and measured S-parameters. (b) Simulated and measured P_{out}, gain, and PAE [31]. PAE: power-added efficiency.*

To fulfill the required input impedance Z_{in}, the external coupling can be adjusted by controlling external quality factor Q_e, according to

$$M_{S,1} = \frac{1}{\sqrt{Q_e \cdot FBW}}. \quad (4)$$

The embedded filtering circuit not only realized the impedance matching at the operating frequency but also eliminated the harmonics. Figure 5(a) illustrates the simulated and measured S-parameter results, showing a gain of around 16.4 dB over the passband. Two transmission zeros (TZs) are created at the passband edges to enhance the selectivity. Figure 5(b) gives the simulated and measured P_{out}, gain, and power-added efficiency (PAE) of the power amplifier at a fixed frequency of 2.45 GHz. The PAE is up to 69.8%, and the corresponding output power and gain are 40.1 dBm and 11.8 dB, respectively. With the integrated filter, the skirt selectivity is increased, and the total size of the integrated component is $0.65\,\lambda_g \times 0.48\,\lambda_g$, smaller than the cascaded power amplifier and filters.

Substrate Integrated Waveguide Filter–Amplifiers

A substrate integrated waveguide (SIW) becomes an attractive candidate transmission medium as frequencies go higher because of its lower loss compared to microstrip circuits. SIW technology usually presents a good performance for applications under 100 GHz. Also, the good manufacturability of SIWs provides a unique and attractive solution for mass-production or cost-sensitive applications, even though the Q-factor (150–1,000) of SIW resonators is generally lower than that of metallic waveguide resonators (1,000–12,000).

As a planar structure, an SIW is easy to integrate with on-chip active devices. Specifically, broadband amplifiers can be more feasibly achieved using SIW matching structures because they support propagation of transverse electric modes and avoid parasitic transverse magnetic modes. De-embedded coupling slots and stepped impedance transitions are often used in controlling the external coupling strength for impedance transformation. The interresonator couplings are commonly implemented by using irises.

Evanescent (EVA) mode cavity resonators based on SIW technology have been utilized for the design of the narrowband power amplifier's OMN in [24]. The circuit diagram and the physical construction are illustrated in Figure 6. The coupling coefficients are determined by the geometries of the coupling iris, and the external couplings are realized using slot apertures. By tuning the bias line, the second harmonic is terminated in the high-efficiency region, while the fundamental

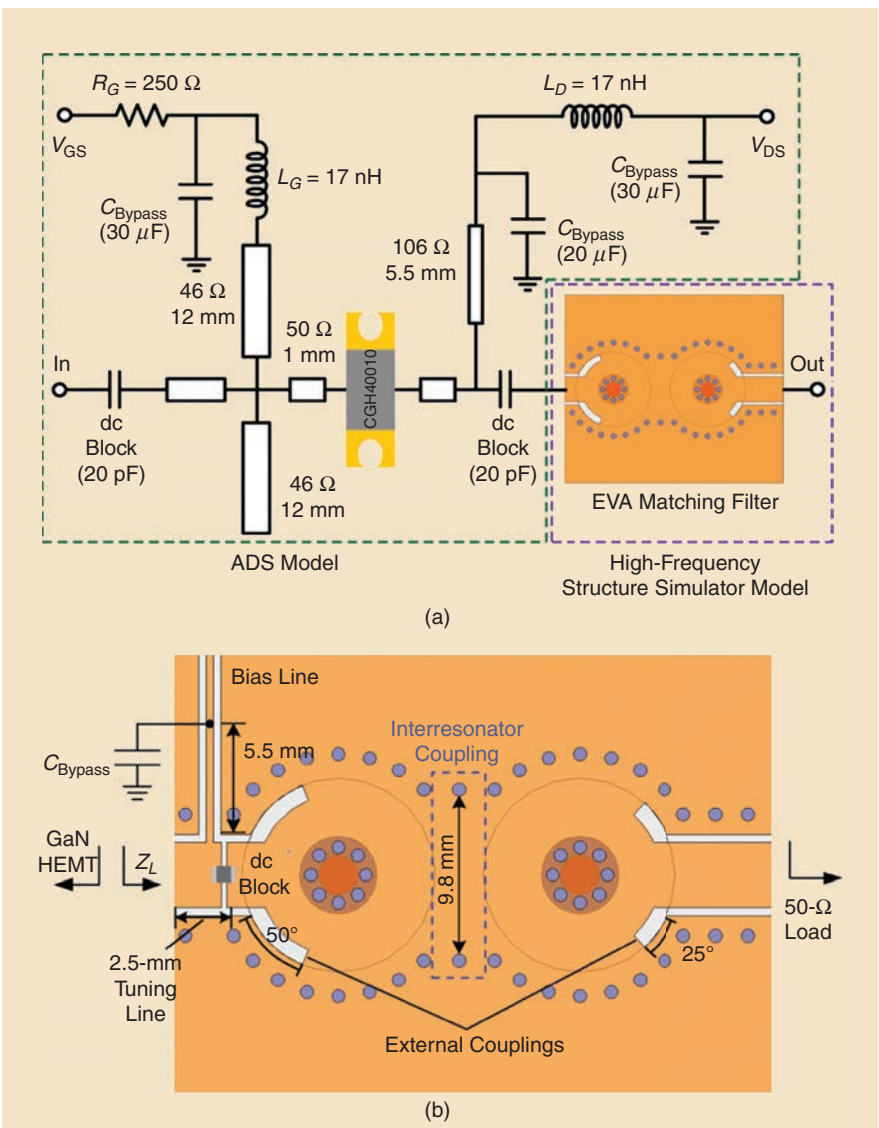

Figure 6. *(a) A circuit schematic of the co-designed filter–amplifier. (b) Construction of the two-pole SIW filter [24]. ADS: Advanced Design System; GaN: gallium nitride; HEMT: high-electron mobility transistor.*

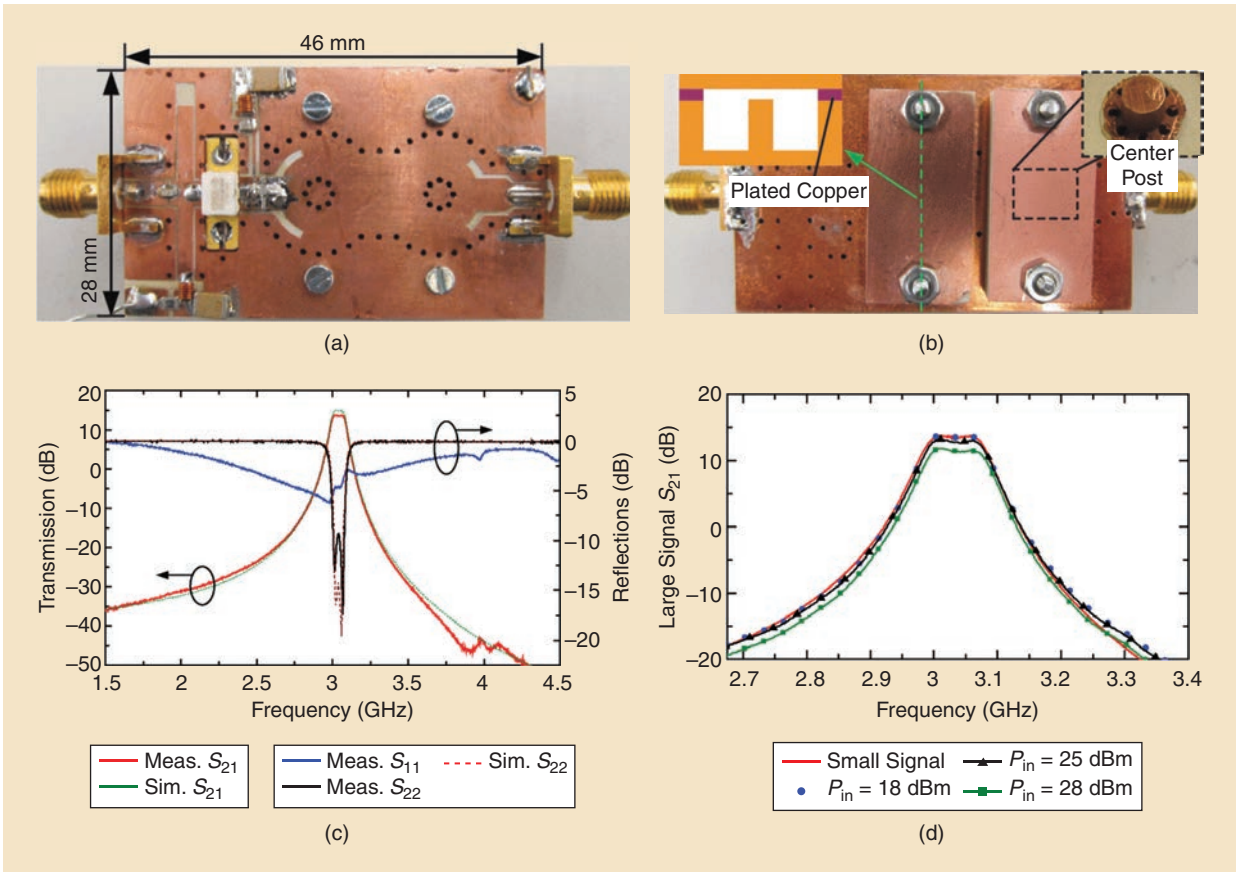

Figure 7. *Photos of the fabricated SIW filtering power amplifier. (a) Front side and (b) backside. (c) Simulated and measured small-signal results. (d) Simulated and measured large-signal results [24].*

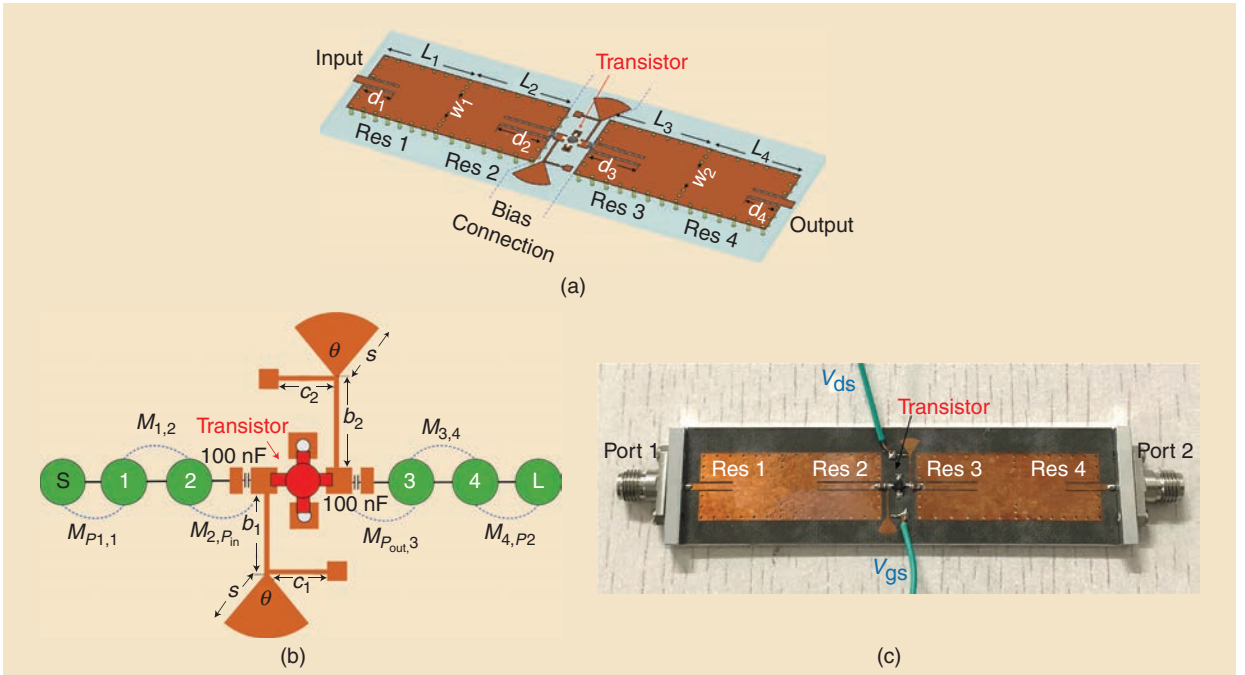

Figure 8. *(a) The layout of the SIW filter–amplifier. (b) A schematic of the filter matching at the input and output of the transistor. (c) The fabricated SIW filter–amplifier [21]. Res: resonator.*

impedance almost remains the same. The small- and large-signal responses of the filter–amplifier are given in Figure 7. Note that the co-design approach enhances the efficiency from 64% (cascaded) to around 72% (co-design) at a power saturation of 40 dBm.

A more general filter–amplifier topology is given in [21], where an all-resonator structure is applied to replace both the IMN and OMN of the transistor, as illustrated in Figure 8. The amplifier geometries can be extracted accurately using the coupling matrix, which resembles the classic passive filter design method. The size of the coupling iris (w_i in Figure 8) can be determined from the coupling coefficients. As shown in Figure 9, the two-pole Chebyshev responses are displayed in both S_{11} and S_{22} responses; S_{21} shows about a 9-dB gain over the passband, and the measured noise figure is around 2.5 dB in the passband. Unlike the previous examples, where the input and output matching filters are modeled individually, the feedback coupling between output and input in the transistor is considered in [21]. This provides an integrated design method for which the physical geometrics can be extracted more accurately, yielding a much reduced electromagnetic simulation time.

Waveguide Filter–Amplifiers

If an even higher frequency or power capacity must be fulfilled in the amplifier applications, the use of high-performance nonplanar components becomes imperative. A metallic waveguide featuring a high Q-factor is an attractive structure at higher frequencies, especially above 100 GHz. 3D metallic filters in the form of rectangular, cylindrical, or spherical shapes are usually selected for loss-sensitive, high-performance, and high-power capacity applications [19], [22], [36]. The main disadvantage is that the structure is bulky in size, and the manufacturing could be costly. One challenge of using 3D metallic waveguides is the transition between on-chip transistor and waveguide.

Transition structures with a high coupling efficiency are not easy to realize. E-plane probes, dipoles, and finlines are the common choices of the transitions. Other contactless or air-filled transitions, such as step ridges, can avoid dielectric loss, with the penalty of increased

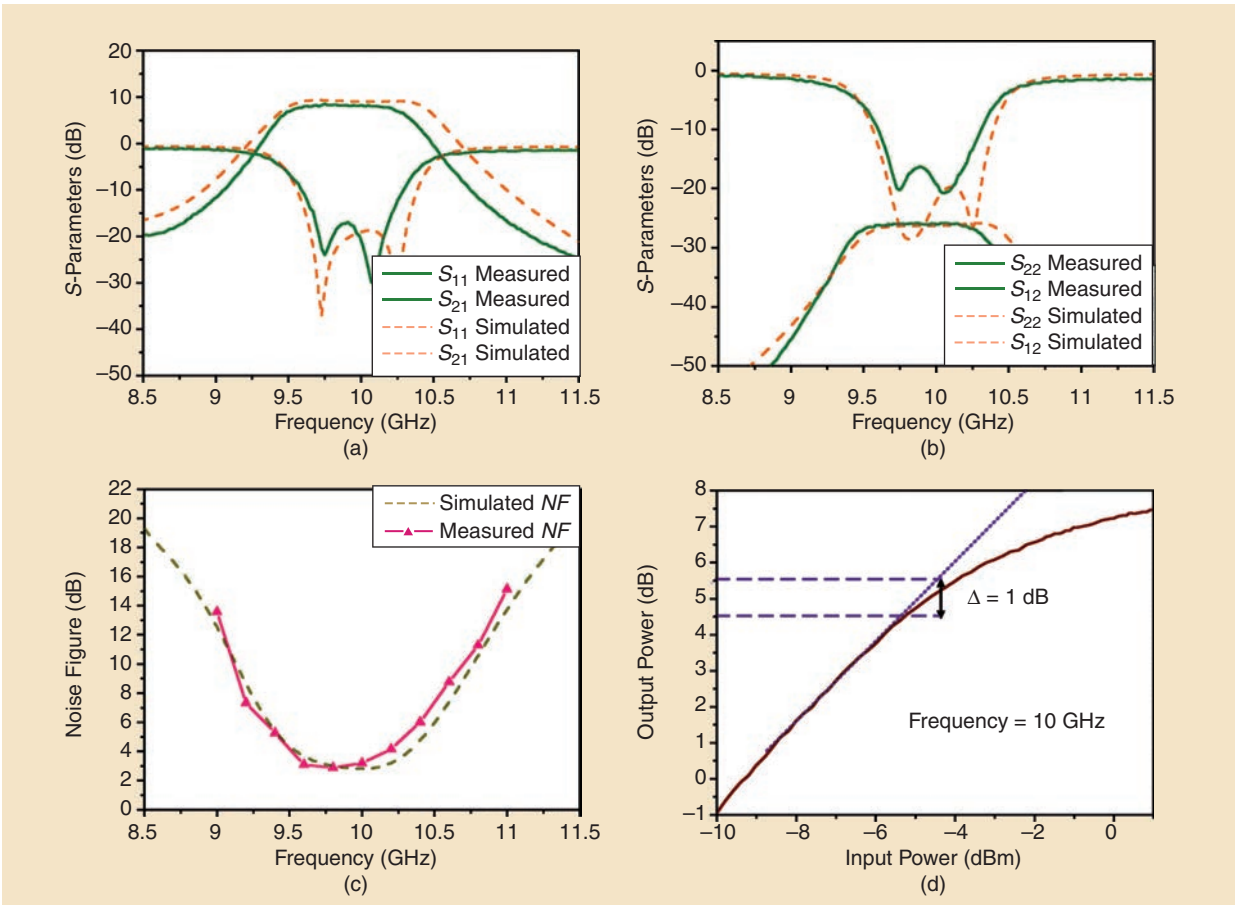

Figure 9. *Simulation and measurement results of the filter–amplifier shown in Figure 8. (a) S_{11} and S_{21}, (b) S_{22} and S_{12}, (c) noise figure, and (d) 1-dB compression point (P1-dB) measurement [21]. NF: noise figure.*

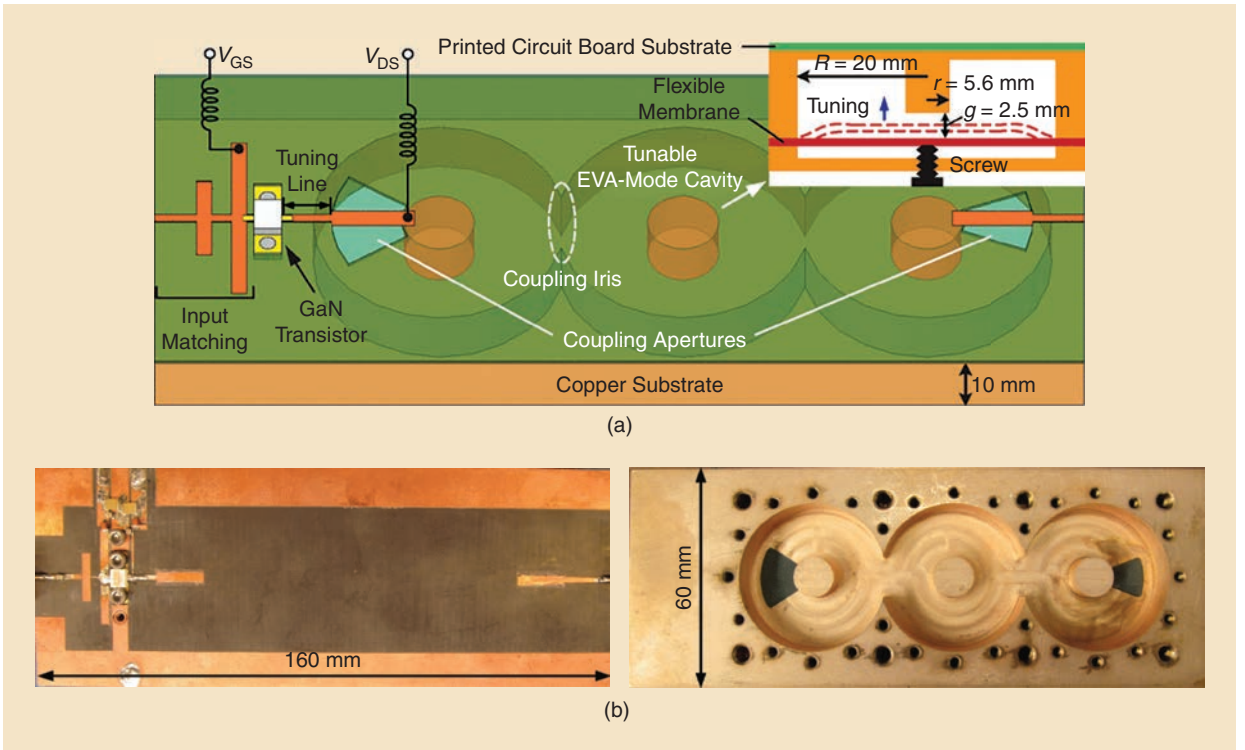

Figure 10. *(a) The physical construction of the power amplifier with a tunable three-pole EVA mode filter. (b) Photos of the fabricated filter integrated power amplifier [23].*

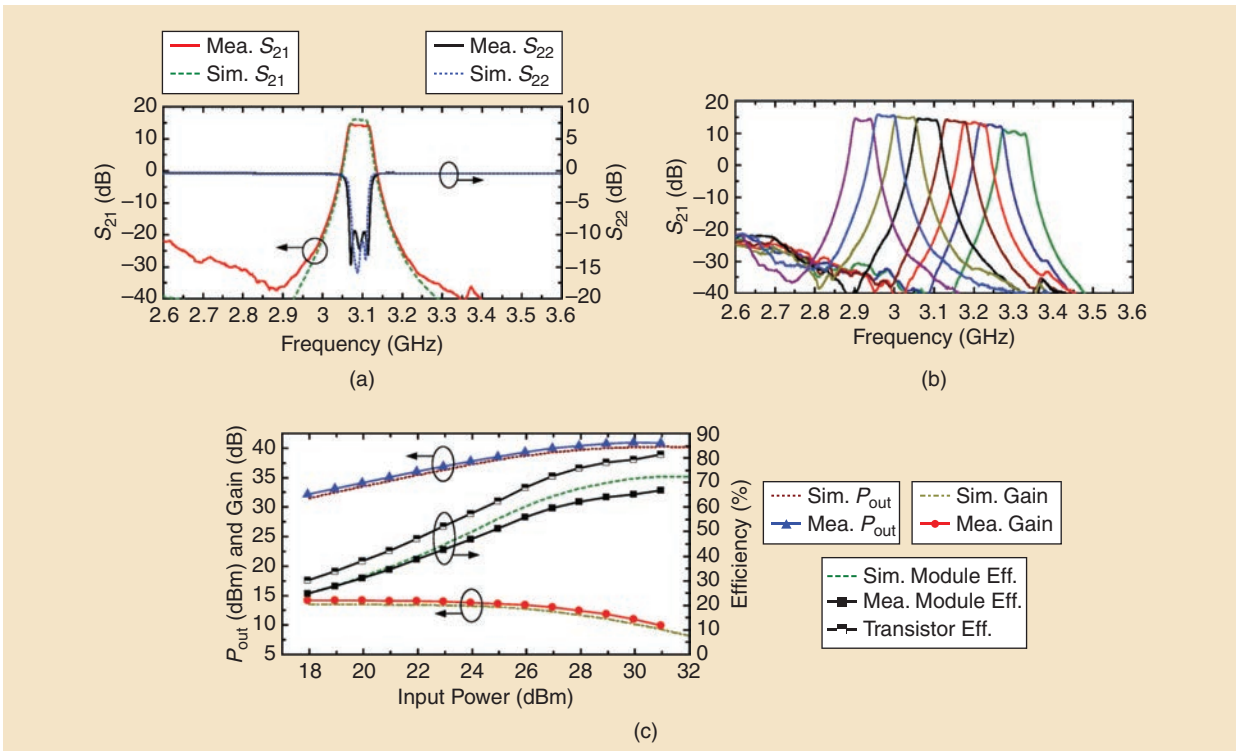

Figure 11. *The performance of the filter–amplifier in Figure 10. (a) Measured and simulated small-signal frequency response at 3.1 GHz. (b) Measured small-signal frequency response over the entire tuning range. (c) Measured output power and gain versus input power at 3.1 GHz [23]. Mea.: measured; Sim.: simulated; Eff.: efficiency.*

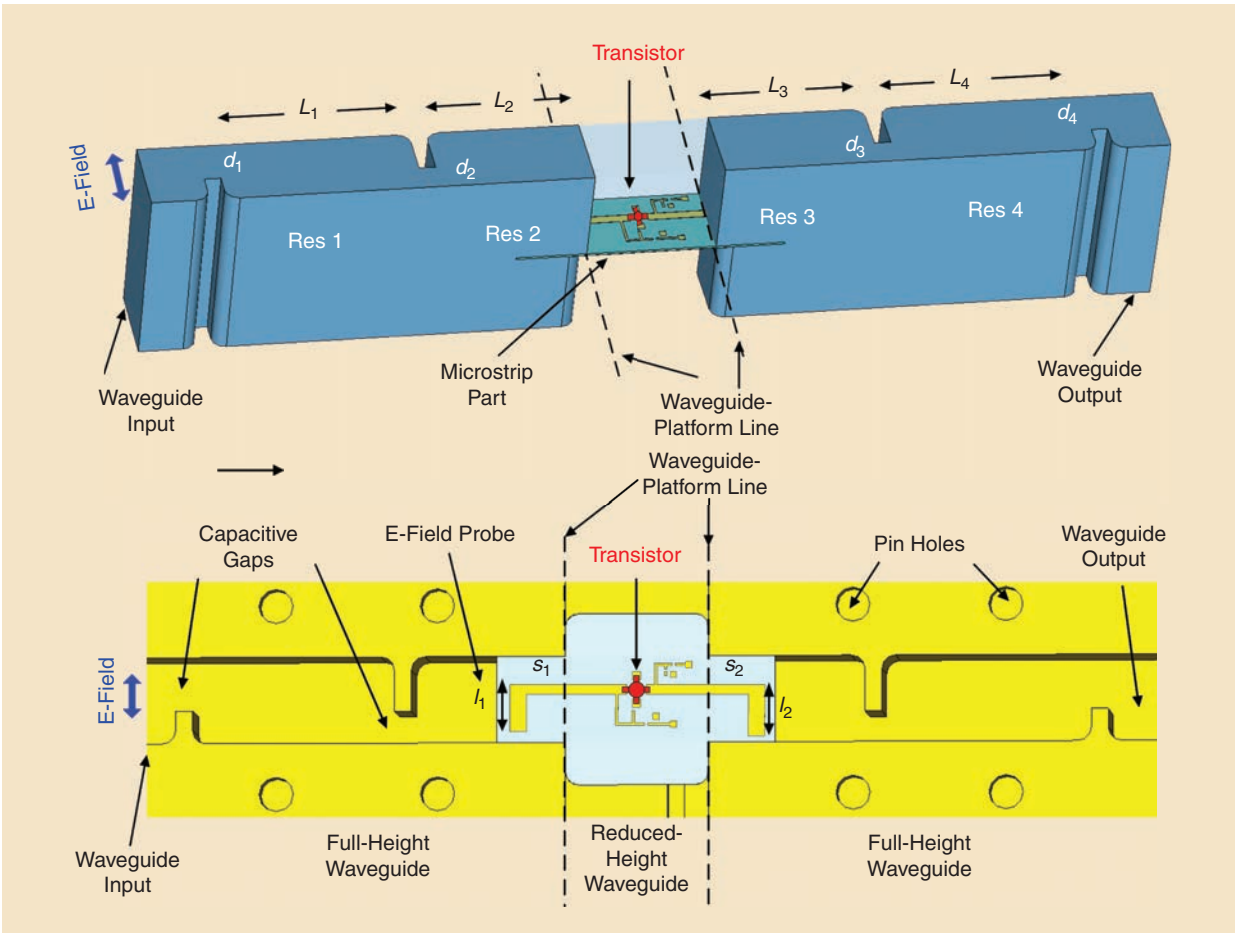

Figure 12. *Diagrams of the waveguide filter–amplifier [20].*

complexity and cost. For waveguide filter–amplifier integration, the active inverter or resonator methods discussed previously no longer apply because it is difficult to model active elements within a 3D construction.

Figure 10 illustrates a tunable filtering power amplifier where the resonators are tuned using screws [23]. The center frequency can be tuned from 2.95 to 3.35 GHz, as shown in Figure 11. The power efficiency reaches its highest point of 67%, and the corresponding gain compression is about 2 dB at the maximum output power of 40 dBm.

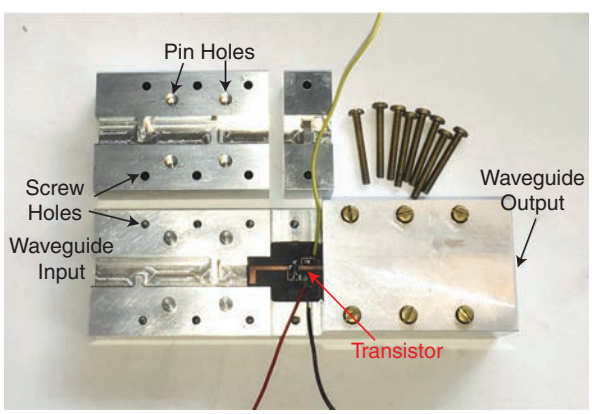

Figure 13. *The fabricated waveguide filter–amplifier [20].*

Figure 12 illustrates a waveguide filter–amplifier with E-plane probes used for coupling the waveguide and the transistor [20]. The interresonator couplings are achieved by the waveguide iris, while the external couplings are determined by the probe structure. A photo of the waveguide amplifier is given in Figure 13. The measured results in Figure 14 show the Chebyshev filtering response of S_{11} and S_{22}. The S_{21} curve indicates a gain of around 11.1 dB over the passband. A brief design procedure of this waveguide filter–amplifier is described in "Design Steps of the Integrated Waveguide Filter–Amplifier."

Dielectric Resonator Filter–Amplifiers

Dielectric resonators (DRs) feature a high Q-factor and lower cost than waveguide cavities [37], [38]. As illustrated in Figure 15, a DR filter was employed to realize output impedance matching of a gallium nitride (GaN) transistor power amplifier [38]. The analytical method was used for the DR-based filter–amplifier

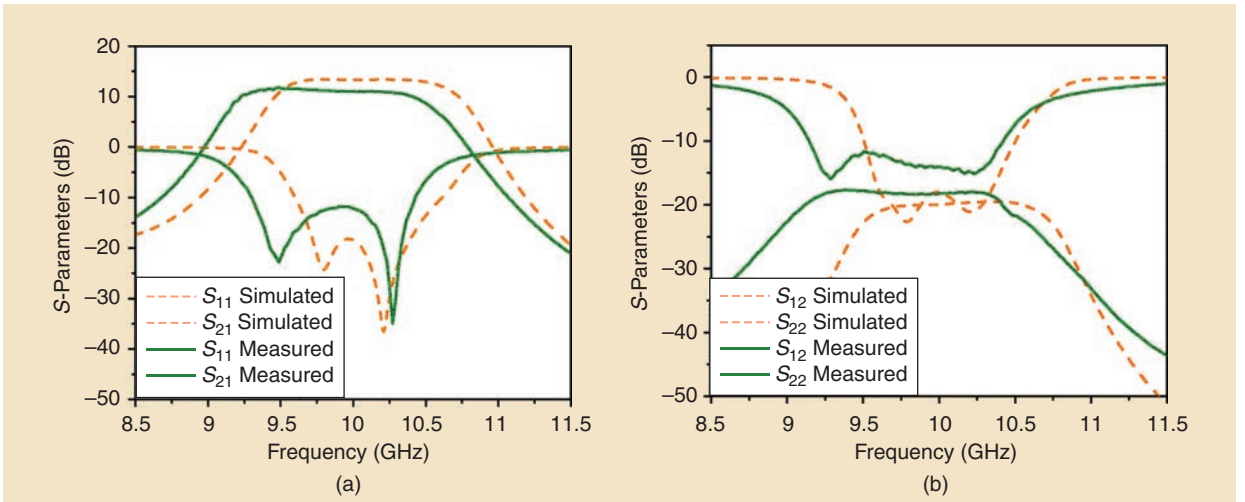

Figure 14. *Simulation (dashed lines) and measurement (solid lines) results of the filter–amplifier in Figures 12 and 13. (a) S_{11} and S_{21} and (b) S_{22} and S_{12} [20].*

design. To realize the filtering response, a transmission line TL11 is used to eliminate the imaginary part of the load impedance. The DR filter converts the real impedance to 50 Ω through tuning of the external couplings, as given by [38]

$$M'_{S,1} = \frac{M_{S,1}}{\sqrt{R_{\text{in}}}}. \tag{5}$$

The filter's selectivity was enhanced by the two TZs near the passband. This integrated DR filter–amplifier achieves a small-signal gain of 18.3 dB with a 3-dB bandwidth of 2.3%. The measured P_{out}, PAE, and drain efficiency (DE) at 1.88 GHz are given in Figure 16. This filter–amplifier exhibits its superiority of high PAE over the microstrip filter–amplifier in [31] and the hybrid microstrip-cavity filter–amplifier in [36] with the same fractional bandwidth.

Broadband Filter–Amplifiers

Broadband filter synthesis methods used to match the frequency-dependent impedance of amplifiers have already been briefly reviewed. In this section, a broadband filter–amplifier is presented as an example, and several recently published broadband filtering amplifiers are summarized in Table 2. In general, the required wideband matching networks are commonly realized using passive *LC*-ladder networks, which are usually based on microstrip structures.

Figure 17 shows an example of a broadband filtering power amplifier [40] employing a right-/left-handed (CRLH) cell and a dual CRLH (D-CRLH) cell that offer filter matching to the amplifier. Matching filters formed by the D-CRLH absorb the bias circuits and allow for a reduced circuit footprint. Note that filter matching at both the fundamental and harmonic frequencies is required over the bandwidth. An optimum impedance of $19.7 + 5.5j\ \Omega$ at the center frequency of 2 GHz was chosen. Real-to-real and real-to-complex transformations were carried out. The measured S-parameters of the filter–amplifier are given in Figure 18(a), where the return loss is around 5 dB, and a TZ is created at 3 GHz. The measured DE and output power versus

Design Steps of the Integrated Waveguide Filter–Amplifier

1) Determine the filter–amplifier specifications (i.e., the center frequency, bandwidth, gain, power, efficiency, and type of filtering response) based on the specific application scenarios.
2) Model the active component and extract the optimum input and output impedances of the transistor at the filter center frequency.
3) Obtain the active coupling matrix through direct synthesis or optimization.
4) Extract the initial dimensions of the filter–amplifier from the nonzero elements of the obtained coupling matrix. Usually, this is undertaken through electromagnetic simulations. The transition geometries (e.g., the E-plane probe and the waveguide cavity shown in Figure 13) can also be determined by the self- and external couplings.
5) Optimize the entire device via electromagnetic simulations to finalize the design and make it ready for fabrication and measurement.

frequency at an input power of 28 dBm are shown in Figure 18(b). Compared with conventional *LC*-ladder based low-pass matching filters, the D-CRLH bandpass filter (BPF) matching network demonstrates its broadband harmonic impedance transformation characteristics.

Comparison of Integrated Filter–Amplifiers

A comparison of the state of the art for integrated filter–amplifiers is given in Table 3. Various filter types (microstrip, DRs, waveguide, hybrid microstrip-to-DR types) together with their advantages/disadvantages are presented. The reviewed examples validate the generality of the filter–amplifier integration theory, which can be applied to both input and output complex impedances of active devices as well as planar or nonplanar filter constructions.

Toward Terahertz Applications

The integrated filter–amplifier configuration can be particularly beneficial for terahertz applications, where loss becomes a major concern. For terahertz amplifiers,

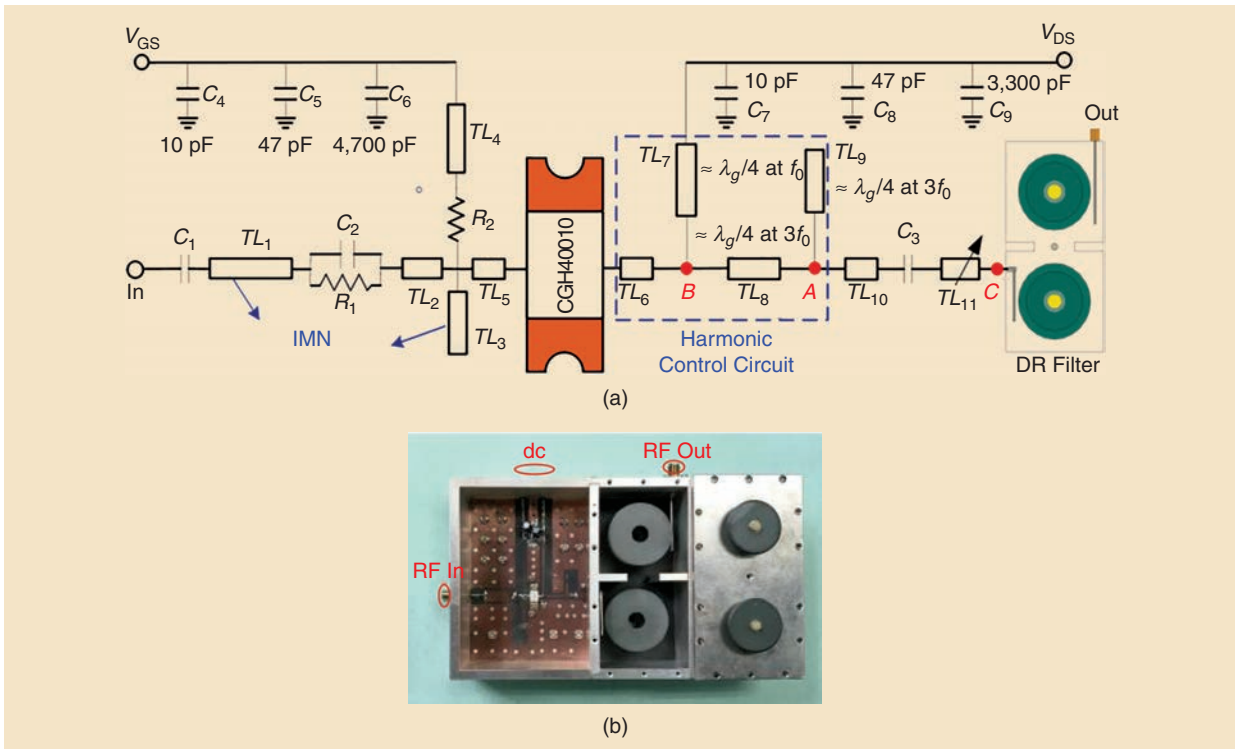

Figure 15. *(a) Configuration of the DR filtering power amplifier. (b) Photograph of the fabricated device [38].*

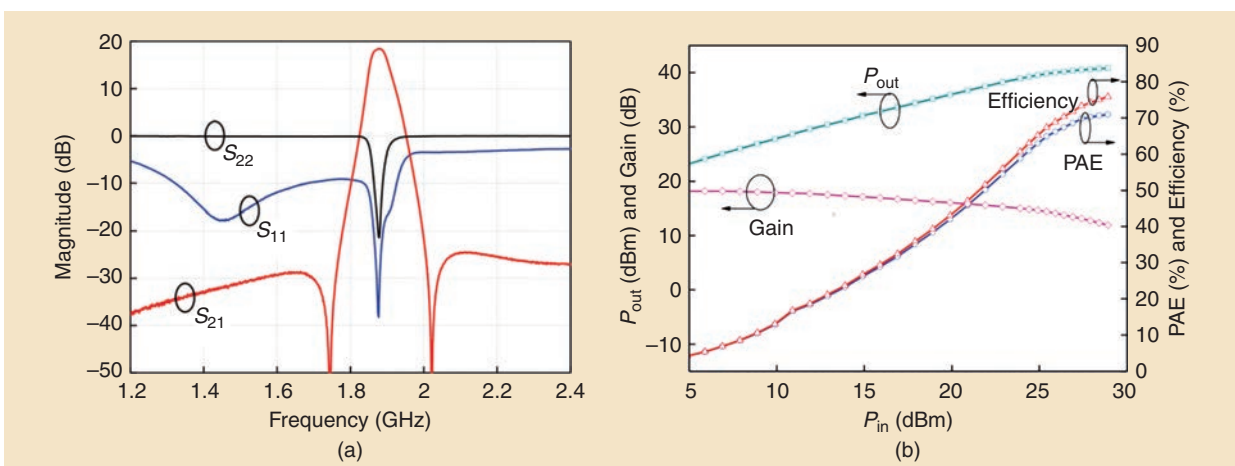

Figure 16. *The performance of the filter–amplifier in Figure 15. (a) Measured and simulated S-parameters and (b) measured P_{out}, gain, efficiency, and PAE versus input power [38].*

monolithic microwave integrated circuits (MMICs) are usually integrated with hollow metal waveguides. For such MMICs, the probe transitions are usually made from substrate materials, such as alumina (with a dielectric constant of 9.6) or quartz (with a dielectric constant of 3.8). Because of the extremely sensitive parasitic parameters, there are stringent requirements on dimensional accuracy for these probes and waveguides. A common E-plane probe and a dipole antenna are illustrated in Figure 19(a) and (b).

Instead of using separate matching networks, the active components can be matched directly using resonators of waveguide cavity filters, and such waveguide cavities have inherently low losses compared to typical matching circuitry based on lossy planar structures. This approach also minimizes the footprint of the entire filter–amplifier. Although the concept of amplifiers matched to filters has been reported extensively, filter–amplifiers operating at terahertz frequencies have not yet been reported in the open literature. However, this method, i.e., using waveguide filters to match active/nonlinear circuits with complex loads, has been successfully applied to the design of millimeter-wave triplers [26], [27] and terahertz subharmonic mixers [28].

TABLE 2. A summary of recently published broadband filtering power amplifiers.

Mode	Bandwidth (GHz, %)	P_{out} (dBm)	Efficiency (%)	Gain (dB)	Filter Matching Technique	Reference
Class J	2–3, 40	40–41.8	58–72	11.5–12.5	Equivalent circuit nonlinear model approximation	[4]
N/A	1.9–4.3, 78	39.5– 41.8	57–72	9–11	Resonant parallel *LC* circuits	[9]
Class F	1.45–2.45, 51	35.7–35.9	70–81	10–12.6	Simplified real frequency technique	[10]
N/A	0.8–3.2, 120	39.7– 42.9	57–74	10.7–13.5	Even–odd-mode analysis technique	[11]
Class E	0.136–0.174, –	39.03	74	11.5–12.2	Reactance-compensation technique	[12]
Class J	1.4–2.6, 60	39.5– 40.4	57–72	11–12	Norton transformer	[39]
N/A	1.2–2.3, 63	40.6–42.6	64.3–77.5	12.4–14.5	D/CRLH BPF	[40]
N/A	2–4, 70.7	35.1–38.9	40–55	9.5–11	Minimum inductor BPF	[41]
N/A	1.9–2.3, –	39–40.4	69–78.2	13.4–15.1	Coupled line-based tuning network	[42]
Class F	1.35–2.5, 60	40.96–42.6	68–82	15.2–17	Modified elliptic low-pass filter	[43]
Class E	1.4–2.7, –	39–41.2	64.5–73.5	9–10.9	Shunt capacitance and shunt filter	[44]
Class E	0.9–2.2, 84	40–43	63–89	10–13	Synthesized low-pass matching network	[45]
N/A	1.7–2.6, 35	28–42	65–78	9.1–10.1	Step-impedance quasi-Chebyshev low-pass filter synthesis	[46]
Class F	0.3–1, 107.7	37–40.3	62–81	12–15.3	Quasi-elliptic low-pass filtering network	[47]
N/A	1.15–2.45, 77.4	39.7–41.7	38.4– 52.2	6.5	Optimum balanced broadband load network	[48]

D/CRLH: dual right-/left-handed; BPF: bandpass filter.

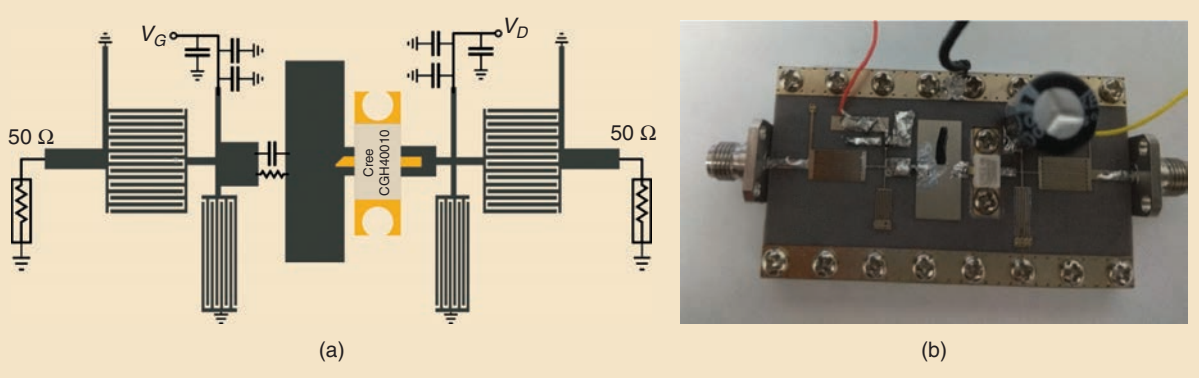

Figure 17. *(a) A schematic of the broadband power amplifier. (b) A prototype of the proposed broadband power amplifier using the D-CRLH bandpass filtering matching method [40].*

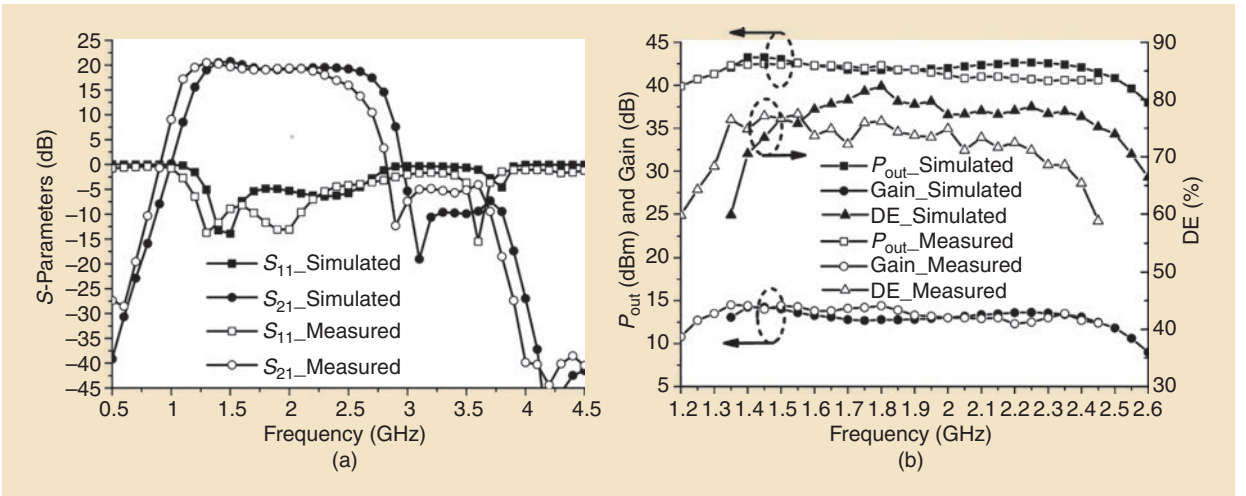

Figure 18. *The performance of the broadband filter–amplifier in Figure 17. (a) Simulated and measured S_{11} and S_{21} and (b) measured and simulated DE output power and gain versus frequency [40].*

TABLE 3. A comparison of integrated filter–amplifiers in the open literature.

Filter Type	Cost	Loss	Volume	Reference	Advantages and Disadvantages
Microstrip	Low	High	Medium	[4], [9] [31]–[35], [39]–[48]	Easy integration with on-chip transistor; low cost; high loss
On chip	High	High	Small	[35]	Extremely small volume; easy integration with monolithic microwave integrated circuit; high loss; costly
DR	Medium	Low	Large	[36]–[38]	Bulky; complex planar-3D coupling structure; low loss; medium cost
Ceramic coaxial resonator	Medium	Low	Medium	[35]	High Q-factor; low loss; medium volume
SIW	Low	Medium	Medium	[21], [24]	Easy integration with on-chip transistor; good tradeoff among cost, loss, and volume
EVA cylinder cavity	High	Low	Large	[23]	High cost; bulky; low loss at very high frequencies
Waveguide cavity	High	Low	Large	[19], [20]	Complex planar-3D coupling structure; high power capacity

MMIC: monolithic microwave integrated circuit.

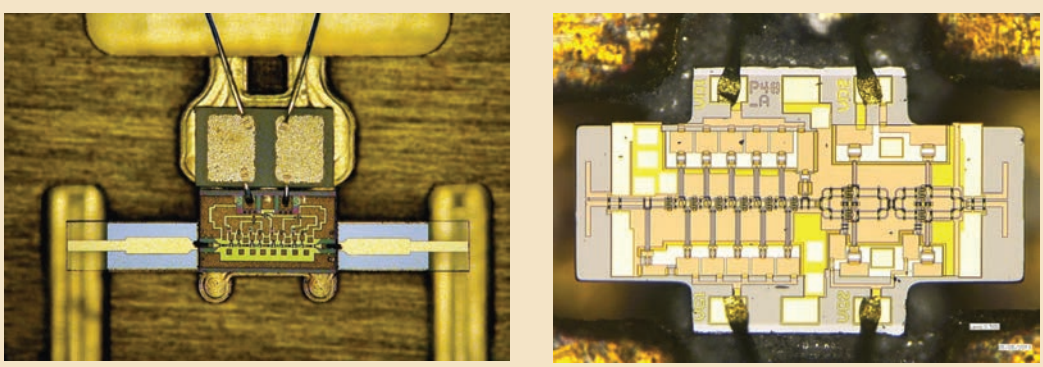

Figure 19. *(a) A 300-GHz mHEMT amplifier using 2-mil-thick quartz E-plane probes [50]. (b) A 650-GHz power amplifier dipole antenna transition [51].*

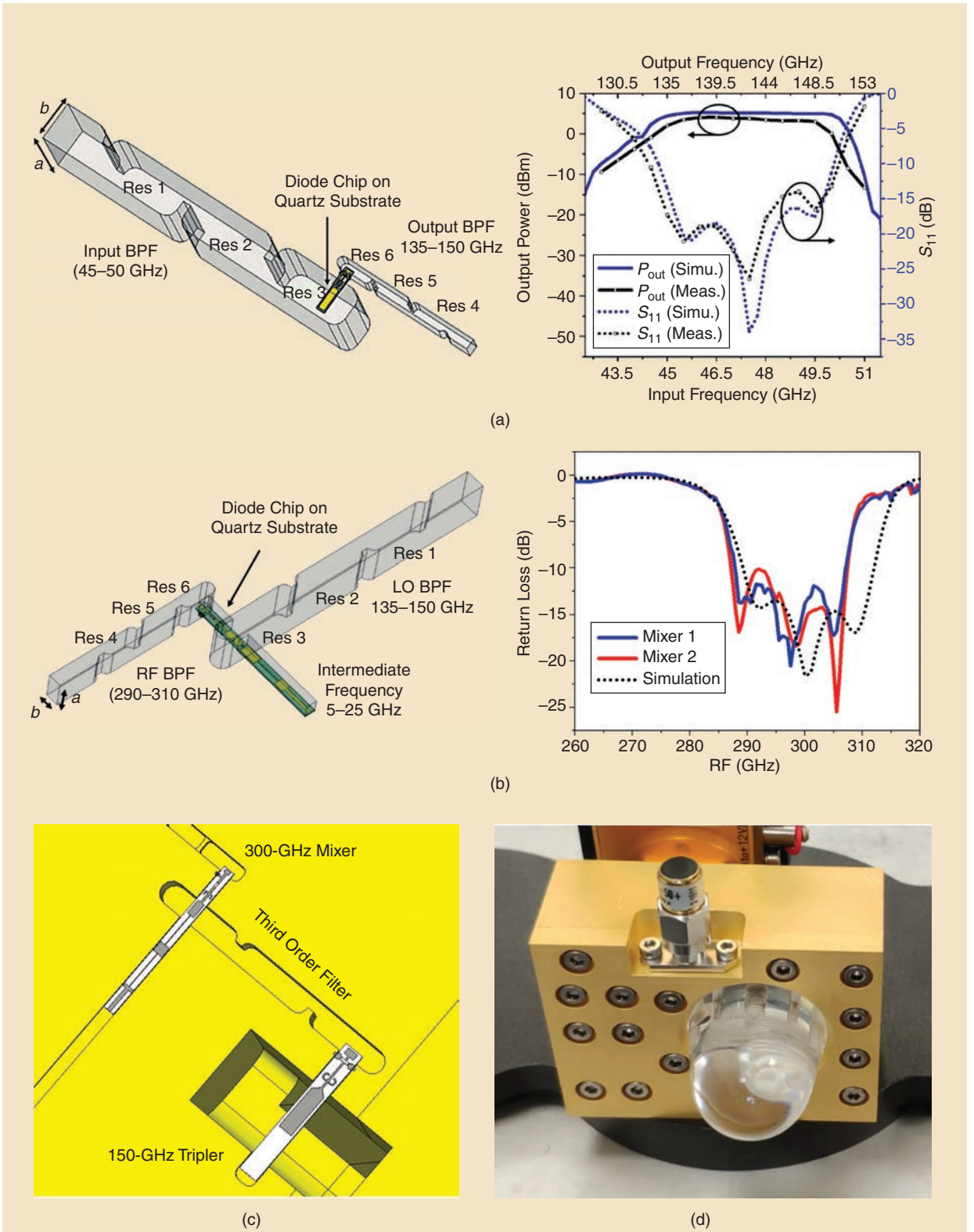

Figure 20. *(a) A 150-GHz tripler, matching directly using resonators of waveguide filters [26]. (b) A 300-GHz subharmonic mixer, matching directly using resonators of waveguide filters [28]. (c) An integrated subsystem based on the tripler in (a) and the mixer in (b). (d) A 300-GHz communication system front end in which the frequency triplers and mixers are based on structures shown in (a)–(c). BPF: bandpass filter; LO: local oscillator.*

All of these components can be eventually assembled to form a system, and the technique is expected to be applicable to multifunctional devices and systems.

In the co-design of terahertz mixers and multipliers with waveguide cavity filters, the complex impedance of the diode chip is matched directly using waveguide filters. This new approach provides a built-in filtering function and removes the need for a separate impedance interface and therefore the associated transmission or transition losses. Excellent performances have been achieved for both the triplers and mixer, as shown in Figure 20(a) and (b). Low-loss hollow waveguides are also widely used for the interconnection of multiple components in terahertz systems. Waveguide filters can be used to simultaneously match the output of one device and the input of the subsequent device, as shown in [49] and in Figure 20(c) and (d), where the output of the 150-GHz frequency tripler and the input of the 300-GHz mixer are matched simultaneously by using the same third-order waveguide filter. This offers a further reduction of the overall size of the system.

Conclusions

This article reviewed the concept of integrated filter–amplifiers and implementation examples. Various types of filters based on waveguide, SIWs, microstrips, and hybrid DRs have been described. This demonstrates the feasibility of replacing conventional matching networks with filters. The integration techniques lead to more compact construction, lower loss, and increased efficiency. As transistors with a complex port impedance/admittance can be matched with narrow/broadband filters, the methodology can be generalized to deal with a wide range of components with complex ports, such as antennas, mixers, and triplers. All of these components can be eventually assembled to form a system, and the technique is expected to be applicable to multifunctional devices and systems. There is still considerable work to be done in many aspects of this concept. The development of filter–amplifier integration techniques as well as other integrated devices and systems remains an active area of research.

Acknowledgments

The authors would like to thank Prof. Michael J. Lancaster (University of Birmingham, U.K.) for his valuable suggestions on this article. The work of Xiaobang Shang was supported by the National Measurement System Programme of the U.K. Government's Department for Business, Energy and Industrial Strategy (BEIS).

References

[1] D. M. Pozar, *Microwave Engineering*. Hoboken, NJ, USA: Wiley, 2011.
[2] I. J. Bahl, *Fundamentals of RF and Microwave Transistor Amplifiers*. Hoboken, NJ, USA: Wiley, 2009.
[3] J. S. Hong and M. J. Lancaster, *Microstrip Filters for RF/Microwave Applications*. New York, NY, USA: Wiley, 2001.
[4] X. Meng, C. Yu, Y. Liu, and Y. Wu, "Design approach for implementation of class-J broadband power amplifiers using synthesized band-pass and low-pass matching topology," *IEEE Trans. Microw. Theory Techn.*, vol. 65, no. 12, pp. 4984–4996, 2017, doi: 10.1109/TMTT.2017.2711021.
[5] H. J. Carlin and J. J. Komiak, "A new method of broad-band equalization applied to microwave amplifiers," *IEEE Trans. Microw. Theory Techn.*, vol. 27, no. 2, pp. 93–99, 1979, doi: 10.1109/TMTT.1979.1129569.
[6] B. S. Yarman and H. J. Carlin, "A simplified 'real frequency' technique appliable to broadband multistage microwave amplifiers," in *Proc. IEEE MTT-S Int. Microw. Symp. Dig.*, Jun. 1982, pp. 529–531, doi: 10.1109/MWSYM.1982.1130781.
[7] R. M. Fano, "Theoretical limitations on the broadband matching of arbitrary impedances," *J. Franklin Inst.*, vol. 249, no. 2, pp. 139–154, 1950, doi: 10.1016/S0016-0032(50)91101-X.
[8] D. E. Dawson, "Closed-form solutions for the design of optimum matching networks," *IEEE Trans. Microw. Theory Techn.*, vol. 57, no. 1, pp. 121–129, 2009, doi: 10.1109/TMTT.2008.2009041.
[9] P. Saad, C. Fager, H. Cao, H. Zirath, and K. Andersson, "Design of a highly efficient 2–4-GHz octave bandwidth GaN-HEMT power amplifier," *IEEE Trans. Microw. Theory Techn.*, vol. 58, no. 7, pp. 1677–1685, 2010, doi: 10.1109/TMTT.2010.2049770.
[10] N. Tuffy, L. Guan, A. Zhu, and T. J. Brazil, "A simplified broadband design methodology for linearized high-efficiency continuous class-F power amplifiers," *IEEE Trans. Microw. Theory Techn.*, vol. 60, no. 6, pp. 1952–1963, 2012, doi: 10.1109/TMTT.2012.2187534.
[11] J. Wang, S. He, F. You, W. Shi, J. Peng, and C. Li, "Codesign of high-efficiency power amplifier and ring-resonator filter based on a series of continuous modes and even–odd-mode analysis," *IEEE Trans. Microw. Theory Techn.*, vol. 66, no. 6, pp. 2867–2878, 2018, doi: 10.1109/TMTT.2018.2819650.
[12] N. Kumar, C. Prakash, A. Grebennikov, and A. Mediano, "High-efficiency broadband parallel-circuit class E RF power amplifier with reactance-compensation technique," *IEEE Trans. Microw. Theory Techn.*, vol. 56, no. 3, pp. 604–612, 2008, doi: 10.1109/TMTT.2008.916906.
[13] J. Rooney, R. Parry, I. Hunter, and R. D. Pollard, "A filter synthesis technique applied to the design of multistage broad-band microwave amplifiers," *IEEE Trans. Microw. Theory Techn.*, vol. 50, no. 12, pp. 2947–2953, 2002, doi: 10.1109/TMTT.2002.805156.
[14] C. Chang and T. Itoh, "Microwave active filters based on coupled negative resistance method," *IEEE Trans. Microw. Theory Techn.*, vol. 38, no. 12, pp. 1879–1884, 1990, doi: 10.1109/22.64569.
[15] Y. Li *et al.*, "A novel low-power notch-enhanced active filter for ultrawideband interferer rejected LNA," *IEEE Trans. Microw. Theory Techn.*, vol. 69, no. 3, pp. 1684–1697, 2021, doi: 10.1109/TMTT.2021.3053264.
[16] Y. C. Li, K. C. Wu, and Q. Xue, "Power amplifier integrated with bandpass filter for long term evolution application," *IEEE Microw. Wireless Compon. Lett.*, vol. 23, no. 8, pp. 424–426, 2013, doi: 10.1109/LMWC.2013.2268457.
[17] Y. S. Lin, J. F. Wu, W. F. Hsia, P. C. Wang, and Y. H. Chung, "Design of electronically switchable single-to-balanced bandpass low-noise amplifier," *IET Microw. Antennas Propag.*, vol. 7, no. 7, pp. 510–517, 2013, doi: 10.1049/iet-map.2012.0426.
[18] K. Wu and W. Meng, "A direct synthesis approach for microwave filters with a complex load and its application to direct diplexer

design," *IEEE Trans. Microw. Theory Techn.*, vol. 55, no. 5, pp. 1010–1017, 2007, doi: 10.1109/TMTT.2007.895175.

[19] Y. Gao, J. Powell, X. Shang, and M. J. Lancaster, "Coupling matrix-based design of waveguide filter amplifiers," *IEEE Trans. Microw. Theory Techn.*, vol. 66, no. 12, pp. 5300–5309, 2018, doi: 10.1109/TMTT.2018.2871122.

[20] Y. Gao, X. Shang, C. Guo, J. Powell, Y. Wang, and M. J. Lancaster, "Integrated waveguide filter amplifier using the coupling matrix technique," *IEEE Microw. Wireless Compon. Lett.*, vol. 29, no. 4, pp. 267–269, 2019, doi: 10.1109/LMWC.2019.2901892.

[21] Y. Gao *et al.*, "Substrate integrated waveguide filter–amplifier design using active coupling matrix technique," *IEEE Trans. Microw. Theory Techn.*, vol. 68, no. 5, pp. 1706–1716, 2020, doi: 10.1109/TMTT.2020.2972390.

[22] K. Chen, X. Liu, W. J. Chappell, and D. Peroulis, "Co-design of power amplifier and narrowband filter using high-Q evanescent-mode cavity resonator as the output matching network," in *Proc. IEEE MTT-S Inter. Microw. Symp.*, Jun. 5–10, 2011, pp. 1–4, doi: 10.1109/MWSYM.2011.5972854.

[23] K. Chen, T. Lee, and D. Peroulis, "Co-design of multi-band high-efficiency power amplifier and three-pole high-Q tunable filter," *IEEE Microw. Wireless Compon. Lett.*, vol. 23, no. 12, pp. 647–649, 2013, doi: 10.1109/LMWC.2013.2283876.

[24] K. Chen, J. Lee, W. J. Chappell, and D. Peroulis, "Co-design of highly efficient power amplifier and high-Q output bandpass filter," *IEEE Trans. Microw. Theory Techn.*, vol. 61, no. 11, pp. 3940–3950, 2013, doi: 10.1109/TMTT.2013.2284485.

[25] Y. Gao, X. Shang, Y. Wang, and M. J. Lancaster, "An x-band waveguide orthomode transducer with integrated filters," *Microw. Opt. Technol. Lett.*, vol. 62, no. 1, pp. 78–81, 2020, doi: 10.1002/mop.31986.

[26] C. Guo *et al.*, "A 135–150-GHz frequency Tripler with waveguide filter matching," *IEEE Trans. Microw. Theory Techn.*, vol. 66, no. 10, pp. 4608–4616, 2018, doi: 10.1109/TMTT.2018.2855172.

[27] C. Guo *et al.*, "A 135–150-GHz frequency Tripler using SU-8 micromachined WR-5 waveguides," *IEEE Trans. Microw. Theory Techn.*, vol. 68, no. 3, pp. 1035–1044, 2020, doi: 10.1109/TMTT.2019.2955684.

[28] C. Guo *et al.*, "A 290–310 GHz single sideband mixer with integrated waveguide filters," *IEEE Trans. THz Sci. Technol.*, vol. 8, no. 4, pp. 446–454, 2018, doi: 10.1109/TTHZ.2018.2841771.

[29] R. R. Mansour, "High-Q tunable dielectric resonator filters," *IEEE Microw. Mag.*, vol. 10, no. 6, pp. 84–98, 2009, doi: 10.1109/MMM.2009.933591.

[30] X. Shang *et al.*, "W-band waveguide filters fabricated by laser micromachining and 3-D printing," *IEEE Trans. Microw. Theory Techn.*, vol. 64, no. 8, pp. 2572–2580, 2016, doi: 10.1109/TMTT.2016.2574839.

[31] L. Gao, X. Y. Zhang, S. Chen, and Q. Xue, "Compact power amplifier with bandpass response and high efficiency," *IEEE Microw. Wireless Compon. Lett.*, vol. 24, no. 10, pp. 707–709, 2014, doi: 10.1109/LMWC.2014.2340791.

[32] M. Furqan, F. You, W. Shi, S. Ahmad, and T. Qi, "A broadband power amplifier using hairpin bandpass filter matching network," *Electron. Lett.*, vol. 56, no. 4, pp. 168–213, 2019, doi: 10.1049/el.2019.3047.

[33] M. F. Haider, F. You, T. Qi, and W. Shi, "A 10W broadband power amplifier with a hairpin resonator filter based on even-odd mode impedance analysis," in *Proc. Eur. Microw. Conf. Central Eur. (EuMCE)*, May 13–15, 2019, pp. 366–369.

[34] Z. Zhuang, Y. Wu, M. Kong, and W. Wang, "High-selectivity single-ended/balanced DC-block filtering impedance transformer and its application on power amplifier," *IEEE Trans. Circuits Syst. I, Reg. Papers*, vol. 67, no. 12, pp. 4360–4369, 2020, doi: 10.1109/TCSI.2020.3015883.

[35] J. A. Estrada, J. R. Montejo-Garai, P. de Paco, D. Psychogiou, and Z. Popović, "Power amplifiers with frequency-selective matching networks," *IEEE Trans. Microw. Theory Techn.*, vol. 69, no. 1, pp. 697–708, 2021, doi: 10.1109/TMTT.2020.3020097.

[36] Q.-Y. Guo, X. Y. Zhang, J.-X. Xu, Y. C. Li, and Q. Xue, "Bandpass class-F power amplifier based on multifunction hybrid cavity–microstrip filter," *IEEE Trans. Circuits Syst., II, Exp. Briefs*, vol. 64, no. 7, pp. 742–746, 2017, doi: 10.1109/TCSII.2016.2600575.

[37] J. Xu and X. Y. Zhang, "Dual-channel dielectric resonator filter and its application to Doherty power amplifier for 5G massive MIMO system," *IEEE Trans. Microw. Theory Techn.*, vol. 66, no. 7, pp. 3297–3305, 2018, doi: 10.1109/TMTT.2018.2829197.

[38] J. Xu, X. Y. Zhang, and X. Song, "High-efficiency filter-integrated class-F power amplifier based on dielectric resonator," *IEEE Microw. Wireless Compon. Lett.*, vol. 27, no. 9, pp. 827–829, 2017, doi: 10.1109/LMWC.2017.2734778.

[39] P. Wright, J. Lees, J. Benedikt, P. J. Tasker, and S. C. Cripps, "A methodology for realizing high efficiency class-J in a linear and broadband PA," *IEEE Trans. Microw. Theory Techn.*, vol. 57, no. 12, pp. 3196–3204, 2009, doi: 10.1109/TMTT.2009.2033295.

[40] Q. Cai, W. Che, G. Shen, and Q. Xue, "Wideband high-efficiency power amplifier using D/CRLH bandpass filtering matching topology," *IEEE Trans. Microw. Theory Techn.*, vol. 67, no. 6, pp. 2393–2405, 2019, doi: 10.1109/TMTT.2019.2909892.

[41] G. Nikandish, R. B. Staszewski, and A. Zhu, "Broadband fully integrated GaN power amplifier with embedded minimum inductor bandpass filter and AM–PM compensation," *IEEE Solid-State Circuits Lett.*, vol. 2, no. 9, pp. 159–162, 2019, doi: 10.1109/LSSC.2019.2927855.

[42] Z. Su, C. Yu, B. Tang, and Y. Liu, "Bandpass filtering power amplifier with extended band and high efficiency," *IEEE Microw. Wireless Compon. Lett.*, vol. 30, no. 2, pp. 181–184, 2020, doi: 10.1109/LMWC.2020.2966067.

[43] M. Yang, J. Xia, Y. Guo, and A. Zhu, "Highly efficient broadband continuous inverse class-F power amplifier design using modified elliptic low-pass filtering matching network," *IEEE Trans. Microw. Theory Techn.*, vol. 64, no. 5, pp. 1515–1525, 2016, doi: 10.1109/TMTT.2016.2544318.

[44] A. Grebennikov, "High-efficiency class-E power amplifier with shunt capacitance and shunt filter," *IEEE Trans. Circuits Syst. I, Reg. Papers*, vol. 63, no. 1, pp. 12–22, 2016, doi: 10.1109/TCSI.2015.2512698.

[45] K. Chen and D. Peroulis, "Design of highly efficient broadband class-E power amplifier using synthesized low-pass matching networks," *IEEE Trans. Microw. Theory Techn.*, vol. 59, no. 12, pp. 3162–3173, 2011, doi: 10.1109/TMTT.2011.2169080.

[46] Z. Zhuang, Y. Wu, Q. Yang, M. Kong, and W. Wang, "Broadband power amplifier based on a generalized step-impedance Quasi-Chebyshev lowpass matching approach," *IEEE Trans. Plasma Sci.*, vol. 48, no. 1, pp. 311–318, 2020, doi: 10.1109/TPS.2019.2954494.

[47] S. Zarghami, M. Hayati, M. K. Kazimierczuk, and H. Sekiya, "Continuous class-F power amplifier using quasi-elliptic low-pass filtering matching network," *IEEE Trans. Circuits Syst., II, Exp. Briefs*, vol. 67, no. 11, pp. 2407–2411, 2020, doi: 10.1109/TCSII.2020.2964895.

[48] H. Kang *et al.*, "Optimized broadband load network for Doherty power amplifier based on bandwidth balancing," *IEEE Microw. Wireless Compon. Lett.*, vol. 31, no. 3, pp. 280–283, 2021, doi: 10.1109/LMWC.2020.3043770.

[49] M. J. Lancaster *et al.*, "GaAs Schottky components for 300 GHz communication systems using a resonator impedance matching approach," in *Proc. 44th Inter. Conf. Infrared, Millimeter THz Waves (IRMMW-THz)*, Sep. 1–6, 2019, p. 1, doi: 10.1109/IRMMW-THz.2019.8874014.

[50] A. Tessmann *et al.*, "A 300 GHz mHEMT amplifier module," in *Proc. IEEE Inter. Conf. Indium Phosphide Related Mater.*, May 10–14, 2009, pp. 196–199, doi: 10.1109/ICIPRM.2009.5012477.

[51] V. Radisic, K. M. K. H. Leong, X. Mei, S. Sarkozy, W. Yoshida, and W. R. Deal, "Power amplification at 0.65 THz using InP HEMTs," *IEEE Trans. Microw. Theory Techn.*, vol. 60, no. 3, pp. 724–729, 2012, doi: 10.1109/TMTT.2011.2176503.

Microwave Power Detectors in Different CMOS Design Architectures

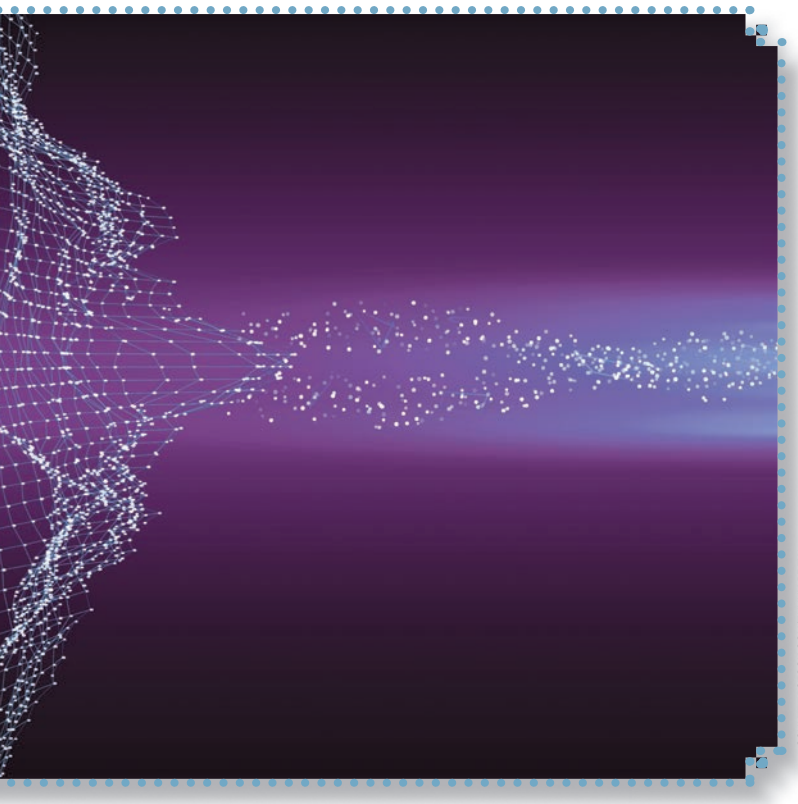

©SHUTTERSTOCK.COM/FUNNY DREW

Jules Guiliary Ravanne, Yi Lung Then, Hieng Tiong Su, and Ismat Hijazin

Transmitted and received power must be controlled quickly and accurately to comply with government regulations, minimize interference, and optimize power consumption. Microwave power detectors (PDs) are critical building blocks employed in applications such as integrated circuit tests and measurements, wireless communication, and automatic-gain-control (AGC) circuits to monitor signal power level. PDs are utilized as received signal strength indicators (RSSIs) to adjust the gain of the intermediate frequency/RF signal via an AGC circuit

Jules Guiliary Ravanne (jgravanne@swinbune.edu.my), Yi Lung Then (ythen@swinburne.edu.my), and Hieng Tiong Su (hsu@swinbune.edu.my) are with the Swinburne University of Technology, Kuching, Sarawak, 93350, Malaysia. Ismat Hijazin (ihijazin@swinbune.edu.au) is with the Swinburne University of Technology, Melbourne, VIC 3122, Australia.

Digital Object Identifier 10.1109/MMM.2022.3155033

Date of current version: 5 May 2022

[1]. They are also used in mobile terminals to monitor the transmitted power, thereby optimizing power consumption. Two popular methods employed to measure the power signal level are root mean square (RMS) value and peak value. Peak detectors capture the input's peak power to provide power information, whereas the RMS PD provides information about the average power [2]. Figure 1 shows a conventional block diagram of a microwave PD employed in an RF transmitter. The directional coupler is used to couple the output signal from the power amplifier to a PD. The signal is then converted to a dc voltage that the power controller utilizes to change the power amplifier's gain, thereby improving the transmitter's linearity.

The specification of PDs relies on the application requirements and design methodologies. Performance metrics such as operating frequency, dynamic range, sensitivity, and power consumption determine PDs' efficiency and accuracy. These critical performance metrics are described next.

Operating Frequency

A consistent response is necessary over the frequency of operation. Two important parameters are required to accomplish this: input impedance matching and the gain variation of the PD versus frequency [3]. Input matching networks are circuitry connected between a load and a source that ensures maximum power transfer to the load, thus, guaranteeing a low voltage standing wave ratio [4]. These two parameters simplify the design and maintain extremely low variation over the frequency of operation.

Sensitivity

PD sensitivity relates to the system's ability to obtain usable information from a low input signal [3]. The minimum output signal level of the PD should be lower than the minimum input signal level. Sensitivity is enhanced with an increase in the gain of the PD; however, if the PD's gain reaches saturation, sensitivity degrades. Sensitivity is highly dependent on the input matching network of the system, and it affects the linearity of the PD [5].

Dynamic Range

Dynamic range is defined as the law-conformance for which the PD satisfies the accuracy level over all operating conditions. Law-conformance is the ripple error arising from the difference between the measured and the ideal transfer characteristics of the PD. The conventional value of law-conformance is ±1 dB, even though a smaller value such as ±0.5 dB is also acceptable [6]. It is often employed to define the accuracy of logarithmic PDs. A PD with a larger dynamic range offers greater flexibility in the selection of system components [7]. As such, PDs with a larger dynamic range are suitable for multiple applications.

Power Consumption

With the continuous downscaling of semiconductors, power consumption has gained major design significance comparable to performance and area [8]. Power consumption is a crucial design parameter as it impacts weight, cost, and size, and it establishes the electrical and thermal limits of designs. Furthermore, there is a reliability issue at high power consumption. High-power systems, which tend to operate at high temperatures, can cause silicon failures [9]. From an environmental perspective, low-power electronic devices are preferred because lower electricity consumption lessens the global ecological impact.

Aside from the application requirements, design methodologies, and performance metrics, the technology utilized to fabricate PDs is also crucial. Various technological processes are currently being used in the market, such as BiCMOS, CMOS, and III–V technologies. BiCMOS technology offers excellent noise performance and ensures high input–output (I/O) speed and switching. BiCMOS also achieves lower power consumption than bipolar technologies and improved speed over CMOS technology [2]. However, the process complexity of BiCMOS results in a higher cost and longer fabrication cycle time compared to CMOS technology [10]. III–V technologies offer higher electron mobility compared to silicon, making them appropriate for low-power and high-speed applications [11]. Although BiCMOS and III–V technologies presently provide superior performance, CMOS technology is the preferred option to fabricate integrated circuits (ICs) due to its ultralow power consumption, higher packing density, and low-cost, making them suitable for mass production [12]. In addition, CMOS technologies provide higher ease of integration for digital and analog functions on the same chip. CMOS

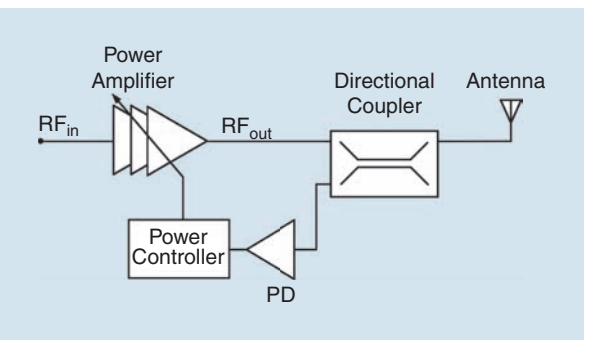

Figure 1. *A conventional microwave PD in an RF transmitter [1].*

technology also has a higher density for digital operations and a high slew rate and gain for analog functions [13]. These advances in microwave integrated circuit performance in standard CMOS technologies in terms of ease of integration, power consumption, and cost has made the design of microwave PDs using CMOS a compelling choice.

Design Methodologies for PDs

PDs can be classified into 1) peak detection, 2) distributed PDs, 3) true RMS detection, and 4) logarithmic detection. This section investigates different design methodologies for these PDs and analyzes these methodologies' advantages and limitations. Circuit implementations and how a given circuit architecture addresses specific applications and performance metrics are described.

Peak Detection

Peak detectors capture the amplitude of the signal at the input. Two types of peak detectors commonly employed are negative peak detectors that measure the input signal's trough and positive peak detectors that measure the input signal's crest [14]. Peak detection is utilized in the design of constant envelope modulated signal applications such as pulse detection, electronic warfare, envelope tracking in power amplifiers, and in the Global System for Mobile (GSM) communication [2]. Peak detectors perform power detection by rectifying the input signal with a full or half-wave rectifier. The output signal is then obtained using a low-pass filter (LPF) to average the input signal. Peak detection is commonly accomplished by employing bipolar transistors or diode-based PDs. However, since bipolar transistors are challenging to implement in CMOS technology, diode-based PDs are the more popular choice for peak detection using CMOS technologies [2].

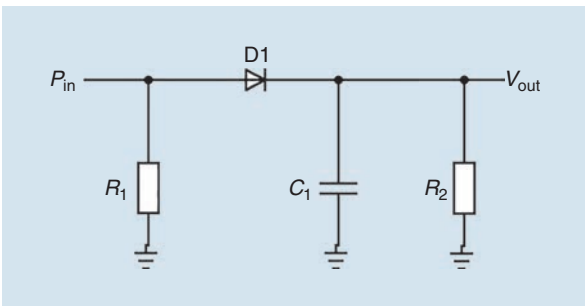

Figure 2. *A diode-based PD.*

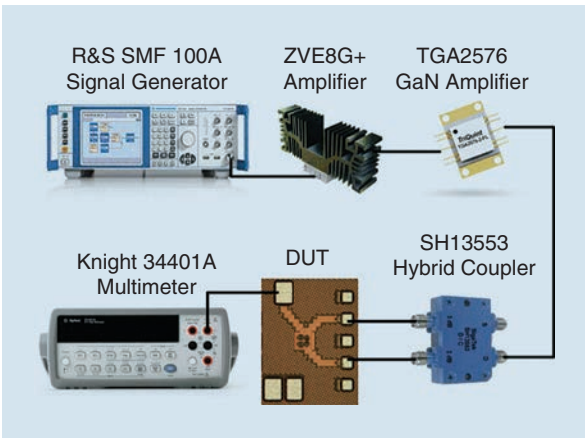

Figure 3. *A proposed measurement setup [17].*

In the early 1990s, diode-based PDs were extensively used in microwave applications due to their high-frequency characteristics [15]. Diode-based PDs exploit diodes' nonlinear characteristics to rectify the input signal, generating a dc output proportional to the input amplitude. These PDs offer the fastest response time constant compared to other designs [8]. Fast response time is a vital specification for applications involving wireless communications. Nevertheless, since the diode junction is temperature dependent, the output rectified voltage changes with temperature [16]. In addition, for applications in the gigahertz region, the cost of a large chip area, power consumption, and matching design are crucial. A simple diode-based PD implementation is shown in Figure 2. The diode D1 is an active element that performs power detection. The resistor R_1 offers resistive input matching and provides a return path for the rectified current. Resistor R_2 acts as the load, and capacitor C_1 filters the signal.

In a recent paper [17], a diode-based PD was developed in a 65-nm CMOS process to improve the maximum input power and dynamic range through a balanced switched capacitor architecture for wireless microwave power transfer applications. Their PD consisted of four p-type and n-type (PN) junction diodes operating as switches, an output filter for high frequency, a load resistor, and two capacitors at the input. The diode's bias voltage is below the threshold voltage, which resulted in low power consumption of 0.7 mW. The diodes operated as PDs both in the negative half-cycle and in the positive half-cycle to enhance linearity, and thus the dynamic range. Figure 3 shows the proposed PD's measurement setup for a device under test.

Figure 4 shows the proposed PD's I/O characteristics when the power level is swept from –5 dBm to 40 dBm at 4 GHz, 5 GHz, and 6 GHz. The measurement results show a dynamic range of 34 dB at 5 GHz with an error of ±1 dB and an operating range of 2 to 6 GHz. The maximum input power was 35 dBm, which is the highest achieved to date [17].

For comparison, commercially available diode-based PDs offer up to a 90-dB dynamic range. A range of –70 to 20 dBm is available for single-path models optimized

for continuous-wave measurements [18]. For instance, ON Semiconductor fabricated an NCS5000 PD with an integrated Schottky diode for applications in communication systems. The PD has a simple configuration for operation up to 2 GHz and a dynamic range of 50 dBm. The PD can operate at a low supply current of 300 µA for a temperature range of –40°C to 85 °C [19].

Distributed PDs

Distributed PDs are a design that solves the issues of wideband input matching arising from established matching methods such as reactive and resistive matching [20]. The principle of operation of such PDs relies on the diode's parasitic junction capacitance coupled with a lumped inductive element to perform RF power detection [21]. Distributed PDs achieve higher bandwidth through absorption of the diode's parasitic junction capacitance in a traveling-wave structure. Input power dissipation through matching resistors is prevented, leading to higher voltage sensitivity that is suitable for communication receiver applications [20].

In a recent review, Qayyum and Negra [22] developed a distributed PD in 130-nm standard CMOS technology using a traveling-wave structure. The transconductance of the transistors for power detection was biased in the subthreshold region to enhance the voltage sensitivity. Figure 5 shows a schematic of the proposed PD. The PD comprises three MOSFETs biased in the subthreshold region, a coupling capacitor ($C_{coupling}$) at the input, a dc-blocking capacitor (C_{block}), resistors, and inductors. The proposed PD transmission line impedance Z_{line} determines the impedance input matching. Z_{line} is expressed by $\sqrt{(L_{line}/L_{in})}$, where C_{in} is the PD-stage input capacitance. The transmission line is terminated by an on-chip dc blocking capacitor and a 50-Ω resistor.

The PD operated from 7 GHz to 70 GHz with an overall voltage sensitivity of 75 dB and power consumption of around 0.156 mW. Qayyum and Negra demonstrated that the minimum detectable input power is within –40 dBm and –37 dBm. However, this design is more suited for sensitive high-voltage microwave applications such as radiometers and communication receivers. Other performance metrics of the PD were not discussed in detail [22].

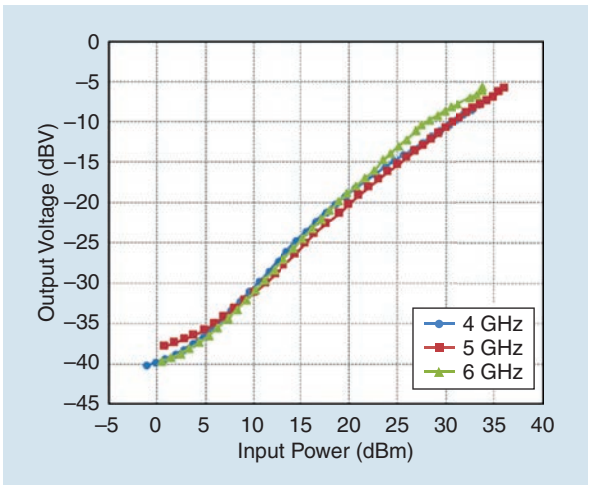

Figure 4. *A measured output voltage of the PD proposed in [17].*

True RMS Detection

The true RMS PD, also referred to as an RMS-to-dc converter, is a popular design methodology due to its insensitivity to the peak-to-average envelope power ratio (PAR) compared to peak and logarithmic detection. These PDs generate a quasi-dc signal representing the power level of an input signal.

Thermal Detection

In theory, thermal detection should be one of the simplest methods for detecting RMS power; however, in practice it is difficult and expensive to realize [23]. Thermal detection is commonly used in communication and sensor applications due to its high accuracy and wide bandwidth [24]. Figure 6 shows a PD implemented with thermal detection. Both the reference voltage and the input signal heat the adjacent thermocouples and a

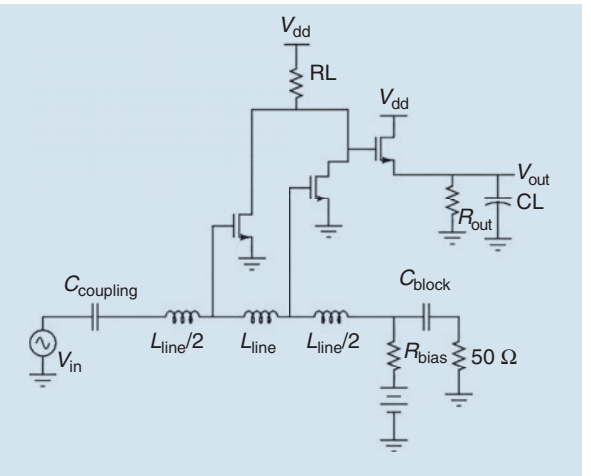

Figure 5. *A schematic of a distributed PD employed in [22].*

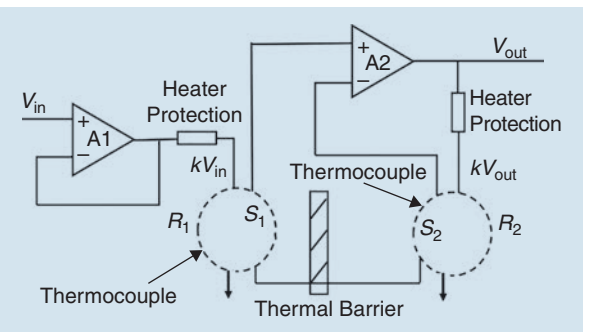

Figure 6. *An implementation of a PD with thermal detection.*

resistor individually. The temperature is proportional to the induced output voltage. The difference between these output voltages is a scaled measure of the input power relative to the reference power.

Thermal isolation and matching between the thermocouples to reduce dependency is crucial to improving accuracy. This implementation has excellent accuracy as the power is proportional to the difference in temperature [18]. However, the system is challenging to integrate and implement in standard CMOS and has high power consumption.

PD Using a Single Field Effect Transistor

Field-effect transistors (FETs) are easier than diode-based and thermal-based PDs to integrate with different technology processes [7]. Furthermore, FETs are more sensitive than Schottky diodes to temperature variations. A PD implemented using a single NMOS is presented in Figure 7. The square-law characteristic of the NMOS transistor M_1 is exploited to perform power detection. The transistor is biased in the saturation region, and the input signal is applied through the drain of the device. Resistor R_3 acts as a load to establish the output voltage while C_3 and R_2 filters the output signal.

Qayyum and Negra [12] designed a high sensitivity PD comprising a single common source NMOS using

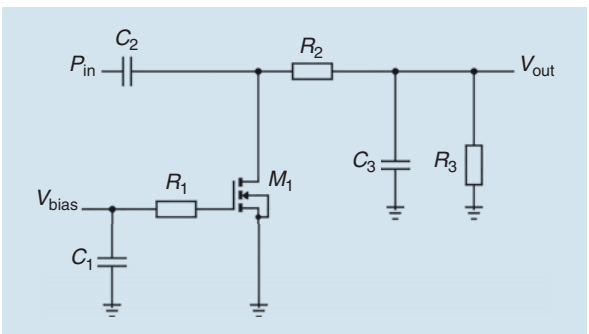

Figure 7. *A PD with single FET. FET: Field-effect transistors.*

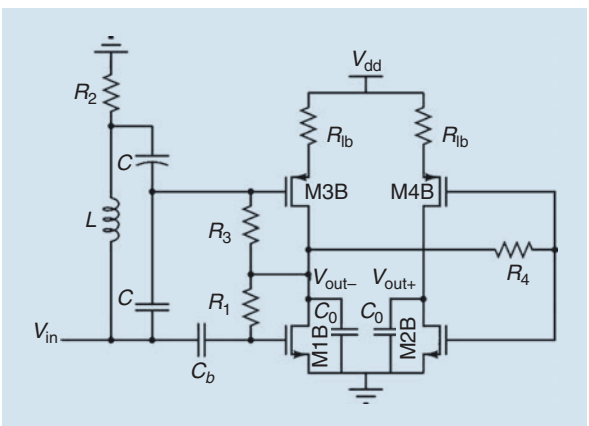

Figure 8. *A self-biased PD proposed in [26].*

65-nm standard CMOS technology. The microwave PD operated in the subthreshold region to boost the device's transconductance, thereby achieving good overall sensitivity and wide input matching. Measurements showed an input reflection coefficient of less than –9.5 dB from 0.1 GHz to 110 GHz, a dynamic range of 35 dBm, high sensitivity of 67 dB, and power consumption of 0.029 mW.

Differential Structure

A single-ended PD's performance suffers from process and temperature variations, which affect the output of the PD [16]. A differential structure would alleviate this issue. Generally, differential PDs have one active device connected to the microwave power input and another similar active device, which acts as a reference point. The second device reduces the dc voltage offset caused by variations in supply voltage, process, and temperature [8]. Moreover, the differential signal has higher immunity to common-mode noise when compared with a single-ended device [25].

A self-biased ultrawideband differential PD shown in Figure 8 was developed using 130-nm CMOS technology. The nonlinear properties of short-channel MOS in the saturation and subthreshold region of operation were used to produce a dc proportional to the input signal power [26]. The PD had an embedded amplifier to improve its sensitivity, and 50-Ω input matching was achieved using a quasi-T-coil matching network. The quasi-T-coil matching network is a circuit configuration that provides wider bandwidth than inductive peaking. From Figure 8, the quasi-T-coil consists of an inductor L, a resistor R_2, and capacitors C. Since the transistors operated in the weak inversion region, their design had a relatively low power consumption of 0.1 mW. The PD had an operating frequency of 125 MHz to 8.5 GHz, a high output sensitivity of 268 mV/dB, and an input dynamic range of 47 dB, making the design suitable for a variety of applications, including communication receivers and reflectometers.

Another differential microwave PD was designed using 130-nm CMOS technology, which exploited MOS transistors' square-law characteristic in the strong inversion region to detect microwave signals [2]. Their proposed design consisted of an exponential current generator, a differential PD unit, and a two-stage operational amplifier. Linear-in-decibel output was obtained by biasing the exponential generator's transistors so that its drain current (I_{DS}) is the exponential of the gate-to-source voltage (V_{GS}). The operating frequency was from low frequency to 8.5 GHz, and the static power consumption was 0.18 mW. However, although a low power consumption was achieved, the PD's 18-dB dynamic range was relatively low compared to other design strategies. Furthermore, since the MOSFETs operating in the weak

inversion region are temperature dependent, the authors [2] suggest that a temperature and process compensation circuit should be included for better accuracy.

Rectifier Implementation

Rectifier microwave PDs are uncommon due to their high power consumption. However, they do have application in on-chip RF measurement. An unbalanced source coupled pair is usually used to design current amplifiers [7].

Garcia et al. [27] employed a class AB rectifier shown in Figure 9 to design a microwave PD using a 350-nm standard CMOS process. The input voltage was converted into current and amplified by a high input impedance input stage. The circuit operated in current mode, and the rectifier then performed full-wave rectification of the current at the first stage. The class AB rectifier rectifies the current only if the operation is in the nonlinear region. The circuit also consisted of an LPF to extract the dc components. The PD had an operating frequency range of 0.9 GHz to 2.4 GHz, a conversion gain of 50 mV/dBm, a dynamic range greater than 30 dB, and power consumption of 8.6 mW, including the bias circuits.

Squaring Cell Detection

Another design strategy for RMS PDs is squaring cells (SQRs). Squaring cells consist of nonlinear elements such as MOSFETs generating an output voltage proportional to the input voltage's square. These squaring cells perform squaring and averaging to obtain the RMS voltage of the input signal. The output of the squaring cells contains power information, and they are classified into three modes: current mode, voltage mode, and voltage/current mode [28]. Furthermore, they can be designed using different methodologies, such as the MOS translinear (MTL) loop and Meyer squaring structure [29]. Choi et al. [30] developed a wide dynamic range RMS PD using a 28-nm CMOS standard process. Their proposed PD consisted of a transimpedance amplifier (TIA), cascading gain amplifiers (GAs), differential-to-single-ended amplifier (D2S), and squaring circuits. A power level segmented detection approach was employed to realize more than 40 dB of dynamic range. The RF input is first applied to the GAs, then it is converted to a squared dc voltage by the squaring cells for averaging. Their proposed design is shown in Figure 10.

The TIA converted the output current from the GAs and squaring cells block to voltage with the help of a feedback resistor. Finally, single-ended voltage is realized using the D2S. The dynamic range could be extended if necessary by using more GAs and squaring cells. A Meyer squaring architecture was utilized to repress odd harmonics terms and common-mode variations. dc offset calibration is required due to mismatches that may arise in the circuit, which affects the dynamic range of the squaring cells considerably. The PD's operating frequency was from 0.7 GHz to 4 GHz with a dynamic range greater than 40 dB and power consumption of 5.8 mW. Squaring cells' insensitivity to modulation form or signal shape due to averaging over time makes them suitable for cellular RFICs applications. One limitation of squaring cells implemented in CMOS technology is mismatches that reduce the detection range.

Logarithmic Detection

High dynamic range is an essential requirement in the design of most microwave PDs. A dynamic range of 50 dB and above is generally realized through

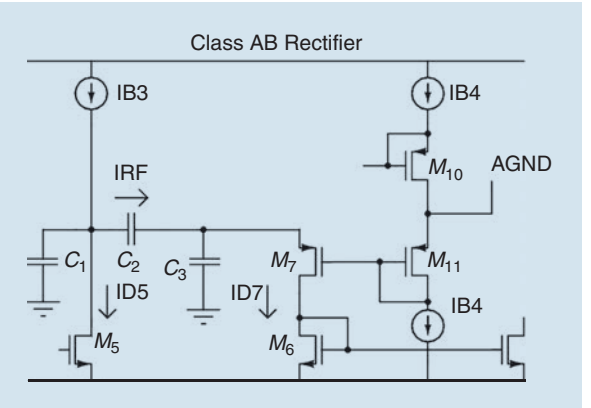

Figure 9. *A schematic of the rectifier with parasitics employed in [27].*

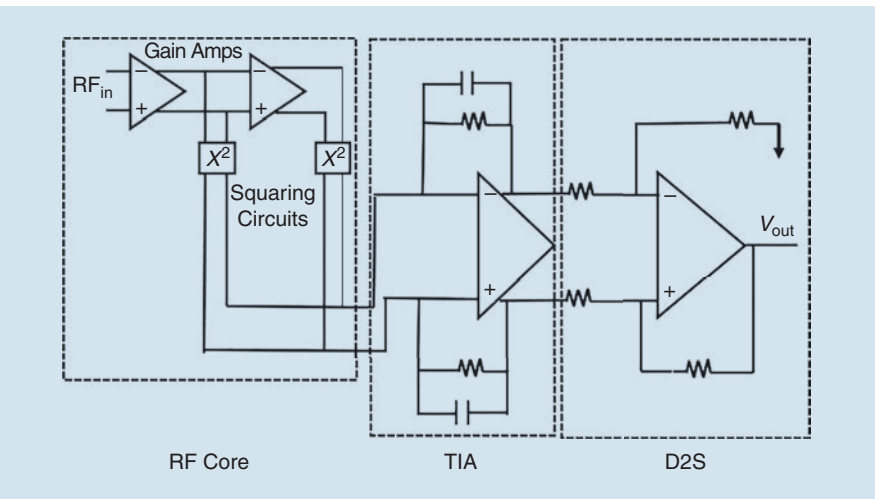

Figure 10. *A microwave PD using squaring cells [30].*

log-amp limiters [7]. Log-amp limiters are a popular and efficient design strategy to extend the dynamic range. The limiter gain stages provide gain and clip the output at a specific voltage level. The limiter closest to the output reaches the maximum level first and then the clipping moves toward the input. The limiters each generate a differential output current and voltage. The differential output voltage is passed to the succeeding limiter while the differential output currents are summed and applied to resistors to generate the linear-in-decibel output [8]. The higher the number of cascaded gain stages, the better the linear-in-decibel performance. However, the power consumption also increases with an increasing number of stages, so design tradeoffs are required.

In an attempt to improve the low dynamic range in [2], a PD with a current mirror active load along with a logarithmic amplifier was designed by [31]. Figure 11 illustrates the architecture of the proposed microwave PD. The microwave PD's architecture consisted of a differential PD unit, a seven-stage logarithmic amplifier, a supply voltage, a process, and a temperature-insensitive current reference circuit for optimum biasing.

The RF input signal was applied to the differential PD unit and converted into a dc output voltage that was further amplified by the seven-stage logarithmic amplifier. Linear-in-decibel output was realized using piecewise linear approximation. Since the PD's output was a dc voltage, the rectifier and filters were omitted from the logarithmic amplifier circuit design, resulting in comparatively low power consumption [31]. A high output resistance was set to achieve a higher conversion gain that considerably improved the PD's sensitivity and linearity. The improved sensitivity makes the PD adequate for a wireless sensor network for fruit farming. The operating frequency was from 0.5 GHz to 3 GHz, and the dynamic range was 50 dB from a supply voltage of 1.8 V [31].

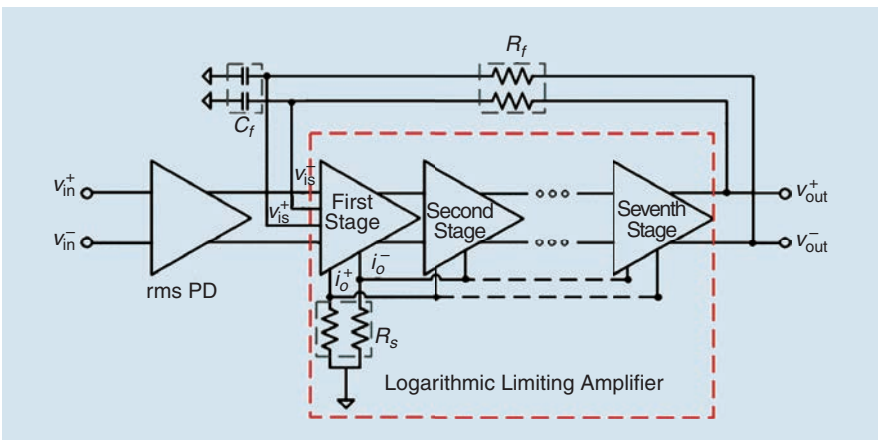

Figure 11. *A log-amp limiter PD [31].*

Another linear-in-decibel microwave PD that relies on a logarithmic amplifier using 180-nm standard CMOS technology was proposed in [32]. A Cherry-Hooper architecture was employed to design limiting amplifiers to accomplish linear RF power detection under high frequency. A common source with PMOS diode-connected load differential amplifier architecture was utilized to design the limiting amplifier. An ac coupling capacitor was also employed as an offset cancellation circuit to compensate for the dc offset due to device mismatch. A wide dynamic range of 40 dB was achieved along with a log-error of ±1dB; however, the PD's power consumption relatively high.

There are also commercially available logarithmic PDs with good performance characteristics. Commercial PDs are usually fabricated using a high-speed SiGe process. Some examples include the ADL5513 and the AD8307, designed and manufactured by Analog Devices [33], [34]. For instance, the ADL5513 PD provides wide bandwidth operation from 1 MHz to 4 GHz with a constant dynamic range of 80 dB. The PD also has a sensitivity of -70 dBm that makes it suitable for applications involving RSSI measurement and power monitoring in radio link transmitters [33]. However, commercial logarithmic PDs also display high power consumption.

Table 1 presents an overview of the different design methodologies' fundamental differences. Table 2 summarizes a list of different design methodologies found in the literature. Their operating parameters and applications are also presented. Table 2 demonstrates that log-amp limiter PDs provide a wider dynamic range of up to 50 dB compared to the other design methodologies. Because cascaded low gain limiting amplifiers and log-amp limiter's can compress wide dynamic range signals into the decibel equivalent, their high dynamic range makes the log-amp limiter suitable for GSM and wireless communications. However, as shown in Table 2, the wide dynamic range comes at the expense of higher power consumption and a larger chip area. This suggests that log-amp limiter PDs are less suitable for applications requiring operation for days with low power and small-chip area. Table 2 also shows that differential structure design methodologies offer a dynamic range between 20 and 27 dB and a much smaller chip area. Their power consumption is relatively low, making them suitable for RF transmitters and communication receivers. As shown in Table 2, the

distributed PD can offer a wide operating frequency range and low power consumption. A wide operating frequency range is crucial in many applications in wireless communications. Table 2 also demonstrates that RMS PDs have relatively low power consumption, low chip area, and reasonably high dynamic range, making them appropriate for a wide range of applications.

TABLE 1. A comparison of implementation strategies for PDs.

Design Methodology	Advantages	Drawbacks
Peak detection	• Simpler circuits • Fast response	• Output voltage varies with PAR • Limited dynamic range • Inaccuracy at high frequencies • Poor temperature stability
Logarithmic detection	• Wide dynamic range • Linear-in-decibel output • Excellent stability and accuracy • Fast response	• High power consumption • Output voltage varies with PAR
Distributed power detection	• Better wideband input matching • Higher sensitivity • Lower NEP	• Limited dynamic range • No linear-in-decibel output
True RMS Power detection	• Output voltage does not vary with PAR • Good stability	• Limited dynamic range • Slow response time

Conclusions

This article presented, a review of microwave PDs using different architectures in standard CMOS. Different PD implementations and their performance metrics were analyzed, and comparisons were drawn. Table 1 shows that each of the available implementations strategies has considerable advantages and disadvantages, so depending on the PD's application requirement, a suitable topology can be chosen. Table 2 demonstrates that logarithmic amplifiers, even though they provide the highest dynamic range, also have the highest power consumption. In contrast, diode-based

TABLE 2. A comparison of existing PD architectures.

Reference	Topology	CMOS Technology (nm)	Operating Frequency (GHz)	Dynamic Range (dB)	P dc (mW)	Sensitivity (dB)	Chip Area (mm^2)	Applications	Date Published
[32]	Log-amp limiter	180	0.1–8	40	70	-	0.98	GSM and AGC	2006
[2]	Differential	0.13	0.1–8.5	20	0.18	-	0.0126	RF transmitter	2008
[27]	Limiter and rectifier	350	0. 9–2.4	30	8.6	-	0.031	RF measurement	2008
[26]	Differential	130	0.8–8.5	27	0.1	-	0.085	Reflectometer and communication receiver	2010
[31]	Differential/ log-amp limiter	180	0.5–3	50	0.9	-	0.0078	Wireless sensor network and telemetry	2012
[25]	Differential	65	0.1–44	20	-	-	-	Microwave and millimeter wave	2014
[1]	Limiter and rectifier	180	0.3–10	42	0.55	-	0.113	Wireless communication	2015
[30]	Squaring cell	28	0.7–4	40	5.8	-	0.1499	RF transmitter	2016
[12]	Single FET	65	0.1–110	-	0.03	67	0.0096	Radio	2017
[22]	Distributed	130	7.0–70	30	0.16	75	0.0684	Wireless communication	2017
[17]	Diode-based	65	4.0–6	32	0.7	-	0.0036	Wireless microwave power transfer	2019
[35]	Log-amp limiter	130	2.0–16	45	35.2	-	-	GSM	2019

and distributed PDs have a lower dynamic range. These fundamental differences among design methodologies are essential in deciding upon a PD circuit configuration for specific application requirements. The significant growth of electronic devices has accentuated the need to control and monitor power at high frequencies. The current market demands smaller size, lower cost, higher frequency capability, and better accuracy. PD designs have become competitive, with improved performance as the ultimate goal. Consequently, to improve PDs' performance, new designs for logarithmic amplifiers with lower power consumption or distributed PDs with a larger dynamic range are areas for future research.

Acknowledgement

The authors would like to acknowledge the Ministry of Education Malaysia for granting funding (FRGS/1/2019/TK04/SWIN/03/1) to support this research work.

References

[1] J. Wang, Y. Zheng, F. Yang, F. Tian, and H. Liao, "A wide band CMOS radio frequency RMS power detector with 42-dB dynamic range," in *Proc. 2015 IEEE Int. Symp. Circuits Syst. (ISCAS)*, pp. 1678–1681, doi: 10.1109/ISCAS.2015.7168974.

[2] Y. Zhou and M. Y. Chia, "A low-power ultra-wideband CMOS true RMS power detector," *IEEE Trans. Microw. Theory Techn.*, vol. 56, no. 5, pp. 1052–1058, 2008, doi: 10.1109/TMTT.2008.921299.

[3] P. Genest, H. Grandry, and H. Chaoui, "Criteria for selecting RF power detectors," *High Freq. Electron.*, vol. 3, pp. 52–55, Jun. 2004, doi: 10.1109/MWSYM.2016.7539988.

[4] B. S. Yarman, *Design of Ultra Wideband Power Transfer Networks*. Hoboken, NJ, USA: Wiley, 2010.

[5] M. Wei, S. Qayyum, and R. Negra, "High sensitivity tunable power detector," in *Proc. 2016 IEEE MTT-S Int. Microw. Symp.*, pp. 1–4, doi: 10.1109/MWSYM.2016.7539988.

[6] J. C. Cowles, "The evolution of integrated RF power measurement and control," in *Proc. 12th IEEE Mediterranean Electrotech. Conf. (IEEE Cat. No.04CH37521)*, 2004, vol. 1, pp. 131–134, doi: 10.1109/MELCON.2004.1346790.

[7] E. Nash. "Ask the applications engineer—28: Logarithmic amplifiers explained." Analog Dialogue. https://www.analog.com/en/analog-dialogue/articles/logarithmic-amplifiers-explained.html (Accessed: Jan. 6, 2020).

[8] A. Thanachayanont, "Design of a low-power wide dynamic range CMOS RF power detector," *Int. J. Electron. Lett.*, vol. 3, no. 4, pp. 213–224, 2015, doi: 10.1080/00207217.2014.917717.

[9] M. Pedram, "Power minimization in IC design: Principles and applications," *ACM Trans. Des. Autom. Electron. Syst.*, vol. 1, no. 1, pp. 3–56, 1996, doi: 10.1145/225871.225877.

[10] D. Harame, "High performance BiCMOS process integration: Trends, issues, and future directions," in *Proc. 1997 Bipolar/BiCMOS Circuits Technol. Meeting*, pp. 36–43, doi: 10.1109/BIPOL.1997.647351.

[11] N. J. Shah and S. Pei, "III-V device technologies for electronic applications," *AT&T Tech. J.*, vol. 68, no. 1, pp. 19–28, 1989, doi: 10.1002/j.1538-7305.1989.tb00643.x.

[12] S. Qayyum and R. Negra, "0.8 mW, 0.1–110 GHz RF power detector with 6 GHz video bandwidth for multigigabit software defined radios," in *Proc. 2017 IEEE MTT-S Int. Microw. Symp.*, pp. 1722–1725, doi: 10.1109/MWSYM.2017.8058975.

[13] G. Zimmer, "Technology for the compatible integration of silicon detectors with readout electronics," *Nucl. Instrum. Methods Phys. Res. Section A, Accel., Spectrometers, Detect. Associated Equip.*, vol. 226, no. 1, pp. 175–184, 1984, doi: 10.1016/0168-9002(84)90186-4.

[14] T. R. Kuphaldt, *Lessons in Electric Circuits – Experiments*, vol. 6, London, U.K.: Koros Press, 2011.

[15] V. Milanovic, M. Gaitan, J. C. Marshall, and M. E. Zaghloul, "CMOS foundry implementation of Schottky diodes for RF detection," *IEEE Trans. Electron Devices*, vol. 43, no. 12, pp. 2210–2214, 1996, doi: 10.1109/16.544393.

[16] L. F. Fei. "Integrated power detector solutions and design strategies." https://www.eetimes.com/integrated-power-detector-solutions-and-design-strategies/# (Accessed: Feb. 14, 2020).

[17] C. Li, X. Yi, C. C. Boon, and K. Yang, "A 34-dB dynamic range 0.7-mW compact switched-capacitor power detector in 65-nm CMOS," *IEEE Trans. Power Electron.*, vol. 34, no. 10, pp. 9365–9368, 2019, doi: 10.1109/TPEL.2019.2908283.

[18] A. S. Brush, "Measurement of microwave power - A review of techniques used for measurement of high-frequency RF power," *IEEE Instrum. Meas. Mag.*, vol. 10, no. 2, pp. 20–25, 2007, doi: 10.1109/MIM.2007.364984.

[19] "Integrated RF Schottky detector," ON Semiconductor, Phoenix, AZ, USA, NCS5000, 2006. [Online]. Available: https://media.digikey.com/pdf/Data%20Sheets/ON%20Semiconductor%20PDFs/NCS5000-D.pdf

[20] S. Qayyum and R. Negra, "Analysis and design of distributed power detectors," *IEEE Trans. Microw. Theory Techn.*, vol. 66, no. 9, pp. 4191–4203, 2018, doi: 10.1109/TMTT.2018.2851954.

[21] R. W. Shillady, "High dynamic range video detector," in *Proc. IEEE MTT-S Int Microw. Symp. Dig.*, 1986, pp. 301–304, doi: 10.1109/MWSYM.1986.1132175.

[22] S. Qayyum and R. Negra, "0.16 mW, 7–70 GHz distributed power detector with 75 dB voltage sensitivity in 130 nm standard CMOS technology," in *Proc. 2017 12th Eur. Microw. Integr. Circuits Conf. (EuMIC)*, pp. 13–16, doi: 10.23919/EuMIC.2017.8230648.

[23] C. Kitchin and L. Counts, *RMS to DC Conversion Application Guide*, 2nd ed. Norwood, MA, USA: Analog Devices, 1983.

[24] H. Erikson and R. W. Waugh. "A temperature compensated linear diode detector." Design Tip. https://olli.vanhoja.net/static/d009.pdf (Accessed: Mar. 16, 2020).

[25] K. Xu, X. Yang, W. Wang, and T. Yoshimasu, "44-GHz, 0.5-V compact power detector IC in 65-nm CMOS," in *Proc. 2014 IEEE Int. Wireless Symp.*, pp. 1–3, doi: 10.1109/IEEE-IWS.2014.6864216.

[26] C. Li, F. Gong, and P. Wang, "A low-power ultrawideband CMOS power detector with an embedded amplifier," *IEEE Trans. Instrum. Meas.*, vol. 59, no. 12, pp. 3270–3278, 2010, doi: 10.1109/TIM.2010.2047131.

[27] A. Valdes-Garcia, R. Venkatasubramanian, J. Silva-Martinez, and E. Sanchez-Sinencio, "A broadband CMOS amplitude detector for on-chip RF measurements," *IEEE Trans. Instrum. Meas.*, vol. 57, no. 7, pp. 1470–1477, 2008, doi: 10.1109/TIM.2008.917196.

[28] M. A. Al-Absi and I. A. As-Sabban, "A CMOS current-mode squaring circuit free of error resulting from carrier mobility reduction," *Analog Integr. Circuits Signal Process.*, vol. 81, no. 1, pp. 23–28, 2014, doi: 10.1007/s10470-014-0319-8.

[29] Z. Tao, W. R. Eisenstadt, and R. M. Fox, "A novel 5GHz RF power detector," in *Proc. 2004 IEEE Int. Symp. Circuits Syst. (IEEE Cat. No. 04CH37512)*, vol. 1, pp. 1–897, doi: 10.1109/ISCAS.2004.1328340.

[30] J. Choi *et al.*, "Wide dynamic-range CMOS RMS power detector," *IEEE Trans. Microw. Theory Techn.*, vol. 64, no. 3, pp. 868–880, 2016, doi: 10.1109/TMTT.2016.2519030.

[31] S. Sakphrom and A. Thanachayanont, "A low-power CMOS RF power detector," in *Proc. 2012 19th IEEE Int. Conf. Electron., Circuits, Syst. (ICECS)*, pp. 177–180, doi: 10.1109/ICECS.2012.6463771.

[32] J. Wu *et al.*, "A linear-in-dB radio-frequency power detector," in *Proc. 2011 IEEE MTT-S Int. Microwave Symp.*, pp. 1–4, doi: 10.1109/MWSYM.2011.5972772.

[33] "1 MHz to 4 GHz, 80 dB logarithmic detector/controller," Analog Devices, Norwood, MA, USA, ADL5513, 2008. [Online]. Available: https://www.analog.com/media/en/technical-documentation/data-sheets/ADL5513.pdf

[34] "Low cost, DC to 500 MHz, 92 dB logarithmic amplifier," Analog Devices, Norwood, MA, USA, AD8307, 2006. [Online]. Available: https://www.analog.com/media/en/technical-documentation/data-sheets/AD8307.pdf

[35] Z. Yijun and M. C. Y. Wah, "A wide band CMOS RF power detector," in *Proc. 2006 IEEE Int. Symp. Circuits Syst.*, p. 4231, doi: 10.1109/ISCAS.2006.1693562.

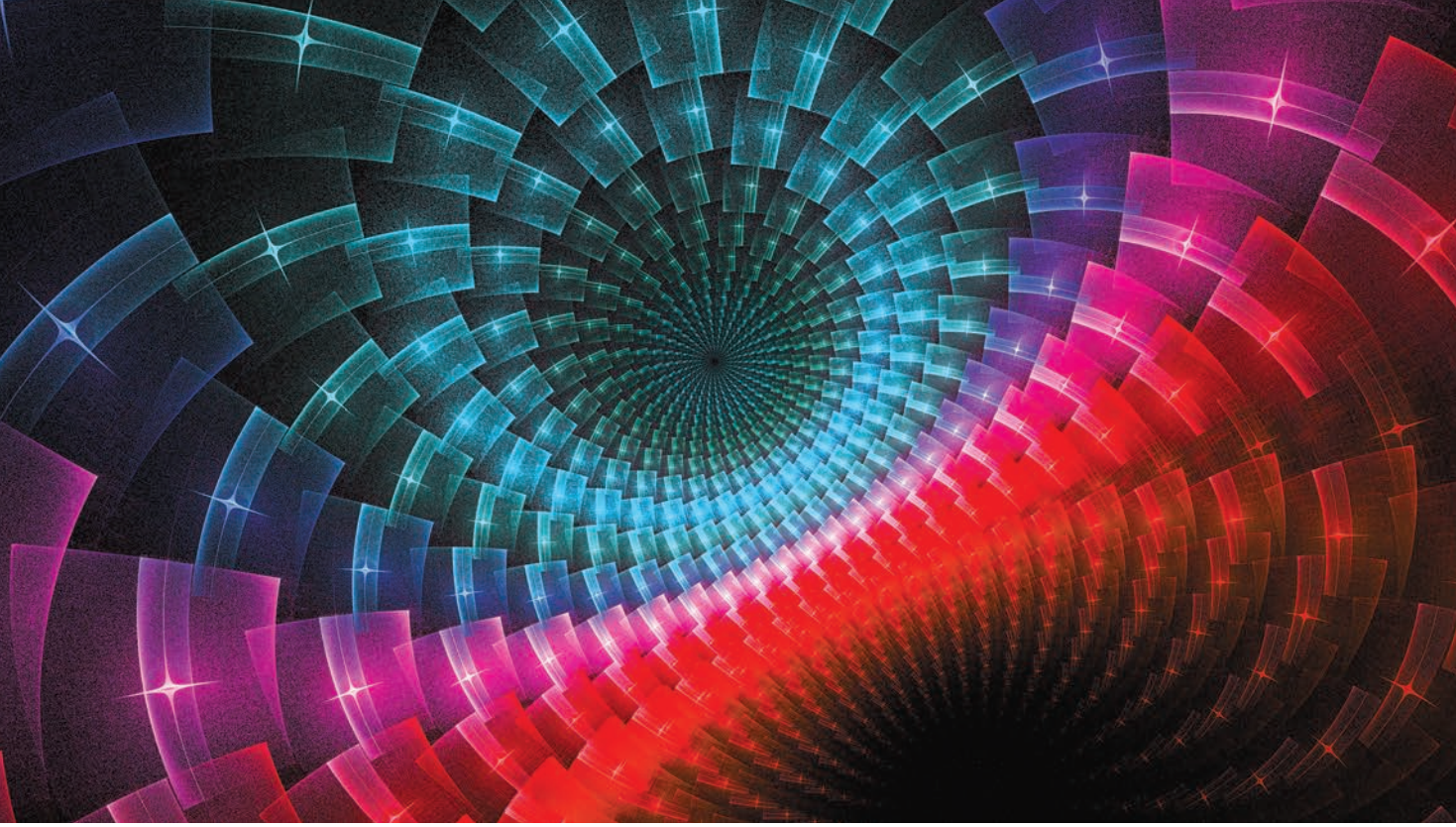

Spatiotemporal Nonreciprocal Filters

Prantik Dutta, Gande Arun Kumar, Gopi Ram, and Dondapati Suneel Varma

Nonreciprocal components are of paramount importance in many electronic systems. Traditionally, reliance on magnetic materials, such as ferrites, has been the basis of the functionality of such components. The internal magnetic moment under the influence of a strong external magnetic bias breaks the reciprocity of the materials [1]. However, today's state-of-the-art systems demand cost-effective, miniaturized, and integrated solutions. This can be achieved with magnetless nonreciprocal devices that are capable of breaking the Lorentz reciprocity

Prantik Dutta (prantikdutta3@student.nitw.ac.in), Gande Arun Kumar (g.arun@nitw.ac.in), Gopi Ram (gopi.ram@nitw.ac.in) and Dondapati Suneel Varma (d.suneelvarma@student.nitw.ac.in) are with the Department of Electronics and Communication Engineering, National Institute of Technology, Warangal, Telangana, 506004, India.

Digital Object Identifier 10.1109/MMM.2022.3157970

Date of current version: 5 May 2022

principle [2]. In the past decade, passive metastructures have also been devised to achieve Faraday rotation without magnetic bias. Spatiotemporal biasing of the metasurfaces initiates frequency translation and harmonic mixing properties that, in turn, generate nonreciprocity [3], [4]. Recently, with the advent of magnetless nonreciprocal devices, time-varying circuits have been viewed as a remarkable breakthrough. This has, in fact, paved the path for researchers to develop nonreciprocal devices such as circulators [5]–[14], isolators [15]–[18], gyrators [19], and even leaky-wave antennas [20], [21]. Still, there remain some areas in the field of nonreciprocity that can be explored with the aid of magnetless time-varying circuits. One such area is the implementation of nonreciprocity in bandpass filters.

Nonreciprocal bandpass filters (NR-BPF) find a broad spectrum of applications in the domain of communication systems. One such application-specific deployment is in the wireless transceiver system shown in Figure 1. The NR-BPF in the transmitter section allows only the in-band frequency components (indicated by green arrows) and prevents any out-of-band frequency components (indicated by brown arrows) to pass to the power amplifier stage in the forward direction, while at the same time preventing any in-band frequency components (indicated by red arrows) to pass back to the mixer stage as a result of reflection from the power amplifier and the antenna. Similarly, in the receiver section, the NR-BPF not only acts as a filter (indicated by green and brown arrows) but also acts as an isolator by attenuating any reflected wave that might pass to the antenna. The advantage of using a single NR-BPF to serve this dual purpose lies in the reduction of losses that would have been incurred by deploying both the filter and the isolator together to manifest the same phenomenon.

Although nonreciprocity in bandpass filters has been implemented using various techniques [23]–[25], implementation using time-modulated resonators is still nascent. Wu et al. proposed a novel concept of an isolating bandpass filter with low forward transmission loss and high reverse isolation at the center frequency [22]. The basic block diagram of a third-order NR-BPF is given in Figure 2. The circuit consists of space-separated time-varying resonators in addition to the capacitors that are generated by virtue of admittance inverters (to be dealt with shortly). Owing to the nonlinear capacitance property of a varactor diode under reverse bias, the modulation of the varactors within the resonators generates intermodulation (IM) products. The significant difference between the RF power distribution among the IM products in the forward and reverse paths generates nonreciprocity in the circuit characteristics. The essence of the time-varying capacitance lies in the generation of IM products, which, unlike time-invariant products, do not generate a reciprocal bandpass response. Interestingly, with only the dc bias applied, the varactor would behave as a normal capacitor and hence would not produce any nonreciprocity. It will be further explained in the "Analysis of Spatiotemporal Transmission Lines" section that the amplitude, frequency, and phase of the ac signal applied to the time-varying capacitance determines the position of the IM products with respect to the RF signal in the frequency domain. Hence, the RF signal is translated to the higher and lower harmonic frequencies owing to the position of the IM products as it travels

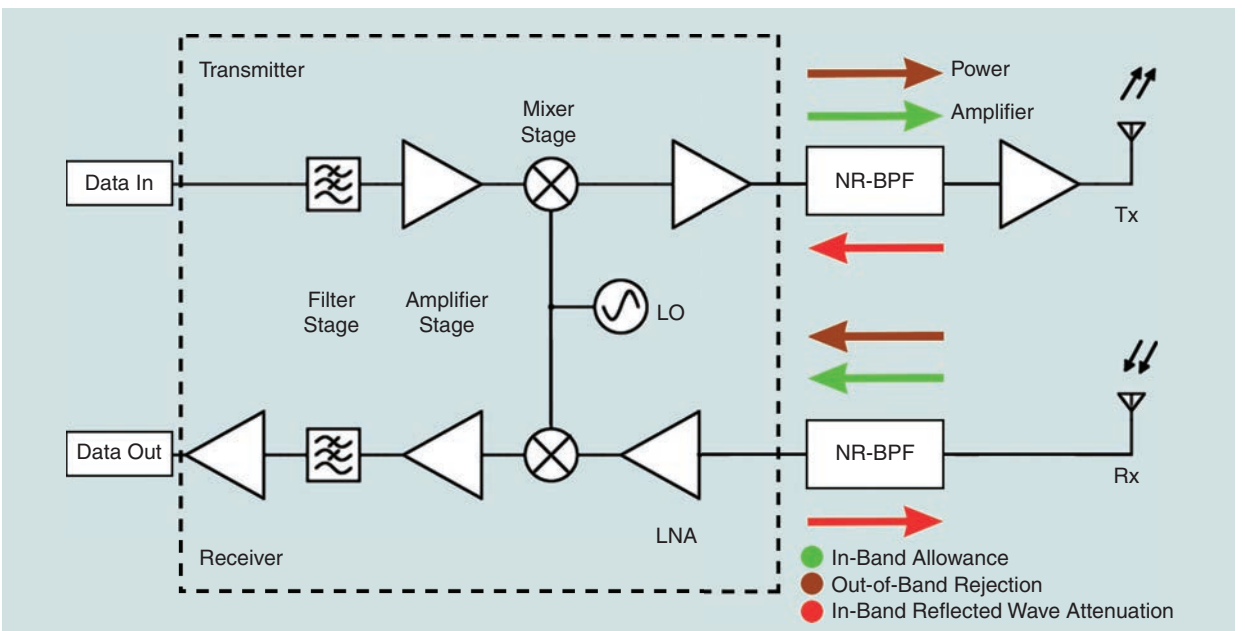

Figure 1. *A block diagram of a transceiver deployed with NR-BPF. LO: local oscillator; LNA: low-noise amplifier.*

from source to load or vice versa. The frequency translation also leads to the distribution of RF power among these harmonics, but a wise choice of the parameters of the ac signal results in the constructive interference of the signals translated to harmonics with the signal at the fundamental frequency, thus reinforcing the RF signal reaching the load in the forward direction. Conversely, destructive interference between the signals in the reverse direction results in an attenuation of RF power reaching the source in the backward direction. This phenomenon causes the bandpass filtering response in the forward direction while triggering an isolation within the passband of the filter in the reverse direction.

The concept of time-varying transmission lines (TVTL) has already proved its usefulness in application-specific domains such as circulators, isolators, and other nonreciprocal communication systems. Nonreciprocal filters with the aid of TVTL, although in the nascent stage, may prove superior to circuits involving conventional bulky and expensive ferrite components.

The objective of this article is to develop basic concepts for the design of time-modulated filters and to survey the current state of practical implementation of these filters. Specifically, the prerequisites for the concept that are historically significant are elaborated to set the foundation for a discussion of nonreciprocal filters. Second, the theory of nonreciprocity in filters at the fundamental frequency using spatiotemporal modulation (STM) is presented. Finally, a survey of practical implementation of the filters in lumped and distributed components is discussed. This review aims to contribute to the understanding of nonreciprocal filters and to open doors for researchers to accelerate the burgeoning development of the field of magnetless nonreciprocal filter design.

Prerequisites to the Concept of Nonreciprocity

Before moving on to decipher the cause of nonreciprocity, it's helpful to understand the concepts that serve as milestones in the development of nonreciprocity and that still underpin modern day technological advances in this domain.

The Parametric Amplifier

Any amplifier can be considered to be a modulator in which the energy of the input wave is transformed to the load impedance by harnessing the energy from the amplifier's energy source. The amplifier's energy source can be either a dc or an ac supply. For a dc source, the amplified output waveform is an exact replica of the input waveform with the amplifier's energy source providing the useful gain. However, for an ac source, the output is not an exact replica of the input. In fact, the frequency of the output waveform is transformed owing to the generation of new frequencies due to the interaction of two waves of different frequencies. The spectral content of the output waveform contains an infinite number of transformed frequencies. These frequencies, denoted as $f_{y,z}$, where y and z are positive, negative, or zero integers, are harmonically related to the input wave frequency (f_0) and the frequency of the modulator's energy source (f_m), also termed the *local oscillator* ($f_{y,z} = yf_0 + zf_m$). This energy conversion from one frequency component to another is governed by general power relations first described by Manley and Rowe [26], which are popularly known as the *Manley–Rowe relations*. These relations consist of two independent equations that govern nonlinear reactance modulators provided the nonlinear characteristic of the element (capacitor or inductor) is single-valued. These equations relate the power at different frequencies obtained after harmonic mixing of the input signal frequency and the local oscillator or modulation frequency. By expanding the charge q and flux linkage ψ for the capacitor and inductor respectively in terms of a Fourier series, the Manley–Rowe equations relating the average power flowing into the nonlinear element, $W_{y,z}$, at the harmonic frequencies $f_{y,z}$ with the individual components f_0 and f_m can be expressed as shown in (1):

$$\sum_{y=0}^{\infty}\sum_{z=-\infty}^{\infty}\frac{yW_{y,z}}{yf_0+zf_m}=0$$
$$\sum_{y=-\infty}^{\infty}\sum_{z=0}^{\infty}\frac{yW_{y,z}}{yf_0+zf_m}=0. \quad (1)$$

For a linear capacitor or inductor, without mixing terms, only two frequency components will be present, that is, either f_0 or f_m and $W_{y,z}=0$ for all y and z, proving that (1) is satisfied. Any circuit analysis that includes nonlinear reactance should be checked with (1) to ensure good gain and stability.

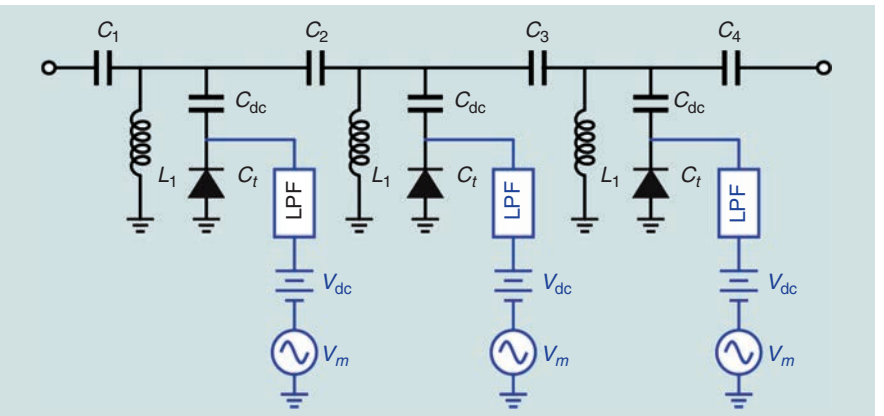

Figure 2. *A block diagram of a third-order NR-BPF using varactor diodes [22]. LPF: lowpass filter.*

Remarkable results can be obtained from (1). If the circuit is designed to allow only the current of harmonic frequency $f_0 + f_m$, denoted as sum frequency f_s with associated power, then W_s is allowed to be present in addition to the individual frequencies f_0 and f_m, and (1) gives

$$\frac{W_m}{f_m} + \frac{W_s}{f_s} = 0$$
$$\frac{W_0}{f_0} + \frac{W_s}{f_s} = 0, \tag{2}$$

where W_0 is the power of the signal source and W_m is that of the power entering the nonlinear element from the local oscillator. Since power is supplied by the currents of frequencies f_0 and f_m, therefore W_0 and W_m are positive whereas W_s is negative, since power is being delivered at the frequency $f_0 + f_m$. Therefore, (2) can be rearranged as

$$-\frac{W_s}{W_0} = 1 + \frac{f_m}{f_0}. \tag{3}$$

Thus, a gain at the sum frequency ($f_s = yf_0 + zf_m$) with respect to the signal frequency is obtained, and this type of amplifier is known as a *parametric up-converter*. The order of the modulation product is the sum of the integer values y and z [27]. An even more interesting result is obtained if, instead of the sum frequency, a difference frequency $f_d = f_m - f_0$ is allowed to flow. If the power delivered to the frequency component is W_d, then the Manley–Rowe equations for such a circuit turn out to be

$$\frac{W_m}{f_m} + \frac{W_d}{f_d} = 0, \tag{4a}$$
$$\frac{W_0}{f_0} - \frac{W_d}{f_d} = 0. \tag{4b}$$

From (4a), it can be seen that the local oscillator supplies energy to the nonlinear reactance; therefore, the power at the difference frequency is negative. This is because power is being delivered by the nonlinear reactance at the difference frequency. Consequently, from (4b), the power at the RF frequency W_0 should be negative. Thus, for this case, the nonlinear reactance offers a negative resistance to the RF signal source. This results in the abstraction of power from the local oscillator and this power is delivered to both the signal source and the signal generated with the difference frequency. This negative resistance creates an instability. The magnitude of the gain in this case is equivalent to that obtained in (3). If the external resistance to the difference frequency is now reduced from a large value, the total signal circuit resistance could approach zero. Under this condition, the external signal source can be removed and the three components, comprising the signal, the modulation, and the difference frequency (f_d), will continue to flow, resulting in free oscillations. This has been experimentally demonstrated in [28], where, the reduction in external resistance facilitated the production of sustained oscillations. The circuit operating under this condition is called a *negative resistance parametric amplifier*.

A magnetic modulator has been demonstrated in [29]. It is shown that for the simplest modulation containing only a single magnetic modulator, the sum frequency introduces a positive resistance while the difference frequency introduces a negative resistance in the signal path. In the carrier or the local oscillator path, both of the frequencies introduce positive resistance. The same phenomenon occurs in case of a variable capacitor circuit [30], [31]. Thus, for any nonlinear reactance, the flow of current comprising the difference frequency causes abstraction of energy from the carrier (f_m) that is delivered to the signal (f_0) while that of the sum frequency results in abstraction of energy from both the carrier and the signal.

A parametric amplifier using semiconductor diodes has been illustrated in [32]. The application of parametric amplification has also been investigated in time-varying distributed reactance in propagating structures [33]. Depending on the phase and group velocity of the propagating wave, which in turn depends on the series reactance and the shunt susceptance of the transmission line, four cases have been studied; each case complies with the Manley–Rowe equations. If the phase and the group velocity are in the same direction, it leads to frequency conversion; that is, the power from one frequency is transferred to the other frequency with the additional power being supplied by the time-variant reactance (capacitor or inductor). If two waves of different group velocities but with the same phase velocities flow, it can be utilized as a filter or a frequency channel selector, which has been further studied in [16].

STM Transmission Line

From parametric amplifier theory, it is clear that nonlinear or time-varying reactance leads to mixing of harmonic frequencies, resulting in generation of IM products. The IM products strictly follow the Manley–Rowe equations, provided the reactance is single-valued. One of the application-specific domains of this frequency-mixing behavior is the separation of spatio-temporally overlapping signals traveling in opposite directions without using bulky ferrite components as has been demonstrated in [34] and [35]. The concept of distributed modulated capacitors (DMC) that can serve as a time-varying transmission line in which varactor diodes are loaded along the length of the transmission line has been proposed in [16] and is shown in Figure 3(a).

The modified telegrapher's equation [37] for TVTL using time-varying capacitance is given by

$$\frac{\partial v(z,t)}{\partial z} = -L\frac{\partial i(z,t)}{\partial t}$$
$$\frac{\partial i(z,t)}{\partial z} = -\frac{\partial [C(z,t)v(z,t)]}{\partial t}, \tag{5}$$

where L is the inductance per unit length and $C(z, t)$ denotes the time-varying capacitance per unit length. The time-varying capacitance $C(z, t)$ is usually implemented using a varactor diode, which is nothing but a voltage controlled capacitor where the reverse bias applied across the varactor changes the capacitance. In fact, the capacitance decreases with the applied reverse bias. So, an ac voltage applied across the varactor results in a corresponding variation in the capacitance, which can be expressed by

$$C(z,t) = C_0 + \Delta C \cos(\omega_m t - \beta_m z + \phi), \tag{6}$$

where C_0 denotes the mean capacitance per unit length and the second part of (6) corresponds to the capacitance due to the applied reverse bias ac voltage across the varactor where ΔC is the amplitude variation per unit length of the capacitance due to the reverse bias, ω_m is the angular frequency, and β_m is the phase constant. In a similar manner, a transmission line embedded in a ferromagnetic medium is demonstrated in [36] as shown in Figure 3(b). Here, the ferromagnetic medium is driven by a local oscillator that actually leads to the time variation in the transmission line. This time-varying ferromagnetic medium, in fact, provides a mutual coupling between the two transmission lines.

Just as in the case of transmission lines loaded with time-varying capacitance per unit length, the modified telegrapher's equation for Figure 3(b) is given in [36]. The characteristic impedance and phase constant of the lines are given as $Z_{0i} = \sqrt{L_i / C_i}$ and $\beta_i = \omega_i \sqrt{L_i C_i}$, where i = 1, 2. The ferromagnetic medium is energized by a traveling wave with a phase constant β and angular frequency ω. Similar to the time-varying capacitance, the time-varying inductance $L(z, t)$ takes the form given in [36]. If the frequency of the waves traveling in lines 1 and 2 are such that $\omega_1 + \omega_2 = \omega$, then, as in the case of parametric amplifiers, the energy of the local oscillator is coupled to the traveling waves in lines 1 and 2 and this leads to exponentially growing waves along the length of the transmission line, leading to exponential amplification. But the drawback of this circuit is that two separate transmission lines are needed for the coupling to occur and for the transfer of energy. So, a time-varying transmission line utilizing a spatiotemporal variation of the capacitance is a better choice.

A time-varying transmission line finds wide application not only in the generation of nonreciprocal components like isolators and circulators but also its unique feature of allowing propagation only in the direction of the carrier signal can be well utilized in the design of nonreciprocal filters, as was demonstrated for the first time in [22]. Let us suppose the angular frequency of the signal and the carrier wave traveling in the transmission line shown in Figure 4 are ω_0 and ω_c, respectively.

The signal arriving from the antenna is modulated by the varactors, and currents at the intermodulation products are generated. These currents travel both right and left along the upper transmission line. If the parametric conversion is considered at only the upper sideband $(\omega_0 + \omega_c)$, the received signals at the left (b_+) and right (b_-) are given in [38]. Analysis of the received signal at either end reveals that, moving toward the receiver end in Figure 4, the signal amplitude gradually increases, whereas, moving toward the transmitter end, the signal amplitude gradually decreases and reaches zero after some wavelengths. As the number of varactors increases, the faster the decay. This analysis proves to be the basis for further application-specific STM transmission lines with distributedly modulated capacitors.

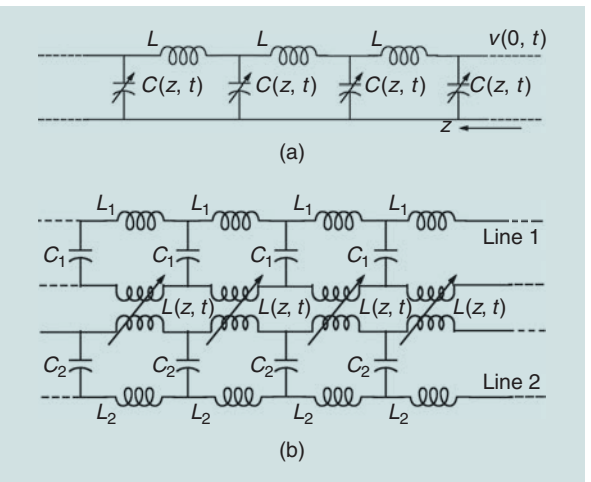

Figure 3. *A time-varying transmission line integrated with spatiotemporally modulated transmission line (a) capacitance per unit length [16] and (b) inductance per unit length [36].*

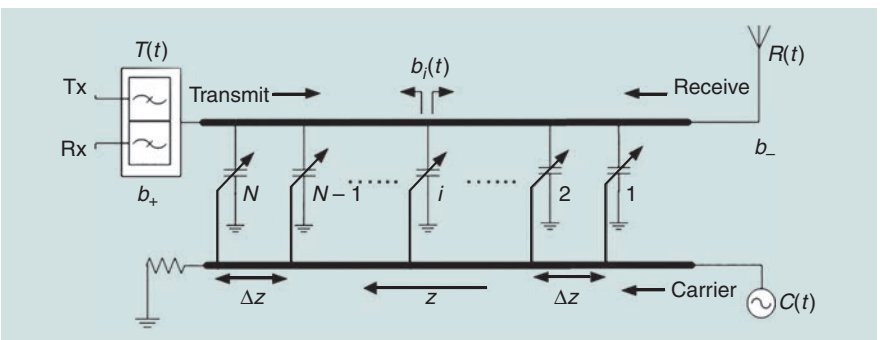

Figure 4. *A concept of DMC as circulator, where* $T(t) = e^{j\omega_0(t+z/v_p)}$, $R(t) = e^{j\omega_0(t-z/v_p)}$, *and* $C(t) = e^{j\omega_c(t-z/v_p)}$ *[38].*

Nonreciprocal Filters

In the previous sections, parametric amplification, frequency mixing, and nonreciprocal behavior in TVTL using STM were explained. Based on these properties of a TVTL, a filter in the forward direction with isolation in the backward direction has been demonstrated in [22]. Prior to digging deeper into the underlying cause of nonreciprocity in filter characteristics, we first discuss the foundations of the insertion loss method in the design of conventional filters.

Analysis of the Insertion Loss Method

The basis for the analysis of any filter function using the insertion loss method is the construction of a characteristic polynomial for the desired insertion loss (IL) and the return loss (RL) level in the lowpass prototype (LPP) domain [37]. Once the characteristic polynomial has been defined in the Laplace (s) domain, the next step is the extraction of the elemental values so as to design a circuit comprising the corresponding reactive elements. The LPP domain can be converted to the bandpass prototype (BPP) domain based on classical lowpass-bandpass transformations. Based on the synthesized parameters, the circuit can then be represented in a coupling matrix form.

The concept of a coupling matrix was first introduced in 1970 by Atia and Williams for the BPP model [39], [40]. Once the g values, frequency independent (FIR) elements, and coupling inverter values are extracted, the total coupled network can be represented in the form of a two-port network. This two-port network, using Kirchhoff's nodal laws, can be represented in a matrix form also known as a *coupling matrix*. It is an integration of the source and load impedances (R_S and R_L), the frequency dependent elements (capacitors and inductors), and the FIR elements, which leads to the mainline and cross-couplings represented by the matrix **M**. Further details on the synthesis and scaling of the coupling matrix can be found in [41]–[43]. Modeling the elements in matrix form simplifies operations such as scaling, transformation, and inversion. The extracted network from the synthesized polynomials is pictorially shown in [44].

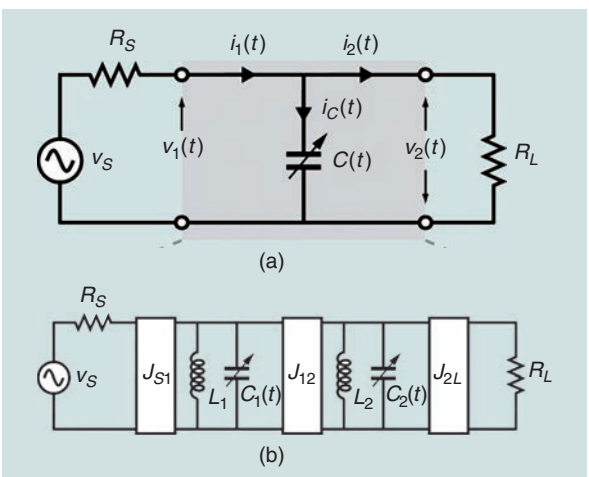

Figure 5. *(a) A simple LTV circuit with a single shunt capacitor modulated by a sinusoidal signal. (b) A generalized circuit topology of a second-order spatiotemporally modulated filter [22].*

Analysis of Spatiotemporal Transmission Lines

A linear time-varying (LTV) transmission line is shown in Figure 5(a). The time-varying shunt capacitor $C(t)$, which can be implemented using the varactor diode, happens to be the primary underlying cause of nonreciprocity (which will be explored in due course). If, in place of a single time-varying element, multiple time-varying elements are added along the transmission line, as shown in Figure 5(b), with each modulated by sinusoidal signals with progressive phase shifts, then the phenomenon is termed *STM* since the time-varying elements are separated in space as well as being time modulated with different phase angles. Since the STM transmission line deals with the harmonics of the signal frequency ω and the modulation frequency ω_m, the analysis should be transformed from the time domain to the frequency domain using Fourier analysis [45]. The time harmonic capacitance variation is given in (6). For our analysis, the spatial part ($\beta_m z$) is ignored and a new term ζ is introduced, which is given by $\zeta = \Delta C/C_0$. Kirchhoff's law applied to the network in Figure 5(a) gives

$$v_1(t) = v_2(t), \tag{7a}$$

$$i_1(t) = j\omega C(t) v_2(t) + i_2(t). \tag{7b}$$

Substituting only the time-varying portion of $C(t)$ from (6) and applying a Fourier transform to the equation set (7), it can be shown that

$$V_1(\omega) = V_2(\omega), \tag{8a}$$

$$I_1(\omega) = j\omega C_0 V_2(\omega) + j\omega\frac{\Delta C}{2} \times [V_2(\omega - \omega_m)e^{j\phi} + V_2(\omega + \omega_m)e^{-j\phi}] + I_2(\omega). \tag{8b}$$

Similar expressions can be obtained at the generated intermodulation frequencies ($\omega \pm \omega_m$) from (8) and can be integrated into a spectral admittance matrix [46] as given in [22]. When an LC resonator with an FIR element is used in place of the time-variant capacitor alone, extra $1/j\omega L$ and jB terms are added to the admittance matrix. For the BPP, the admittance of a resonator comprising the unmodulated capacitance of the varactor C_0, the inductor L, and a FIR element B at the nth IM product is denoted in (9):

$$Y_q^{(n)} = jC_0(\omega + n\omega_m) + \frac{1}{jL(\omega + n\omega_m)} + jB. \tag{9}$$

If, additionally, two terms $P^{(p)}$ and $Q^{(p)}$ corresponding to the pth resonator are defined as

$$P^{(p)} = \frac{\zeta}{2} e^{-j\phi_p}, \tag{10a}$$

$$Q^{(p)} = \frac{\zeta}{2} e^{j\phi_p}, \tag{10b}$$

the spectral admittance matrix of the pth resonator is given by (11). In terms of Fourier series representation, the modulation of the varactor generates an infinite number of IM products ($\omega \pm n\omega_m$), but only a limited range of IM products will suffice.

In the matrix shown in (11) at the bottom of the page, IM products only up to $n = \pm 2$ are considered for analysis. Apart from the center element of the matrix, the other diagonal elements depict the new resonators formed due to the generated IM products while the off-diagonal elements represent the couplings between the different harmonic components of the same resonator [44]. A closer look into the matrix in (11) shows that the matrix is not symmetric. This implies that apart from the mainline couplings (the J inverters), the couplings between the harmonic resonators are related by a nonreciprocal admittance inverter that, for a coupling between two different harmonics $(n-1)$ and n for a resonator p, is given by

$$J_p^{(n,n-1)} = Q^{(p)}[\omega + n\omega_m], \tag{12a}$$

$$J_p^{(n-1,n)} = P^{(p)}[\omega + (n-1)\omega_m]. \tag{12b}$$

The first equation of (12) represents an up-conversion from the $(n-1)$th to the nth harmonic while the second one represents the down-conversion. The equivalent circuit of the spectral admittance matrix is shown in Figure 6.

On the basis of (11) and (12), a coupling topology has been framed in [44], which delves deeper into the underlying cause of nonreciprocity. In the coupling topology, the mainline $J_{i,i+1}$ inverters couple the different resonators within the same harmonics (ω or $\omega \pm k\omega_m$), but the inverters of (12) show the coupling between contiguous harmonic components of the same resonator. Since these couplings between the adjacent nonlinear harmonics are nonreciprocal, the response of the system is also nonreciprocal [47]. It is clear that the phase terms associated with these couplings between adjacent nonlinear harmonics [(12)] are the underlying cause of nonreciprocity.

Figure 7(a) and (c) represent the traveling of electromagnetic (EM) waves to and from port 1 and port 2 only through the resonators and the mainline couplings. This traveling wave does not encounter any phase differences as is evident from the fact that there are no phase terms linked with the diagonal elements in the admittance matrix shown in (11). This indicates that, without modulation, there is no nonreciprocity. Now, if Figure 7(b) and (d) are observed, they show the traveling of EM waves through the nonlinear harmonic resonators generated due to the modulation of the capacitor. If the phase difference between the resonators is considered as $\Delta\phi$ and the phase of the first resonator as $\phi_1 = 0^\circ$, then the total phase difference encountered by the wave in the forward direction is $+\phi_1 + \phi_2 - 2\phi_3 = -135^\circ$ and that in the backward direction is $-\phi_1 - \phi_2 + 2\phi_3 = 135^\circ$. The phase difference between the forward and backward traveling wave is 90°, thus explaining the concept of nonreciprocity. Alternately, if the $ABCD$ parameters of the 2-pole filter shown in [22] are found to be

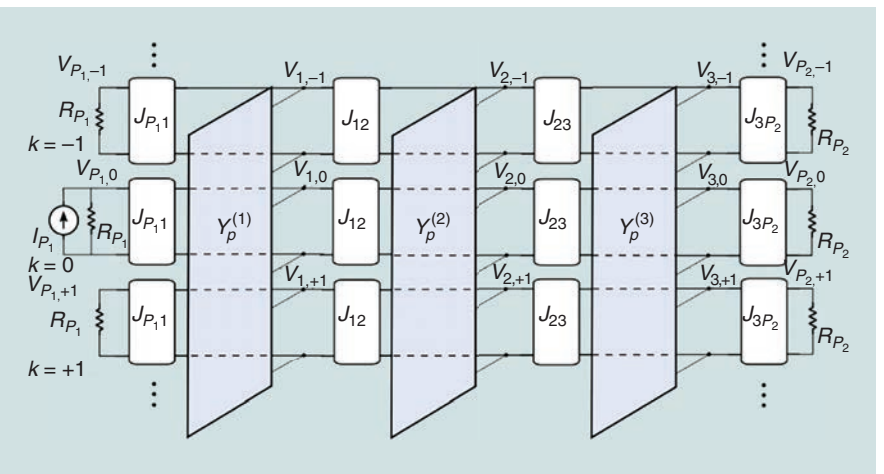

Figure 6. *An equivalent circuit transformed from the basic coupled resonator circuit showing the generated nonlinear harmonics [44].*

$$\mathbf{Y}_r^{(p)} = \begin{bmatrix} Y_q^{(-2)} + jB_p & jP^{(p)}(\omega - 2\omega_m) & 0 & 0 & 0 \\ jQ^{(p)}(\omega - \omega_m) & Y_q^{(-1)} + jB_p & jP^{(p)}(\omega - \omega_m) & 0 & 0 \\ 0 & jQ^{(p)}\omega & Y_q^{(0)} + jB_p & jP^{(p)}\omega & 0 \\ 0 & 0 & jQ^{(p)}(\omega + \omega_m) & Y_q^{(+1)} + jB_p & jP^{(p)}(\omega + \omega_m) \\ 0 & 0 & 0 & jQ^{(p)}(\omega + 2\omega_m) & Y_q^{(+2)} + jB_p \end{bmatrix}. \tag{11}$$

$$AD - BC = \frac{C_0^2\omega_1^2 - J_{12}^2 + \frac{C_0^2\zeta^2(\omega-\omega_m)\omega e^{-j\Delta\phi}}{4} + \frac{C_0^2\zeta^2(\omega+\omega_m)\omega e^{j\Delta\phi}}{4}}{J_{12}^2} + j\frac{C_0^2 J_{S1}\omega_1^2}{J_{12}}, + j\frac{C_0^2 J_{S1}\zeta^2(\omega-\omega_m)\omega e^{-j\Delta\phi}}{4J_{12}} + j\frac{C_0^2 J_{S1}\zeta^2(\omega+\omega_m)\omega e^{j\Delta\phi},}{4J_{12}} \quad (13)$$

where $\omega_1 = \omega - 1/\omega LC_0$. When there is no modulation, $\zeta = 0$ and at the center frequency, $\omega_0 = 1/\sqrt{LC_0}$ and thus ω_1 turns out to be 0. Then the AD – BC of (13) becomes

$$AD - BC = 1. \quad (14)$$

Thus, mathematical analysis proves that the modulation frequency ω_m and modulation index ζ, along with the phase difference between the resonators $\Delta\phi$, generate the nonreciprocity in these spatiotemporal circuits. Although this analysis relies on the manifestation of nonreciprocity by the time-varying circuits, the underlying cause of the phenomenon remains somewhat unclear.

Figure 8(a) shows the underlying phenomena encountered by the EM wave when it traverses from port 1 to port 2 (forward direction). The direction of the orange arrows indicate the probable paths taken by the EM wave in the forward journey through the mainline resonators as well as the resonators generated at the first harmonic frequency. Although the resonators at only the first harmonics are shown, the same holds for the higher order harmonics. The thickness of the arrows indicates the approximate energy content in the EM wave at the particular position. The blue arrows indicate the reflected wave at port 1, their direction and thickness conveying the same information as the orange ones. The energy of the EM wave is distributed among the fundamental and the harmonics, thereby incurring a loss just after encountering the first resonator. The remainder of the energy is further distributed in the corresponding mainline resonators as well as being redistributed among other higher order harmonics as it advances. By proper choice of circuit parameters, the energy of all of the harmonics can be made to converge again at the fundamental frequency, thereby nullifying the IL. If the energy from the various

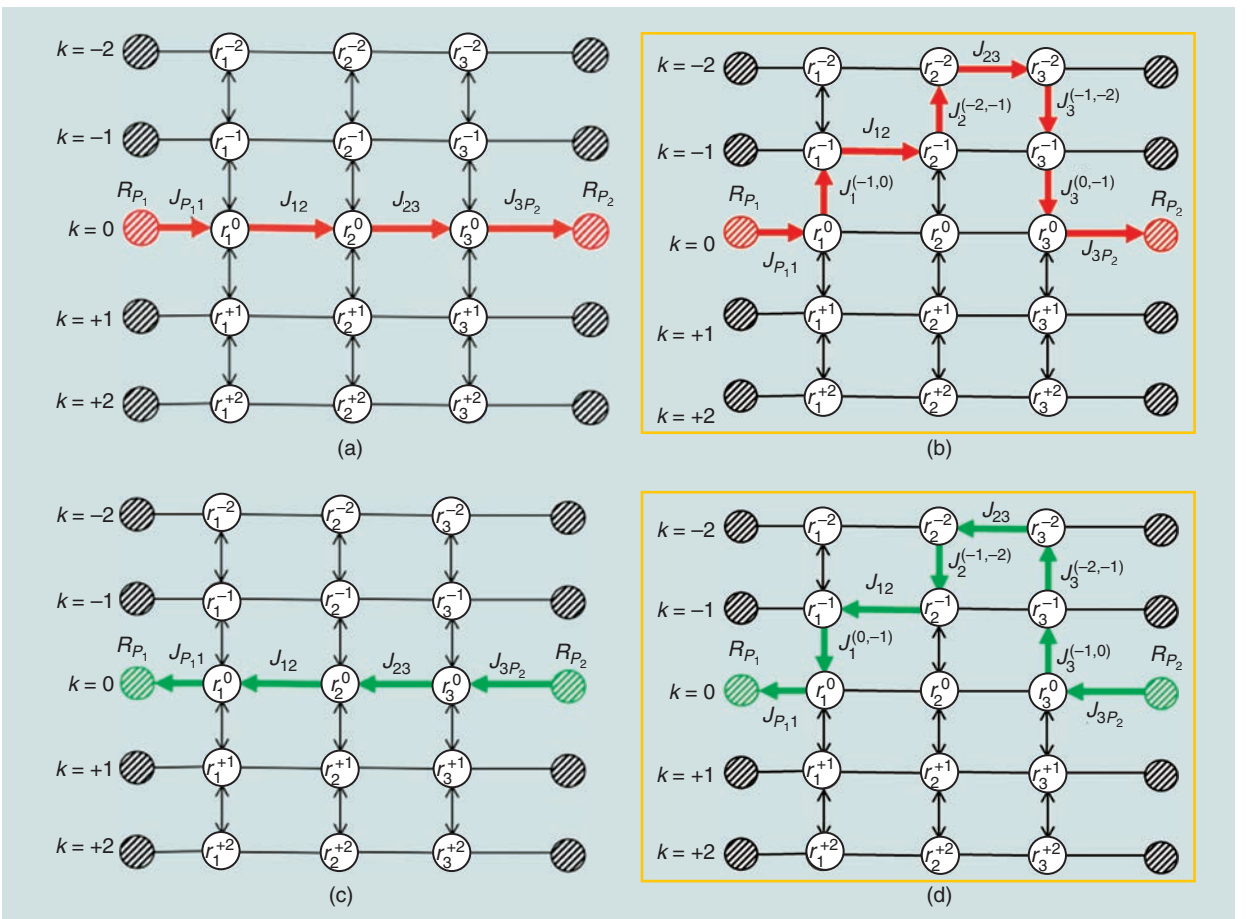

Figure 7. *The different paths for the EM waves to traverse from (a) and (b) port 1 to 2 and (c) and (d) port 2 to 1 shown in the coupling topology in [44].*

harmonics does not up-convert and then down-convert back to the fundamental frequency, a considerable IL is encountered at the fundamental frequency, even if the circuit is lossless. Another important parameter that needs to be considered in the forward direction is the energy at port 1 that is reflected from the various harmonics back to the fundamental frequency. As the energy is up and down-converted to the higher order harmonics, reflected waves from various harmonics are in turn up-converted and down-converted back to the fundamental frequency, as indicated by vertical blue arrows in the vicinity of port 1. This phenomenon is responsible for additional energy being reflected back to port 1, thereby incurring an additional RL apart from the RL due to the fundamental frequency alone. As the RL increases, the energy of the wave at the fundamental frequency reduces, thereby degrading the IL in the passband of the filter. So, in the forward direction, proper engineering of the circuit as well as the parameters is essential to reject higher order harmonics at both port 1 and port 2.

Figure 8(b) shows the traversal of the EM wave from port 2 to port 1 (backward direction). Nonreciprocity demands isolation in the backward direction; the backward traveling EM wave must incur an IL in this path. As has already been discussed in the case of a forward traveling wave, nullification of harmonics at both the ports would promote low IL. Under this constraint, significant isolation can be achieved only if port 2 can be engineered in such a way that much of the energy is reflected by the higher order harmonics back to the fundamental frequency, in addition to the reflected wave at the fundamental frequency. Since the first constraint precludes the coupling of energy to the higher order harmonics in port 1, the only port that can be manipulated is port 2.

Additionally, the progressive phase difference ($\Delta\phi$) between the resonators should be chosen so that the total phase encountered by the EM wave while traversing the fundamental and IM products does not result in a destructive interference of the signal power at the load end in the forward direction. On the other hand, for the

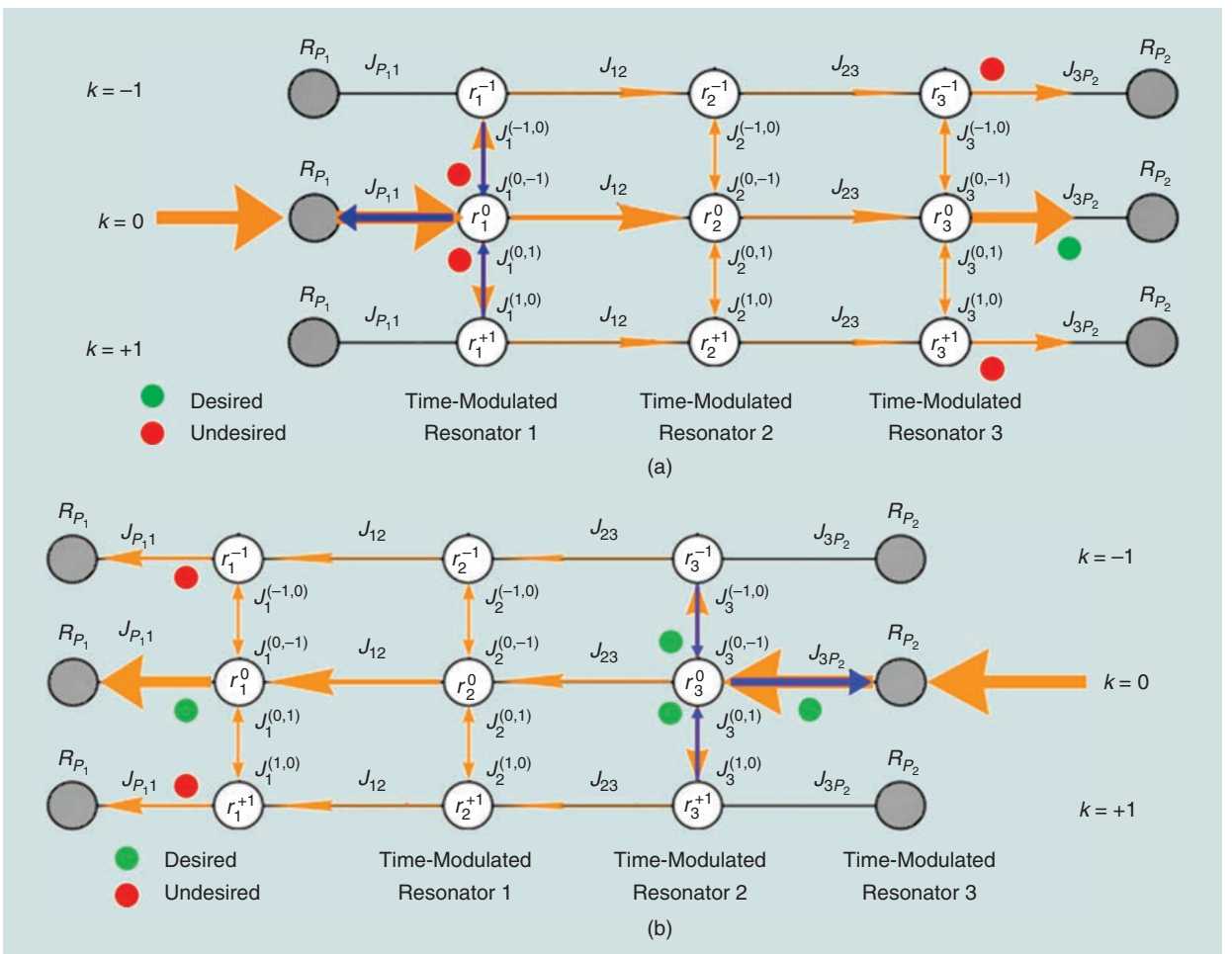

Figure 8. *A pictorial representation of the transmission and reflection paths taken by the EM waves within the fundamental frequency and the first harmonics in the (a) forward direction and (b) backward direction.*

EM wave traveling in the backward direction, the total phase encountered must destructively interfere with the signal power, thereby increasing the backward IL considerably. Furthermore, it should be noted that the increase in the number of time-varying resonators results in an increase in the degrees of freedom for the EM energy traveling in the forward direction to converge back to the fundamental frequency from the harmonics, thereby enhancing the IL. A similar phenomenon occurs in the backward direction. The increase in the number of resonators results in an enhancement of the conversion of EM energy from the fundamental to the harmonics in addition to the reflection incurred at port 2.

Implemented Filters and Discussion

It has been observed that with only one time-varying resonator, the circuit does not exhibit nonreciprocity at the center frequency, because the available power from the carrier frequency is distributed among both the carrier and the IM frequencies, and the latter exhibits loss only at the center frequency. Conversely, with more than one time-varying resonator, the power from the transmitted and reflected harmonic products is up-converted and down-converted back to the carrier frequency. Since the frequency translation is nonreciprocal as has been shown in (10)–(12), S_{21} at the center frequency becomes nonreciprocal as well.

From Figure 9, one can see that the performance is enhanced when the number of resonators is increased. Comparison of the results of a three-pole filter with different numbers of harmonics has been elaborated in [22]. The results of that study show that convergence issues arise in the numerical results when the dimension of the spectral matrix increases from three to seven. This leads to variation in the transmission and the reflection curves. Good convergence as well as stable results are obtained when the dimension of the spectral matrix is 7, which indicates that the signal power is mostly contained within the range $\omega - 3\omega_m$ to $\omega + 3\omega_m$ for a three-pole filter.

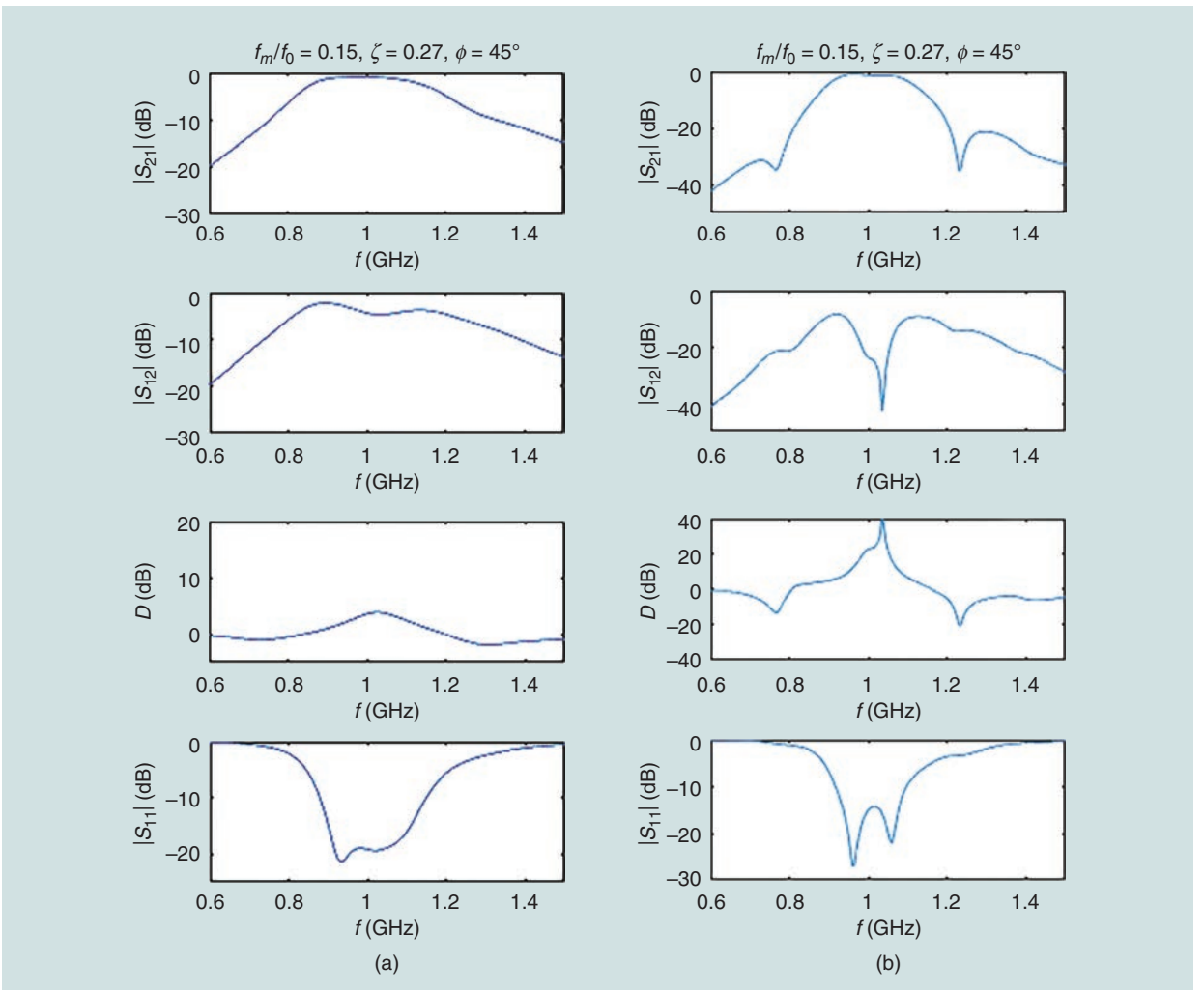

Figure 9. *The S-parameters along with Directivity (D (dB)) for (a) two resonators and (b) three resonators [22].*

Furthermore, a 0.043 dB equiripple filter exhibiting nonreciprocity with the circuit configuration shown in Figure 2 has been built using lumped components with a center frequency (f_0) at 200 MHz and a bandwidth (BW) of 30 MHz [22]. First, the LPP (g) values were obtained corresponding to an IL of 0.043 dB using the procedures listed in the "Analysis of the Insertion Loss Method" section. The mean value of the capacitor (Cr) in the resonator was set to a feasible value of 13.2 pF. Correspondingly, $L_r = 1/\omega^2.C_r$, where $\omega_0 = 2\pi f_0$. Based on the extracted values of the admittance inverters and replacing them with physical inverters with capacitors arranged in a π configuration, a filter using lumped components was built. The dc signal applied to the varactor (SMV1236) fixes the nominal capacitance value, whereas the superimposition of the ac signal results in a swing of the capacitance value from its nominal position, as has been theoretically shown in (6). The magnitude of the ac voltage swing depends on the magnitude of the chosen modulation index (ζ). The modulation signal is applied to the varactor through an LPF with a cutoff frequency much less than f_0 to prevent its interference with the modulation signal (f_m). The dc blocking capacitors (C_{ds}) isolate the shunt inductor from the dc path. The response of the circuit is shown in Figure 10 and clearly reveals a directivity D of more than 20 dB in the passband. As has already been elaborated, the energy of the EM wave in the backward direction is distributed among the IM frequencies and, hence, the value of ω_m was set at 30 MHz, which ensures that the reflected energy at port 2 falls within the stopband of the filter.

Another implementation of a NR-BPF using lumped components was carried out in [48]. The varactor configuration for the resonator is shown in Figure 11. The first step in the design of the desired unmodulated BPF is to choose the appropriate capacitor for the resonator. Once the capacitor value is fixed, the required dc biasing of the varactor is chosen to achieve the required capacitance value. This is followed by the optimization of the ac parameter values such as frequency, voltage, and the progressive phase shifts of the modulating signals so as to achieve a minimum IL in the passband in the forward direction and high reverse isolation. The analysis and the parameter extraction procedures followed here are based on the analysis in [22]. Furthermore, a parametric study was used to obtain the optimized values of the circuit parameters ζ, ω_m, and ϕ corresponding to the best response of the filter.

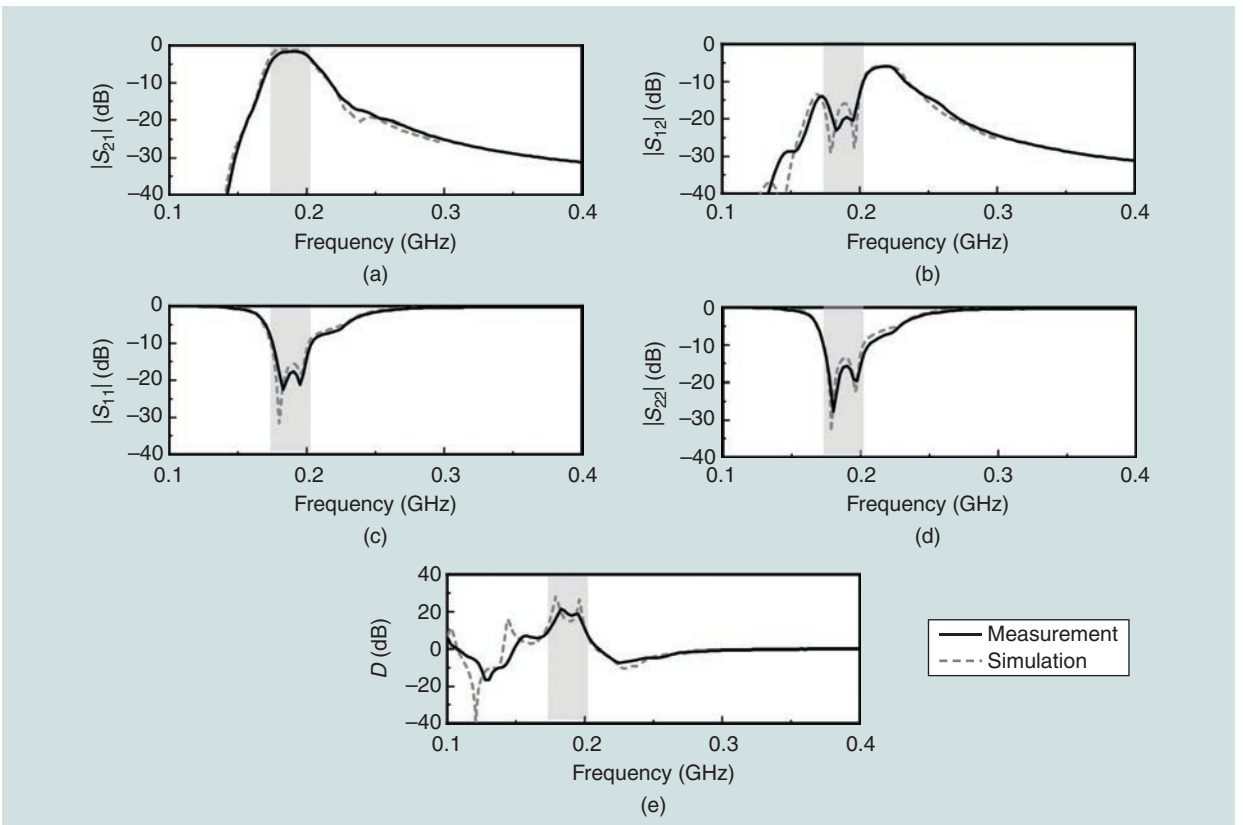

Figure 10. *A comparison of the measured and simulated modulated responses for the circuit of Figure 2. (a) IL | S_{21} |. (b) Reverse isolation | S_{12} |. (c) Reflection | S_{11} |. (d) Reflection | S_{22} |. (e) Directivity D [22].*

Figure 12(a) shows that the best response is obtained when the modulation frequency f_m is less than the bandwidth of the filter. This result is consistent with the fact that the reflected energy from port 2 does not fall in the passband. Too low of a modulation frequency results in a higher RL from the harmonics at port 2 within the passband, while too high of a modulation frequency results in more energy coupling to the higher order harmonics, resulting in an increase in the IL in the passband. Figure 12(b) shows that enhanced performance in terms of IL as well as directivity is obtained when $\Delta\phi = 60^\circ$. It also shows that the variation in the modulation signal amplitude, which in turn is related to the parameter ζ, has an effect on the bandwidth and directivity of the filter. Lower ζ values result in wider bandwidth at the cost of degraded directivity while higher ζ values degrade the bandwidth, but the RL as well as the directivity are enhanced.

The optimized filter characteristics corresponding to the circuit in Figure 11 are shown in Figure 13. The measured bandwidth is 27.5 MHz (19.2%) with the center frequency at 143 MHz. The measured minimum IL in the passband of the forward transmission response ($|S_{21}|$) and the maximum isolation in the reverse direction ($|S_{12}|$) were found to be 3.7 dB and 52.8 dB, respectively. This circuit also possesses the potential to have a tunable center frequency from 136 MHz to 163 MHz, simultaneously achieving nonreciprocity as shown in Figure 14. This is done by uniformly altering the dc bias voltage on the three resonators. Although the IL is degraded in this case compared to [22], this is still the first ever reported NR-BPF with tunable center frequency.

The filters in [22] and [48] used lumped components, which can be difficult to work with in the high frequency domain. So, the foundations laid in [22] were extended into a coupling matrix for the first time in [44], in which a three-pole filter and a four-pole filter were analytically formulated, simulated, and implemented using microstrip line showing nonreciprocity at the center frequency. The modulation signal parameters are optimized to maximize the energy that is coupled to the nonlinear harmonics, thus ensuring that most of the energy is transferred to the operating frequency. A coupling matrix is used to obtain the values of the circuit elements and obtain the desired response, followed by the optimization of the ac parameters, as explained earlier, in the analysis of the IL method for filter design.

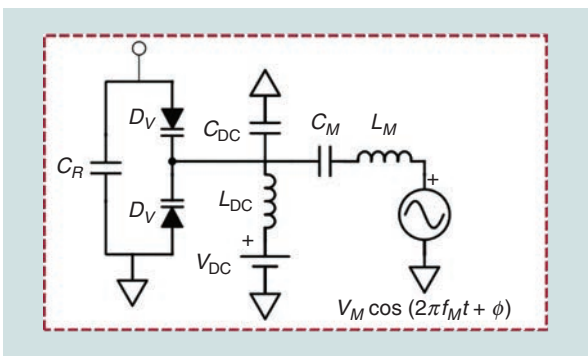

Figure 11. *The capacitor network configuration to harness the resonant frequency modulation [48].*

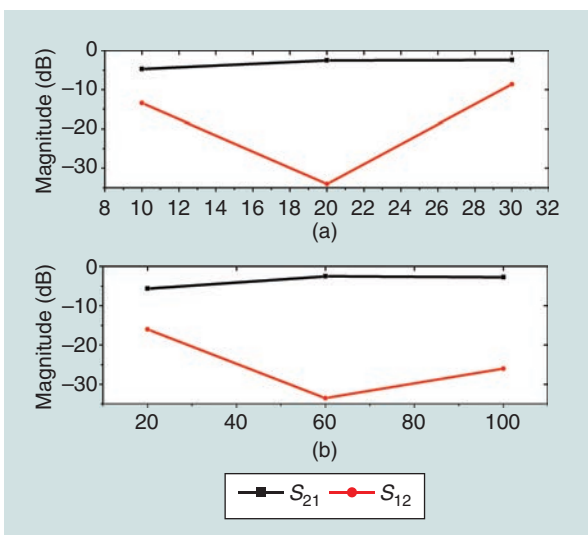

Figure 12. *(a) The variation of IL and isolation with variation of f_m. (b) The variation of IL and isolation with variation of $\Delta\phi$.*

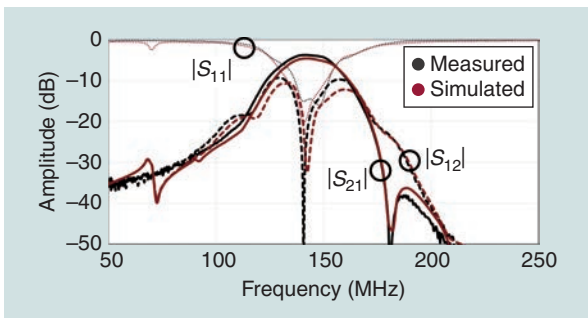

Figure 13. *The contrast between the simulated and measured responses of power transmission and reflection for the fabricated prototype in Figure 11 [48].*

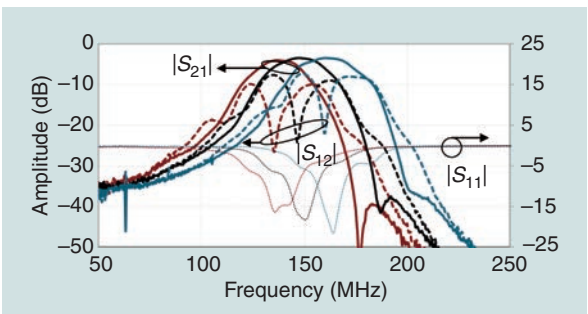

Figure 14. *An RF measured variation of the center frequency of the fabricated prototype in Figure 11 by modifying the dc bias to the varactors [48].*

A pictorial representation of the energy flow in the forward and reverse direction is shown in Figure 7. Numerical analysis shows that decreasing the modulating signal frequency enhances directivity at the cost of narrower bandwidth. For the built filter, quarter-wave microstrip lines terminated with a via hole on one side and connected to varactors on the other side were used. Both third- and fourth-order filters were fabricated and compared with the simulation results. The geometry of the third-order filter is shown in Figure 15 and the corresponding *S*-parameters are shown in Figure 16.

As in the case of lumped circuits, the RF and the modulating signals are isolated using choked inductors. Moreover, to increase the isolation further, the two signals are supported on two different planes of the substrate. Measured results exhibit slightly more IL in the passband owing to parasitic cross-coupling between nonadjacent resonators. After a resistor was connected in parallel to the resonators to model the losses incurred in the measured results good correspondance was achieved between the simulated and measured results. The directivity for the fourth-order filter is 13.8 dB as compared to the 13.6 dB for the third-order filter. Although the simulation and the measured results show good correlation, the complicated biasing design somewhat degrades the response.

Another distributed realization of a nonreciprocal filter using microstrip lines is shown in [49]. Initially, a parametric study was carried out to optimize the modulation frequency, followed by implementation of a two-pole filter using microstrip lines. The parametric study provides neat and useful results, which can be utilized to choose the values of the parameters.

Table 1 represents the variation in filter characteristics with changes in parameters ζ, f_m, and $\Delta\phi$. Here, an ↑ beside the parameter name represents that the parameter value is increasing. For example, f_m ↑ means the effect of increasing f_m on the filter characteristics. Similarly, for the filter characteristics, an ↑ indicates an enhanced result is obtained, a ↓ indicates degradation of that particular characteristic, a ! mark before the ↑ or ↓ indicates a slight increase or decrease respectively and ↑↓ indicates that the characteristic first enhances and then degrades. It can be concluded that among the other parameters, $\Delta\phi$ plays a dominant role in determining the bandwidth of the response. It is also evident that increasing $\Delta\phi$ beyond 90° results in degradation of the response. This can be explained using the coupling topology given in [44]. If the EM wave traverses a path $J_{P_1 1} \rightarrow J_1^{(-1,0)} \rightarrow J_{12} \rightarrow J_{23} \rightarrow J_3^{(0,-1)} \rightarrow J_{3P_2}$ in the forward direction, then the total phase encountered by the wave is $\phi_1 - \phi_3 = -2\Delta\phi$. Conversely, in the backward direction, the total phase encountered is $2\Delta\phi$. Thus, the total phase difference incurred by the wave in the forward and backward direction is $4\Delta\phi$. So, as $\Delta\phi$ increases from 0° to 90°, the phase difference increases until it reaches its maximum, that is $360° = 0°$, hence a phase cancellation occurs at this point. Further increase in the $\Delta\phi$ results in the repetition of the same cycle starting from the minimum, thereby degrading the performance. If f_m increases

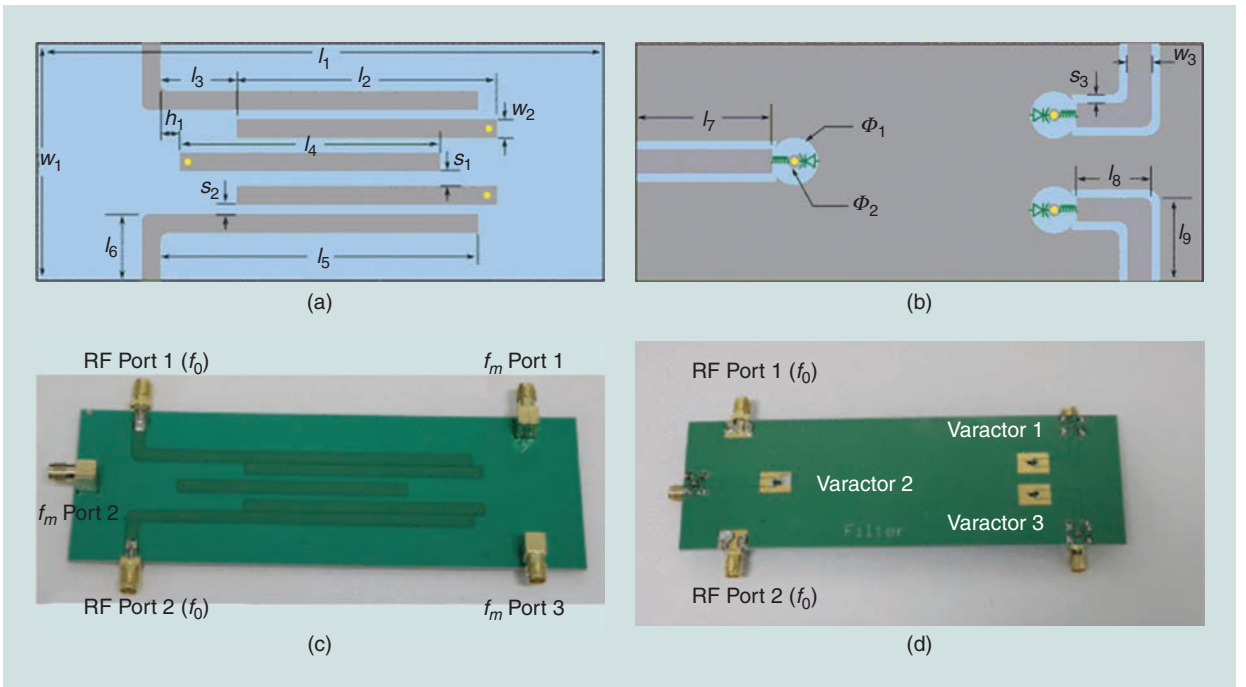

Figure 15. *A distributed implementation of the third-order nonreciprocal filter using microstrip technology. The layout design of the (a) top and (b) bottom metalization layer, respectively. The fabricated (c) top and (d) bottom metalization layers, respectively [44].*

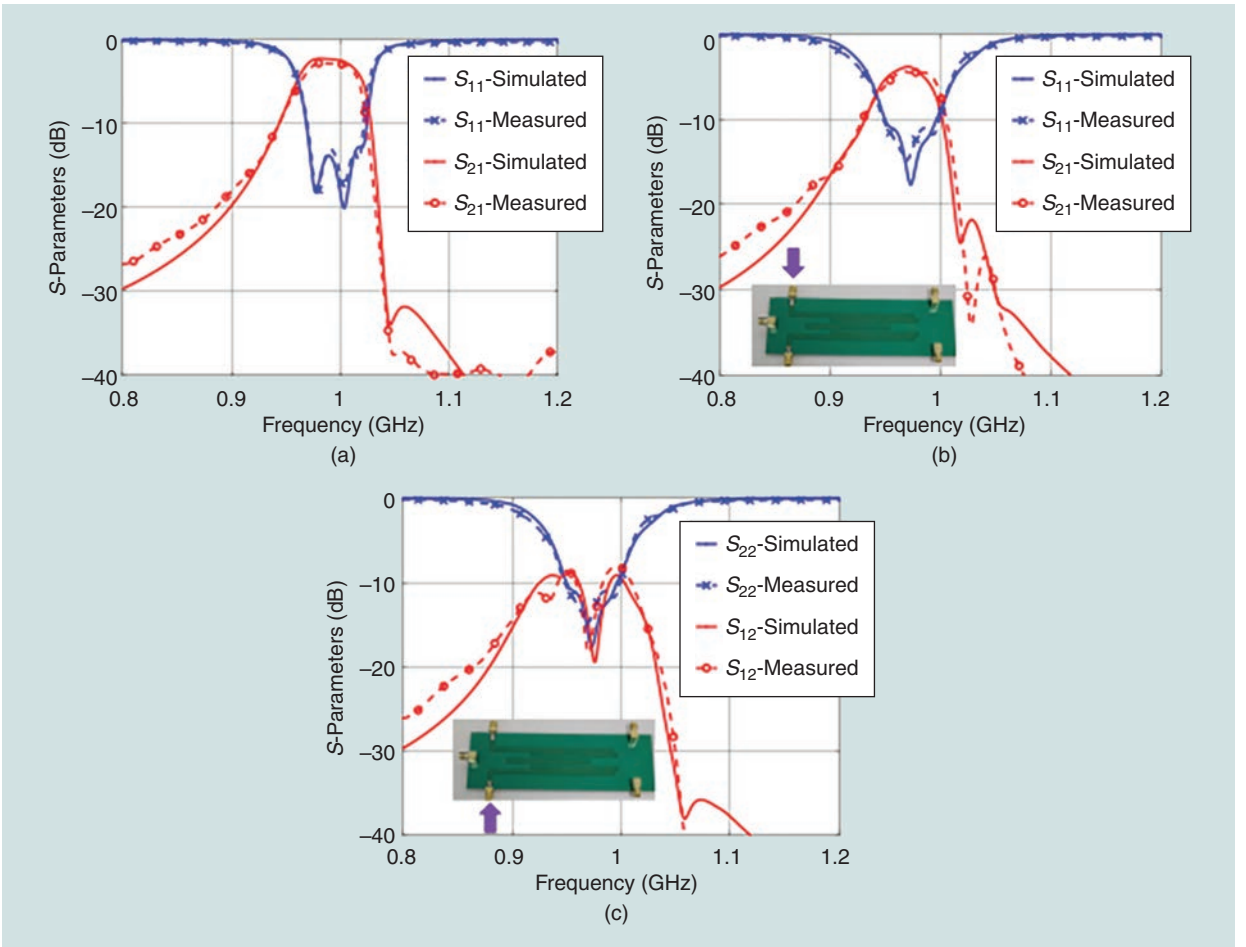

Figure 16. *(a) The two-pole unmodulated response of the filter in Figure 15. (b) and (c) The modulated response of the fabricated filter upon excitation by the modulating signal at the ports specified by the arrows [44].*

to a large value, the IM products fall outside the bandwidth of the filter. As a result, the conversion of energy to the harmonics reduces, thereby increasing the bandwidth at the cost of reducing the nonreciprocity at the center frequency. On the other hand, reduction of f_m to a very small value results in the reduction of the number of reflection zeroes within the passband with a simultaneous generation of transmission zeroes outside the band. This phenomenon not only increases the selectivity of the filter, but also degrades the bandwidth. This compels the proper choice of the f_m value to obtain optimum results in terms of bandwidth and isolation. Works addressing the enhancement of bandwidth in nonreciprocal filters are still, to the authors' knowledge, unavailable and demand further research in this domain. With higher numbers of harmonics and more paths available for traversal, the phase cancellation of all of the waves happens at no particular point, thus preserving the nonreciprocity at every instance.

TABLE 1. The variation of filter characteristics corresponding to parametric variations.

	S_{21}	S_{11}	D	BW
$f_m \uparrow$	↑	↑	↓	!↓
$\zeta \downarrow$	↑	↑	↓	!↑
$\Delta\phi \uparrow$	↑↓	↓	↑↓	↑

The fabricated filter is fed with the modulating sources at the center of the half-wavelength resonators. This configuration nullifies the first odd-resonance voltage at the center, thus precluding any biasing components to separate the RF frequency f_{RF} from the modulation frequency f_m as was the case for [44] where a choke lumped inductor was used to separate the RF and the modulation path. This novel design reduces circuit complexity. The layout design of the distributed implementation is shown in Figure 17.

The fabricated filter along with its response is shown in Figure 18. While the lumped component representation shown earlier had better directivity, the distributed response is worse, showing a directivity D = 6.2 dB for the fabricated circuit compared to D = 12 dB for the simulated response. The presence of lengthy cables at the modulating signal ports excites even order

resonant modes and introduces loading effect on the resonator, which is likely the cause of this discrepancy.

Similarly, a second-order NR-BPF using a microstrip structure has also been simulated in [50]. Parametric studies have been carried out that show an increase in the nonreciprocity with an increase in the modulation voltage, but the increased nonreciprocity degrades the IL in the forward path. The circuit model is similar to the other works and the microstrip layout is shown in Figure 19 and the corresponding *S*-parameters in Figure 20. Simulation results show a clear nonreciprocity at the center frequency with a directivity of 4.7 dB.

The nonreciprocity in both the lumped and the distributed circuits discussed thus far depends solely on the incremental phase difference of the applied modulation signal to the varactors. Hence the power handling capabilities of the designed circuits depend largely on the varactor used and its breakdown voltage.

In sum, the recent literature, simulated comparisons, and mathematical analysis all corroborate the genesis of nonreciprocity in time-varying resonators owing to the incremental phase difference of the applied modulation signal. In addition to the incremental phase difference ($\Delta\phi$) and the effects of its variation, the other parameters that are equally important are the modulation index (ζ) and the modulation frequency (ω_m). With an increase in ζ from a nominal value, more energy is coupled to the higher order harmonics. As a result, the RL from the harmonics back to the fundamental frequency increases in both the ports, which in turn results in the degradation of IL in the forward direction while the isolation enhances in the reverse direction. Thus, a proper choice of $\Delta\phi$ is required to optimize the bandwidth and isolation of the filter, whereas that for the ζ results in optimization between the isolation and IL within the passband. The modulation frequency ω_m translates the reflected and transmitted wave to frequencies away from the fundamental frequency. A

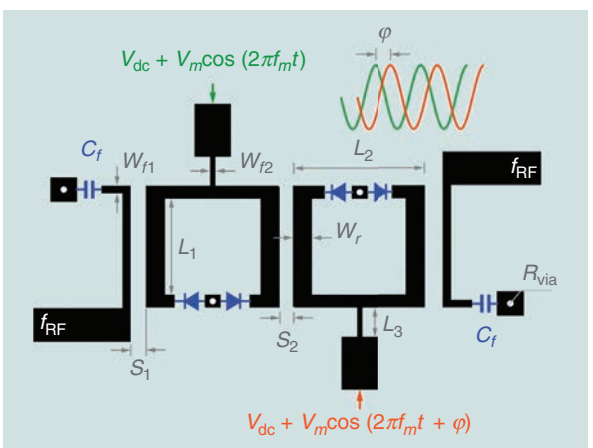

Figure 17. *The layout design of the microstrip implementation of the proposed nonreciprocal filter [49].*

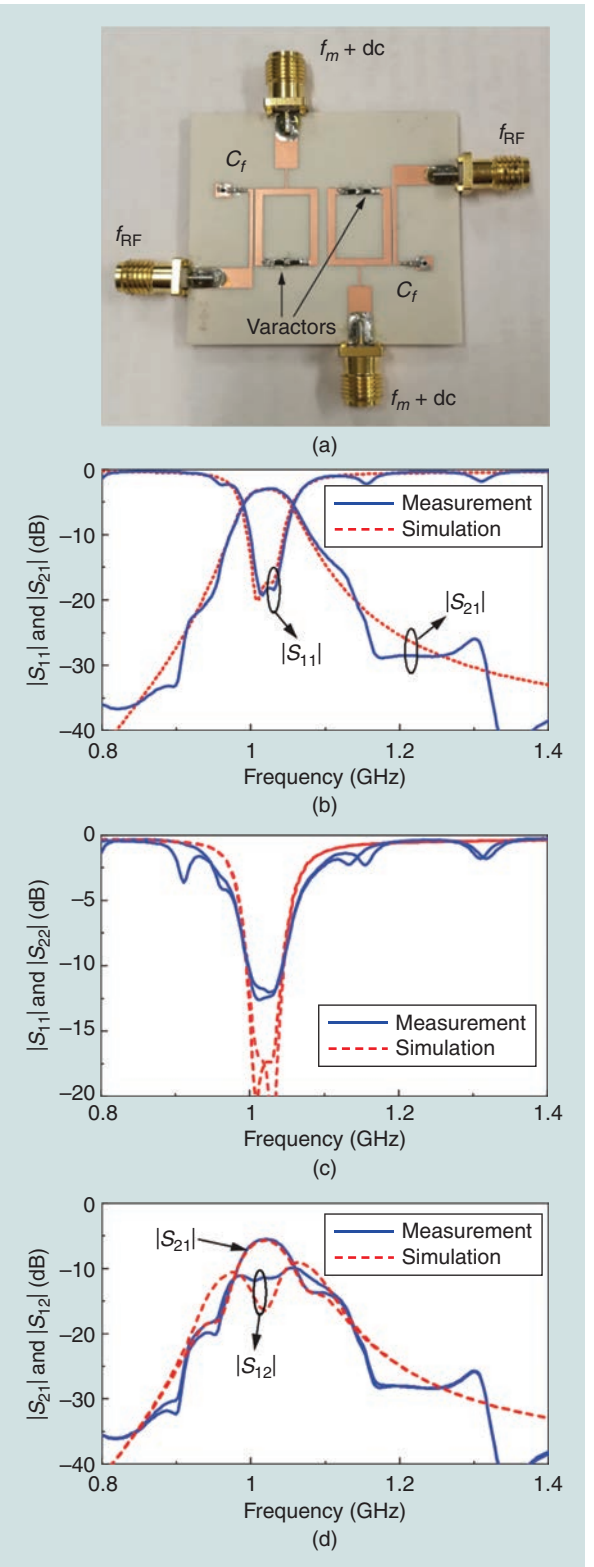

Figure 18. *(a) A picture of the fabricated two-pole nonreciprocal filter. (b) The simulated and measured results of the filter without modulation. (c) The simulated and measured S_{11} and S_{22} of the filter with modulation. (d) The simulated and measured S_{21} and S_{12} of the filter with modulation [49].*

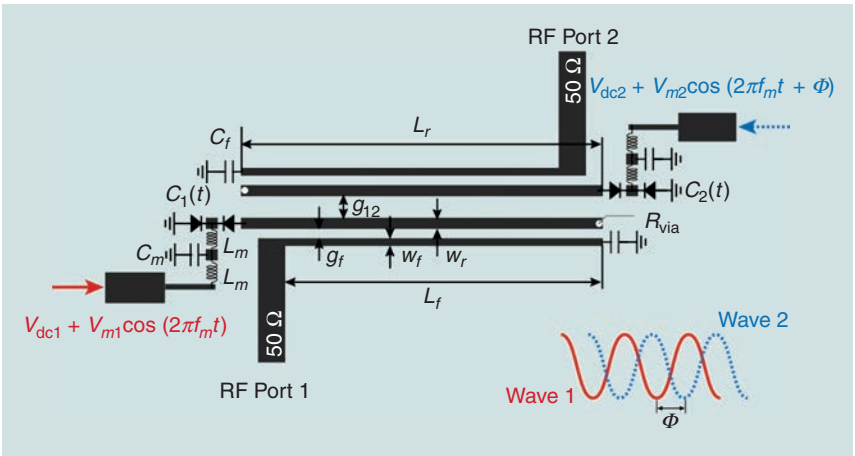

Figure 19. *The layout design of the microstrip implementation of the second-order spatiotemporally modulated nonreciprocal filter using time-modulated quarter wavelength resonators in [50].*

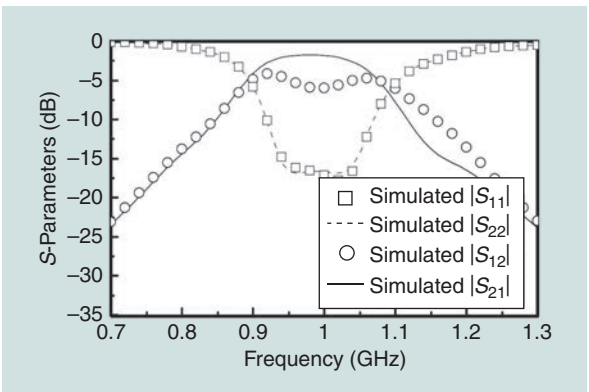

Figure 20. *The simulated result showing clear nonreciprocity for the circuit in Figure 19 [50].*

good response is obtained when the value of f_m is chosen such that $BW/2 < f_m < BW$. This indicates that the reflected energy from the first harmonics back to the fundamental frequency falls within the stopband of the filter. It is worthwhile to mention that the generated frequencies and their associated powers strictly adhere to the Manley–Rowe equations [1]. This implies that the power associated with the up-converted and down-converted signals depends on the frequency ω_m. Thus, the ω_m value needs to be properly optimized, not only to keep the reflected energy in the stopband, but also to maintain the power at the sum and difference frequencies, so as to obtain the IL within a reasonable limit.

Conclusions

Spatiotemporal nonreciprocal filters were reviewed and discussed in this article. An extensive study was carried out starting from the parametric amplifier, which serves as the key to understanding the STM followed by an analysis of time-varying transmission. These concepts serve as the prerequisites for the study of nonreciprocity in microwave filters. The role of synthesis and extraction of lumped components in the fabrication of filters was also discussed. The primary concept and the underlying cause of nonreciprocity was deciphered, followed by the responses of the filter networks and the recent technological advances in this field. Most of the notable work accomplished thus far in this field is on narrowband filters, leaving scope for broadband implementation in the near future. This domain, still relatively unexplored, leaves plenty of room for further research and development in the realization of cost-effective solutions with higher directivity and lower IL, which meet state-of-the-art technological demands.

References

[1] C. E. Fay and R. L. Comstock, "Operation of the ferrite junction circulator," *IEEE Trans. Microw. Theory Techn.*, vol. 13, no. 1, pp. 15–27, 1965, doi: 10.1109/TMTT.1965.1125923.

[2] C. Caloz, A. Alù, S. Tretyakov, D. Sounas, K. Achouri, and Z.-L. Deck-Léger, "Electromagnetic nonreciprocity," *Phys. Rev. Appl.*, vol. 10, p. 047001, Oct. 2018, doi: 10.1103/PhysRevApplied.10.047001.

[3] Z. Wu, C. Scarborough, and A. Grbic, "A spatio-temporally modulated metasurface as a free-space N-path system," in *Proc. 2020 14th Eur. Conf. Antennas Propag. (EuCAP)*, pp. 1–3, doi: 10.23919/EuCAP48036.2020.9135884.

[4] D. Ramaccia, D. L. Sounas, A. Marini, A. Toscano, and F. Bilotti, "Achieving electromagnetic isolation by using up-and down-converting time-varying metasurfaces," in *Proc. 2020 14th Int. Congr. Artif. Materials Novel Wave Phenomena (Metamaterials)*, pp. 1–2, doi: 10.1109/Metamaterials49557.2020.9285032.

[5] A. Kord, D. L. Sounas, and A. Alù, "Achieving full-duplex communication: Magnetless parametric circulators for full-duplex communication systems," *IEEE Microw. Mag.*, vol. 19, no. 1, pp. 84–90, 2017, doi: 10.1109/MMM.2017.2759638.

[6] T. Kodera, D. L. Sounas, and C. Caloz, "Magnetless nonreciprocal metamaterial (MNM) technology: Application to microwave components," *IEEE Trans. Microw. Theory Techn.*, vol. 61, no. 3, pp. 1030–1042, 2013, doi: 10.1109/TMTT.2013.2238246.

[7] R. Fleury, D. L. Sounas, C. F. Sieck, M. R. Haberman, and A. Alù, "Sound isolation and giant linear nonreciprocity in a compact acoustic circulator," *Science*, vol. 343, no. 6170, pp. 516–519, 2014, doi: 10.1126/science.1246957.

[8] N. A. Estep, D. L. Sounas, J. Soric, and A. Alù, "Magnetic-free nonreciprocity and isolation based on parametrically modulated coupled-resonator loops," *Nature Phys.*, vol. 10, no. 12, pp. 923–927, 2014, doi: 10.1038/nphys3134.

[9] N. Reiskarimian and H. Krishnaswamy, "Magnetic-free non-reciprocity based on staggered commutation," *Nature Commun.*, vol. 7, no. 1, pp. 1–10, 2016, doi: 10.1038/ncomms11217.

[10] N. A. Estep, D. L. Sounas, and A. Alù, "Magnetless microwave circulators based on spatiotemporally modulated rings of coupled resonators," *IEEE Trans. Microw. Theory Techn.*, vol. 64, no. 2, pp. 502–518, 2016, doi: 10.1109/TMTT.2015.2511737.

[11] N. Reiskarimian, J. Zhou, and H. Krishnaswamy, "A CMOS passive LPTV nonmagnetic circulator and its application in a

full-duplex receiver," *IEEE J. Solid-State Circuits*, vol. 52, no. 5, pp. 1358–1372, 2017, doi: 10.1109/JSSC.2017.2647924.

[12] T. Dinc, M. Tymchenko, A. Nagulu, D. Sounas, A. Alu, and H. Krishnaswamy, "Synchronized conductivity modulation to realize broadband lossless magnetic-free non-reciprocity," *Nature Commun.*, vol. 8, no. 1, pp. 1–9, 2017, doi: 10.1038/s41467-017-00798-9.

[13] A. Kord, D. L. Sounas, and A. Alù, "Magnet-less circulators based on spatiotemporal modulation of bandstop filters in a delta topology," *IEEE Trans. Microw. Theory Techn.*, vol. 66, no. 2, pp. 911–926, 2018, doi: 10.1109/TMTT.2017.2757470.

[14] A. Kord, D. L. Sounas, and A. Alu, "Pseudo-linear time-invariant magnetless circulators based on differential spatiotemporal modulation of resonant junctions," *IEEE Trans. Microw. Theory Techn.*, vol. 66, no. 6, pp. 2731–2745, 2018, doi: 10.1109/TMTT.2018.2818152.

[15] J. Chang, J. Kao, Y. Lin, and H. Wang, "Design and analysis of 24-ghz active isolator and quasi-circulator," *IEEE Trans. Microw. Theory Techn.*, vol. 63, no. 8, pp. 2638–2649, 2015, doi: 10.1109/TMTT.2015.2442976.

[16] S. Qin, Q. Xu, and Y. E. Wang, "Nonreciprocal components with distributedly modulated capacitors," *IEEE Trans. Microw. Theory Techn.*, vol. 62, no. 10, pp. 2260–2272, Oct. 2014, doi: 10.1109/TMTT.2014.2347935.

[17] M. M. Biedka, R. Zhu, Q. M. Xu, and Y. E. Wang, "Ultra-wide band non-reciprocity through sequentially-switched delay lines," *Scientific Rep.*, vol. 7, no. 1, p. 40,014, 2017, doi: 10.1038/srep40014.

[18] D. L. Sounas, J. Soric, and A. Alu, "Broadband passive isolators based on coupled nonlinear resonances," *Nature Electron.*, vol. 1, no. 2, pp. 113–119, 2018, doi: 10.1038/s41928-018-0025-0.

[19] A. Nagulu *et al.*, "Nonreciprocal components based on switched transmission lines," *IEEE Trans. Microw. Theory Techn.*, vol. 66, no. 11, pp. 4706–4725, 2018, doi: 10.1109/TMTT.2018.2859244.

[20] D. Correas-Serrano, J. S. Gomez-Diaz, D. L. Sounas, Y. Hadad, A. Alvarez-Melcon, and A. Alù, "Nonreciprocal graphene devices and antennas based on spatiotemporal modulation," *IEEE Antennas Wireless Propag. Lett.*, vol. 15, pp. 1529–1532, 2016, doi: 10.1109/LAWP.2015.2510818.

[21] S. Taravati and C. Caloz, "Mixer-duplexer-antenna leaky-wave system based on periodic space-time modulation," *IEEE Trans. Antennas Propag.*, vol. 65, no. 2, pp. 442–452, 2017, doi: 10.1109/TAP.2016.2632735.

[22] X. Wu, X. Liu, M. D. Hickle, D. Peroulis, J. S. Gòmez-Dìaz, and A. Àlvarez Melcòn, "Isolating bandpass filters using time-modulated resonators," *IEEE Trans. Microw. Theory Techn.*, vol. 67, no. 6, pp. 2331–2345, 2019, doi: 10.1109/TMTT.2019.2908868.

[23] J. Wu, X. Yang, S. Beguhn, J. Lou, and N. X. Sun, "Nonreciprocal tunable low-loss bandpass filters with ultra-wideband isolation based on magnetostatic surface wave," *IEEE Trans. Microw. Theory Techn.*, vol. 60, no. 12, pp. 3959–3968, 2012, doi: 10.1109/TMTT.2012.2222661.

[24] L. X.-H, H.-M. Zhou, Q. shi Zhang, and H. W.-W, "Lumped modeling with circuit elements for nonreciprocal magnetoelectric tunable band-pass filter," *Chin. Phys. B*, vol. 25, no. 11, p. 117,505, Nov. 2016.

[25] M. Ghatge, G. Walters, T. Nishida, and R. Tabrizian, "A non-reciprocal filter using asymmetrically transduced micro-acoustic resonators," *IEEE Electron Device Lett.*, vol. 40, no. 5, pp. 800–803, 2019, doi: 10.1109/LED.2019.2907089.

[26] J. M. Manley and H. E. Rowe, "Some general properties of nonlinear elements-Part I. General energy relations," *Proc. IRE*, vol. 44, no. 7, pp. 904–913, Jul. 1956, doi: 10.1109/JRPROC.1956.275145.

[27] J. M. Manley, "Some general properties of magnetic amplifiers," *Proc. IRE*, vol. 39, no. 3, pp. 242–251, Mar. 1951, doi: 10.1109/JRPROC.1951.231835.

[28] C. F. Spitzer, "Sustained subharmonic response in non-linear series circuits," *J. Appl. Phys.*, vol. 16, no. 2, pp. 105–111, 1945, doi: 10.1063/1.1707553.

[29] J. M. Manley and E. Peterson, "Negative resistance effects in saturable reactor circuits," *Elect. Eng.*, vol. 65, no. 12, pp. 870–881, Dec. 1946, doi: 10.1109/EE.1946.6440006.

[30] R. V. L. Hartley, "Oscillations in systems with non-linear reactance," *Bell Syst. Tech. J.*, vol. 15, no. 3, pp. 424–440, Jul. 1936, doi: 10.1002/j.1538-7305.1936.tb03559.x.

[31] A. Van Der Ziel, "On the mixing properties of non-linear condensers," *J. Appl. Phys.*, vol. 19, no. 11, pp. 999–1006, 1948, doi: 10.1063/1.1698106.

[32] L. Blackwell and K. Kotzebue, *Semiconductor-Diode Parametric Amplifiers* (Electrical Engineering Series). Englewood Cliffs, NJ, USA: Prentice Hall, 1961.

[33] P. K. Tien, "Parametric amplification and frequency mixing in propagating circuits," *J. Appl. Phys.*, vol. 29, no. 9, pp. 1347–1357, 1958, doi: 10.1063/1.1723440.

[34] Y. E. Wang, "Non-reciprocity with time-varying transmission lines (TVTLs)," in *Proc. 2012 IEEE Int. Conf. Wireless Inf. Technol. Syst. (ICWITS)*, pp. 1–4, doi: 10.1109/ICWITS.2012.6417737.

[35] Y. E. Wang, "Time-varying transmission lines (TVTL): A new pathway to non-reciprocal and intelligent RF front-ends," in *Proc. 2014 IEEE Radio Wireless Symp. (RWS)*, pp. 148–150, doi: 10.1109/RWS.2014.6830149.

[36] P. K. Tien and H. Suhl, "A traveling-wave ferromagnetic amplifier," *Proc. IRE*, vol. 46, no. 4, pp. 700–706, 1958, doi: 10.1109/JRPROC.1958.286770.

[37] D. Pozar, *Microwave Engineering*, 4th ed. Hoboken, NJ, USA: Wiley, 2011.

[38] S. Qin and Y. E. Wang, "Parametric conversion with distributedly modulated capacitors (DMC) for low-noise and non-reciprocal RF front-ends," in *Proc. 2013 IEEE MTT-S Int. Microw. Symp. Dig. (MTT)*, pp. 1–3, doi: 10.1109/MWSYM.2013.6697751.

[39] A. Atia and A. Williams, "New types of waveguide bandpass filters for satellite transponders," *Comsat Tech. Rev.*, vol. 1, no. 1, pp. 20–43, 1971.

[40] A. E. Williams and A. E. Atia, "Narrow-bandpass waveguide filters," *IEEE Trans. Microw. Theory Techn.*, vol. 20, no. 4, pp. 258–265, 1972, doi: 10.1109/TMTT.1972.1127732.

[41] R. J. Cameron, C. M. Kudsia, and R. R. Mansour, *Microwave Filters for Communication Systems: Fundamentals, Design, and Applications*. Hoboken, NJ, USA: Wiley, 2018.

[42] H. C. Bell, "The coupling matrix in low-pass prototype filters," *IEEE Microw. Mag.*, vol. 8, no. 2, pp. 70–76, 2007, doi: 10.1109/MMW.2007.335531.

[43] Y. He, G. Wang, and L. Sun, "Direct matrix synthesis approach for narrowband mixed topology filters," *IEEE Microw. Wireless Compon. Lett.*, vol. 26, no. 5, pp. 301–303, 2016, doi: 10.1109/LMWC.2016.2549098.

[44] A. Alvarez-Melcon, X. Wu, J. Zang, X. Liu, and J. S. Gomez-Diaz, "Coupling matrix representation of nonreciprocal filters based on time-modulated resonators," *IEEE Trans. Microw. Theory Techn.*, vol. 67, no. 12, pp. 4751–4763, 2019, doi: 10.1109/TMTT.2019.2945756.

[45] A. Oppenheim, A. Willsky, and S. Nawab, *Signals and Systems* (Signal Processing Series). Englewood Cliffs, NJ, USA: Prentice Hall, 1997.

[46] C. Kurth, "Steady-state analysis of sinusoidal time-variant networks applied to equivalent circuits for transmission networks," *IEEE Trans. Circuits Syst.*, vol. 24, no. 11, pp. 610–624, 1977, doi: 10.1109/TCS.1977.1084283.

[47] S. Darlington, "Linear time-varying circuits-matrix manipulations, power relations, and some bounds on stability," *Bell Syst. Tech. J.*, vol. 42, no. 6, pp. 2575–2608, 1963, doi: 10.1002/j.1538-7305.1963.tb00978.x.

[48] D. Simpson and D. Psychogiou, "Magnet-less non-reciprocal bandpass filters with tunable center frequency," in *Proc. 2019 49th Eur. Microw. Conf. (EuMC)*, pp. 460–463, doi: 10.23919/EuMC.2019.8910732.

[49] X. Wu, M. Nafe, A. A. Melcón, J. Sebastián Gómez-Díaz, and X. Liu, "A non-reciprocal microstrip bandpass filter based on spatiotemporal modulation," in *Proc. 2019 IEEE MTT-S Int. Microw. Symp. (IMS)*, pp. 9–12, doi: 10.1109/MWSYM.2019.8700732.

[50] X. Wu, M. Nafe, and X. Liu, "Non-reciprocal 2nd-order bandpass filter by using time-modulated microstrip quarter-wavelength resonators," in *Proc. 2019 Int. Conf. Microw. Millimeter Wave Techn. (ICMMT)*, pp. 1–3, doi: 10.1109/ICMMT45702.2019.8992839.

IMS

Connecting Minds. Exchanging Ideas.

PROGRAM PREVIEW

Join Us
In-Person

Register Now

19-24 June
Denver, CO

ims-ieee.org

Digital Object Identifier 10.1109/MMM.2022.3158166

IEEE

MTT-S
IEEE MICROWAVE THEORY & TECHNOLOGY SOCIETY

RFIC

ARFTG

Keynotes & At A Glance

The Future of RFIC is Digital

Dr. Curtis Ling
MaxLinear

RFICs into the Roaring 20's: Hot and Cold

Prof. Sorin Voinigescu
University of Toronto

A Quantum Technology Landscape

Prof. Dana Z. Anderson
University of Colorado and ColdQuanta, Inc.

Space, Changing the Way We Live, Enabled by Microwave Innovations

Gregory E. Edlund
Lockheed Martin Space Systems Company

Learning from the Lightning: How Nikola Tesla Formulated a Scheme for Wireless Power in Colorado Springs

Prof. W. Bernard Carlson
University of Virginia and National University of Ireland Galway

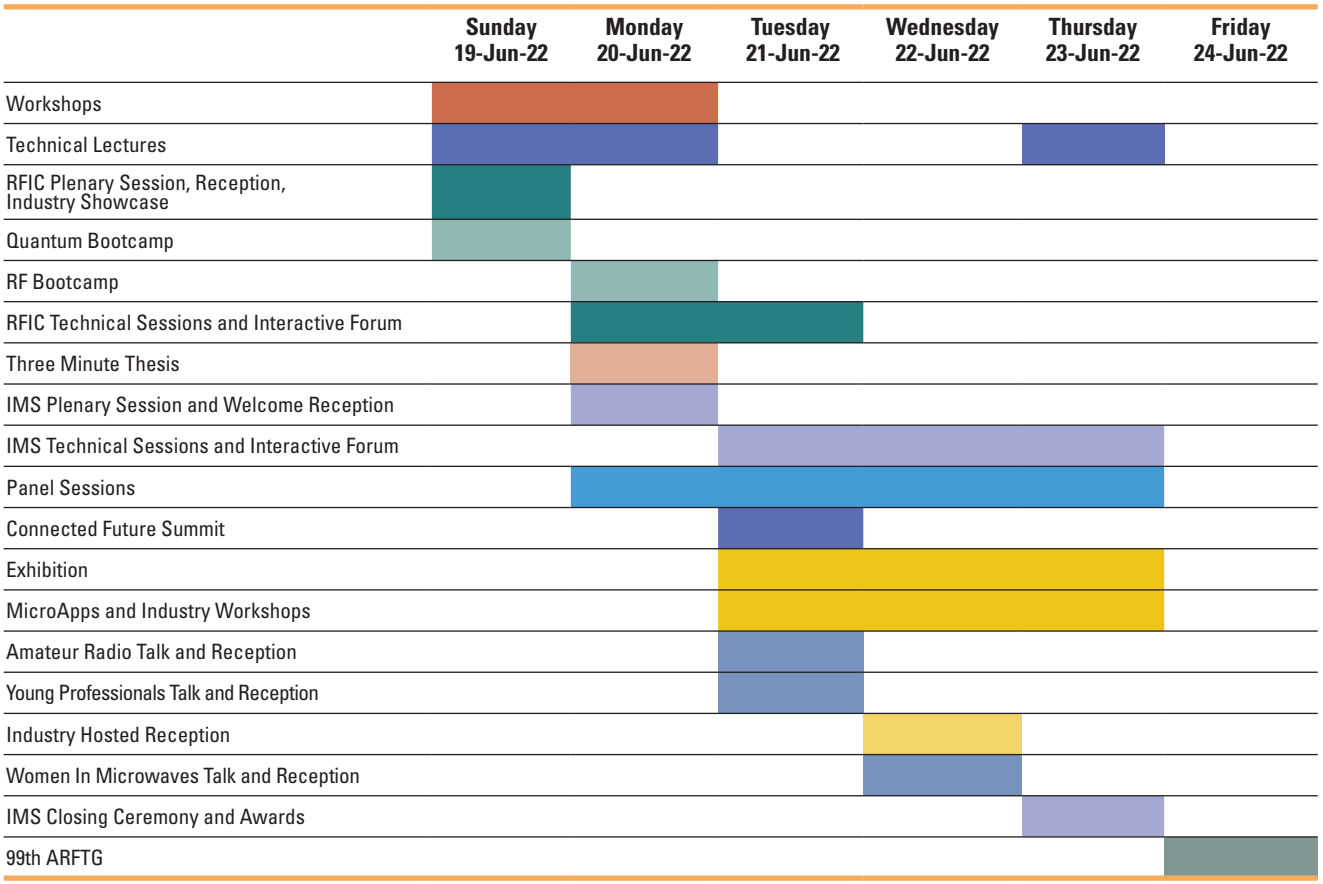

Panel Sessions, Technical Lectures & Workshops

PANEL SESSIONS

- Industry vs. Academia: Who is Leading Whom?
- This is the Right Way to Architect the Microwave Control for Quantum Computers!
- Race to the Next G – Ride the mmWave or Wave Goodbye!
- The Trend of Tiny AI: Will Ultra-Low-Power Fully-Integrated Cognitive Radios Become a Reality?
- Small Satellites and Constellations: Who Will Be the Winners of the New Race to Space?
- Wearables – Our Life Depends on Them!
- Modern Phased Arrays and OTA Testing: A Design or a Measurement Challenge?

TECHNICAL LECTURES

- Fundamentals of Noise, and Understanding its Effects on RFICs
- Electromagnetic Fundamentals Underlying Health Impact of Millimeter-Wave Radiations
- Semiconductor Electronics for High Power/High Speed Reconfigurable RF and Microwave Electronics

WORKSHOPS

- Advanced Manufacturing and Design Techniques for Emerging 3D Microwave and mm-Wave RF Filters
- Advances in SATCOM Phased-Arrays and Constellations for LEO, MEO and GEO Systems
- Emerging MIT/PCM Based Reconfigurable Microwave Devices
- Front-End Module Integration and Packaging for 6G and Beyond 100GHz Communication and Radar Systems
- In-Band Full-Duplex Integrated Devices and Systems
- Superposition and Entanglement: When Microwaves meet Quantum
- Supply Modulation Techniques: From Device to System
- RF Large-Signal Transistor Performance Limits Related to Reliability and Ruggedness in Mobile Circuit Applications
- GaN/GaAs Technology Development and Heterogeneous Integration for Emerging mm-Wave Applications
- Microwave Techniques for Coexistence between 5G and Passive Scientific Systems
- On-Wafer mm-Wave Measurements
- Measurement and Modeling of Trapping, Thermal Effects and Reliability of GaN HEMT Microwave PA Technology
- Hands-On Phased Array Beamforming Using Open Source Hardware and Software
- AI/ML-Based Signal Processing for Wireless Channels
- Commercial Applications of Medical RF, Microwave and mm-Wave Technology
- Quantum RF Receivers: Using Rydberg Atoms for Highly Sensitive and Ultra Wideband Electric Field Sensing
- Large-Scale Antenna Arrays: Circuits, Architectures, and Algorithms
- SWIPT — Simultaneous Wireless Information and Power Transmission for Future IoT Solutions
- Health Aspects of mm-Wave Radiation in 5G and Beyond
- Micro and Nano Technology Challenges to Address 6G Key Performance Indicators
- Wideband and High Efficiency mm-Wave CMOS PA Design for 5G and Beyond
- Emerging Low-Temperature/Cryogenic Microwave Techniques and Technologies for Quantum Information Processing
- mm-Wave Design Challenges and Solutions for 6G Wireless Communications
- mm-Wave and THz Systems for Near-Field Imaging, Spectroscopy and Radar Sensing Applications
- Advanced Interference Mitigation in Integrated Wireless Transceivers
- System Design Considerations for Advanced Radios
- Toward Tbps Optical and Wireline Transceivers: a Tutorial for RFIC Designers
- Wireless Proximity Communication
- Recent Developments in Sub-6GHz PAs and Front-End Modules
- Digitally Intensive PAs and Transmitters for RF Communication
- Human Body Communications

IMS Technical Sessions

Tuesday, 21 June

- Tu1A: Advances in Synthesis and Design Techniques for Non-Planar Filters
- Tu1B: Advances in Numerical and Computational Techniques for Simulation and Design Optimization
- Tu1C: Advances in RFID Technologies
- Tu1D: Advanced Frequency Synthesis
- Tu1E: Microwave Technologies for Quantum-System Integration
- Tu2A: Advances in Non-Planar Filter Technologies
- Tu2B: A Retrospective and a Vision of Future Trends in RF and Microwave Design Optimization
- Tu2C: Advances in RF Sensors
- Tu2D: Advanced mm-wave-sub-mm-wave Mixers, Switches and Phase Shifters
- Tu2E: Cryogenic Microwave Circuits for Control of Quantum Systems
- Tu3A: Reconfigurable Multi-Mode Resonators and Filters
- Tu3C: Rectenna and Signal Design for RF Power Transmission and Energy Harvesting
- Tu3D: HF-VHF-UHF Power Amplifiers and Systems
- Tu3E: Cryogenic Measurement and Characterization for Quantum Systems
- Tu4A: Integrated Filters in the GHz and sub-THz Range
- Tu4B: Components for Advanced Systems and Applications
- Tu4C: Low-Frequency Wireless Power Transfer and Harvesting Systems
- Tu4D: Advanced High-Speed Mixed-Signal Circuits For Optical and mm-Wave Systems
- Tu4E: Next-Generation mm-wave GaN Technologies and MMICs for 5G-6G and DoD Applications

Wednesday, 22 June

- We1A: High-Density Integration of Transmission Line Structures
- We1B: Advances in High Frequency Device Modeling
- We1C: Advanced 5G Wireless System Architectures and Underlying Over-the-Air Characterization Techniques
- We1D: Nonlinear Analysis and Design of Microwave Signal Generation and Processing Circuits
- We1E: High Power GaN RF and Microwave Power Amplifiers
- We1F: Radar from Space to Ground (and Below) - The Synergy Between Commercial, Government, and Metrology Applications
- We1G: Millimeter-Wave and Terahertz Power Amplifiers and Frontend Modules
- We2A: Advancements in Planar and Substrate Integrated Filters and Multiplexers
- We2B: Advances in the Characterization of Microwave and Millimeter-Wave Materials and Components
- We2C: AI-ML for RF and mmWave Applications
- We2E: Advanced Linearization Techniques for PAs and MIMO Transmitters
- We2F: Advanced Concepts for 77 GHz Radar
- We2G: Millimeter-wave and Terahertz System Demonstrations and Concepts
- We3A: Advances in Passive Devices
- We3B: Advances in Interconnects
- We3C: Towards Physically Secure Communication and Computation
- We3D: LNAs and Receivers at W-band and Beyond
- We3E: New Advances in RF Circuits and Systems
- We3F: Cognitive Radar
- We3G: Millimeter-Wave and Terahertz Signal Generation
- We4A: Advances in mmWave Passive Components & Systems
- We4B: Advanced Manufacturing and Novel Substrates
- We4C: Advanced System Architectures and Concepts
- We4D: Advances in Low Power CMOS Low Noise Amplifiers (LNAs)
- We4E: Special Session in Memory of Professor Tatsuo Itoh
- We4F: Advanced Radar Imaging and Signal Processing
- We4G: Millimeter and Terahertz Integrated Circuits and Components

Thursday, 23 June

- Th1A: Microwave Interaction and Characterization of Biological and Semiconductor Materials
- TH1B: Advances in SAW and Acoustic Components Technology
- Th1C: Microwave and Terahertz Photonics
- Th1E: Compound Semiconductor Power Amplifiers
- Th1F: Efficient Characterization and Test of Phased Array Antenna Systems: Is it Really a Nightmare?
- Th2A: Measurement and Instrumentation Techniques for Evolving Standards in Future Technologies
- Th2B: Recent Advances on Acoustic Resonators and Filters
- Th2C: Nano-Devices and Their High Frequency Applications
- Th2E: Recent Advances in Microwave Semiconductor Technology
- Th2F: Antenna Systems for 5G and SATCOM Applications
- Th3A: MHz-to-THz Instrumentation for Biological Measurements and Healthcare Applications
- Th3B: Emerging Phase-Change and SIW Technologies for mmWave to sub-THz Applications
- Th3C: Silicon Based Digital Power Amplifier Architectures
- Th3E: Reconfigurable RF Systems for 5G mmWave Communications
- Th3F: Advances in Integrated Transceivers for Beamforming and RADAR Applications

Technical Track Key:

- Field, Device and Circuit Tech.
- Passive Components & Packaging
- Active Devices
- Emerging Technologies
- Focus or Special Sessions
- RFIC Sessions
- Systems & Applications

For the latest on IMS and Microwave Week visit ims-ieee.org

RFIC Technical Sessions

Monday, 20 June

- RMo1A: mm-Wave Transmitters & Receivers for Communication & 5G Applications
- RMo1B: Cryogenic and Advanced Front-End Circuits
- RMo1C: RFIC Systems and Applications: Custom RFICs for Emerging Systems
- RMo2A: Multi-Gigabit Transceivers & Modules for Point-to-Point & Emerging Applications
- RMo2B: Power Switches, Amplifiers and Power Dividers for mm-wave and sub-THz Applications
- RMo2C: RF & mm-Wave Transmitters
- RMo3A: Millimeter-Wave & Sub-THz Circuits & Systems for Radar Sensing and Metrology
- RMo3B: Mixed-Signal Building Blocks for Next-Generation Systems
- RMo3C: Frequency Generation Techniques for 5G and IoT
- RMo4A: Power Amplifiers for 100+GHz Applications
- RMo4B: Switch Technology, CMOS Reliability, and ESD
- RMo4C: RF, mmWave and Sub-THz VCOs

Tuesday, 21 June

- RTu1A: mm-wave and Wide Band Low-Noise CMOS Amplifiers
- RTu1B: Efficiency Enhancement Techniques for Power Amplifiers
- RTu3A: Circuits and Techniques for Full Duplex Transceivers
- RTu3B: Millimeter-Wave-THz Devices and BIST-Calibration, and Circuits for Emerging Applications
- RTu4A: Emerging Wireless Communications
- RTu4B: Building Blocks for Next Generation Frequency Synthesis

The Systems Forum, Connected Future Summit, and Boot Camps

With a special focus on systems design across three days, The Systems Forum includes technical topics showcased in the Connected Future Summit, panel sessions, focused sessions, and an interactive Systems Pavilion on the show floor.

Connected Future Summit

The Connected Future Summit will be held on Tuesday, 21 June 2022. The Summit will review core technologies for future wireless networks along with their human and societal impacts. Topics will include future trends of 6G and beyond; standardization of both cellular (3GPP) and Wi-Fi Alliance; broadband wireless with satellite constellations and other high-altitude platform; V2X technology with beyond 5G; semiconductor technologies; reconfigurable front ends and system architectures; and test and measurement challenges impacting next-generation connectivity evolution.

Visit **ims-ieee.org/connectedfuturesummit** to view the agenda and speakers.

RF Boot Camp

Join us for an introduction to RF basics on Monday, 20 June 2022! This one day course is ideal for newcomers to the microwave world, such as technicians, new engineers, college students, engineers changing their career path, as well as marketing and sales professionals looking to become more comfortable in customer interactions involving RF & Microwave circuit and system concepts and terminology. The format of the RF Boot Camp is similar to that of a workshop or short course, with multiple presenters from industry and academia presenting on a variety of topics.

Visit **ims-ieee.org/RFbootcamp** to view the agenda and speakers.

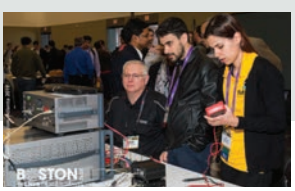

NEW! Quantum Boot Camp

This course will provide an introduction to the basics of quantum engineering, targeting microwave engineers who want to understand how they can make an impact in this emerging field. The intended audience includes new engineers, engineers who may be changing their career path, marketing and sales professionals, as well as current university students. Speakers will cover quantum engineering basics with a focus on the control and measurement of quantum systems and will conclude with a hands-on introduction to the design of superconducting qubits using modern microwave CAD tools.

Visit **ims-ieee.org/quantumbootcamp** to view the agenda and speakers.

Exhibition, MicroApps, Industry Workshops and Mobile App

EXHIBITION OVERVIEW

The exhibition at IMS2022 includes 380+ exhibitors from around the world, showcasing their products and services. All conference pass holders gain free access to the exhibition. "EXPO only" passes are also available. You can sign up for a FREE EXPO only pass for the Wednesday exhibition or gain access to three days of exhibition and show-floor presentations in the MicroApps Theater for $30.

SHOW HOURS

Tuesday, 21 June 2022	Wednesday, 22 June 2022	Thursday, 23 June 2022
09:30-17:00	09:30-18:00	09:30-15:00

SHOW FLOOR NETWORKING HIGHLIGHTS

- Continental Breakfast each morning Tuesday-Thursday
- Sweet Treat Tuesday (during afternoon)
- Coffee breaks throughout the day Tuesday, Wednesday, and Thursday
- Industry Hosted Reception, Wednesday, 22 June 2022, 17:00-18:00
- Societies Pavilion
- Systems Pavilion
- Three networking lounges with charging stations

MICROAPPS

The Microwave Application seminars (MicroApps) offered Tuesday, 21 June through Thursday, 23 June 2022, provide a unique forum for the exchange of ideas and practical knowledge related to the design, development, production, and test of products and services. MicroApps seminars are presented by technical experts from IMS2022 exhibitors with a focus on providing practical information, design, and test techniques that practicing engineers and technicians can apply to solve the current issues in their projects and products. View the complete MicroApps schedule at https://ims-ieee.org/exhibition/microapps/microapps-seminars.

INDUSTRY WORKSHOPS

The Industry Workshops are 2-hour industry-led presentations featuring hands-on, practical solutions often including live demonstrations and attendee participation. These Workshops are open to all registered Microwave Week attendees for $25 per Workshop. View the complete Industry Workshop schedule at https://ims-ieee.org/exhibition/microapps/industry-workshops.

IMS MICROWAVE WEEK MOBILE APP

The IMS Microwave Week app is now available in the Apple App store and Google Play store. Install the app on your Android or iOS device to view the full schedule of Workshops, Technical Lectures, IMS and RFIC Technical Sessions, ARFTG, Panel Sessions, Social Events and Exhibition information. On-site during Microwave Week you will be able to download IMS and RFIC papers and presentations, access Workshop materials, locate exhibitors and explore all that Denver, CO, has to offer! Download today!

Apple App Store

Google Play Store

Follow us on:

#IMS2022

For the latest on IMS and Microwave Week visit ims-ieee.org

Exhibitor List

2pi-Labs GmbH
3D Glass Solutions Inc
3G Shielding Specialties
3RWAVE
A-Alpha Waveguide Inc.
ACE-Accurate Circuit Engineering
ACEWAVETECH
AdTech Ceramics
Advanced Assembly
Advanced Circuitry International
Advanced Test Equipment Corp.
Aerospace & Defense Technology
AFT Microwave Inc.
AGC Multi Material America Inc.
Agile Microwave Technology Inc.
AI Technology Inc.
A-INFO Inc.
AJ Tuck Co.
Akoustis Inc.
ALMT Corp.
Altum RF
AMCAD Engineering
AMD-Xilinx
American Microwave Corp.
American Standard Circuits Inc.
Amotech Co. Ltd.
Ampleon
AmpliTech Inc.
Analog Devices Inc.
AnaPico Inc.
Anoison Electronics LLC
Anokiwave
Anritsu Co.
Ansys
APITech
AR Modular RF
AR RF/Microwave Instrumentation
Artech House
ASI CoaxDepot
Association of Old Crows
Astronics Test Systems
AT Wall Company
Auden Techno
Avalon Test Equipment
B&Z Technologies
Barry Industries Inc.
Benchmark Electronics Inc.
Berkeley Nucleonics Corp.
Boonton
Cadence Design Systems Inc.
Cernex/Cernexwave
Charter Engineering Inc.
ChongQing Ceratronics Technology Ltd.
Ciao Wireless Inc.
Cicor Group
Cinch Connectivity Solutions
CML Microcircuits
Colorado Engineering Inc.
Colorado Microcircuits Inc.
CommAgility
Communications & Power Industries
Component Distributors Inc.
Conduant Corporation
Connectronics Inc.
Copper Mountain Technologies
Corning Inc.
Corry Micronics LLC
Crane Aerospace & Electronics
Criteria Labs Inc
Crystek Corp.
Custom Cable Assemblies Inc.
Custom Microwave Components Inc.
CW Swift & Associates Inc.
CX Thin Films
Dalicap Tech
dB Control
Delta Electronics Mfg. Corp.
Denka Corporation
DeWeyl Tool Company
Diamond Antenna & Microwave Corp.
Diramics
DiTom Microwave Inc.
dSPACE Inc.
Ducommun LaBarge Technologies Inc.
Eclipse MDI
ED2 Corporation
Egide USA
Electro Ceramic Industries
Electro Rent Corp.
Element Six
Elite RF
EM Labs Inc.
EMC Elektronik Ltd.
Empower RF Systems Inc.
EMSS Antennas
ENGIN-IC Inc.
Eravant
ETL Systems Ltd.
ETS-Lindgren
Eureka Aerospace Inc.
European Microwave Week
Evans Capacitor Company
Everything RF/Microwaves 101
evissaP Inc
EZ Form Cable, a Trexon Company
F&K Delvotec Inc.
Filtronetics Inc.
Filtronic Broadband
Fine-Line Circuits Limited
Flann Microwave Ltd.
Flexco Microwave Inc.
Focus Microwaves Inc.
FormFactor Inc.
Fortify
Geib Refining Corp.
Gel-Pak
General Microwave Corporation
GGB Industries Inc.
Glenair Inc.
Global Communication Semiconductors
GLOBALFOUNDRIES
Golden Loch Ind. Co. Ltd.
Guerrilla RF
Harbour Industries LLC
HASCO INC
Hermetic Solutions Group
Herotek Inc.
Hesse Mechatronics
High Frequency Electronics
Hirose Electric USA
Holzworth
HRL Laboratories LLC
Hughes Circuits Inc.
HYPERLABS
IEEE Future Directions: LEO Sats Project
IHP GmbH
IMS Connector Systems
IMST GmbH
InCompliance Magazine
Indium Corp.
Innertron Inc.
Innovative Power Products Inc.
InPack
In-Phase Technologies Inc.
iNRCORE
Inspower Co. Ltd.
Integra Technologies Inc.
Intelliconnect LLC
International Manufacturing Services Inc.
inTEST Thermal Solutions
Ironwood Electronics
Isola/Insulectro
ITF Co. Ltd.
IVWorks Co. Ltd.
IW Microwave Products
JFW Industries Inc.
Johanson Technology Inc.
JQL Technologies Corporation
Junkosha Inc.
Keysight Technologies
Knowles Precision Devices
KOSTECSYS Co. Ltd.
KREEMO Inc.
KRYTAR
KVG Quartz Crystal Technology GmbH
Kyocera AVX
Kyocera International Inc.
LadyBug Technologies LLC
Lake Shore Cryotronics Inc.
Laser Processing Technology Inc.
Leader Tech Inc.
Leonardo
Liberty Test Equipment Inc.
Linear Photonics
Linearizer Technology Inc.
Linwave Technology
Logus Microwave
Low Noise Factory AB
LPKF Laser & Electronics
M2 Global
MACOM
Marki Microwave Inc.
Maury Microwave
MaXentric Technologies LLC
MCV Microwave
Measure Tech Inc.
MECA Electronics Inc.
Mega Circuit Inc.
MegaPhase
Menlo Microsystems Inc.
Mercury Systems
Metamagnetics Inc.
Mician GmbH
Micro Harmonics Corporation
Micro Lambda Wireless Inc.
MicroFab Inc.
Micro-Mode Products Inc.
Microsanj LLC
Microsembly
Microwave Applications Group
Microwave Development Labs
Microwave Engineering Corp.
Microwave Journal
Microwave Product Digest
Microwave Products Group
Microwaves & RF
Millimeter Wave Products Inc.
Milliwave Silicon Solutions Inc.
Mini-Circuits
Mini-Systems Inc.
MISOTECH
Mitsubishi Electric US Inc.
Modelithics Inc.
Modular Components National
Morion US LLC
Mouser Electronics Inc.
MPI Corp.
MRSI Systems, Mycronic
MtronPTI
Muegge Gerling
MWS Wire Industries
Nano Dimension
Narda-MITEQ
NDK America
Networks International Corp.
NI
Ningbo Somefly Technologies
Nisshinbo Micro Devices Inc.
Noisecom
Norden Millimeter Inc.
Northrop Grumman
Nxbeam Inc.
Ohmega Technologies
Ophir RF Inc.
Optomec
Orbel Corp.
Orolia USA
Otava Inc.
Pasquali Microwave Systems
Passive Plus Inc.
Pasternack
PCB Power Inc
PCB Technologies
Pickering Interfaces
Piconics Inc.
Planar Monolithics Industries
Plymouth Rock Technologies
PM Industries Inc.
Polyfet RF Devices
PPG Cuming Microwave
PPI Systems Inc.
Presidio Components Inc.
PRFI Ltd.
pSemi Corporation
Purecoat North LLC
Q Microwave Inc.
QIQ Systems Inc.
Qorvo
QP Technologies
Quantic Electronics
Quarterwave Corp.
Queen Screw & Mfg Inc
QuinStar Technology Inc.
QWED Sp. z o.o
R&K Company Limited
Rapidtek Technologies Inc.
Reactel Inc.
RelComm Technologies Inc.
Reldan
Remtec Inc.
Renaissance Electronics/HXI
Renesas Electronics America Inc
Res-Net Microwave
Response Microwave Inc.
RF Globalnet
RF Morecom Corea
RF Superstore
RFHIC Corp.
RF-Lambda USA LLC
RFMTL
RFMW
Richardson Electronics Ltd.
Richardson RFPD
RJR Technologies Inc.
RLC Electronics Inc.
Rogers Corp.
Rohde & Schwarz USA Inc.
Rosenberger North America
SAF North America LLC
Samtec Inc.
San-tron Inc.
Sawnics Inc.
Schlegel Electronic Materials
Schmid & Partner Engineering AG
Scientific Microwave Corp.
SemiDice (Micross Components)
SemiGen
Sensorview Co. Ltd.
Sentec E&E Co. Ltd.
SGMC Microwave
Shimifrez Inc.
Siglent Technologies NA
Signal Hound
Signal Integrity Journal
Signal Microwave
SignalCore Inc.
Skyworks Solutions Inc.
Smiths Interconnect
SOMACIS
Sonnet Software Inc.
Southwest Microwave Inc.
Space Machine & Engineering Corp.
SpaceForest sp z.o.o.
SRTechnology Corp.
SSI Cable Corporation
Starwave Sdn Bhd
State of the Art Inc.
Statek Corp.
Stellant Systems Inc.
Stellar Industries Corp.
StratEdge Corp.
Sumitomo Electric Device Innovations
Sung Won Forming
SuperApex Corporation
Susumu International (USA) Inc.
SV Microwave
Switzer
SynMatrix Technologies Inc.
Tagore Technology Inc.
Tai-Saw Technology Co. Ltd.
Taitien
TDK Corporation of America
TDK-Lambda Americas
Tecdia Inc.
Teledyne Technologies
Telegartner Inc.
Telonic Berkeley Inc.
TESLA Consortium
TEVET
Texas Instruments
The Boeing Company
The Goodsystem Corp.
Thin Film Technology Corp.
TICRA
Times Microwave Systems
TMY Technology Inc.
Tower Semiconductor
TPT Wire Bonder
Transcat Inc.
Transcom Inc.
Transline Technology Inc.
TRF Electronics
TRM Microwave
TRS-RenTelco
Ulbrich Specialty Wire Products
Ultra
United Monolithic Semiconductors
University of Texas at Dallas
UTE Microwave Inc.
Vanteon Corporation
Varioprint AG
Vaunix Technology Corp.
Ventec International Group
Virginia Diodes Inc.
Vishay Intertechnology Inc.
Waka Manufacturing Co. Ltd.
Wave Mechanics Pvt. Ltd
WAVEPIA Co. Ltd.
WavePro
Wavice
WayvGear
Weinschel Associates
Wenzel Associates Inc.
Werlatone Inc.
West Bond Inc.
Wevercomm Co. Ltd.
Wiley
WIN Semiconductors Corp.
Winchester Interconnect
WIPL-D
Wireless Telecom Group
Withwave Co. Ltd
WL Gore & Associates Inc.
Wolfspeed Inc.
XMA Corporation
X-Microwave
Xpeedic Technology Inc.
Z-Communications Inc.

First time exhibitors are noted in white.

This information is accurate as of 16 March

For the latest on IMS and Microwave Week visit ims-ieee.org

Thank You to Our Sponsors

PLATINUM

ANALOG DEVICES
AHEAD OF WHAT'S POSSIBLE™

qorvo®

GOLD

AMPLITECH GROUP

ROHDE&SCHWARZ
Make ideas real

SILVER

Anokiwave
mmW Solutions. Enabling a new world

cadence®

ERAVANT
FORMERLY SAGE MILLIMETER

MACOM®

Maury Microwave

MI-WAVE®
Millimeter Wave Products Inc.

OFFICIAL MEDIA SOURCE OF MTT-S

IEEE microwave MAGAZINE
for the Microwave & Wireless Engineer

MEDIA PARTNERS

Microwave Journal

Microwaves&RF

MEDIA SPONSORS

everythingRF

HIGH FREQUENCY ELECTRONICS

MPD MICROWAVE PRODUCT DIGEST

RF Globalnet

For the latest on IMS and Microwave Week visit ims-ieee.org

Women in Microwaves

IMS2022 Women in Microwaves Retrospective: We've Come a Long, Long Way

■ **Sherry Hess**

It's been 12 years since I first raised my hand and volunteered to coordinate the Women in Microwaves (WIM) reception at the 2010 IEEE International Microwave Symposium (IMS2010) in Los Angeles, despite not knowing what it was and never having attended. Since then, I've been deeply committed to the IEEE Microwave Theory and Techniques Society (MTT-S) WIM organization, advocating for the greater involvement of women in the MTT-S.

I'm not sure how far back the IMS WIM reception goes, but, after signing up to host the 2010 event (Figure 1), I remember asking myself, "There aren't that many of us; why had I not been previously invited to attend, and why had I not heard of it?" Such a small percentage of engineers in the RF and microwave realm are women to begin with, and it appeared even more difficult to get the word out about this reception.

Sherry Hess (sherry.hess.us@ieee.org), an IEEE MTT-S Women in Microwaves committee member, is with Cadence Design Systems, San Jose, California, 95134, USA.

Digital Object Identifier 10.1109/MMM.2022.3157969
Date of current version: 5 May 2022

I quickly got to work making sure all MTT-S women were aware of the reception. I knew we had to be aggressive with our outreach to increase awareness of our group and fully promote the many benefits and opportunities that the RF and microwave industry offers women. I am happy to share that we had women from all facets of IMS attend that event—overall, we had more than 75 people (men and women) attend, which was more than double the prior year's participation.

Earlier WIM events typically took place in a convention center conference room with only a handful of women

COURTESY OF LYLE PHOTOGRAPHY

Figure 1. *Sherry Hess (right) with Jeannette Wilson and Neil Craig at the IMS2010 WIM reception.*

attending. Since 2010, however, the reception has grown into a full program that embraces keynote addresses, guest speakers, and panel discussions as well as a vibrant, standing-room-only networking reception at a fun venue.

For instance, at IMS in 2016 (San Francisco), the WIM social event was augmented by an all-female technical track followed by a "Diversity in Engineering" panel session. In 2017 (Hawaii), the reception expanded to include a half-day panel discussion, "Inspiring the Next Generation of Women Engineers," which, for the first time ever, sought to reach out to women of all ages and career stages by opening the session to audiences ranging from middle school girls to professional women. Discussions ranged around finding out what it takes to "make it" in this male-dominated occupation, and the panel members shared their personal journeys and advice on becoming successful microwave engineers.

WIM receptions and panel discussions were soon added to the agenda of microwave conferences around the world, and I found myself speaking globally at conferences like the European Microwave Week (EuMW) (Europe), Asia-Pacific Microwave Conference (Asia), IEEE International Conference on Microwaves, Communications, Antennas, Biomedical Engineering, and Electronic Systems (Israel), IEEE MTT-S International Microwave and RF Conference (India), and more. In addition to the "larger" events, we are also making inroads at regional ones. As a case in point, in 2019, the IEEE Coastal Los Angeles Section Technical Symposium jumped onboard and hosted a women's networking luncheon.

Fast-forward some 10 years since I first learned of WIM to 2020, when I became the fourth female voting member of the MTT-S Administrative Committee, working with the first woman MTT-S president, Dominique Schreurs (2019), and incoming Rashaunda Henderson, the second female and first Black president. We all continue to focus on the important work of encouraging and mentoring women to join and stay in our field. As part of the IEEE MTT-S Member and Geographic Activities WIM subcommittee, I have seen tremendous growth in women "leaning in" to WIM, with the organization expanding to four subcommittee executives and 15 regional coordinators covering the Americas; Europe, the Middle East, and Africa; and the Asia-Pacific region. We continue to expand!

This retrospective on the blossoming of the WIM organization leads up to yet another unique event that recently happened: the IMS 2022

Digital Object Identifier 10.1109/MMM.2022.3158034

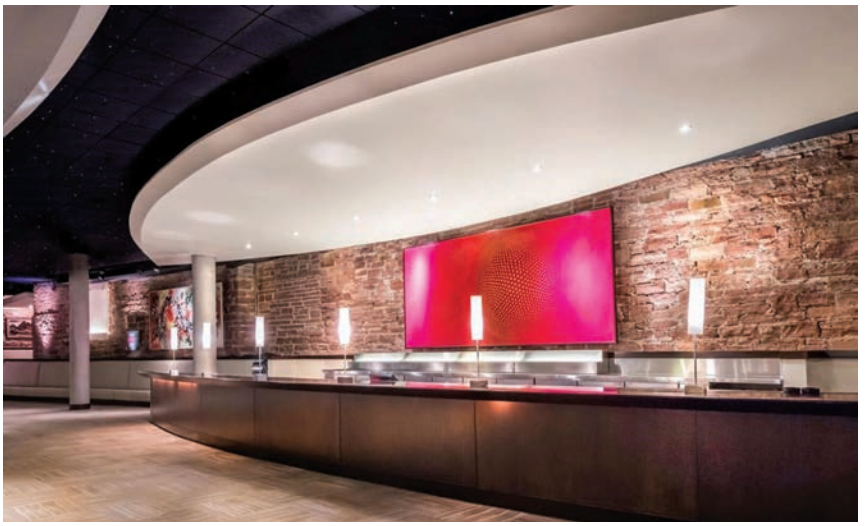

Figure 2. *The reception room and bar at the Ellie Caulkins Opera House. (Photo courtesy of Visit DENVER, the Convention and Visitors Bureau.)*

(Denver) WIM reception, held at the Denver Center for the Performing Arts in the Ellie Caulkins Opera House (Figure 2). Unlike past events, the organizing committee this time was more than just one or two—it was a true team lead by Prof. Zoya Popovic of the University of Colorado, Boulder that included not only her daughter but also numerous graduate students (both men and women).

WIM at IMS2022 is just one of many WIM events being held globally this year. Last year's EuMW2021 in London and EuMW2022, being held in Milan in September, both include WIM programs (presentations and networking). There is also the International Microwave Workshop Series on Advanced Materials and Processes for RF and THz Applications in November, which is already in the works. The list goes on ... a very good thing! To see where/when a WIM program is taking place in 2022, visit the MTT-S WIM page at https://mtt.org/wim for up-to-date news and information.

WIM is growing as more women realize the value of mutual support, networking, and mentorship. We're finding new and innovative ways to attract and maintain more women in our field by encouraging them to get involved and make their voices heard. As for the MTT-S WIM reception, it has morphed from a lackluster meeting room with a dozen attendees to exciting venues with hundreds of attendees—we've come a long, long way!

2022 IEEE Fellows Elevation and Recognition *(continued from page 43)*

MTT-S Members Elevated to Fellow of the IEEE Evaluated by Other Societies

We would also like to recognize our members who have been elevated to Fellow by other Societies or Councils. Currently, there are 39 Societies and seven Technical Councils in IEEE. Members elevated to the level of Fellow by other Societies who are also members of the MTT-S are listed here in alphabetical order according to the evaluating Society or Council:

- Hongsheng Chen, by the AP-S, for contributions to electromagnetic metamaterial and invisibility cloaks
- Tommaso Isernia, by the AP-S, for contributions on antennas synthesis and inverse scattering problems
- Xiuyin Zhang, by the AP-S, for contributions to the design of filtering antennas
- Jiang Zhu, by the AP-S, for contributions to antenna design for wireless communications
- Mikko Valkama, by the IEEE Communications Society, for contributions to physical layer signal processing in radio systems.

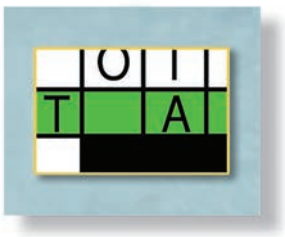

Enigmas, etc.

Solution to Last Month's Quiz

■ **Takashi Ohira**

We remember the truncated cosine waveform

$$i(t)=\begin{cases} I_1\cos\omega t - I_2 & \text{for off} \\ -\dfrac{R_2}{R_1}I_2 & \text{for on} \end{cases} \tag{1}$$

formulated in the previous puzzle. For (1) to satisfy current continuity at the turn-on moment $\omega t=\phi$, the two right-hand sides must balance as

$$I_1\cos\phi - I_2 = -\frac{R_2}{R_1}I_2. \tag{2}$$

Takashi Ohira (ohira@tut.jp) is with Toyohashi University of Technology, Aichi, 441-8580, Japan. He is a Life Fellow of IEEE.

Digital Object Identifier 10.1109/MMM.2022.3157966
Date of current version: 5 May 2022

This equation may look slightly complicated. However, at the specified condition $R_1=R_2$, the equation reduces to $\cos\phi=0$. Thus, we conclude that

$$\phi = 90^\circ. \tag{3}$$

Therefore, the correct answer to last month's quiz is "d." See Figure 1 to review the circuit diagram and current waveform with the emphasis of word balloons.

Looking at the circuit diagram again, one may think that the condition $R_1=R_2$ implies the usual source-to-load impedance matching. Is it true that the usual matching theorem applies to the diode rectifier even though R_1 is RF resistance while R_2 is dc resistance? This is a mysterious (but instructive) question for nonlinear RF circuit designers. Although currently uncertain, the truth will be revealed step by step in this journey. Next month's quiz will consider what happens to ϕ when $R_1\neq R_2$.

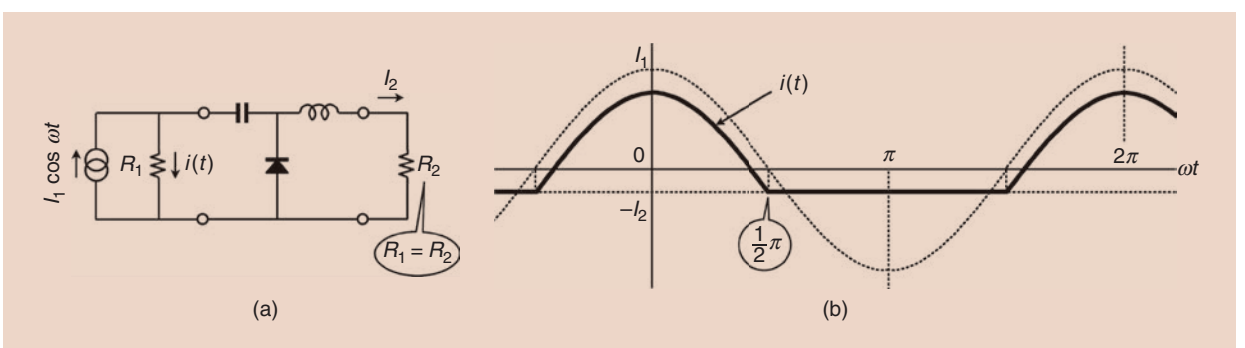

Figure 1. *The rectifier operated under the condition of $R_1=R_2$: the (a) circuit diagram and (b) current waveform.*

Conference Calendar

Editor's Note: Please check the website of each conference for any changes to paper or workshop deadlines or conference dates, and modality (in person, virtual, or hybrid).

JUNE 2022

2022 IEEE/MTT-S International Microwave Symposium (IMS 2022) (co-located with 2022 IEEE Radio Frequency Integrated Circuits Symposium (RFIC), and 2022 99th ARFTG Microwave Measurement Conference (ARFTG)
19–24 June 2022
Location: Denver, Colorado, United States

JULY 2022

2022 Fifth International Workshop on Mobile Terahertz Systems (IWMTS)
4–6 July 2022
Location: Duisburg, Germany

2022 Wireless Power Week (WPW)
5–8 July 2022
Location: Bordeaux, France

2022 IEEE MTT-S International Conference on Numerical Electromagnetic and Multiphysics Modeling and Optimization (NEMO)
6–8 July 2022
Location: Limoges, France

Digital Object Identifier 10.1109/MMM.2022.3144801
Date of current version: 5 May 2022

2022 IEEE MTT-S International Conference on Microwave Acoustics and Mechanics (IC-MAM)
18–20 July 2022
Location: Munich, Germany

2022 International Telecommunications Conference (ITC-Egypt)
26–28 July 2022
Location: Alexandria, Egypt

AUGUST 2022

2022 IEEE International Symposium on Radio-Frequency Integration Technology (RFIT)
29–31 August 2022
Location: Busan, South Korea

SEPTEMBER 2022

2022 47th International International Conference on Infrared, Millimeter, and Terahertz Waves (IRMMW-THz)
4–9 September 2022
Location: Rotterdam, The Netherlands

2022 IEEE Global Humanitarian Technology Conference (GHTC)
8–11 September 2022
Location: Santa Clara, California, United States

2022 24th International Microwave and Radar Conference (MIKON) and 2022 23rd International Radar Symposium (IRS)
12–14 September 2022
Location: Gdansk, Poland

2022 52nd European Microwave Conference (EuMC), 2022 17th European Microwave Integrated Circuits Conference (EuMIC), and 2022 18th European Radar Conference (EuRAD)
26–30 September 2022
Location: Milan, Italy

OCTOBER 2022

2022 IEEE International Topical Meeting on Microwave Photonics (MWP)
4–6 October 2022
(Virtual Conference)

2022 IEEE 31st Conference on Electrical Performance of Electronic Packaging and Systems (EPEPS)
9–12 October 2022
Location: San Jose, California, United States

2022 IEEE International Symposium on Phased Array Systems & Technology (PAST)
11–14 October 2022
Location: Waltham, Massachusetts, United States

2022 IEEE BiCMOS and Compound Semiconductor Integrated Circuits and Technology Symposium (BCICTS)
16–19 October 2022
Location: Fort Lauderdale, Florida, United States

IEEE Microwaves, Antennas and Propagation Conference (MAPCON)

www.ieeemapcon.org

Dec 12-16, 2022 | Bangalore, India

Chief Patrons:
S. Somanath
Secretary, DoS / Chairman, ISRO
G. Satheesh Reddy,
Secretary, DDR&D/ Chairman, DRDO

General Chairs:
Puneet Kumar Mishra
Mrinal Kanti Mandal

TPC Chairs:
Ashutosh Kedar
Meenakshi Rawat

Finance Chair:
Chandrakanta Kumar

MAPCON Executive Committee
Yahia Antar (Co-Chair)
Goutam Chattopadhyay (Co-Chair)
Rajeev Jyoti, Shiban Koul
Debatosh Guha, K J Vinoy
Puneet K Mishra, Jaleel Akhtar
Chinmoy Saha, Sherry Hess

IEEE MTT-S and IEEE AP-S have come together and signed a MoU for combining two flagship conferences of the respective societies in India (IMaRC and InCAP) to a single conference: Microwave, Antennas, and Propagation Conference (MAPCON). The first edition of MAPCON is planned to be organized in Bangalore, India during Dec 12-16, 2022. MAPCON 2022 will create an international platform for Microwave, Antenna and Propagation experts and technologist from Industry, Academia and Startup ecosystem to collaborate and share their vision, expertise and knowledge. MAPCON 2022 will include technical sessions, poster sessions, special sessions, invited talks, workshops, tutorials, focused track on Young Professionals, Women in Engineering and SIGHT. Eminent professionals from International Space Agencies, Defense Establishments, National Research Organizations, Academia, and Industries will deliver expert talks and tutorials and organize special sessions related to recent developments.

Call For Paper : Authors are invited to submit their original research work in the form of paper, 4-6 pages, in following areas (but not limited to) :

- Phased array antennas
- Reflector and reflect-array antennas
- Horn antennas & Feed components
- Planar Antennas
- Frequency selective surfaces
- Radar and remote sensing antennas
- Satellite antennas and payloads
- Aircraft antennas
- Antennas for seekers and defense applications
- Ultra Wide Band and multi-band antennas
- RFIDs
- Scattering & Diffraction
- Dielectric resonator antennas
- Metamaterial, metasurface and EBG antennas
- Reconfigurable antennas
- EM theory and computational EM
- Characterization of Antennas/Payloads/Radomes
- MIMO and 5G antennas
- Millimeter-wave & Terahertz antennas
- Embedded and wearable antennas
- Conformal antennas
- Beamforming techniques
- Propagation studies and experiments
- Antenna Measurements (Compact Range, Near Field, Far Field, Drones etc.)
- RFICs and MMICs
- Evolution of Semi Conductor Technologies in RF, Microwaves, mmwave, THz
- Passive components and circuits
- TR Modules
- High power Microwaves
- MIMO techniques
- Novel waveguides and new phenomena in waveguides
- Plasmonic devices and their applications
- Microwave, millimeter-wave and THz systems
- Radar, SAR and microwave imaging
- RF sensors and testing techniques
- Microwave materials and processing
- Emerging areas including nanotechnology and biomedical applications
- Wireless and cellular architectures, components, and circuits
- Electromagnetic Interference and Compatibility (EMI/EMC)
- Medical and industrial applications of microwaves
- RF energy harvesting and wireless power transfer
- RF systems for emerging telecommunication infrastructure
- RF technologies for Space and Defense applications
- RF Technologies for 5G/6G and beyond
- Additive Manufacturing Techniques
- Doppler, Short Range, Autonomous Vehicle Radars

Important Dates:

Paper Submission Starts	:	May 15, 2022
Paper Submission Ends	**:**	**July 31, 2022**
Notification of Acceptance	:	Sep 30, 2022

Early Submission Advantage : Discount on Registration Fees, if papers are submitted before May 30, 2022

Awards:

MAPCON Best Paper Award (Academia & Industry)	: ₹ 50,000
Dr. C J Reddy Best YP Paper Award (Male & Female)	: ₹ 15,000
Mrs Ranjana Pal Award for Practical Application and design (Male & Female)	: ₹ 5,000
MAPCON Best Student Paper Award (1st)	: ₹ 10,000
MAPCON Best Student Paper Award (2nd)	: ₹ 5,000

Digital Object Identifier 10.1109/MMM.2022.3168890

Advertisers Index

ADVERTISER	PAGE	URL	PHONE
Anokiwave	11	www.anokiwave.com/	
Besser Associates	8	www.BesserAssociates.com	
Cadence Design Systems	2	www.cadence.com/go/awr/try	
Cicor	23	www.cicor.com	
Coilcraft	33	www.coilcraft.com	
Comsol	7	www.comsol.com/feature/rf-innovation	
dSPACE	13	www.dspace.com	
Mician GmbH	9	www.mician.com	+49 42116899351
Mini-Circuits	1	www.minicircuits.com	+1 718 934 4500
Polyfet RF Devices	23	www.polyfet.com	+1 805 484 4210
Remcom	5	www.remcom.com	+1 888 7 REMCOM
Rosenberger GMbH & Co.KG	15	www.rosenberger.com	
Sonnet Software	CVR 4	www.sonnetsoftware.com	+1 877 7 SONNET
Taitien, USA	21	www.Taitien.com	
Transline Technology, Inc	19	www.translinetech.com	+1 714 533 8300
West • Bond, Inc	27	www.westbond.com	+1 714 978 1551
WIPL-D	17	www.wipl-d.com	

445 Hoes Lane, Piscataway, NJ 08854

IEEE MICROWAVE MAGAZINE REPRESENTATIVE
Aviva Rothman
Naylor Association Solutions
Phone: +1 352 333 3435
arothman@naylor.com

Digital Object Identifier 10.1109/MMM.2021.3133032

IEEE Journal of Microwaves

"Expanding Science, Technology & Connectivity Around the Globe"

Announcing a very Special Issue

Celebrating the 70th Anniversary of the MTT Society

Initial Manuscript Submission Deadline: Monday, October 3rd, 2022

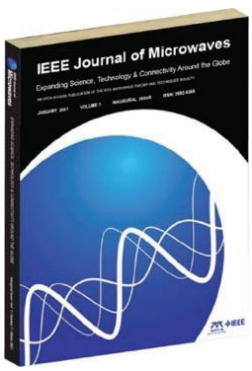

The Microwave Theory and Technology Society is celebrating 70 years of service to the microwave engineering and science communities throughout 2022. This special issue of the **IEEE Journal of Microwaves** will document some of the many topic areas and significant contributions that have been made over the years.

General interest review articles, historic accounts, and new contributions highlighting developments that have come out of our rich historic narrative are all welcome.

If you have a particular idea or topic you would like to contribute please contact our special issue guest editor: **Professor Ke Wu**, Ecole Polytechnique, Montréal, Canada (ke.wu@polymtl.ca) or **Peter Siegel**, JMW Editor-in-Chief (phs@caltech.edu).

The deadline for submission of initial manuscripts is Monday, **October 3rd, 2022.** Final upload of accepted paper proofs is **December 1, 2022**. All production ready manuscripts will be posted on IEEE Xplore Early Access and will appear in final paginated sequence in the Special Issue – scheduled for final release in January 2023.

Manuscripts should be formatted and submitted using the instructions, templates and links that can be found at: https://mtt.org/publications/journal-of-microwaves/manuscript-submission/. Contributed papers should be targeted at ten pages but review and special invited papers can be longer. All submissions will be reviewed in accordance with the normal procedures of the Journal. Please tag uploaded papers as "Special Issue" at Manuscript Central.

Additional multidisciplinary topics and regular research articles will also be considered. Prospective authors should contact our Guest Editor or Editor-in-Chief if they wish to suggest or discuss specific contributions.

We hope you will consider contributing to this Special Issue of *IEEE Journal of Microwaves* and continue to support the journal through your regular research submissions.

IEEE

MTT-S

Digital Object Identifier 10.1109/MMM.2022.3160252

SONNET®
v18

18.54 is available now!

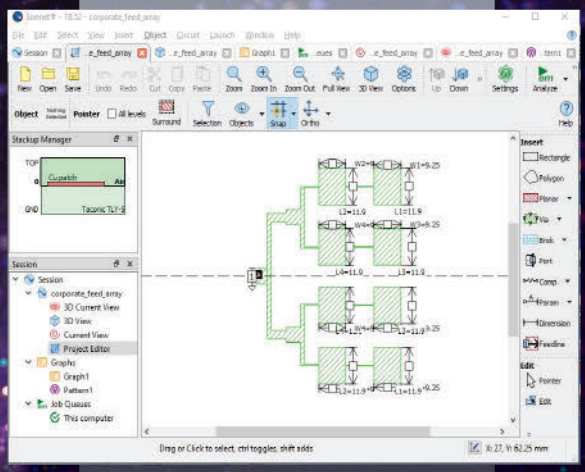

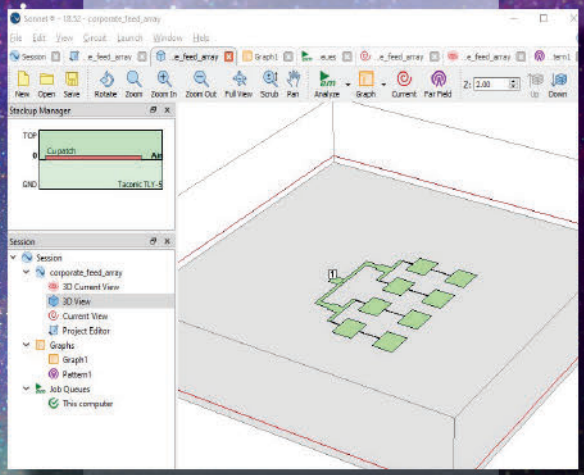

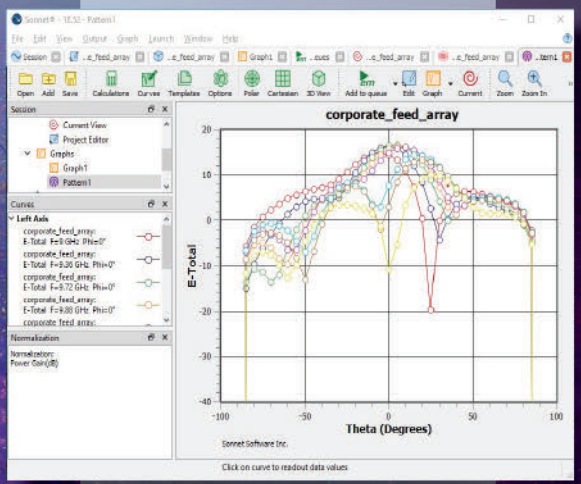

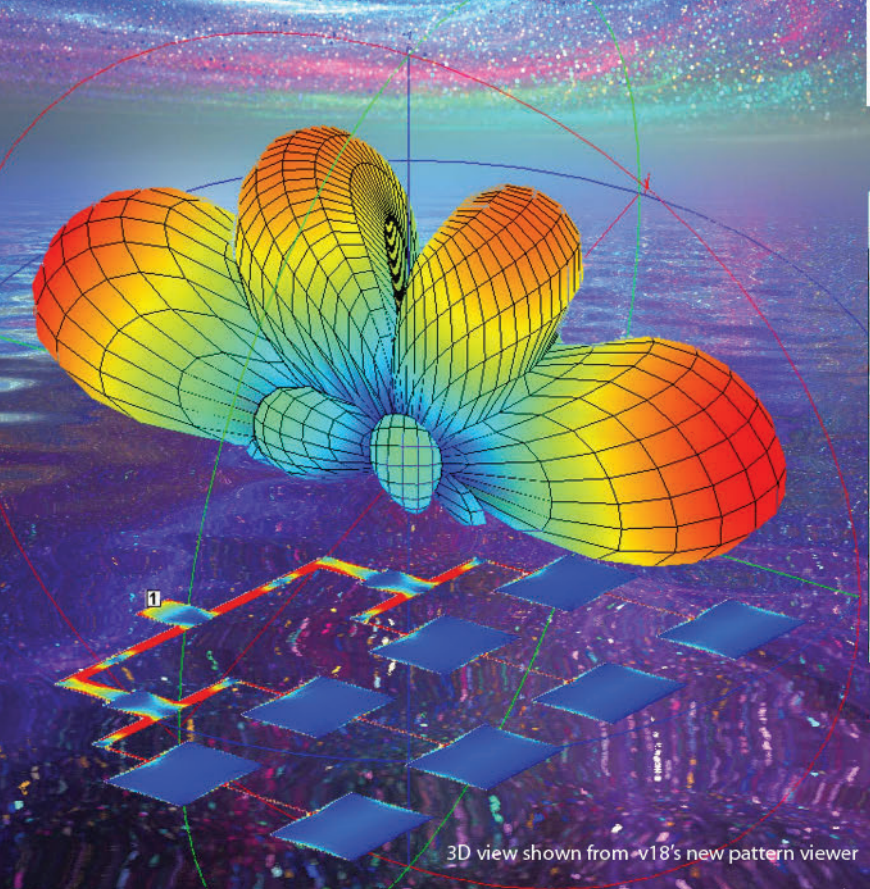

3D view shown from v18's new pattern viewer

www.sonnetsoftware.com
(877) 7 Sonnet